COPPER(II) ARYLCARBOXYLATES : SUBSTITUENT EFFECTS ON STRUCTURE, THERMAL PROPERTIES, MAGNETISM, REDOX AND CARBON-CARBON BOND-FORMING REACTION OF CARBONYLS

MOHAMMAD ISA BIN MOHAMADIN

FACULTY OF SCIENCE
UNIVERSITY OF MALAYA
KUALA LUMPUR

2011

COPPER(II) ARYLCARBOXYLATES : SUBSTITUENT EFFECTS ON STRUCTURE, THERMAL PROPERTIES, MAGNETISM, REDOX AND CARBON-CARBON BOND-FORMING REACTION OF CARBONYLS

MOHAMMAD ISA BIN MOHAMADIN

THESIS SUBMITTED IN FULFILLMENT OF THE
REQUIREMENT FOR THE DEGREE OF
DOCTOR OF PHILOSOPHY

DEPARTMENT OF CHEMISTRY
FACULTY OF SCIENCE
UNIVERSITY OF MALAYA
KUALA LUMPUR

2011

ABSTRACT

This research focused on the synthesis, structural elucidation, and physical characterisations of copper(II) arylcarboxylates of general formula $[Cu_2(p\text{-}XC_6H_4COO)_4L_2]$, where X = H, NO_2, OH, NH_2, F, Cl, Br and I, and a complex with the chemical formula $[Cu_2(3,5\text{-}(NO_2)_2C_6H_3COO)_4L_2]$, and L = CH_3CH_2OH and/or H_2O.

A total of nine binuclear copper(II) arylcarboxylates were successfully prepared, and their magnetic, thermal and redox properties were determined. In addition, suitably selected complexes were also subjected to reaction with selected carbonyls namely acetone, and a mixture of benzaldehyde and acetophenone, in order to determine their role in the carbon-carbon bond-formation reaction.

The instrumental analyses used to characterize these complexes were CHN elemental analyses, atomic absorption spectroscopy (AAS), FTIR and UV-vis spectroscopies, X-ray crystallography (for crystalline complexes), magnetic susceptibility by the Gouy method, thermogravimetry, differential scanning calorimetry, and cyclic voltammetry. In addition, NMR (^{1}H- and ^{13}C-) and GCMS were used to elucidate the structure of the product(s) obtained from the reaction with carbonyls.

All complexes were dimeric with square pyramidal geometry at copper(II) centres with *syn-syn* coordination mode of carboxylate ligand in the solid states. However, complexes having strong electron-withdrawing group, namely X = NO_2, 3,5-$(NO_2)_2$ and F, have a more distorted geometry around copper(II). The structures were stable in CH_3OH-CH_3COOH solvents, but formed monomeric structures in strong coordinating ligands, namely DMSO

and DMF. Especially were the copper(II) complexes with NO_2- and I-substituted arylcarboxylates ligands, which dissociated in DMSO-$CHCl_3$.

The complexes showed antiferromagnetic interaction of variable strengths. The values of μ_{eff} and 2J range from 1.80 B.M. to 2.54 B.M, and from -382 cm^{-1} to -133 cm^{-1}, respectively. However, no direct correlation between the type of substituent and the strength of the magnetic interaction could be established.

The complexes were thermally stable up to 240°C. The decomposition pathway involved the decarboxylation of the ligands, leaving residues assumed to be mainly copper(II) oxide. Complexes with electron-donating group were less thermally stable compared to those with electron-withdrawing groups.

All complexes were redox-active. Facile reduction depended on the type of substituent as well as on the geometrical distortion at copper(II) centres. Complexes with electron-donating group were reduced at more negative potential (harder to be reduced) compared to those with electron-withdrawing group. The redox reactions were quasi-reversible involving extensive structural reorganization and chemical reactions (the EC mechanism).

The reaction of CuB with CH_3COCH_3 in acidic condition formed a black mixed-valence complex, $[Cu(II)Cu(I)(R)_3(RH)_2L_4].CH_3COCH_3$, where R = C_6H_5COO; L = $CH_3COCH_2C(OH)(CH_3)_2$. The ligand L was a product of the carbon-carbon bond-forming reaction between CH_3COCH_3 molecules. The mixed-valence complex was thermally stable (T_{dec} = 126°C), strongly antiferromagnetic (μ_{eff} = 1.33 B.M.; 2J = - 556 cm^{-1}), and has a highly delocalized electron with surprisingly low band gap energy of 1.2 eV.

Under similar conditions, $CuNO_2B$, CuOHB and CuClB reacted with CH_3COCH_3 to form the mixed-valence complexes $[Cu(II)Cu(I)(R)_3(RH)_2L_{10}].3CH_3COCH_3$, $[Cu(II)Cu(I)(R)_3(RH)_5L_5].CH_3COCH_3$ and $[Cu(II)Cu(I)(R)_3(RH)_2L_{15}].CH_3COCH_3$ (where R = 4-$NO_2C_6H_4COO$, 4-HOC_6H_4COO and 4-ClC_6H_4COO respectively, L = $CH_3COCH_2C(OH)(CH_3)_2$). The copper(II) complex substituted with a strong electron-withdrawing group (NO_2) formed the mixed-valence product in higher yield compared to that with electron-donating group (OH).

Some of the findings of this project were published in six (6) ISI journals, one (1) non-ISI journal, and presented at three (3) national and five (5) international conferences (**Appendix 1**).

ABSTRAK

Fokus utama penyelidikan ini adalah sintesis, elusidasi struktur dan pencirian fizikal bagi kuprum(II) arilkarboksilat dengan formula umum [Cu_2(*p*-$XC_6H_4COO)_4$], iaitu X = H, NO_2, OH, NH_2, F, Cl, Br and I, dan satu kompleks dengan formula kimia [$Cu_2(3,5\text{-}(NO_2)_2C_6H_3COO)_4$].

Sejumlah sembilan kuprum(II) arilkarboksilat binuklear berjaya disintesiskan, dan sifat magnetik, terma dan redok ditentukan. Di samping itu, kompleks yang sesuai dipilih bagi melihat peranan komplek-kompleks ini dalam tindak balas pembentukan ikatan karbon-karbon.

Peralatan yang digunakan untuk mencirikan semua kompleks adalah analisis unsur CHN, spektroskopi penyerapan atom (AAS), spektroskopi FTIR dan UV-vis, kristalografi sinar X (bagi kompleks berhablur), kerentanan magnet melalui kaedah Gouy, termogravimetri, kalorimetri pembeza imbasan, dan voltametri siklik. Sebagai tambahan, peralatan NMR (^{1}H- dan ^{13}C-) dan GCMS digunakan untuk menentukan struktur hasil-hasil yang diperoleh daripada tindak balas dengan karbonil.

Semua kompleks adalah dimerik dengan geometri piramid sisi empat sama pada kuprum(II) dan karboksilat titian *syn-syn*. Struktur kompleks adalah stabil dalam pelarut CH_3OH-CH_3COOH, tetapi tidak stabil dan membentuk struktur monomerik dalam pelarut DMSO and DMF. Terutama adalah kompleks kuprum(II) dengan ligan arilkarboksilat tertukarganti NO_2 dan I yang tercerai dalam DMSO-$CHCl_3$.

Kompleks-kompleks ini menunjukkan saling tindakan antiferomagnetik dengan pelbagai kekuatan. Nilai μ_{eff} dan 2J adalah dalam

julat 1.80 B.M. hingga 2.54 B.M, dan -382 cm^{-1} hingga -133 cm^{-1} masing-masing. Walaubagaimanapun, kekuatan saling tindakan magnetik tidak bergantung secara langsung dengan jenis kumpulan tertukar ganti dalam komplek tersebut.

Semua kompleks adalah stabil secara terma sehingga suhu 240^oC. Laluan penguraian melibatkan pendekarboksilan ligan, dengan baki utama dianggapkan kuprum(II) oksida. Kompleks dengan kumpulan penderma elektron adalah kurang stabil secara terma berbanding kompleks dengan kumpulan penarik elektron.

Semua kompleks adalah aktif redoks. Penurunan mudah bergantung pada jenis penukarganti dan pengherotan geometri pada kuprum(II). Komplek dengan kumpulan tertukar ganti penderma elektron adalah lebih susah diturunkan berbanding dengan komplek yang mempunyai kumpulan tertukar ganti penarik elektron. Tindak balas redoks adalah kuasi-berbalik dan melibatkan pengubahan semula struktur secara ektensif dan tindak balas kimia (mekanisme EC).

Tindak balas CuB dengan CH_3COCH_3 dalam keadaan berasid membentuk kompleks valens tercampur $[Cu(II)Cu(I)(R)_3(RH)_2L_4]$. CH_3COCH_3, iaitu R = C_6H_5COO; L = $CH_3COCH_2C(CH_3)(OH)CH_3$, yang berwarna hitam. Ligan L adalah hasil daripada proses pembentukan ikatan karbon-karbon antara molekul-molekul CH_3COCH_3. Kompleks valens tercampur ini adalah stabil secara terma ($T_{terurai}$ = 126^oC), antiferomagnetik kuat (μ_{eff} = 1.33 B.M.; 2J = - 556 cm^{-1}), dan mempunyai elektron ternyahtempatan secara meluas dengan tenaga jurang jalur yang agak rendah , iaitu 1.2 eV.

Pada keadaan yang serupa, $CuNO_2B$, CuOHB dan CuClB bertindak balas dengan CH_3COCH_3 untuk membentuk kompleks valens tercampur $[Cu(II)Cu(I)(R)_3(RH)_2L_{10}].3CH_3COCH_3$, $[Cu(II)Cu(I)(R)_3(RH)_5L_5].CH_3COCH_3$ and $[Cu(II)Cu(I)(R)_3(RH)_2L_{15}].CH_3COCH_3$ (iaitu R = $4\text{-}NO_2C_6H_4COO$, $4\text{-}HOC_6H_4COO$ and $4\text{-}ClC_6H_4COO$ masing-masing, L = $CH_3COCH_2C(OH)(CH_3)_2$). Kompleks kuprum(II) tertukarganti dengan kumpulan penarik electron kuat (NO_2) membentuk hasil valens tercampur dalam hasilan yang lebih tinggi berbanding dengan kumpulan penderma electron (OH).

Beberapa penemuan daripada projek ini telah diterbitkan dalam enam (6) jurnal ISI dan dibentangkan secara lisan atau poster di tiga (3) persidangan kebangsaan dan lima (5) persidangan antarabangsa (**Lampiran 1**).

ACKNOWLEDGEMENTS

Alhamdulillah, all praises are due to Allah SWT for His greatness and for giving me the strength and courage to sail through this life-changing odyssey.

To my supervisor, Assoc. Prof. Dr. Norbani Abdullah, words are too little to describe my appreciation for her patience, guidance and encouragement throughout the completion of this work. Her kindness and persistence in helping me with my work has made my learning and research experience very lucrative and eye-opening.

I am also very grateful to all of my colleagues from Inorganic Chemistry Research Laboratory, Physical Chemistry Research Laboratory and all staff in the Chemistry Department, Science Faculty, University of Malaya. Without their cooperation and kindness, this project could not have been completed.

I also would like to thank Universiti Teknologi MARA for the financial support in sponsoring fully my study. A special appreciation also goes to the University of Malaya for the research grants (PS146/2007B and PS191/2008A).

Most of all, I wish to thank my wife, Nor Hazizah and all my kids, Abid, Sofea and Imran, and my parents and parents-in-law, for their enduring support and encouragement throughout this project.

TABLE OF CONTENTS

CHAPTER 1

INTRODUCTION

Dinuclear, trinuclear and polynuclear complexes of copper(II) ion have interesting structural diversity [1] and peculiar physical properties [2-5]. Studies done on these complexes with different type of ligands [6-9] have revealed numerous evidences on the direct impact of ligands on the structures and physical properties of such complexes [10].

Among the most common ligands studied are the carboxylates ($RCOO^-$), and nitrogen- and sulfur-containing groups [11-13]. The specially high interest in carboxylates comes from the ability of these ligands to bond to the central metal ion through various coordination modes [14], thus making it possible to tune their structures, and to allow them to be use as key building blocks for the synthesis of polynuclear complexes, from discrete dimers to supramolecular 1-D, 2-D and 3-D networks [15,16].

Earlier works on copper(II) carboxylates was sparked by the discovery of subnormal magnetic moment of copper(II) acetate monohydrate, $[Cu(CH_3COO)_2(H_2O)]$ [17]. This complex was later structurally resolved to be binuclear in which the two Cu atoms are bridged by four CH_3COO groups, while two H_2O molecules occupy the axial positions [18] (**Figure 1.1**).

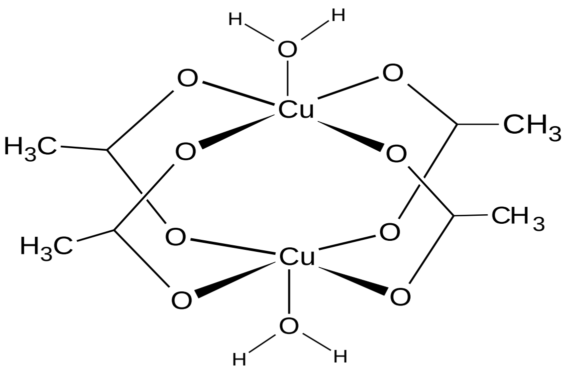

Figure 1.1: Structure of [$Cu_2(CH_3COO)_4(H_2O)_2$]

A remarkable feature of this structure, now famously known as the paddle-wheel structure, is the short distance between the two Cu atoms of 2.64 Å. This interatomic distance is comparable to the interatomic distance of 2.56 Å in metallic Cu. Surprisingly, the magnetic moment of this complex was found to be around 1.4 B.M., which is substantially smaller than the spin-only value of 1.73 B.M. [10,19]. Since then, extensive works have been done by many researchers in order to explain this anomaly and its correlation to the structures of copper(II) carboxylates [10].

The structural and magnetic studies of copper(II) carboxylates have always gone hand-in-hand, particularly for the purpose of understanding the electron transport in the compound [20-21]. The abnormally low value of magnetic moments actually indicates a very strong interaction between the unpaired electron on each Cu(II) centre [10]. In earlier studies, such observation was suggested to be caused by a direct interaction (either δ or σ) between the two Cu(II) ions due to the short Cu-Cu distance in the compounds [20,22]. But, as the structures of more compounds made up of different ligands as well as metal ions became known, a superexchange interaction via the bridging carboxylate ligands becomes more feasible [23,24].

Throughout time, the study on copper(II) carboxylates has grown extensively and was not limited to dinuclear complexes and magnetic properties. With a great development in the field of synthesis, different types of ligands were developed, thus giving birth to a large and diverse group of copper(II) coordination compounds with interesting structures and properties with a lot of potential application in many areas [25]. With such a huge structural diversity, the study on copper(II) carboxylate or metal(II) carboxylate has partly turned to the study of supramolecular compound with promising industrial applications. The ability of this compound to form multi-dimensional frameworks by joining the metal ions and organic carboxylate bridges has given birth to the formation of metal organic frameworks (MOFs). The development and analysis of these types of materials provide not only an interesting window into nanochemistry but also the potential for novel application of the pores, channels and chains that these compounds display.

Undeniably, the work on metal carboxylates is still intensively progressing especially in the field of metal organic frameworks. May be due to this scenario, the work on the chemical properties of metal carboxylates seemed to be forgotten and left behind. The chemical properties, especially the catalytic role of the compounds, are a very promising area of research and could give some useful insight on another potential application of metal carboxylates. Unfortunately, there only exist few researches on the catalytic properties of such compounds. Copper(II) ion particularly has shown catalytic properties for many chemical reactions, and as shown by Irie et al. [26], metal(II) complexes do have catalytic properties to certain degree. Aldol condensation reaction, one of the most important C-C bond-forming reactions in synthetic chemistry, has been reported to be catalysed by transition metal(II) ions [27].

While the literature on the structure of binuclear copper(II) carboxylates is considerable, only a relatively small number of benzoate compounds have been the subject of structural characterization. In addition, the literature available for the physico-chemical properties of such complexes is also limited.

It is rather surprising that copper or other metal ions with arylcarboxylate anions have been scarcely studied. There are some magneto-structural studies on copper(II) complex with benzoate ion and few of its derivatives as ligands with sole objective to establish their magnetic properties in relation to their structure [28-31]. There are also papers on complexes of rare earth metal ions with 2,4-dimethoxy-, 3,4-dimethoxy-, 4-chloro-2-nitro- and 4-chloro-3-nitrobenzoate [32-34], 3,5-dimethoxybenzoate with Cu(II), Ag(I), Zn(II) and Pb(II) [35], and 3,6-dichloro-2-methoxybenzoate with Cu(II), Hg(II), Pb(II) and Zn(II) [36].

The structure of copper(II) benzoate have also been shown to be varied, from dimeric paddle-wheel to polymeric, depending upon the method of preparation [39-40]. The formation of binuclear structure with two metal ions in close proximity is a great promise in biomimetic studies of binuclear metalloenzyme and metalloproteins due to their peculiar catalytic properties, their stabilizing properties of unusual oxidation states and potential electronic and magnetic interaction between two metal ions [41-43]. In physicochemical aspects, such complexes can also significantly lead to the development of new inorganic materials capable of showing peculiar magnetic and redox properties and hence can have a wealth of application in magneto chemistry.

Thus, this project was undertaken to thoroughly study the structural, physical and chemical properties of nine copper(II) arylcarboxylates of general formula $[Cu(4\text{-}XC_6H_4COO)_2]$ where X = H, NO_2, OH, NH_2, F, Cl, Br, I, and for $[Cu(3,5\text{-}(NO_2)_2C_6H_3COO)_2]$. These substituents are postulated to bring a significant impact on the structure of the complexes, especially in terms of electron polarizability and steric hindrance, and thus will also directly affect the physical properties of the complexes. Specifically for copper(II) arylcarboxylates, the structures were reported to depend predominantly on the steric effect. For example, bulky *ortho*-substituents were shown to form dinuclear complexes [44]. However, in the absence of steric effect, the reduction of the charge on the copper(II) ion is imperative. Higher σ electron density on the carboxylate oxygen atoms, normally measured from the pK_a value of the parent acid, and adducts which lower the residual charge on the copper(II) ions, favour the formation of dinuclear complexes [44-47].

A synthetic method chosen to prepare these complexes was a metathesis reaction between [$Cu(CH_3COO)_2$] and the corresponding arylcarboxylic acid [48]. The structures of these complexes were deduced from CHN elemental analyses, FTIR spectroscopy, UV-vis spectroscopy, and X-ray crystallography (for crystals). The physical properties studies were focused on their magnetic, and on the less explored thermal and electrochemical properties. Such studies will enable a better understanding on the correlation between structure and physical properties of these complexes. The thermal properties were studied using thermogravimetry (TGA), differential scanning calorimetry (DSC), the magnetic susceptibility by the Gouy method, and the redox properties by cyclic voltammetry (CV).

The chemical property studied for these arylcarboxylates arises from a preliminary work on the reaction of copper(II) benzoate with acetone in the presence of hydrochloric acid under reflux [49]. The product from the reaction was a black, shiny and fragile solid, but its identity was not fully confirmed. Initial findings suggest that the product formation involves redox and C-C bond-forming reactions. The black shiny appearance of the solid is a promising criterion for further development into functional materials, particularly as photonic nanomaterials. Hence, this study was undertaken to optimize the reaction conditions, thoroughly understand the reaction mechanism, and to deduce the structure of the black solid.

The study was then extended to see the scope of this reaction to other carbonyls and other copper(II) arylcarboxylates. The carbonyls chosen were acetophenone and benzaldehyde to ascertain C-C bond-forming reaction, while the complexes chosen were copper(II) 4-nitrobenzoate, copper(II) 4-hydroxybenzoate and copper(II) 4-chlorobenzoate. The analytical techniques used in this part of the study were CHN elemental analyses, FTIR spectroscopy, UV-vis spectroscopy, NMR (^{1}H- and ^{13}C-), GCMS, magnetic susceptibility, TGA, DSC and cyclic voltammetry.

To summarise, the main objectives of this research were to deduce the structures of selected copper(II) arylcarboxylates, to determine their magnetic, thermal and electrochemical properties, and to understand the mechanism, identify the reaction product, and study the scope of the reaction between copper(II) arylcarboxylates with carbonyls.

Some of the findings from this research were accepted and published in ISI (six articles) and non-ISI journals (one article), and were presented either orally or as posters at three national and five international conferences respectively. These are listed below.

1. Norbani Abdullah, Mohammad Isa Mohamadin, Ng Seik Weng and Edward R.T. Tiekink, "*A three-component co-crystal and a mono crystal isolated from the same crystallisation of a copper(II) carboxylate*" has been accepted for publication in Zeitschrift fuer Kristallographie (Manuscript ID : zkri-D-11-1439R1).
2. Norbani Abdullah and Mohammad Isa Mohamadin, *Mixed-Valence Low Bandgap Photovoltaic Material:*

$[Cu(II)Cu(I)(R)_3(RH)_2L_4].CH_3COCH_3$ $(R = C_6H_5COO;$ $L = CH_3COCH_2C(OH)(CH_3)_2)$, Journal of Advanced Materials Research, 2011 (Manuscript ID : E2763.)

3. M.I. Mohamadin and A. Norbani, *Spectroscopic, Thermal, Magnetic and Electrochemical Studies of Tetrakis-μ-p-fluorobenzoatodicopper(II)*, International Journal of Physical Science, 2011 (Manuscript ID : IJPS-10-306).
4. Mohammad Isa Mohamadin and Norbani Abdullah, *Thermal stability and electrochemical behaviour of Tetrakis-μ-benzoatodicopper(II)*, (2010) Central European Journal of Chemistry, Volume 8, Number 5, 1090-1096.
5. N. Abdullah, M.I. Mohamadin, A.P. Safwan and E.R.T Tiekink, *Aqua(2,2'-bipyridine-*κ^2*N,N')(3,5-dinitrobenzoato-*κO^1*)copper(II) tetrahydrofuran Monosolvate,* Acta Cryst. (2010), E66, m1055–m1056.
6. Mohammad Isa Mohamadin, Norbani Abdullah, Kong Mun Lo and Seik Weng Ng *Aqua(2,2'-bipyridine-*κ^2*N,N')bis(4-iodobenzoato-κO)copper(II)*. Acta Cryst. (2010). E66, page 1530.
7. Norbani Abdullah, Mohammad Isa Mohamadin, Zaimatul‟ Azian, Jia Ti Tee, Lailatun Nazirah Ozair, Ahmad Nazeer Che Mat, Nur Syamimi Ahmad Tajidi, Yasameen Al-Hakem, and Annie Johana Ahmad. *Thermally Stable Low-Dimensional Magnetic* $[MM'(RCOO)_4]$ $(M, M' = Cu(II), Fe(II), Ni(II);$ $R = p\text{-}HOC_6H_4,$ $p\text{-}H_2NC_6H_4,$ $p\text{-}NO_2,$ $CH_3(CH_2)_{14}),$ Bilateral Symposium between University of Malaya and University of Hyderabad, 26-28 October 2010) (oral presentation).

8. Norbani Abdullah, Ahmad Nazeer Che Mat, Mohammad Isa Mohamadin, Ramlah Ngatten, *bis-(p-aminobenzoato)bis(hexadecanoato)dicopper(II): A low-temperature and thermally-stable functional metallomesogen*, UM-HU Bilateral Seminar, 26-28 October 2010, University Malaya. (poster)
9. Mohammad Isa Mohamadin, Norbani Abdullah, *Thermal Stability and Electrochemical Behaviour of Tetrakis-μ-benzoatodicopper(II)*, Program with Professor Deevi Basavaiah, Hyderabad University, 7 June 2010, Jabatan Kimia, University Malaya. (oral paper)
10. Mohammad Isa Mohamadin and Norbani Abdullah, *Structural, Magnetic, Thermal, Electrochemical and Chemical Properties of Copper(II) Benzoate,* Proceedings of the Second International Conference and Workshops on Basic and Applied Sciences and Regional Annual Fundamental Science Seminar 2009, Volume I, pp 24-28.
11. Mohammad Isa Mohamadin and Norbani Abdullah, *Solvent-Dependent Electrochemical Behaviour of Copper(II) Complexes with para-substituted Benzoato Ligand*, 10th Asian Conference on Analytical Sciences and 22nd Malaysian Symposium on Analytical Chemistry (ASIANALYSIS X/SKAM 22) (2009) (oral paper).
12. Mohammad Isa Mohamadin and Norbani Abdullah, *Magnetic, Structural and Thermal Stability Studies of Copper(II) Benzoate and Its Derivatives*, The 2nd Penang International Conference For Young Chemists (Penang ICYC) 2008 (oral paper).

13. Mohammad Isa Mohamadin and Norbani Abdullah, *Potential novel copper complex: a product formed through reaction of* $Cu_2(C_6H_4COO)_4$ *and ketone in acidic condition*, Ninth Tetrahedron Symposium, „Challenges in Organic and Bioorganic Chemistry, 22-25 July 2008, Berkeley , CA , USA (poster).
14. Mohammad Isa Mohamadin and Norbani Abdullah, *Thermal, Spectral and Electrochemical Properties of Copper(II) Benzoate and Its Derivatives*, International Graduates Congress 2007 (3rd MPSGC) 12th – 14th December 2007 (oral paper).

This thesis is divided into five chapters. Chapter 1 introduces the objectives of the research and publications of research findings. Chapter 2 presents the relevant theories and literature reviews on copper(II) carboxylates, analytical techniques used in structural deduction, namely elemental analysis, FTIR and UV-vis spectroscopies, and concepts of magnetic, thermal, electrochemistry (focusing on cyclic voltammetry), and carbon-carbon bond-forming reaction. Chapter 3 presents the experimental part of the research covering the methods used to synthesize the complexes, the C-C bond-forming reactions, and the instrumental techniques used in the analyses. Chapter 4 contains the results and discussions, and Chapter 5 presents the conclusions and suggestions for future works. A list of references is included at the end of each chapter. The appendixes are included at the end of the thesis.

References

[1] M. Melnik, *Coord. Chem. Rev.* 42 (1982) 259.

[2] M.P. Suh, M.Y.Han, J.H. Lee, K.S. Min and C. Hyeon, *J. Am. Chem. Soc.* 120 (1998) 3819.

[3] E.I. Solomon, *Pure Appl. Chem.* 55 (1983) 1069.

[4] V. Mckee, *Adv. Inorg. Chem.* 40 (1993) 323.

[5] B. Waller, J.D. Lipscomb, *Chem. Rev.* 96 (1996) 2625.

[6] Y.H. Chung, H.H. Wei, Y.H. Liu, G.H. Lee and Y. Wang, *Polyhedron* 17, (1988) 449.

[7] L.P. Battaglia, A.B. Corradi, and L. Menabue, *J. Chem. Soc., Dalton Trans*. (1986) 1653.

[8] R.D. Harcourt, F.L. Skrezenek and R.G.A.R. Maclagan, *J. Am. Chem. Soc.* 108 (1986) 5403.

[9] M. Gonzalez-Alvarez, G. Alzuet, J. Borras, B. Macias and A. Castineras, *Inorg. Chem.* 42 (2003) 2992.

[10] M. Kato, H.B. Jonassen, and J.C. Fanning, *Chem. Rev.* 64 (1964) 99.

[11] G. Christou, *Acc. Chem. Res*. 22 (1989) 328.

[12] K. Wieghardt, *Angew. Chem. Int. Ed. Engl.* 28 (1989) 1153.

[13] Y. Akhriff, J. Server-Carrior, A. Sancho, J. Garcia-Lozano, E. Escriva, J.V. Folgado, and L. Soto, *Inorg. Chem.* 38 (1999) 1174.

[14] G.B. Deacon and R.J. Philips, *Coord. Chem. Rev.* 33(1980) 227.

[15] M. Eddaoudi, J. Kim, N. Rosi, D. Vodak, J. Wachter, M.O‛Keeffe, and O.M. Yaghi, *Science* 295 (2002) 469.

[16] Y. Kim and D.-Y. Jung, *Inorg. Chem*. 39 (2000) 1470.

[17] B.N. Figgis and R.L. Martin, *J. Chem. Soc.* (1956) 3837.

[18] Nierkek and Schoening, *Acta Cryst.* 6 (1953) 227.

[19] P.W. Jotham, S.F.A. Kettle, and J.A. Marks, *J. Chem. Soc. Dalton Trans.* (1972) 428.

[20] D.H. Richard, L.S. Frances, and G.M. Robert, *J. Am. Chem. Soc.* 108 (1986) 18.

[21] M. Jerzy, *Coord. Chem. Rev.* 249 (2005) 2534.

[22] L.S. Forster, and C. Ballhausen, *J. Acta. Chem. Scand.* (1962) 16.

[23] D.M.L. Goodgame, N.J. Hill, D.F. Marshall, A.C. Skapski, M.L. Smart, and P.G.H. Troughton, *J. Chem. Soc. Chem. Commun.* (1969) 629.

[24] P.J. Hay, J.C. Thibeault, and R. Hoffman, *J. Am. Chem. Soc.* 97 (1975) 4884.

[25] B. Kozlevcar, I. Leban, M. Petric, S. Petricek, O. Roubeu, J. Reedijk and P. Segedin, *Inorg. Chim. Acta* 357 (2004) 4220.

[26] K. Irie, and K. Watanabe, *Bull. Chem. Soc. Jpn.* 53 (1980) 1366.

[27] M. Sato, K. Okawa, and S. Akabori, *Bull. Chem. Soc. Jpn.* 30 (1957) 937.

[28] U. Schatzschneider, T. Weyhermuller and E. Rentscheler, *Inorg. Chim. Acta*. 337 (2002) 122.

[29] W. Lewandowski, M. Kalinowska and H. Lewandowska, *J. Inorg. Biochem.* 99 (2005) 1407.

[30] S. Takamizawa. E. Nakata and T. Saito, *Inorg. Chem. Comm.* 7 (2004) 1.

[31] J. Lewis and R.C. Thompson, *Nature* (1963) 468.

[32] W. Ference and A. Walkow-Dziewulska, *J. Therm. Anal. Cal.* 61 (2000) 923.

[33] W. Ference and A. Walkow-Dziewulska, *J. Therm. Anal. Cal.* 63 (2001) 865.

[34] W. Ference and A. Walkow-Dziewulska, *J. Therm. Anal. Cal.* 63 (2001) 309.

[35] S. Erre, L. Micera and G. Cariati, *Polyhedron* 6 (1987) 1869.

[36] A. Turek, J. Kobylecka and B. Ptaszynski, *J. Therm. Anal. Cal.* 78 (2004) 523.

[37] W. Harrison, S. Rettig, and J.J. Trotter, *Chem. Soc. Dalton.* (1972) 1852.

[38] T. Kawata, H. Uekusa, and S. Ohba, *Acta. Cryst.* B48 (1992) 253.

[39] W. Ference, A. Walkow-Dziewulska and P. Sadowski, *J. Therm. Anal. Cal.* 82 (2005) 365.

[40] M. Melnik, and M. Dunaj-Jurco, *Inorg. Chim. Acta*. 86 (1984) 185.

[41] C.J. Cairns, and D.H. Busch, *Coord. Chem. Rev.* 69 (1986) 1.

[42] A.J. Atkins, D. Black, A.J. Blake, A. Marin-Bacerra, S. Parsons, L. Ruiz-Ramirez, M. Schroder, *Chem. Commun.* (1996) 457.

[43] P. Guerriero, S. Tamburini, and P.A. Vigato, *Coord. Chem. Rev.* 139 (1995) 17.

[44] W. Harrison, S. Rettig and J. Trotter, *J. Chem. Soc. Dalton,* (1972) 1852.

[45] W.E. Hatfield and R. Whyman, *Transition Metal Chem*. 5 (1969) 47.

[46] F.G. Herring, B. Landa, R.C. Thompson and C.F. Schwerdtfeger, *J. Chem. Com. (A)* (1971) 528.

[47] J. Lewis, F.E. Mabbs, L.K. Royston and W.R. Smail, *J. Chem. Soc. (A)* (1969) 291.

[48] C.S. Fountain and W.E. Hatfield, *Inorg. Chem.* 4 (1965) 1368.

[49] N. Abdullah and M. H. Chisholm, *Role of* $Cu_2(XC_6H_4COO)_4$ *in facile C-C bond-forming reaction of carbonyls,* International Conference on Molecular Chemistry, (2008) 54.

CHAPTER 2

LITERATURE REVIEW

2.1 INTRODUCTION

Structural and magnetics studies of binuclear and polynuclear complexes containing multidentate bridging ligands, in which such metal-metal interaction as magnetic coupling, energy or electron transfer and intervalence transfer may occur, are of considerable interest from the standpoints of inorganic, bio-organic and coordination chemistry [1-3]. Hence, this area of research has become the subject of many studies for many years. In addition, a great interest has also been devoted in the field of structural design and molecular magnetism, especially using polynuclear complexes to synthesize new magnetics materials and to investigate the role of the structural variety in the polymetallic active sites in biological system. One of the most interesting features in molecular magnetism is the ability of some polyatomic ligands to provide pathways for exchange coupling between atoms that are not directly bonded. The study of intramolecular exchange interactions has been extended to large number of dinuclear and polynuclear compounds with a variety of bridging ligands, such as carboxylato, hydroxo, oxalato and pseudohalides of the type XCN (X = O, S, Se). Among the systems, Cu(II) carboxylate have been the subject of numerous magneto-structural investigation, and have been extensively studied from different points of view, due to the unique feature of the carboxylato anions that can exhibit different bonding modes, which ultimately will influence the overall properties of the compounds. Most of them are biologically active substances like metal ion drug [4-6].

2.2 COPPER(II) CARBOXYLATES

Copper(II) carboxylates normally refer to large and diverse group of coordination compounds which are interesting due to their possible application in many areas [7]. Such diversity of properties is often related to the coordinated ligands, although special attention is also devoted to structures of compounds, which may differ significantly. The structure and bond properties of Cu(II) compounds are also of continuous interest for many researchers, especially those with N donors ligands as well as with some carboxylic acid and their derivatives which also play an important role in biological processes [8-10], and have been a subject of numerous investigation [11,12]. The ability of carboxylate groups to have a different coordination mode to a metal lead to the formation mononuclear and polynuclear structures [13,14]. In recent years, great attention has been given to magneto-structural studies of complexes of Cu(II) with carboxylate bridges which act as a superexchange pathways [15,16]. Magnetically, dinuclear(II) carboxylates differ from other polymeric and monomeric copper(II) complexes by their lower magnetic moment. It is also important to note that low molecular weight coordination compounds like Cu(II) carboxylates are often used to study correlations between structure, magnetism and spectroscopy [17,18].

Historically copper(II) carboxylates, especially the dimeric structures of the compounds, have captivated the interest of chemists for over seven decades. This fact is evidenced by the numerous review articles focusing on the magnetic, electronic and structural properties of these compounds [11, 19-22]. Using structural criteria, these binuclear copper(II) complexes can be classified into two distinct groups. In the first group, the copper(II) ions are connected by monoatomic bridges (**Figure 2.1)**.

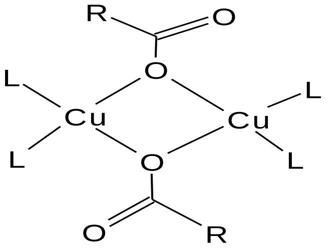

Figure 2.1: Monoatomic bridging coordination mode of $RCOO^-$ ion to copper(II) ions

The second group, which continue to receive great attention, is illustrated using the copper(II) acetate monohydrate structure. The structure contains four three-atom-carboxylate bridges between two copper(II) ions, forming a paddle-wheel structure (**Figure 2.2**).

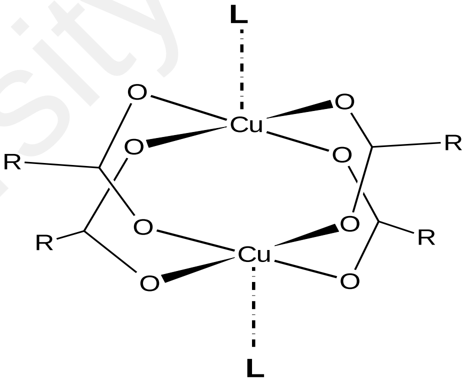

Figure 2.2 Paddle-wheel structure of copper(II) carboxylate

The largest subgroup in the dinuclear family of compounds is isolated dinuclear compounds, where there are additional ligands coordinated at the apical positions of the central dicopper tetracarboxylate core. Inter-dinuclear connection is also possible via H-bonding or weaker association. Also, a small group of polymeric dimers is also known to exist, where direct Cu-O (carboxylate) coordination bonds enable an infinite chain of the dinuclear units (**Figure 2.3)** [23-27].

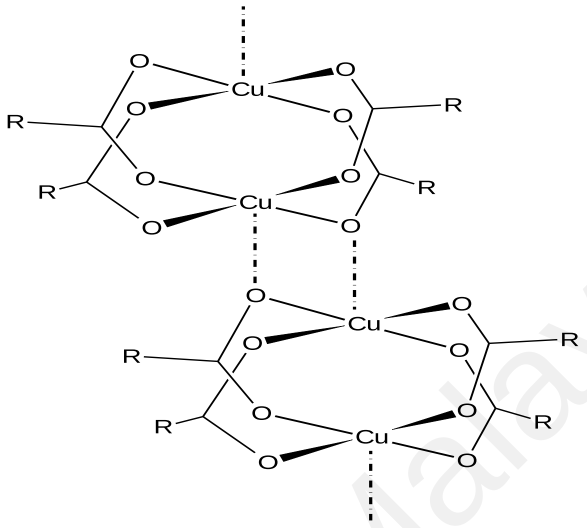

Figure 2.3: Structural type in polymeric dinuclear copper(II) complexes

In general, the carboxylate moiety in copper(II) complex can bond to the central metal ion via three different configurations [28] (**Figure 2.4)**.

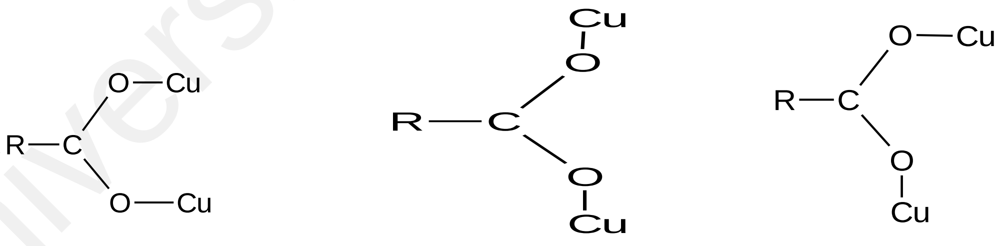

(a) (b) (c)

Figure 2.4: Carboxylate bonding configurations: (a) *syn-syn*; (b) *anti-anti*; (c) *syn-anti*

The different coordination bonding mode of the carboxylate has led to significant structural and physical differences, especially in the magnetic properties of copper(II) complexes.

2.2.1 Structural Study

The structural study of copper(II) carboxylates is very imperative and has always gone hand-in-hand with the study of their magnetic properties. For one-atom acetate bridges between two paramagnetic transition metals centers, the magnetic interaction has been related to the magnitude of the bridging angle and other structural feature [29]. This has been especially studied for oxygen-bridged metal atom, such as Cu-O-Cu. It was discovered that small bridging angles of about 96^o leads to a ferromagnetic interaction, while larger values make the interaction increasingly strongly antiferromagnetic [30,31].

The magneto-structural correlation in copper(II) compounds stands out due to the different coordination mode of the carboxylate groups. From the magnetic point of view, the range of magnetic behaviour as a function of different coordination mode was pointed out, from strongly coupled to moderate or weak antiferromagnetic compounds and even ferromagnetic ones. For copper(II) complexes, three possible possibilities can be observed: (a) the *syn-syn* conformation of carboxylate bridge mediates strong antiferromagnetic interaction, (b) the *syn-anti* conformation mediates weak antiferromagnetic or ferromagnetic interaction [32], and (c) the *anti-anti* conformation mediates weak to moderate antiferromagnetic interaction [33-35].

The *syn-syn* conformation in copper(II) carboxylates is always desirable, but due to the close proximity of copper ions in the binuclear structure, this structure will be unstable and the *anti-anti* and *anti-syn* conformations are favoured if a large residual charge remains on the copper ions after bonding with the carboxylate groups [36]. The acid dissociation constant, pK_a of the parent organic acids are taken as an indication of the available sigma (σ) electron density on the carboxylate oxygen atom. Stronger acids than acetic acid form carboxylate ligands which are less polarisable than the acetate group, and this have less available σ electron density on the carboxylate oxygens. This leaves greater residual charge on the copper ions, and thus favours the *anti-anti* or *anti-sy*n arrangements, such as found in the formates. In addition, the higher effective charge on copper(II) centre will contract the *d* orbitals, which may modify considerably the overlap in the metal-metal bond, and significantly affect the stability of the dimeric unit.

2.2.2 Copper(II) Alkylcarboxylates

It is quite safe to state that the early interest on copper(II) carboxylates stems from unique findings on structural features of copper(II) acetate, $Cu(O_2CCH_3)_2$, which was originally driven by the lower value of its magnetic moment. Through the work of van Nierkerk et al. [37], the structure of $Cu(O_2CCH_3)_2$ was solved. The structure (**Figure 2.5**), famously known as paddle-wheel structure, consists of four bidentate acetate, bridging in the *syn-syn* fashion, to two copper(II) centres forming a centrosymmetric dimeric unit. The Cu-Cu distance of ~2.615 Å is the most striking feature when compared to that found in metallic copper (2.56 Å). The copper atoms are displaced by 0.22 Å out of plane of the oxygen atoms away from the neighboring copper. The O-C-O and Cu-O-C angles were 124.9^o and 122.8^o respectively. Each dimer interacts with four adjacent neighbours via eight intermolecular hydrogen bonds.

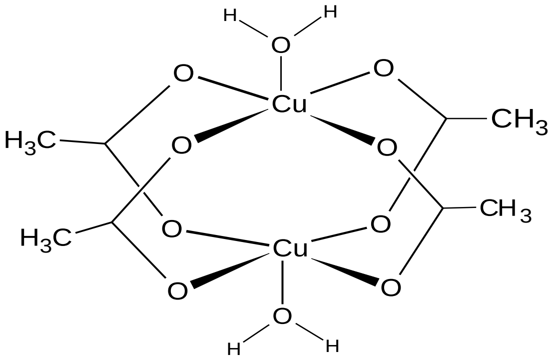

Figure 2.5: Structure of $[Cu_2(O_2CCH_3)_4(H_2O)_2]$

Since the discovery of the dimeric paddle-wheel structure for copper(II) acetate, many more studies on the structural aspect of similar complexes were intensively pursued, focusing mostly on the dimeric complexes, as depicted in **Table 2.1**. In addition, an orthorhombic and monoclinic form of copper(II) acetate with pyridine adduct have also been identified [38,39]. The orthorhombic structure possesses a center of symmetry while the monoclinic form has an arrangement of dimeric units which creates twofold rotation axis through copper ions and pyridine. This form also has a slightly shorter Cu–Cu and Cu–N distances, as well as having the planes of the pyridine rings inclined to each other at 60^o.

The occurrence of mononuclear copper(II) complexes has also been studied. Ahmed and Abu Hijleh [40] reported an investigation on copper(II) acetate complexes with pyridine, α–picoline and γ–picoline as axial ligands. They isolated and characterized not only the usual 1:1 dimers, but also a bis-adduct, $[Cu(O_2CMe)_2.2L]$ (**Figure 2.6**) These 1:2 adducts are presumed monomeric on the basis of their electronic and ESR spectra as well as their room-temperature magnetic moment. The electronic spectra of these compounds consists of one broad asymmetric band at 650 nm (ε = 65) and 658 nm (ε = 84) for the pyridine and γ–picoline adducts respectively, with no evidence of the characteristic 370 nm band found in mono-adducts. The effective magnetic moments, calculated from powdered and solution samples, are temperature independent in the range of 263 – 310 K. Powdered sample of the pyridine-containing compound yielded a room-temperature moment of 1.85 B.M., while the sample in solution yield a slightly higher value of 1.93 B.M. They concluded that the tendency of copper(II) acetate for forming dimeric complexes is attrituble to the requirement of the axial ligands requiring specific orientations which minimize steric repulsion with neighbouring groups.

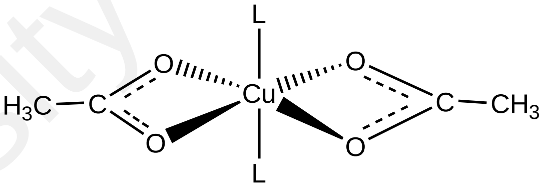

Figure 2.6: Structure of [Cu($CH_3COO)_2L_2$] where L = pyridine, α–picoline or γ–picoline

Another structural studies on copper(II) acetate by Koo [41] also showed a mononuclear complex. The complex, [Cu($CH_3COO)_2$(2,2'-bpy)], was obtained by adding 2,2'-bipyridine to [Cu($CH_3COO)_2$].H_2O in dimethylformamide (DMF). The structure (**Figure 2.7**) reveals that the complex was square planar with CH_3COO^- and 2,2'-bipyridine as monodentate and chelating bidentate ligand, respectively.

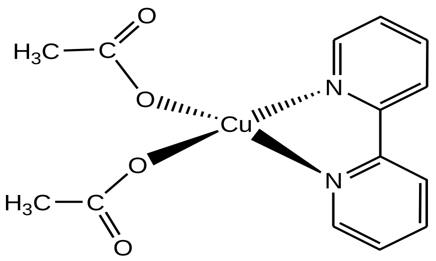

Figure 2.7: The structure of [Cu(CH_3COO)$_2$(2,2'-bpy)]

Table 2.1: Structural data for binuclear copper(II) alkylcarboxylates

Compound	Cu-Cu (Å)	Cu-O (basal) (Å)	Cu-L (apical) (Å)	O-C (Å)	Cu-basal plane (Å)	Cu-O-C (deg.)	O-C-O (deg.)
$Cu(CH_3(CH_2)_2COO)_2$	2.565	1.982	O 2.245	1.243	0.19	123.8	123.3
$Cu(CH_3COO)_2C_4H_4N_2$	2.576	1.964	N 2.167	1.259	0.28	122.5	124.8
$Cu(C_2H_5COO)_2$	2.578	1.94	O 2.28	1.28	0.22	130	113
$Cu(CH_3COO)_2.CH_3OH$	2.597	1.961	O 2.159	1.26			
$Cu(CH_3COO)_2.H_2O$	2.614	1.969	O 2.161	1.259	0.19	123.0	124.9
$Cu(CH_3COO)_2CH_4N_2O.H_2O$	2.637	2.00	O 2.09	1.25			119.9
$Cu(C_2H_5COO)_2C_5H_5N$	2.642	1.96	N 2.17	1.26			125
$Cu(C_2H_5COO)_22C_6H_7N$	2.647	1.97	N 2.21	1.24		126	
$Cu(ClCH_2COO)_23C_6H_7N$	2.685	1.974	N 2.269	1.235	0.228	122.7	127.8
$Cu(Cl_3CCOO)_2$ $2C_5H_4ClN$	2.766	1.957	N 2.145	1.229	0.28	123.8	128.4
$Cu(F_3CCOO)_2C_9H_7N$	2.886	1.972	N 2.107	1.242	0.32	124.9	129.0

2.2.3 Copper(II) Arylcarboxylates

The structural and magnetics properties of copper(II) acetate and other copper alkylcarboxylates have been the subject of many investigation. However, relatively, little attention has been paid to the binuclear copper(II) arylcarboxylates and thus progresses relatively at a slower phase. Earlier work on such compounds might be by Ploquin [42], who reported the results of his magnetic investigations on copper salts of several aliphatic and aromatic carboxylic acids. Since then, the structures of copper(II) arylcarboxylates, such as copper(II) benzoate, $Cu(C_6H_5COO)_2$, have always been deduced from the value of magnetic moment, and compared to that of copper(II) acetate.

In the early studies of copper(II) arylcarboxylates, the magnetic moment of copper(II) salicylate tetrahydrate, $Cu(2\text{-}HOC_6H_4CO_2)_2.4H_2O$ has been determined to be 1.44 B.M. [42,43]. This subnormal reading apparently contradicts the result of a complete X-ray crystal analysis carried out by Hanic and Michalov [44]. Their studies has shown that planar centrosymmetric molecules of $[Cu(2\text{-}HOC_6H_4CO_2)_2].2H_2O$ were linked in the structure by a system of hydrogen bonds in which two remaining water molecules also took part. The shortest Cu-Cu distance in the structure is 3.728 Å and there are no pairs of copper atoms of close distance of approach in the crystals. The magnetic moment of this compound has been determined to be 1.92 B.M., indicating the presence of separate rather than paired Cu atoms. The difference in the magnetic moments in these two similar compounds was explained by Inoue et al. [45] to be due to the existence of magnetically different crystal modification of the compound, based on their preparation method. Inoue et al. has successfully prepared several modification of copper(II) salicylate tetrahydrate which show different magnetic moment.

Inoue et al. [45] has also succeeded in synthesizing copper(II) compound with benzoate ligand but having a normal magnetic moment of 1.87 B.M. The X-ray crystal analysis on a single crystal of the compound showed the Cu-Cu distance of 3.15 Å, and they are bridged by two oxygen atoms and one Cu-O-C-O-Cu link to form a linear chain (**Figure 2.8**). This is basically the first instance of crystalline Cu(II) compounds ever reported to have a short Cu-Cu distance and a normal magnetic moment at room temperature. This situation can be explained through three reasoning, based on their structural feature: (a) copper atoms are linked to form a one-dimensional chain structure instead of forming separate pairs of copper atoms as in copper(II) acetate monohydrate or acetylacetonemono(o-hydroxyanil)copper(II), (b) neighboring copper atoms are bridged by two oxygen atoms, each bonded to an aromatic ring as in the tricoordinated copper(II) complex, and (c) the two copper atoms and two bridging oxygen atoms do not lie on a single plane, instead they are coplanar in the tricoordinated copper(II) complex.

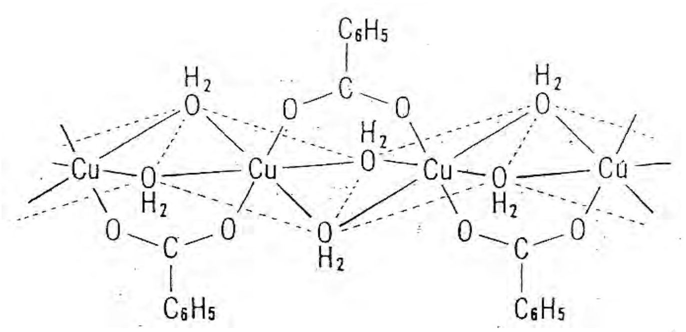

Figure 2.8: Structure of polymeric copper(II) benzoate trihydrate

The anhydrous Cu(II) benzoate has also been shown to have a varied magnetic moments, depending on their method of preparation. Three different modifications were obtained: a normal moment for α modification, and a subnormal moment for β and γ modifications [45]. A series of adducts of copper(II) benzoate with different axial ligands, namely benzoic acid, ethanol and urea, also give subnormal magnetic moments.

Many works have then taken off to further explore the dimeric paddle-wheel structure and its correlation with the magnetic moment in copper(II) arylcarboxylate, especially copper(II) benzoate and its derivatives. Fountain et al. [46] showed that the structural properties of copper(II) benzoate depended not only on the method of preparation, but also on the history of the sample itself. The anhydrous copper(II) benzoate and anhydrous copper(II) *p*-methylbenzoate, Cu(*p*-$CH_3C_6H_4COO)_2$, were easily prepared by heating hydrated copper(II) benzoate and ethanol adducts of copper(II) *p*-methylbenzoate respectively at different temperature. As with copper(II) alkylcarboxylate, the magnetic moment of copper(II) benzoate prepared is temperature dependent, but the value was different from each sample depending on their method of preparation. The prepared Cu(II) compounds showed subnormal magnetic moments at room temperature, and from this, their structures were concluded to be similar to that of copper(II) acetate.

Similarly, Hatfield et al. [47] has also studied the structural-magneto correlation on a series of copper(II) salts of substituted benzoic acids. The copper(II) benzoates under studies were claimed to have the dimeric structure owing to the similarity of the spectral and magnetic properties with those of copper(II) acetate monohydrate and other copper(II) alkanoates. The reflectance spectra of all compounds exhibit a well defined band at ca. 700 nm and a shoulder at ca. 350 – 400 nm, the latter being claimed as a characteristic of binuclear copper(II) carboxylates.

However, the conclusion made for dimeric, paddle-wheel structure based on the value of the magnetic moment must be taken cautiously. Structurally, there is no simple correlation between the structural parameters, in particular the Cu-Cu, Cu-O and Cu-O-C-O-Cu distances, and the magnetic properties of copper(II) carboxylate. The magnitude of the magnetic exchange interaction is highly dependent on the identity of the parent acid and the adduct, in cases where one is present. Melnik [11] in his review has focused on the relationship between structural information and the magnetic properties of binuclear copper(II) carboxylates. Although the value of -2J is insensitive to the Cu-Cu distance, it is affected by the nature of the apical ligand, the distance Cu-O-C-O-Cu bridge and the associated bridging angle. A decrease in the value of -2J is accompanied by an elongation of the bridge and concurrent contraction of the bridging angle [11].

The occurrence of dinuclear complexes and the degree of magnetic interaction between the copper atoms are governed by a few factors, as were noted in some articles [48-51]. In the arylcarboxylates, the steric effect predominates, whereby a bulky substituent can result in the formation of dinuclear complexes. When there is no steric effects, reduction of the charge on copper ions is important. High ζ electron density on the carboxylate oxygen atoms (as measured by the pK_a value of the parent acid) and adducts which lower the residual charge on the copper ions make the formation of dinuclear complexes favourable. It was proposed in the early study that the pK_a value can influence the facile formation of dinuclear complexes; a high pK_a value favours the formation of a dinuclear complex as greater electron polarizability can take place. This effect is attributed to further reducing of the positive charge on the copper ions, which reduces any repulsions between them and allow the metal orbitals to expand giving better overlap [51]. However, the conclusion on the effect of pK_a value on complex structure was solely made based on the magnetic studies [49,50]. It was later found that the magnetic properties of dinuclear complexes depend very much on the electronic structure of the OCO moiety, which is directly related to the effect of the axial ligand instead [52-54]. In addition, the work of Hatfield et al. on copper(II) complexes with substituted benzoic acid also seems to show no apparent correlation between pK_a and magnetic properties [47].

Even though the chemistry of copper(II) arylcarboxylates was extensively studied, it was not until the early 70s that the crystal structures of these complexes were known. One of the earliest compounds studied was dimeric copper(II) aspirinate, $Cu(o\text{-}C_2H_3O_2C_6H_5CO_2)_2$, which has the Cu-Cu bond distance of 2.621(8) Å [55]. In addition to that, Harrison et al. [56] also reported the crystal structure of copper(II) *ortho*-bromobenzoate, $[Cu(o\text{-}BrC_6H_4CO_2)_2(H_2O)]_2$. The structure, which showed a centrosymmetric dinuclear unit with four bidentate *ortho*-bromobenzoate anions forming a *syn-syn* bridges between the two copper atoms separated by 2.624(7) Å, agreed well with Cu-Cu distance in copper(II) aspirinate as well as to that of copper(II) acetate. The coordination about the copper atoms is square pyramidal and five of its nearest neighbours are oxygen atoms, four of these being from the carboxylate anions, and the fifth from water molecules [57].

Another crystal structural work on copper(II) benzoate by Melnik et al. [57] also showed a dimeric structure, with a square pyramidal geometry at each copper center. The Cu-Cu distance was 2.627(3) Å, and they were bridged by four carboxylate groups with DMSO as the apical ligand. However, the IR and electronic spectra of the complex were different for carboxylate stretching frequencies and λ_{max} for the *d-d* band respectively when compared to those found for DMSO adducts of copper(II) benzoate studied by other authors. The differences were postulated to be due to the different method of preparation and possibilities that the compounds were isomeric.

A few other copper(II) benzoate with different apical ligands, as shown in **Table 2.2**, have also been the subject of investigation [57]. It could be seen from the table that the axial ligand plays a role in determining the Cu-Cu distance. There were differences between the chromophore CuO_5 and CuO_4N respectively. For instance, the sum of all interatomic distances in CuO_5 and CuO_4N is approximately 11.33 Å and 11.42 Å, respectively. Also, the Cu-O (basal) distances are somewhat longer in the CuO_4N chromophore (1.97 Å) than in the CuO_5 chromophore (1.96 Å). The values are the same as those reported for copper(II) compounds containing binuclear units of this type [10]. Some variation also exists in the Cu-L (apical) distances, but this is as expected.

Table 2.2: Structural data for binuclear copper(II) benzoates

Compound	Cu-Cu (Å)	Cu-O (basal) (Å)	Cu-L (apical) (Å)	O-C (Å)	Cu-O-C (deg.)	O-C-O (deg.)
$Cu(C_6H_5COO)_2(C_4H_8O_2)_{2..5}$	2.593(3)	1.963(8)	2.178(9)	1.25(1)		124.7(8)
$Cu(C_6H_5COO)_2(CH_3OH)_2$	2.606(3)	1.95(2)	2.24(1)	1.26		125(2)
$Cu(C_6H_5COO)_2C_{10}H_9N$	2.671(2)	1.969(9)	2.186(8)			
$Cu(C_6H_5COO)_2C_5H_5N$	2.681(1)	1.978(5)	2.184(7)	1.271(4)	122.8(5)	125.0(7)

Strinna and co-workers [58] described the structure of copper(II) 2,6-dimethoxybenzoate. The compounds crystallized in the orthorhombic space group, and have a normal centrosymmetric dinuclear unit with four bidentate carboxylate anions forming bridges between the copper atoms. The coordination around the Cu atom is square pyramidal and Cu…Cu distance of 2.619 (1) Å with water as axial ligands. The complexes which was prepared by reacting copper(II) nitrate with 2,6-dimethoxybenzoic acid in an acidic solution exhibits anticipated exchange integral, -2J of 325 cm^{-1}, a value comparable to other dimeric copper(II) arylcarboxylate. The molecular framework of copper(II) carboxylates as a whole seem to be rather flexible and can undergo small rearrangements in response to the bonding requirements of the carboxylate ligands or packing factors.

2.3 SPECTROSCOPIC STUDIES OF COPPER CARBOXYLATES

2.3.1 Fourier Transform Infrared Spectroscopy

Fourier Transform Infrared Spectroscopy (FTIR) involves the absorption of electromagnetic radiation in the infrared region of the spectrum which results in changes in the vibrational energy of molecules. Since, usually all molecules will be having vibration (stretching and bending), the absorbed energy will be utilized in changing the energy levels associated with these. The spectrum may be recorded for organic and inorganic samples, if they can absorb light energy with the frequency in the IR region at 4000-400 cm^{-1} [59].

In a molecule, the atoms are not held rigidly apart. Instead they can move, as if they are attached by a spring of equilibrium separation. This bond can either bend or stretch. If the bond is subjected to infrared radiation of specific frequency (between 300 – 4000 cm^{-1}), it will absorb the energy, and the bond will move from the lowest vibrational state, to the next highest. In a simple diatomic molecule, there is only one direction of vibrating namely stretching. This means there is only one band of infra red absorption. If there are more atoms, there will be more bonds, and therefore more modes of vibrations. This will produce a more complicated spectrum.

However, there is one important limitation. A molecule will only absorb radiation if the vibration is accompanied by a change in its dipole moment. A dipole will occur when there is a difference of charge across a bond. If the two oppositely charged molecules get closer or further apart as the bond bends or stretches, the moment will change. Hooke's law [60] is used to calculate the frequency of light absorbed.

$$\nu_m = \frac{1}{2\pi}\sqrt{\kappa\frac{m_1+m_2}{m_1 m_2}}$$

where k is the force constant indicating the strength of the bond, and m_1 and m_2 are the two masses of the two atoms. This equation indicates that if there is a high value of k (strong bond), it will absorb at high frequency of light as well. Hence, a C=C double bond would absorb a higher frequency of light than C-C single bond. Also, the larger the two masses, the lower the frequency of light absorbed.

In the absence of crystal structure, infrared spectroscopy is invaluable as it can be used to infer the relationship between carboxylate coordination and carbon-oxygen stretching frequencies. In fact, such relationship has provided a topic for discussion in many papers and review articles [61-65]. Vibrational spectra often yield useful information about structure and symmetry within complexes. This is due impart to the usual reduction in symmetry which accompanies coordination of a ligand to a metal. A spectrum may also exhibit a splitting of vibrations arising from degenerate infrared vibrations in the free ligand.

As stated earlier, there are four possible modes of coordination for the bridging carboxylate moiety with metals, *syn-syn*, *anti-anti*, *anti-syn* and monoatomic. Considerable differences are lacking in the infrared spectrum, however, owing to the low symmetry of the free carboxylate ion (C_{2v}). The infrared technique has been used for the recognition of unidentate carboxylate coordination as well as the identification of complexes containing bridging bidentate ligands. The separation (Δ) between ν_{as}(COO) and ν_{s} (COO) for unidentate carboxylates is greater than that found in ionic compounds (164-171 cm^{-1}) [66]. Bridging and/or chelating ligands often exhibit Δ values less than the ionic counterparts. For example, the acetato complexes having chelating and/or bridging carboxylates groups have been shown to have the Δ values of less than 150 cm^{-1}. The shifts are the result of the elimination of the nodal plane of the COO^- (asymmetric) band in the excited state, thus, placing electron density about the carbon for interaction with the bonded groups. The symmetric band remains constant for it is nodal at the carbonyl groups. A sharp asymmetric stretch is observed between 1605 and 1590 cm^{-1} for copper(II) carboxylates. This vibration was once considered characteristic of binuclear structures. It is currently recognized that considerable variation exists for the asymmetric stretch when the metal ions were changed. The asymmetric frequency remains generally consistent with the free ion value. **Table 2.3** shows the IR absorption of asymmetric and symmetric stretching vibration of some copper(II) carboxylates.

Table 2.3: Infrared spectral data (in cm^{-1}) for copper(II) and sodium carboxylates

Compound	**ν_{as}(COO)**	**ν_s (COO)**	**Δ**	**Ref**
Copper(II) acetate	1590	1441	149	67
Copper(II) acetate monohydrate	1602	1441	161	67
Copper(II) acetate monourea	1595	1440	155	68
Copper(MCPA)$_2$[1]	1638	1448	190	69
Copper(II) *o*-aminobenzoate[2]	1551	1384	167	70
Copper(II) *m*-aminobenzoate[2]	1572	1406	166	70
Copper(II) *p*-aminobenzoate[2]	1580	1385	195	70
Cu(dicamba)$_2$.2H$_2$O[3]	1541	1406	135	71
Copper(II) 3,5-dimethoxybenzoate[4]	1581	1392 1428	189 153	72
Copper(II) suprofen hydrated[5]	1603	1411	192	73
CH_3COONa	1578	1414	164	74
CF_3COONa	1680	1457	223	43
NaMCPA	1608	1446	162	70
Na(dicamba)	1603	1404	199	71

MCPA = 4-chloro-2-methylphenoxyacetic acid; Dicamba = 3,6-dichloro-2-methoxybenzoic acid; suprofen = α-methyl-4-(2-thienyl-carbonyl)phenylacetic acid; [1]bidentate bridging unsymmetrical; [2]possibly monodentate with both O and N coordinatively bonded to Cu; [3]bidentate, symmetric chelating; [4]bidentate, bridging and chelating; [5]Bridging, bidentate structure.

2.3.2 UV-visible Spectroscopy

The UV-vis spectroscopy involves the absorption of electromagnetic radiation by subtances in the visible and ultraviolet regions of the spectrum. This will result in changes in the electronic structure of ions and molecules (UV: 200-400 nm; visible: 400-800 nm). The technique deals very much with electronic transitions, from lower to higher energy levels. The excitations of electron(s) can occur between a bonding or lone pair orbital and an unoccupied non-bonding or antibonding orbital. The electronic energy levels and electronic transitions are shown in **Figure 2.9**.

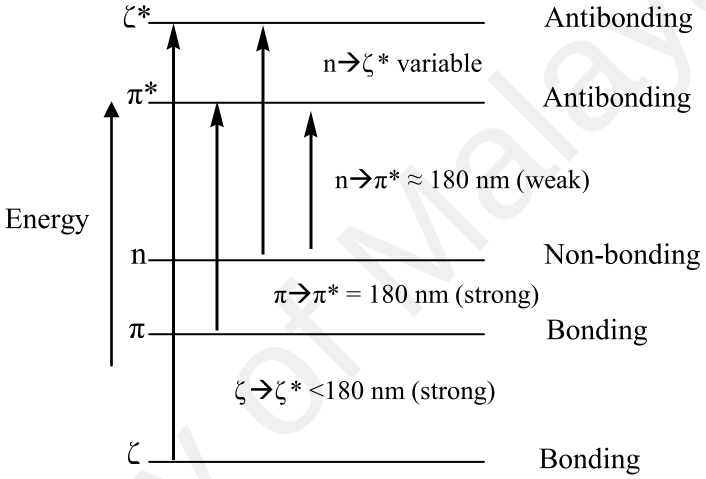

Figure 2.9: Electronic energy levels and electronic transitions

The electronic transitions of transition metal compounds can be categorized into three types: charge transfer, *d–d* spin–allowed, and *d–d* spin–forbidden. Charge transfer bands occur when the excited electron moves from a metal centered orbital to a ligand–centered orbital (metal-to-ligand charge transfer, MLCT) or when the excited electron moves from a ligand-centered orbital to a metal centered orbital (ligand-to-metal charge transfer, LMCT). MLCT bands are more common than LMCT. Spin–allowed and spin–forbidden d–d transitions find the excited electron moving from one d orbital to another d orbital. In the spin–allowed transition, the spin quantum number (or more accurately, the spin angular momentum) in the ground and excited states are the same while in the spin–forbidden transition, the spin state changes during the excitation. These three types of transitions are distinguished by the molar absorption coefficient (ε in the Beer–Lambert law: A = εcl): charge transfer bands have large ε, generally in the range of 1000 to 10000 L mol^{-1} cm^{-1}; spin–allowed *d–d* transition have ε values of 10–100 L mol^{-1} cm^{-1} for octahedral complexes and 500–1000 L mol^{-1} cm^{-1} for tetrahedral complexes; and spin–forbidden bands have ε values less than 5 L mol^{-1} cm^{-1}. Spin–forbidden bands are often not observed.

The first row transition metals are characterized by their ability to form a wide range of coordination complexes in which the octahedral, tetrahedral and square planar geometries predominate. The copper(II) ion is a typical transition metal ion with respect to its formation of coordination complexes, but less typical in its reluctance to form regular octahedral or tetrahedral. The $3d^9$ valence electron configuration of the copper(II) ions lacks cubic symmetry, and hence yields distorted forms of these basic geometries [75]. The coordination numbers of four, five and six are found, but variations of each structure occur through bond length or bond angle distortions due to the Jahn-Teller effect. This phenomenon occurs when the orbital state on a non-linear molecule is degenerate. To relieve this unfavourable condition, the molecular framework will suffer a spontaneous distortion until the Cu(II) ion assumes a ligand field of lower symmetry, and consequently lower energy [76]. This can occur when the molecule is in the ground states or in the excited states. For example, consider the tetragonal distortion of Cu(II) in an octahedral field by elongation of two axial bonds (**Figure 2.10**).

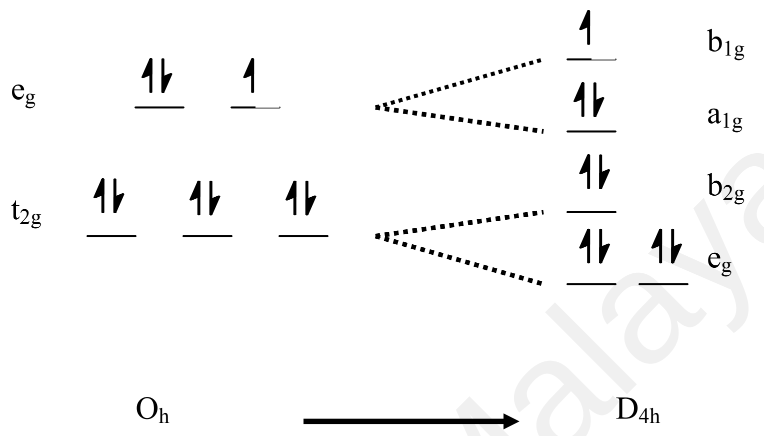

Figure 2.10: Tetragonal Jahn-Teller distortion to relieve degeneracy and reduce the overall energy of the system

The doubly-degenerate (e_g) orbitals split into the b_{1g} and a_{1g} orbitals and the triply degenerate (t_{2g}) orbitals split into the b_{2g} and the doubly degenerate e_g orbitals. Since two electrons are in the stabilized a_{1g} orbitals and only one is in the destabilized b_{1g} orbital, the molecule as a whole is stabilized. For most Cu(II) system, the Jahn-Teller stabilization processs will generally result in the elongation of compression of the two axial bonds with respect to the octahedral structure. The process pictured in **Figure 2.10** is for elongation. Generally, the two orbitals of higher energy in the e_g degenerate octahedral state are the $d_{x^2-y^2}$.

Electronic spectra of dimeric copper(II) carboxyates, both in solution and as single crystals, have been the subject of numerous studies [43,77-79]. Dimeric copper(II) compounds exhibit three bands: Band I at about 699 nm, Band II at about 370 nm, and Band III at about 303 nm. In some instances, Gaussian analysis of Band I has allowed resolution of a second band at about 900 nm, labeled as Band Ia.

The assignment of these bands has been discussed for quite some time [80]. Band I was assigned as *d-d* transition of copper(II) corresponding to $d_{xz,\ yz} \rightarrow d_{x^2-y^2}$; Band Ia for $d_{xy} \rightarrow d_{x^2-y^2}$. If Band II is considered a *d-d* transition, it could be assigned as a $d_{z^2} \rightarrow d_{x^2-y^2}$. However, if it is not a *d-d* transition, then Band Ia may be regarded as $d_{z^2} \rightarrow d_{x^2-y^2}$ transition.

The most studied of the three bands is Band II, which usually appears as a shoulder on Band III. Originally, Band II was thought to be indicative of a copper– copper interaction, and as such characteristic of copper(II) dimeric complexes. A correlation between the magnetic moment and the presence of Band II was recognized by Kato et al. [43]. It was shown that Band II was present for copper(II) complexes having subnormal magnetic moments (< 1.73 B.M.) and this band was absent when complexes exhibited normal magnetic moments. This idea was somewhat abandoned when some known monomeric copper(II) compounds were found to possess an absorption in this region [81-82].

Dubicki and Martin [83] favored a charge transfer assignment for Band II. This is based on their observation that this band shifts to lower energy with variation of the axial ligand, specifically when changing to a more electron withdrawing ligand. Charge transfer is also favored by the observation that chlorine substitution of methyl groups on acetate bridges results in bathochromic shift of Band I as the ligand field strength decreases, while a hypsochromic shift is observed for Band II.

A ligand-to-metal charge transfer (LMCT) assignment has been made for the very intense Band III [77] as the absorptivity coefficient (ε) for this band are of the order of $10^3 – 10^4$ L mol^{-1} cm^{-1}.

The electronic properties of mononuclear copper(II) complexes and their relationship to the stereochemistry have been reviewed by Hathaway and Biling [82]. Electronic spectra are available for solution, solid (diffuse reflectance) and single crystal samples. Solution samples yield accurate ε data while single crystals provide polarization data capable of allowing absolute assignment of spectral bands to energy levels. Above 300 nm, four types of transitions may be observed: ligand combination and overtone vibrations, intraligand transitions, charge-transfer and pure *d-d* transitions. For copper(II) complexes, charge-transfer and intraligand transitions are observed below 500 nm while pure *d-d* as well as the combinations and overtone transitions occur above this wavelength. Relative to *d-d* spectra, the combination and overtone spectra tend to be sharp and easily distinguished.

Hathaway and Billing [82] concluded that the electronic spectra support the following conclusions for copper(II) complexes. Firstly, the sequence of one-electron orbitals for a given stereochemistry remains constant with differing ligand effects reflected in the ligand contribution to the value of crystal field parameter, Δ_o. Secondly, electronic spectra substantiate a correlation diagram relating the energy levels for the CuO_x and CuN_x chromophores. They noted that spectra are in general more sensitive to variations in bond lengths rather than bond angles. Thirdly, the concept of varying tetragonal distortion, established from crystallographic bond length data, is supported substantially by the correlation between the tetragonality (T) and the energy of the $d_{z^2} \rightarrow d_{x^2-y^2}$ transition. Fourthly, a significant lowering of the $d_{z^2} \rightarrow d_{x^2-y^2}$ or d_{xy} transition can be expected if chelation occurs such that the extent of compression or elongation is restricted. Conversely, compounds showing chelation with no concurrent changes in bond length or bond angles exhibit minimal changes in the electronic spectra. Fifthly, there is no spectral evidence for copper(II) complexes possessing an orbitally-degenerate ground state. Examples of d_{z^2}, $d_{x^2-y^2}$ and d_{xy} have all been observed. Electronic spectra cannot be used to distinguish between the possibility of d_{z^2} and $d_{x^2-y^2}$ ground state for the same symmetry. Finally, electronic spectra are insensitive to the presence or absence of a center of symmetry. Variation in intensity is apparently a function of the ligand atoms rather than a center of symmetry. This is supported by the observation that complexes with nitrogen-donor ligands have more intense colours than the oxygen-donor analogues. Lower energy CT bands in the oxygen-donor ligands could account for this [83].

2.4 SELECTED PROPERTIES OF COPPER(II) CARBOXYLATES

2.4.1 Magnetism

Magnetism is a property characteristic of all materials that contain electrically charged particles. A moving electrical charge (i.e. electric current) gives rise to a magnetic field in a material. In an atom, the magnetic field is due to the coupled orbital and spin magnetic moments associated with the motion of electrons. The orbital magnetic moment is due to the motion of electrons around the nucleus whereas the spin magnetic moment is due to the precession of the electrons about their own axes. The resultant of the orbital and spin magnetic moments of the constituent atoms of a material gives rise to the observed magnetic properties. Knowledge about the magnetic properties of materials is an important aspect in the study and characterization of substances.

Often magnetic properties of materials are studied by applying a magnetic field and measuring the induced magnetization in these materials. The magnetic induction, B, that a substance experiences when placed in an applied external magnetic field, H, is given by the expression:

$$B = H + 4\pi M \quad (1)$$

where M is the magnetic moment of the compound per unit volume or the magnetization.

The two most important responses observed are characterized as diamagnetic and paramagnetic moment [84]. As shown in this **Figure 2.11**, the applied magnetic field remains unaffected in a vacuum but is attracted by a paramagnetic, and repelled by a ideal diamagnetic media.

In diamagnetic materials , all the electrons in the atoms are paired and the resultant magnetic moment is zero due to the absence of unpaired electrons. The external magnetic field induces a current whose associated magnetic field is directed opposite to the applied field. The induced magnetic moment associated with this field is called a diamagnetic moment and is negative relative to the applied magnetic field and independent of temperature. The magnitude of the diamagnetic susceptibility is usually small, in the range of 10^{-6} c.g.s units.

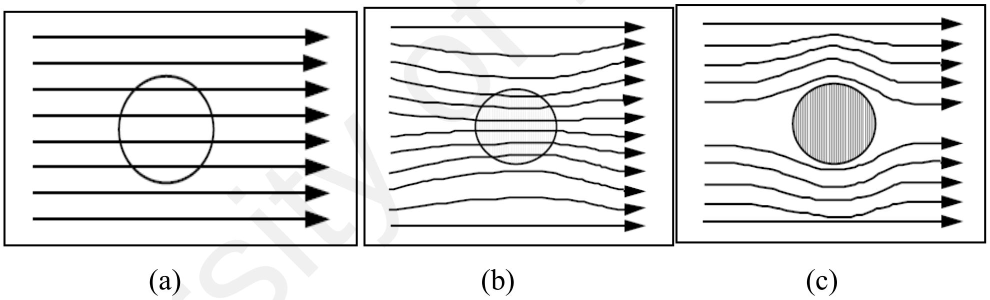
(a) (b) (c)

Figure 2.11: Behavior of applied magnetic field in different media: (a) vacuum (b) paramagnet (c) ideal diamagnet

In paramagnetic materials, the constituent atoms have unpaired electrons resulting in a net magnetic moment. Generally at room temperature, the individual magnetic moments are randomly oriented as shown in **Figure 2.12**. If an external magnetic field is applied to these randomly oriented intrinsic magnetic moments, they will tend to become alligned in a direction parallel to the external magnetic field. The magnetic moment induced in such materials by the application of an external magnetic field is called a paramagnetic moment. The magnitude of the susceptibility of paramagnetic substances is in the range of 10^{-3} to 10^{-6} c.g.s units and is positive.

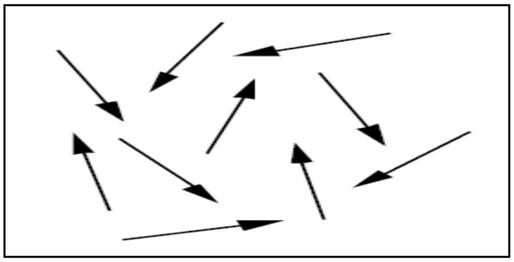

Figure 2.12: Random Orientation of Magnetic moments in Paramagnetic Material (Applied field, H = 0)

Paramagnetic materials, besides having unpaired electrons, contain paired electrons in the inner (closed) shells of the constituent atoms. The presence of these paired electrons makes diamagnetism an inherent property of all materials. Thus the magnetic moment measured is in fact the sum of both paramagnetic (positive quantity) and the associated diamagnetic (negative quantity) moment. Since the presence of an intrinsic magnetic moment in a substance results in a large paramagnetic moment, the diamagnetic effects are often neglected in the calculations. However, if the paramagnetic and diamagnetic moments of the substance under investigation are of comparable magnitude, and where accurate measurements are desired, corrections due to the diamagnetic contributions are made to the measured magnetic moments.

In paramagnetic materials, the magnetic spins are essentially independent spins acted upon only by the applied magnetic field. In the presence of the applied field, the spins tend to align parallel to the field, but since they are independent spins, thermal agitation ensures a random orientation when the applied field is removed. Often, however, the individual spins interact with neighboring spins in a cooperative fashion where the direction of one spin influences the directions of its neighboring spins. These interactions are short-ranged and only important between nearest neighbors, but, in bulk, they can lead to long-range magnetic ordering in the absence of an applied field below a certain critical temperature. A few basic types of bulk magnetic properties include ferromagnetism, antiferromagnetism, and ferrimagnetism [85].

In ferromagnetic materials the spins align in the same direction below a certain critical temperature in the absence of an external magnetic field. In this type of material, the individual spins are ferromagnetically coupled to their neighboring spins meaning that the direction of one spin favors the parallel alignment of the neighboring spin(s). A ferromagnet consists of spins that are all aligned parallel (**Figure 2.13**). Above the critical temperature of ferromagnetic materials, referred to as the Curie temperature (T_C), they typically behave as paramagnets since the surrounding thermal energy is strong enough to overcome the strength of the ferromagnetic coupling. In antiferromagnetic materials, the spins of unpaired electrons align in an antiparallel fashion in the absence of an external magnetic field and below a certain critical temperature called the Néel temperature (T_N). In antiferromagnets, the direction of an individual spin causes neighboring spin(s) to align in an antiparallel direction. This is referred to as antiferromagnetic coupling. Above the T_N, antiferromagnets typically behave as paramagnets, like ferromagnetic materials. In a special case of antiferromagnetism, called ferrimagnetism, the magnetic moments are arranged antiparallel, however, the magnetic moments are not equal. This leads to net magnetization since the opposing moments do not cancel each other out. Ferrimagnets typically behave like paramagnets above the T_N (T_C is not used to describe the critical temperature since the main interactions in ferrimagnetic materials are antiferromagnetic).

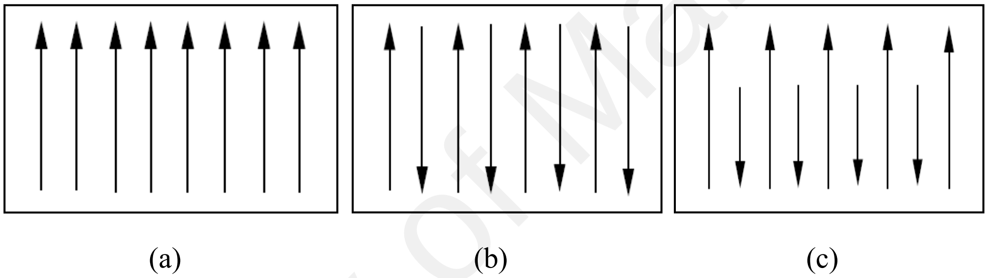

Figure 2.13: Types of magnetic ordering: (a) ferromagnetic, (b) antiferromagnetic, (c) ferrimagnetic

The magnetic properties of a compound can be deduced from its effective magnetic moment (μ_{eff}), calculated using the following relationship:

$$\mu_{\text{eff}} = 2.828(\chi_M^{\text{corr}}T)^{½}$$

where χ_M^{corr} is the corrected molar magnetic susceptibility, and T is the temperature in kelvin (K).

The value of χ_M^{corr} at room temperature can easily be determined using a Gouy balance. This instrument consists of a sensitive balance from which the sample hangs and lies in between the poles of magnet. The balance may be calibrated against a standard with an accurately known susceptibility, such as H_2O (-0.77×10^{-6} c.g.s), $CoCl_2.H_2O$ ($+4.081\times10^{-5}$ c.g.s), $MnSO_4.H_2O$ ($+6.52\times10^{-5}$ c.g.s), $CuSO_4.5H_2O$ ($+0.6\times10^{-5}$ c.g.s) or $Hg[Co(SCN)_4]$ ($+1.644\times10^{-5}$ c.g.s).

The value directly obtained from the Gouy balance is the gram susceptibility, χ_g. The next steps are to calculate the diamagnetic contribution, χ_{dia}, of each atom in the molecule from the Pascal's constant [86], and then the molar susceptibility, χ_m, by multiplying the value of χ_g with the molecular weight. The value of χ_M^{corr} is then obtained from the relationship: $\chi_M^{corr} = \chi_m - \chi_{dia}$.

Copper(II) ion is a $3d^9$ system and therefore has one unpaired electron. Its compounds are expected to be paramagnetic with magnetic moments close to the spin-only value of 1.73 B.M., irrespective of the bond type involved. Actually, the observed values of the magnetic moment are 1.9 – 2.2 B.M., for most of copper(II) compounds with ionic or rather weak covalent bonds, and 1.72 – 1.82 B.M. for the compounds with strong covalent bonds (3*d*4*s*4*p* type) [87-88]. Thus, copper(II) compounds having subnormal magnetic moments of less than 1.73 B.M. may be considered a distinct novelty.

Initial interest in copper(II) carboxylates can be safely said to start with the work on copper(II) acetate monohydrate, which stemmed from the reported abnormal physical properties. These include magnetic behavior in contradiction to the Curie-Weiss law, an abnormally low magnetic moment, and an anomalous electron spin resonance spectrum. In 1952, Guha [89] reported the first variable temperature magnetic study of copper(II) acetate monohydrate single crystal. This study revealed that a susceptibility maximum occurred at 270 K, and decreasing rapidly with decreasing temperature. Lifshitz and Rosebohm [90] also recorded a magnetic moment of 1.4 B.M., a value not only lower that the calculated spin-only moment, but considerably lower than the range of 1.8 – 2.2 B.M. usually accepted for copper(II) salts [21]. In 1952, Bleaney and Bowers [77] reported the electron spin resonance spectrum for copper(II) acetate monohydrate and made the suggestion that the anomalous susceptibility could be explained on the basis of isolated pairs of copper atoms coupled by exchange forces. Two energy levels, a singlet with anti-parallel spins and a triplet with parallel spins, would result from the electron spin interaction. The thermal distribution of the molecules between these states is reflected by the shape of the susceptibility-temperature curve. Mathematically, the magnetic properties can be reconciled by the inclusion of spin coupling term within the Hamiltonian used to describe the system. This was the first explanation of the unusual magnetic properties of copper(II) carboxylates utilizing the Heisenberg-Dirac-Van Vleck (HDVV) model. Since then, there have been a large number of successful applications of the HDVV model to magnetically coupled dimeric copper complexes [21]. From the HDVV model, an expression for the magnetic susceptibility as a function of various parameters can be derived. These parameters include the exchange integral, J_{ij}, between each interacting pair of ions, temperature, and the g values of the metal ions. The expression for paramagnetic susceptibility by the HDVV model, for the case of interacting ions with a spin of ½ is:

$$\chi_M = \frac{g^2\beta^2N}{3kT}\,[1 + {}^{1}/_{3}\exp(-2J/kT)]^{-1} + N\alpha$$

where *g* is the magnetic field splitting factor, β is the Bohr magneton, 2J is the exchange integral of magnetism theory, and Nα is the temperature independent paramagnetism per mole ions. A triplet ground state and a ferromagnetic interaction are indicated by a positive 2J value, while a singlet ground state and an antiferromagnetic interaction are signified by a negative 2J value. The paramagnetic triplet level becomes increasingly populated as the temperature is raised above absolute zero at the expense of the singlet level until a maximum susceptibility value is reached. The temperature at which this maximum is reached is referred to as the Neel temperature, T_N.

The magnetic studies on other copper(II) carboxylates were then intensively pursued in order to further understand the magnetic interaction within the compounds. Most researches converged into one thing: that dimeric copper(II) carboxylate are generally antiferromagnetic with 2J values of around -300 cm^{-1} [12,52] or having low magnetic moments at room temperature. This could be seen in anhydrous copper(II) acetate, copper(II) acetate monohydrate, copper(II) acetate monopyridine adduct, and many more as shown in **Table 2.4** and **Table 2.5** [11,52]. From the many magnetic studies done, the energy separation between the triplet state and singlet ground state is usually similar for dimeric copper(II) system if: (a) the electron donation of the substitution R bonded to the carboxylate C atom is the same, (b) the square pyramidal coordination around Cu atom is not deformed and (c) the ζ donation of the axial ligand is similar [91].

The magnetic studies on copper(II) carboxylates led to the understanding of electron transport as well as electronic communication in these compounds. A great debate had focused on their anomalous magnetic behavior, and generally it was agreed that this was due to some form of strong coupling between the unpaired electrons on adjacent copper atoms through exchange forces. At the same time, many theories were formulated on the mechanisms of the exchange forces. The magnetic interaction between the unpaired electrons on the copper(II) ions is well established to take place on either of the following phenomena or may be both: (a) direct spin interaction between the adjacent copper atoms, and (b) interaction through Kramer's super-exchange type, acting through intermediate oxygen atoms.

Table 2.4: The exchange integral (-2J in cm^{-1}) for binuclear copper(II) carboxylates

Compound	**-2J**
$Cu(CH_3(CH_2)_2COO)_2$	322
$Cu(CH_3COO)_2(H_2O)$	284
$Cu(2\text{-}BrC_6H_4COO)_2(H_2O)$	250
$Cu(CH_3COO)_2(H_2O)$	270
$Cu(C_2H_5COO)_2(C_5H_5N)$	350
$Cu(C_2H_5COO)_2(C_6H_7N)$	364
$Cu(Cl_3CCOO)_2.(C_5H_4ClN)_2$	217
$Cu(F_3CCOO)_2(C_{10}H_9N)$	310
$Cu(CH_3COO)_2(C_5H_3Cl_2N)$	349
$Cu(ClCH_2COO)_2(C_5H_5N)$	333
$Cu(Me_3CCOO)_2(C_5H_5N)$	366

Table 2.5: Magnetic moment (in B.M.) for binuclear copper(II) carboxylates

Compound	μ_{eff}
$Cu(CH_3COO)_2$	1.39
$Cu(CH_3COO)_2.(H_2NCONH_2)$	1.37
$Cu(C_2H_5COO)_2$	1.36
$Cu(C_3H_7COO)_2.(H_2O)$	1.35
$Cu(ClCH_2COO)_2$	1.42
$Cu(C_6H_5COO)_2$	1.44
$Cu(C_{10}H_7COO)_2$	1.44

In the 50s and 60s, the magnetic interaction in copper(II) acetate was believed to be due to direct interaction of copper atoms owing to the short distance between the two Cu atoms. Based on this, Figgis and Martin [92] proposed that the direct interaction may be described as the overlap of atomic orbitals of the two copper atoms. The authors has specifically described the bonding orbitals in each binuclear copper(II) acetate unit using valence-bond in favour over molecular-orbital approach. The observed exchange interaction between the unpaired spins on adjacent copper atoms arises from lateral overlap of $3d_{x^2-y^2}$ orbitals oriented with their lobar planes parallel. This δ bonding is considered to be so weak that the configuration of the binuclear molecule can be maintained only by the four bridging acetate groups.

It is also worth mentioning that if the magnetic interaction of copper(II) carboxylates originates from the direct metal-to-metal linkage, the interaction is expected to be affected by the distance between the metal ions. The magnetic interaction between metals is postulated to become larger as the metal distance becomes shorter. The example taken to support this are copper(II) acetate monohydrate and copper(II) salicylate tetrahydrate. The former, which is known to be a dimer, have a Cu-Cu bond distance of 2.64 Å, leading to a fairly large magnetic interaction between the copper(II) ions (1.43 B.M.) while the latter, having magnetic moment of 1.92 B.M., which is in conformity with the longer Cu-Cu distance of 3.728 Å.

Apart from Cu-Cu distance, magnetic interaction is also affected by the nature of the attached ligand. The magnetic interaction will become larger as the ligand supplies more electron density to the central metal ion. The greater electron transfer makes the metal orbitals larger and results in a larger overlap. The terminal ligand will also give the same promotion. To support this observation, the magnetic susceptibilities of copper(II) chloroacetate were referred. The results showed a good parallel between the pK_a values of the acid and the magnetic moment of the compounds; a larger pK_a value (weaker acid) results in a larger magnetic interaction (low value of magnetic moment). The pK_a value is a good measure of the electron-donation power of the carboxylate ion to the metal ion. The same parallelism can also be seen for the copper(II) salts of monosubstituted benzoic acid. Those with high pK_a values showed low magnetic moments. However, there also exist some irregularity for certain compound but it was attributed to a structure that is different from the dimeric one.

The factors discussed above, namely the Cu-Cu bond and the ligand effect, actually focus in two different aspects. The ligand effect will give way to interaction along the bridge, between Cu and $RCOO^-$ which can be dominant as compared to direct Cu-Cu bond. So the superexchange interaction could always be possible even if for short Cu-Cu bond. In his review, Kato et al. [12] has grouped together the compounds with larger Cu-Cu bond distance as having magnetic interaction with superexchange pathway, while those with smaller Cu-Cu bond as having direct copper-to-copper interaction.

A direct interaction concluded based on Cu-Cu bond has not been always available for all situations, and throughout the year has gradually been left out. It has been shown that the Cu…..Cu distance is not directly related to the magnetic property [10,11]. Also, the -2J value appears to be insensitive to the structural factors related to the axial ligand. In addition, there exist few contradictory results on the relationship between Cu-Cu bond distance and magnetic moments. For instance, copper(II) salicylate has a magnetic moment per copper atom of about 1.44 B.M. [42]. This very strong magnetic interaction does not agree with the X-ray crystal data of the compound which show the Cu-Cu bond of 3.728 Å [44]. Nevertheless, Inoue et al.[45] has justified that the phenomena was caused by the existence of two different crystal modifications of copper(II) salicylate tetrahydrate: the one that has a longer Cu-Cu bond indeed has a normal magnetic moment. However, the existence of the other compound has not been supported by any X-ray crystal data. The anomaly between Cu-Cu bond distance and magnetic moment continues to emerge in the case of copper(II) benzoate trihydrate. The X-ray crystal studies revealed that the neighbouring copper atoms are 3.15 Å apart but the magnetic moment was 1.87 B.M. The reason given was merely based on some structural feature believed to be responsible in reducing the magnetic coupling. The structure of copper(II) benzoate trihydrate (**Figure 2.8**) showed the two Cu atoms bridged by two oxygen atoms from water and one Cu-O-C-O-Cu link to form linear chains [93]. Also, it is worth noting that copper(II) formate tetrahydrate, $Cu(HCO_2)_2.4H_2O$, the structure of which was completely elucidated by X-ray analysis (**Figure 2.14**), has Cu-Cu bond distance of 5.80 Å but with subnormal magnetic moment of 1.64 B.M. [94]. The magnetic interaction in this compound was suggested to be primarily due to the superexchange through a π-pathway, set up by using $3d_{yz}$ or $3d_{xz}$ orbitals of the copper ion and of $2p_x$ orbitals of the bridging HCOO ligand [36].

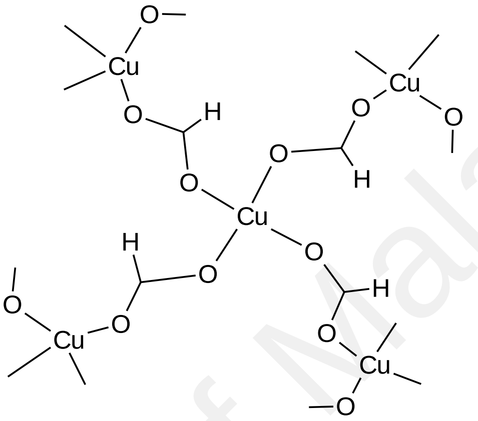

Figure 2.14: The structure of [$Cu(HCOO)_2.4H_2O$] (axially ligated H_2O molecules are not shown in the drawing)

The works of other researchers have also [20, 95-97] shown that the spin coupling between the unpaired electrons of copper(II) ions operates predominantly by a superexchange interaction through the bridging carboxylato ligands rather than by direct Cu-Cu interaction. Accordingly, the magnetic interaction will become stronger as the Cu-O bonds become stronger.

The structural and magnetic results of some copper(II) carboxylates has confirmed the insensitivity of the singlet-triplet separation (-2J) to the Cu-Cu distance [11]. This indicates the predominance of a superexchange rather than of direct mechanism for coupling [95]. The apical ligands also clearly play a role in determining the 2J value in binuclear compounds [91]. The value of 2J increase as the terminal ligands become stronger electron donors. Thus the 2J value tends to increase according to the series of terminal groups:

aniline < water $\leq$ anhydrous < pyridine, picolines, SCN, ethanol < dioxin

It is also worth noting that the main factor which determines the magnitude of the antiferromagnetic interaction in the dimeric copper(II) carboxylates is the electronic structure of the bridging moiety [52].

Through electron density distribution study, Yamanaka et al. [52] showed that the greater the electron density on the carboxylate C atom (specifically $2p_x$ orbital population), the stronger the antiferromagnetic interaction in the binuclear copper(II) carboxylate. This is in accord with the tendency of the spin-exchange interaction to increase as the carboxylate substituent becomes a stronger electron donor [98,99]. In some series of binuclear copper(II) carboxylates, the -2J values tend to increase as the pK_a values of the parent acid of the bridging ligand increase. However; there are some exception, such as formate ($HCOO^-$) and trifluoroacetate (CF_3COO^-) [12,100-104]. Through this study, the authors proposed that the anomaly of the formate ion may originate from the difference in the electronic structure of its carboxylate C atom, which influences the super spin-exchange interaction directly, but not the acidity. Similarly, the trifluoroacetate ion was found to have larger effective negative charges on their O atoms (higher electron population) than trichloroacetate ion, but the pK_a values is relatively smaller for the former. This may explain why copper(II) trifluoroacetate showed a stronger spin-exchange interaction than expected from its pK_a value.

So, in general the mechanism governing the magnetic exchange interaction in copper(II) carboxylate dimers was subjected to considerable controversies since the study of Figgis and Martin [92] on copper(II) acetate monohydrate (the δ bond mechanism). A large number of studies was conducted to see how the structural and physico-chemical properties correlate with the -2J values: pK_a of carboxylic acids, the apical ligands, the *d-d* band energy, the Cu-Cu, Cu-O-C-O-Cu and (plane of O_4)-Cu distances, the Cu-Cu-L and O-Cu-L angles, polarizability of R, and other factors. It can be safely said that the magnetic interaction in copper(II) carboxylates depends very much on the overall structure of the compounds, which then depends on the carboxylate ligand, apical ligand and the synthetic method used.

In addition, the -2J values for several copper(II) benzoate and its adduct are listed in **Table 2.6**. The value of -2J for copper(II) benzoate rarely differ from its average value by more than 30 cm^{-1}. It is also clear that the terminal ligands influence these values. The -2J value tends to increase according to the following series of terminal ligands: nicotine < antipyrine < benzoic acid ~ aryl N-Oxides < dimethylsulphoxide, butanol < pyridine < anhydrous ≤ ethanol. However, copper(II) alkylcarboxylates do not follow this trend [11,105]. This indicates that the variation of -2J with the terminals ligands is not a simple function of the base strength of the ligands.

Copper(II) benzoate and its methyl-substituted derivatives have also been prepared and studied to further elucidate the electron-spin delocalization in the bridging ligand in support of the super-exchange interaction mechanism. The dimeric structure of the compounds with acetone as axial ligands was concluded based on the IR spectral studies as well as their elemental analyses and molecular weight calculation. These compounds were found to also have subnormal magnetic moments when measured as a solution in acetone by the Evans method [106]. Through contact shift study via NMR, Zelonka and co-worker [107] has shown that spin density from the copper ions is indeed delocalized into the molecular orbitals of the bridging ligands.

Table 2.6: The exchange integral (-2J in cm^{-1}) for copper(II) benzoate and its derivatives ($X = C_6H_5COO^-$)

Compound	-2J (cm^{-1})
CuX_2	340[a] 312[b]
$CuX_2C_2H_5OH$	340
$CuX_2C_4H_9OH$	306
$CuX_2C_6H_5COOH$	310
CuX_2DMSO	304
$CuX_2C_5H_5N$	310
$CuX_2C_{10}H_{14}N_2$	253
$CuX_2C_6H_5NH_2$	320
$CuX_2(4,4'\text{-}C_{10}H_8N_2)_{0.5}$	300

[a]Methanol adduct of copper(II)benzoate was heated in vacuum at the temperature of boiling CCl_4 for 3 hours. [b]Trihydrate copper(II) benzoate was refluxed in acetone for several hours.

2.4.2 Thermal Stability

A good thermal stability of a compound is a sought-after property if it was meant for many applications. Owing to a unique and peculiar physico-structural identity, numerous transition metal complexes are of special interest in industries, medicine, and biology, e.g. the electrical and thermochromic properties, antioxidation, vulcanization acceleration, protection of paintings, catalysts and antibacterial properties. All these applications are generally related to room temperature structures of the compounds as well as their thermal stability. Thus, a clear picture should be given on the nature of interrelation between structure and thermal stability. The different factors affecting the thermal stability of the transition metal complexes would be valuable information in order to relate composition, structure and material processing with those properties suitable for various technological applications.

The measurement of thermal stability of a solid complex is usually carried out by estimation of the heat of reaction from the metal salts with the ligands. As reported by Donia in his review paper [108], early works on thermal stability based on caloric measurement on the reaction enthalpy of the hydrates took place in the early twentieth century. Nowadays, the thermal analysis has grown quite extensively using modern techniques, such as differential scanning calorimetry (DSC) and thermogravimetry (TGA).

The decomposition of compounds are studied by DSC, which indicates in heat flow as a function of temperature, and TGA, which in turns shows mass loss as a function of temperature. With such analytical techniques, studying the structures and properties of metal complexes, namely reaction rate and mechanism, are now possible.

Thermal analyses of metal carboxylates, as well as the interpretation thereof, are in many cases complicated by the richness of their phase behaviour. Solid-solid state transitions, as well as smectic-isotropic liquid phase transition, are possible. However, the great variety in the thermal behaviour of metal carboxylates largely depends on many factors, from the type of coordinated ligands to the inclusion of counter ion/molecules into the coordination sphere of the complexes [108,109]. It also very interesting to note that generally for metal complexes, certain findings has shown that the nature and structure of the ligand, and consequently the structure of the complex, is considerably greater in the determination of their thermal stability, than the effect of the strength of the coordinate bond [110].

The decomposition process of copper(II) complexes in general normally consists of a few steps, depending upon their chemical formula and structural feature. Normally, the weight loss at temperatures less than 150°C is assigned to the release of noncoordinated solvent molecules, such as water (dehydration process), which were normally involved in hydrogen bonding. Such process is also clearly indicated by the presence of small endotherm in the DSC plot [111,112]. The release of water molecules or other solvents for that matter, can also take place at much higher temperature (above 200°C), especially when the molecules are coordinated to the metal atom [113,114]. However, it is very important to note that processes such as solid-solid transition (or restructuring) and melting could occur prior to weight loss. These events normally do not show up in a thermogram, but may be seen in a DSC plot as a small sharp endotherm [115,116]. Further weight loss after this process can be associated with the ignition and degradation process of the major ligands coordinated to the metal atom, normally taking place along with the rupture of the bond and the formation of a residue. It has also been reported that the decomposition process at this stage is normally followed by the reduction of Cu(II) to Cu(I) due to electron transfer mechanism and probably the oxidation of the ligands. An intermediate formed at this stage may undergo chemical reaction(s) as a consequence of the secondary processes of thermal degradation with numerous products in a gaseous state [69,71,109]. In a DSC plot, such process is indicated by an exotherm with a high enthalpy change as it is composed of the sum of the different effects in the process of the complex thermal decomposition. Hence, ultimately, no endothermic peak can be observed within this region even though a high percentage of weight loss is involved [109,116].

In the thermal investigation performed on metal complexes with ammonia, such as $[Cu(NH_3)_6]X_2$ (X = Cl, Br, I and NO_3), it was noted that the complexes normally showed two to three deammination reactions. The overall thermal stability of the complex depends predominantly on the presence of the counterion X in both inner and outer sphere. In general, the iodo-containing complexes showed a lower stability due the ease of oxidation of iodide ion to free iodine [117,118]. On the other hand, in the aliphatic diamine metal complexes, such as $[Cu(X)(H_2O)_2]_2$, where X is mono-, bis- and tris- (ethylenediamine), bis(1,2-propanediamine) and bis(1,3-propanediamine), their thermal stabilities were largely attributed to the chelate ring size as well as the steric factor of the methyl group (in the case of propanediamine complexes). A bigger chelate size will increase the stability of the complexes rather significantly [119,120]. However, it is interesting to note that the initial temperature for the decomposition of a complex and the temperature for the formation of the residue does not depend on the molecular weights of the ligand [115].

The metal coordination and position of the functional groups also has been shown to greatly affect the thermal stability of metal complexes. Metal complexes with Schiff base derivatives of 1H-indole-3-ethylenesalicyaldimine (sal TPA) (**Figure 2.13**), with different functional groups at different position on the phenyl ring (3-methoxy, 5-methoxy or 5-bromo), shows thermal stability in the following order: 3-MeOSal TPA < sal TPA < 5-MeOsal TPA < 5-Bromosal TPA. The sequence observed was attributed to the larger steric hindrance of 3-OCH_3 because of the greater proximity of this group to the chelate ring. For the same ligand, the stability order is: Cu < Co ≈ Ni. The higher thermal stability of nickel and cobalt is attributed to the type of ligand, which favours planar coordination around the metal. Moreover, in both metals, the *trans*-planar chromophore MO_2N_2 is less distorted than in the copper complexes [121,122].

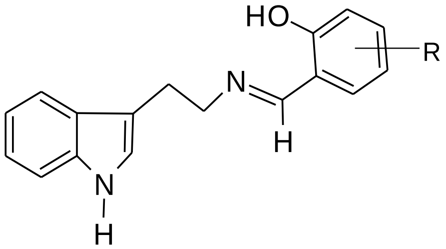

Figure 2.13: Structure of 1H-indole-3-ethylenesalicyaldimine where R = 3-methoxy; 5-methoxy or 5-bromo

The studies have also shown a direct effect of ligands basicity to the thermal behaviour of the complexes. Transition metal complexes with pyridine and substituted pyridines showed that the thermal stability increases with ligand basicity. Such observation was attributed to the stronger metal-ligand bond when the ligand basicity increases. However, ligands such 4-aminopyridine and 4-methylpyridine showed a counter effect. This is due to the pronounced effect of the amino and methyl groups at this position, which give rise to the existence of resonance structures that lowers the tendency to form metal-ligand π-bonds [123-125].

It is also very interesting to observe that the surrounding atmosphere was reported to influence significantly the thermal behaviour of complexes, especially on the final products. The thermochemical studies on 1,2-dithiooxalato-S,S'-complexes namely $Pd(S_2C_2O_2)_2$, $Pt(S_2C_2O_2)_2$ and $Ni(S_2C_2O_2)_2$ gave a mixture of nickel(II,III) oxide and sulphide, palladium(II) oxide and metallic platinum respectively in an oxidative atmosphere. However, in an inert atmosphere, nickel(II) and palladium(II) sulphides and platinum(O) were identified as final products [126-128]. However, for copper(II) carboxylates with ligands majorly consisting of C, H and O atoms, copper(II) oxide will be the major residues especially in an inert atmosphere [69,72,112].

2.4.3 Redox Properties

Voltammetry has proved to be very useful for analyzing dilute solution, both quantitatively and qualitatively, for inorganic, organic and biological components, measuring thermodynamic parameters for metal-ion complexes and oxidation-reduction systems, and studying the kinetic of chemical reactions. Voltammetric techniques are based on controlling the electrode potential and measuring the resulting current [129]. Here, the potential of the test electrode in an electrochemical cell is linearly changed at a known rate, and the resulting current is measured. A current is produced as a result of a redox reaction occurring at the working electrode. Commonly, two electrodes are used. One electrode has a relatively large surface area (the auxiliary electrode), while the other electrode has a very small surface area (the working electrode). A third electrode is known as the reference electrode [130]. The auxiliary electrode has a very small current density while the working electrode has a high current density.

The working electrode is the electrode where the excitation function is being applied (voltage ramp) and the response functions is being monitored (current). As such, this electrode is the heart of an electrochemical cell, though it cannot function without the other two electrodes. The auxiliary electrode simply provides a surface for the opposite electrochemical reaction to take place with respect to the working electrode; thus the current path is between the auxiliary and working electrodes. Most often in cyclic voltammetric experiments, the auxiliary electrode is an inert solid conductor (e.g. platinum wire) dipped in the same solution as the working electrode. The most familiar and widely used working electrode is the dropping mercury electrode (DME), hanging mercury drop electrode (HMDE), carbon paste electrode, glassy carbon electrode, gold electrode, platinum electrode and silver electrode. The purpose of the reference electrode is to provide a stable, reproducible voltage to which the working electrode potential may be referenced. Ideally if a small current is passed through the electrode, the potential change is negligible and, in any case, returns to the initial value when the current ceases. The most common reference electrodes are the silver/silver chloride (Ag/AgCl) and mercury/mercurous chloride (calomel) electrodes. The electrode reactions responsible for generating the reference potential are:

$$AgCl + e^- \rightleftharpoons Ag + Cl^-$$

$$Hg_2Cl_2 + 2e^- \rightleftharpoons 2Hg + 2Cl^-$$

A voltammogram is a plot of current as a function of potential. The basic equation related the potential applied to the electrode is:

$$E = E^o + \frac{0.059}{n} \log \frac{C_O}{C_R}$$

where E = applied electrode potential, E^o = formal electrode, n = number of electron transfer, C_o = concentration of oxidant, and C_R = concentration of reductant.

The important parameters of a cyclic voltammograms are the magnitude of the anodic peak current (I_{pa}) and cathodic peak current (I_{pc}), and the anodic peak potential (E_{pa}) and cathodic peak potential (E_{pc}).

A common example on electrochemical behaviour studied by cyclic voltammogram is on ferrocene ([$Fe(C_5H_5)_2$]). A simulated voltammogram of ferrocene is shown in **Figure 2.16.**

The potential is initially swept in a positive direction in order to oxidise the starting compound.

$$[Fe(C_5H_5)_2] \longrightarrow [Fe(C_5H_5)_2]^+ + e^-$$

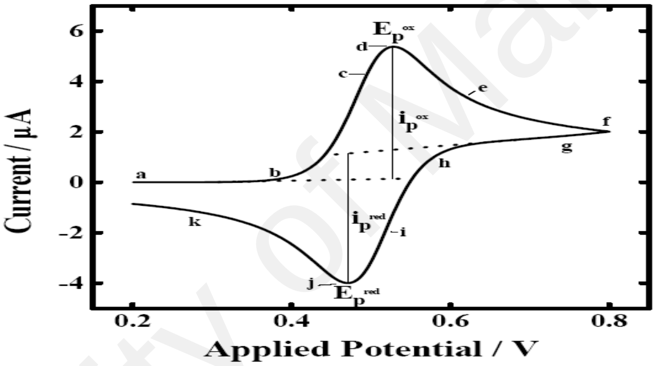

Figure 2.16: A simulated cyclic voltammogram of 0.5 mM [$Fe(C_5H_5)_2$] in an organic solvent (electrode area = 2.54 mm^2, scan rate = 100 mV s^{-1})

Note that in **Figure 2.16**, the positive direction on the current scale is oxidation current. The oxidation current increases rapidly (*b* to *d*) until the concentration of [$Fe(C_5H_5)_2$] at the electrode surface is significantly diminished. This causes the current to peak at a maximum value E_{pa} and then decay (*d* to *g*) as controlled by the rate diffusion of [$Fe(C_5H_5)_2$] from the bulk. The scan direction is switched at about 0.8 V and then the potential is swept in a negative direction in order to reduce the newly formed [$Fe(C_5H_5)_2$]$^+$. Oxidation current is still flowing even though the potential is now being swept in a negative direction. It is not until the potential is negative enough to reduce the $[Fe(C_5H_5)_2]^+$ that the reduction current is observed.

$$[Fe(C_5H_5)_2]^+ + e^- \longrightarrow [Fe(C_5H_5)_2]$$

Again the current rapidly increases (*i* to *k*) to give a maximum value of E_{pc} as the concentration of $[Fe(C_5H_5)_2]^+$ is depleted at the electrode surface and diffusion control gives rise to current decay after a maximum value (*j* to *k*).

A redox couple in which both species rapidly exchange electrons with the working electrode is termed an electrochemically reversible couple. Such a couple can be easily identified from a cyclic voltammogram by measurement of the potential difference between the two peaks potential, ΔE (in V):

$$\Delta E = E_{pa} - E_{pc} = 0.059/n$$

where n = number of electron transferred. The above equation applies to a system which is both electrochemically and chemically reversible. The ΔE value is independent of scan rate for a reversible couple. The potential midway between the two peak potentials is the standard electrode potential, corrected to the reference electrode being used, of the couple.

Electrochemical irreversibility is caused by slow electron exchange of the redox species with the working electrode. In this case, the above equation is not applicable. Electrochemical irreversibility is characterized by ΔE value greater than 0.059/n volt, and dependent on the scan rate (ΔE increases as the scan rate increases) [131].

The total current passing through the cell is the diffusion current (I_d) plus migration current (I_m):

$$I = I_d + I_m$$

The rate of diffusion of the ions to the electrode surface is given by Fick's law [132]:

$$\frac{C}{t} = D\frac{C}{X^2}$$

where D = diffusion coefficient, C = concentration of redox species, t = time, and X = distance from the electrode surface.

In the absence of an electroactive species, a small current known as the residual current flows through the cell. The residual current is a combination of the current flowing as a result of the reduction or oxidation of any impurities in solution. It is also called a charging current, and is the proportion of the total current that is controlled by the diffusion of an electroactive species to the electrode surface. In other words, the diffusion current is the difference between the total current flowing in the cell and the plateau of the wave of the residual current.

As far as binuclear copper(II) complexes are concerned, the electron transfer behaviour has been a subject of considerable interest especially from the point of view of understanding and replicating the redox function of ‘type 3’ copper proteins.

The biological role of copper usually involves association with certain specific proteins, referred to as copper proteins. These proteins generally behave as typical metalloproteins, whereby copper constitutes an integral part of their function. Extensive studies have been carried out on many copper proteins but still there are several questions concerning the stability of the metallic reaction site. This is due to the fact that the copper(II)-copper(I) electron transfer couple is very unique. Unlike other redox couples of the transition series, such as iron, cobalt, and ruthenium, copper has different preferred coordination number and stereochemistry in the two oxidation states. In polar solvents, copper(II) complexes exist predominantly as five- or six-coordinate species (tetragonal), whereas copper(I) complexes are expected to prefer four (tetrahedral) or more likely lower coordination number. Both states are highly labile and stereochemically flexible.

Thus, if a Cu(II) complex, whatever its geometry, is sufficiently flexible to allow a structural reorganization to the tetrahedral geometry, it will probably manifest a reversible access to the corresponding Cu(I) complex. On the other hand, if it is rigidly planar, it is likely that it will exhibit a reversible access to the corresponding Cu(III) complex. If such reorganization is not structurally allowed, the respective electrode processes will be irreversible. Furthermore, if the geometry of the initial Cu(II) complex shows some predisposition towards that of the associated redox state, the relative process will occur at low potential values (weakly negative or even positive for reduction; weakly positive or even negative for oxidation). Thus, electron transfer between copper(II) and copper(I) will therefore normally be accompanied by major structural and stereochemical changes.

Compounds that contain two copper centers with identical geometries and have very low or no magnetic interaction (that is, the metal centers are remotely located) undergo either one-step two-electron transfer or overlapping sequential one-electron reductions [133,134]. In the case of strongly coupled binuclear complexes, electron transfer generally takes place in one of the following ways: (a) two sequential one-electron reduction at different potentials yielding the mixed-valence species [Cu(II)Cu(I)] as the intermediate product [135,136], or (b) the transfer of two electrons at the same potential, producing [Cu(I)Cu(I)] species as the sole product [137,138]. While mechanism (a) is expected on statistical grounds and indeed has been observed in majority of cases, mechanism (b) is more intriguing and has been reported so far in bis(1,3,5-triketonato)dicopper complexes by Fenton et al. [137].

Generally, two mechanisms have been proposed for the electron transfers in binuclear copper(II) complexes, particularly for those having moderately strong antiferromagnetic interaction ($J \leq -300\ cm^{-1}$). The first mechanism [134] suggests that the first electron transfer occurs at the lowest unoccupied orbital of the singlet state. This mechanism predicts that the complex with the greatest antiferromagnetic interaction should have the lowest-potential first reduction step. The addition of the second electron will be also at the lowest potential for the one having greatest J value.

For the second mechanism [139], the electron transfer occurs at the triplet state. It was shown that the observed potential for a system having J value of about -300 cm^{-1} differed by only 6 mV from the potential calculated for a hypothetical system with J = 0. This would predict that for related compounds, the potentials for the first reduction step would be virtually independent of the extent of magnetic interaction. In their studies on binuclear complexes, Mandal et al. [140] showed that besides having different J values, the potential of the first reduction step remained practically invariant throughout the series. This clearly supports the mechanism involving the reduction of triplet copper(II) ion.

As in the case of their structural features and magnetic properties, the electrochemical behaviour of dinuclear copper(II) complexes has also been found to be dependent on the nature of the donor atoms and the structural arrangement of ligands around the central metal ion. These factors give rise to significant effects, such as steric, electronic and conformation interaction, which normally take place in the realm of copper(II) complexes structure.

The electrochemical studies on mononuclear Cu(II) complexes [Cu(dta)X], where X = Cl, ClO_4 and imidazole, while dta = 2,2'-dithiodianiline, showed a direct effect of the ligand. The reduction potential for Cu(II) to Cu(I) was found to be positive (~ + 0.6 V) compared to $CuCl_2$ (- 0.150 V) [141].

This ligand-dependent electrochemical behaviour was also observed by Zhou et al. on $[Cu(pbbt)Cl_2]_2.CH_3OH$ and $[Cu(bbbt)_{1.5}Cl_2]_n$ (pbbt = 1,1'-(1,3-propylene)bis-1H-benzotriazole, bbbt = 1,1'-(1,4-butanediyl)bis-1H-benzotriazole) (**Figure 2.17**). The two complexes showed lower reduction and higher oxidation potentials compared to $CuCl_2$, with a difference of about 35 mV [142].

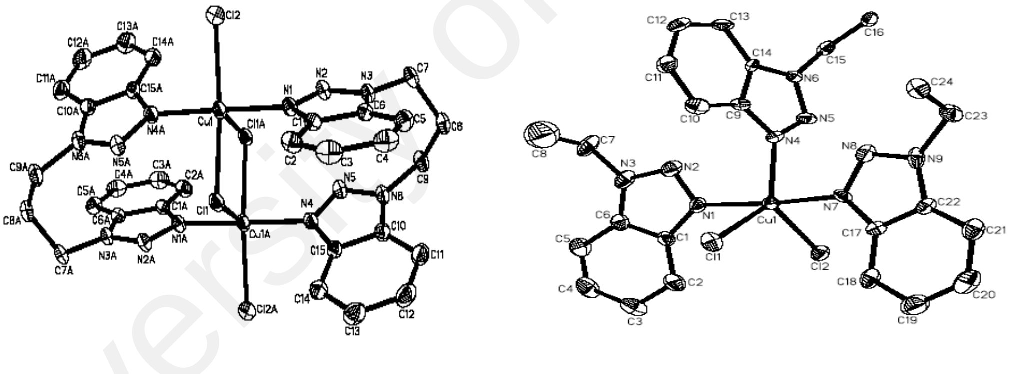

(a) (b)

Figure 2.17: Structures of (a) $[Cu(pbbt)Cl_2]_2.CH_3OH$, and (b) $[Cu(bbbt)_{1.5}Cl_2]_n$

In addition, Amuda et al. in their studies on phenoxo-bridged dicopper(II) complexes, $[Cu_2L(X)]ClO_4]$ (X = OH, Br, OAc ; L = 4-bromo-2-[4(methylpiperazin-1-yl)methyl]-6-[N-(3,5-dimethyl-2-hydroxy-benzy)-N-methylaminomethyl]phenol) (**Figure 2.18**), showed that the reduction potential was exogenous donor dependent, and follows the order $CH_3COO < Br < OH$.

Although CH_3COO is a better electron donor than Br and OH, the reduction was observed at less negative potential. This behaviour seems to be associated with the increased number of atoms involved in the acetate bridge, which may offer more flexibility for the acetate-bridged complexes as opposed to the bromo- and hydroxo- bridged complexes [143]. This geometrical dependent factor was also found in the study by Mosa et al. on dinuclear copper(II) compound, $[(Cu_2bphenim)(H_2O)_4]NO_3$, where bphenim = 4,5-bis(phenylalanyl-N-methyl)-2-methylimidazole. The two copper(II) ions were reduced at different potentials due to the asymmetrical arrangement of the ligands. The copper(II) ion which was coordinated to the amine and carboxylate group was only reduced at a lower potential compared to the copper(II) ion which was additionally coordinated to an imidazolic nitrogen [144].

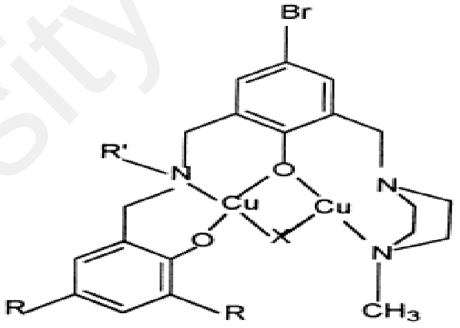

Figure 2.18: Structural formula of $[Cu_2L(X)]ClO_4]$

For carboxylates as ligands, the presence of substituents can also influence the facile reduction of copper(II) ion. The presence of electron donating or withdrawing group can significantly affect the electron density around the central copper(II) ion. The presence of electron-withdrawing group will conceptually reduce the electron density around copper(II), making the reduction process much easier due to reduced electronic repulsion. Such conclusion was supported by the work of Amudha et al. [143], as described above. The reduction process at less negative potential observed for the bromo complex when compared to the hydroxide was suggested to be due to the poor electron- donating nature of the bromide ion. In addition, their work on dinuclear copper(II) complex with bis[3,5-diX-2-hydroxybenzyl]-N-alkylamines (where X = CH_3, Cl), also showed similar trends. The complex with chloro-substituted ligand was reduced at lower potential due the strong electron-withdrawing effect of the atom (which reduced the electron density around copper(II) ion [143]. Similar trend was also portrayed in the work of Bharati et al. [145], who studied different electron-withdrawing effect by the substituted group, namely CHO, $C(O)CH_3$, and $C(O)OCH_3$ at the *para* position of the phenoxide of the phenyl ring of their studied complexes. The reduction potentials of the complexes decrease accordingly as the electron-withdrawing nature of the substituent increases [145].

In the absence of significant electron-donating or withdrawing factors, the geometrical distortion plays a vital role in influencing the electrochemical behaviour of binuclear complexes. Normally, structural distortion takes place due to the presence of highly steric factor by the ligands, ligated either equatorially or axially. The presence of a strong ligating ligand can also influence the facile reduction of the complex as it can weaken the equatorial bond. A weaker ζ coordinate bond with Cu(II) will make it easier to distort the geometry, and thus producing a less antibonding lowest unoccupied $d_{x^2-y^2}$ orbital. Senggottuvelan et al. studies electrochemical behavour of [CuL(X)], where L is 1,4-bis[2-hydroxy-3-(formyl)-5-methylbenzyl]piperazine, and X is Cl, NO_3 or ClO_4, showed that the reduction potential of the complexes was in the following order: $ClO_4 > NO_3 > Cl$. The facile reductions of the complexes having NO_3 and Cl were postulated to be due to easier geometrical distortion by the axial coordination of these anions since they were less sterically hindered [146]. Similar result was obtained by Saravanakumar et al. The reduction process of their complexes, $[Cu(L^2)(ClO_4)]$, where L^2 is $HONC(CH_3)C(CH_3)NCH_2CH(NH_2)CH_3$ (N-β-aminomethyl ethylisonitrosoethyl methyl ketimine), took place at lower negative potential (a difference of 0.11 V) than $[Cu(L^1)(ClO_4)]$, where L^1 is $HONC(CH_3)C(CH_3)NCH_2CH(NH_2)C_2H_5$ (N-β-aminoethyl isonitrosoethyl methyl ketimine). Such potential discrepancy was attributed to the direct impact of the CH_3 substituted group on the ligand periphery, which caused a distortion in the geometry on the complex [147].

Apart from structural distortion, a different geometry at copper(II) centre can also influence the redox potential of the complex. Electrochemical studies on some symmetrical Schiff base copper(II) complexes namely, Salen, Salpr and Salbu, showed an increase in the redox potential as the copper(II) moiety changed from a planar (Salen) towards a distorted tetrahedral (Salbu) geometry. Using the plane angle of N-Cu-O, an assessment of the impact of geometry on redox potential confirmed that a significant change (~10 $mV/^{o}$) has occurred [148].

2.4.4 Carbon-Carbon Bond-Forming Reaction

The carbon-carbon bond-forming reaction is one of the key criteria in forming a new compound in organic synthesis; and one of the most important reactions is aldol condensation. There has been a great interest in such a reaction due to the possible formation of optically active compounds, important in the field of organic synthesis, medicinal chemistry and pharmaceutical industry. For instance, crossed-aldol condensation of aromatic aldehydes with cyclic ketones is an important synthetic reaction for the preparation of α,α'-bis(substituted)benzylidene cycloalkanones. These benzylidene derivatives are intermediates of various pharmaceuticals, agrochemicals and perfumes [149], frequently used for the synthesis of bioactive pyrimidine compounds [149], and also find applications in the preparation of nonlinear optical materials [150] and liquid-crystalline polymers.

Aldol condensation reaction is indeed an important synthetic reaction. In classical methods, this reaction is performed in the presence of strong acids or bases [151,152]. Acids and bases promote the reversible formation of aldols from enolisable aldehydes and ketones. Generally, the reaction occurs by nucleophilic addition of enolate ion of the donor molecule to the carbonyl group of the acceptor molecule, yielding a tetrahedral intermediate that is protonated to give the alcohol as the final product. This β-hydroxy ketones or β-hydroxy aldehydes can be easily dehydrated to yield conjugated enones. In fact, it is this loss of water that gives the aldol condensation its name, since water condenses out of the reaction when the enone product forms.

Aldol reaction was discovered independently by Borodin and Wurtz [153] in 1870. Since then, it has become a versatile method for preparing new C-C bonds [154]. Furthermore, as both of these carbon atoms may end up as chiral centers, there has been much recent research into the asymmetric aldol addition reaction [155].

The typical mechanism of an aldol condensation reaction, using strong acids or bases as catalyst, is illustrated in **Figures 2.19-2.22**.

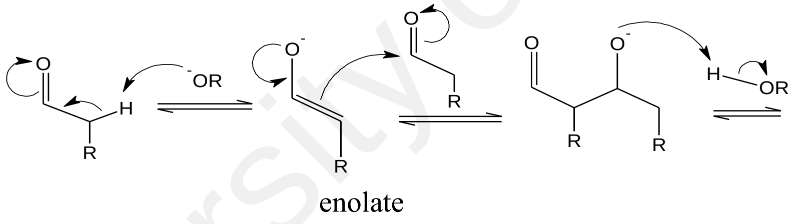

Figure 2.19: Base-catalyzed aldol reaction (base = ⁻OR)

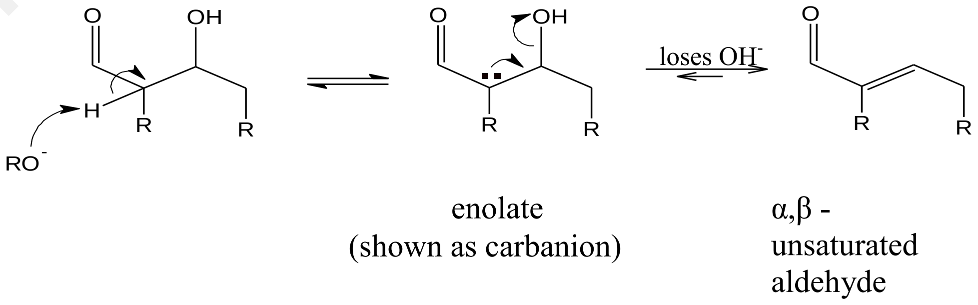

Figure 2.20: Base-catalyzed dehydration (sometimes written as a single step)

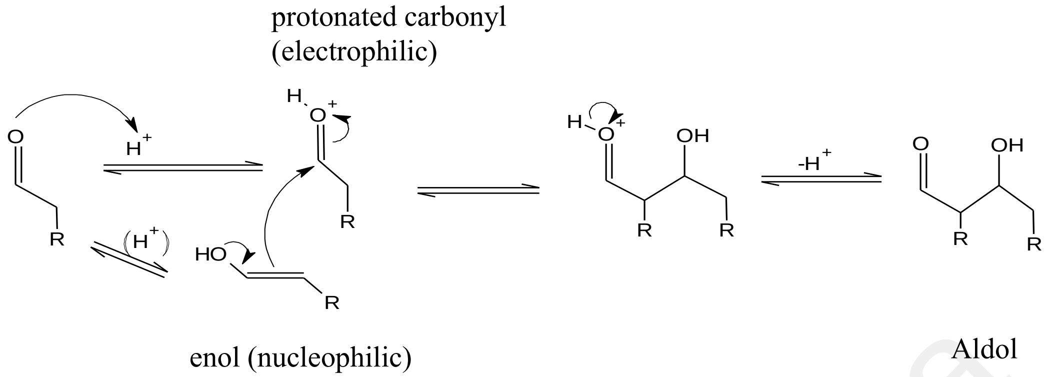

Figure 2.21: Acid-catalyzed aldol reaction

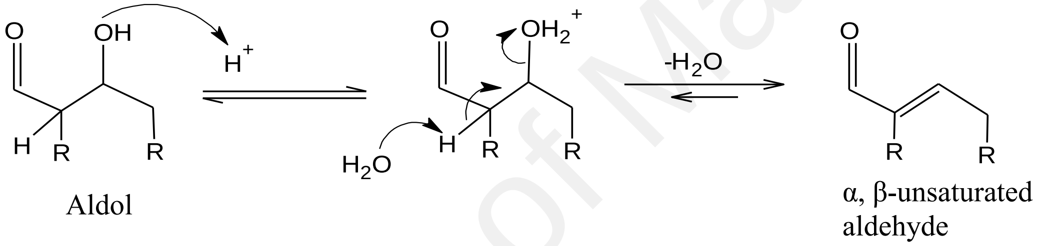

Figure 2.22: Acid-catalyzed dehydration

There are a number of condensation reactions that have essentially the same key mechanistic steps as the aldol condensation. In these reactions, a base (such as hydroxide, alkoxide, amine, acetate) removes an acidic proton to form a carbanion (resonance-stabilized enolate anion), which then attacks a carbonyl carbon. Many of these reactions are named after the chemist(s) who discovered and/or developed the reaction. An example is Claisen-Schmidt condensation.

Theoretically, a mixed aldol condensation between an aldehyde and a symmetrical ketone yields four products (**Figure 2.23**).

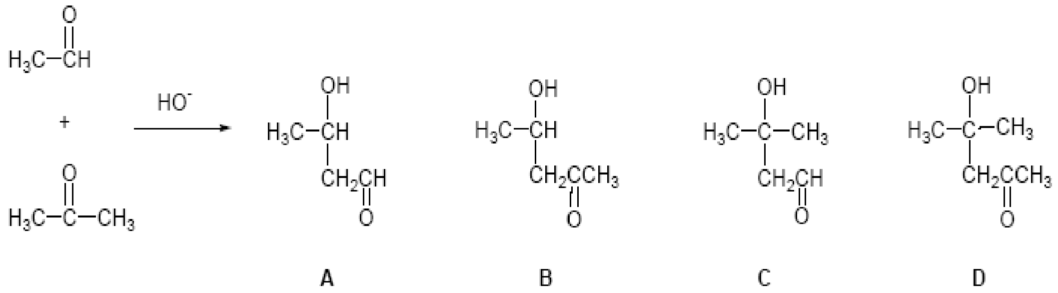

Figure 2.23: Possible products of mixed aldol condensation between a ketone and an aldehyde

In practice, however, products A and B are the major products because the aldehyde carbonyl carbon is more reactive toward nucleophilic attack. If an aldehyde with no α-hydrogen is used, self-condensation of the aldehyde (product A) cannot occur and a good yield of a single product (product B) is obtained. The use of dilute aqueous NaOH to catalyze the condensation of a ketone with an aromatic aldehyde possessing no α-hydrogen is called the Claisen-Schmidt condensation (**Figure 2.24**). At higher temperatures, the aldol addition product usually undergoes spontaneous dehydration to form a C=C double bond, which brings the carbonyl into extended conjugation with the aromatic ring. Some examples from the literature are shown below [156].

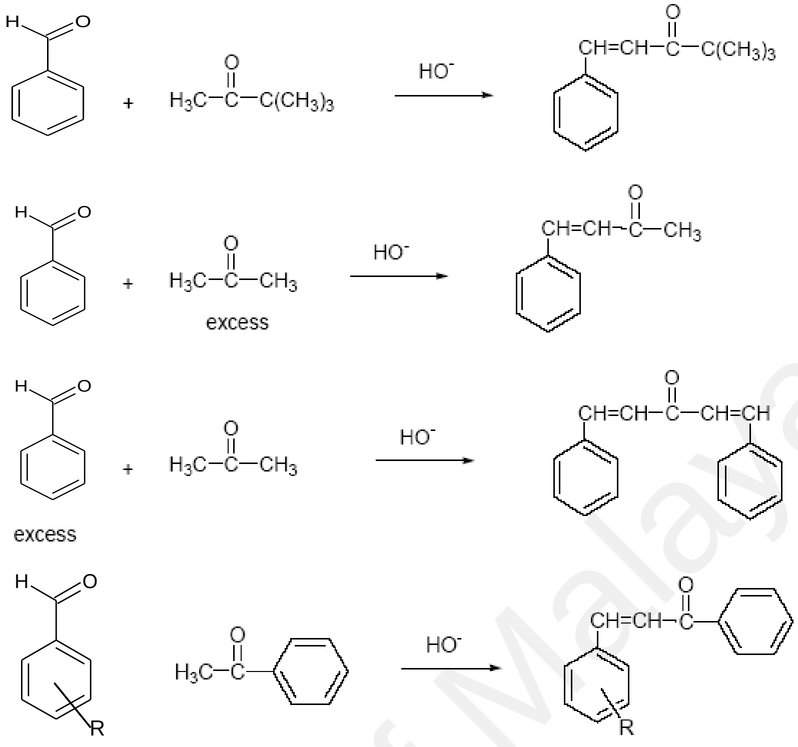

Figure 2.24: Aldol condensation of ketones and aromatic aldehydes possessing no α-hydrogen

Aldol condensation via classical method is no longer favourable as the process suffers from reverse and side reactions resulting in low yields of the products. This has given great limitation to the reaction. However, the effort to increase the versatility of the reaction has not stopped. The use of various kind of catalyst has been performed in order to achieve high asymmetric aldol reaction.

In an attempt to perform an aldol condensation reaction under various conditions, some metal ions were used as catalyst or reagent. The work on this type of compound can be said to be initiated by Irie and co workers [157] in 1980. Nevertheless, the work on aldol condensation reaction mediated specifically by copper(II) ion was initiated by Iwata and co workers [158,159] in 1974. The quest of finding the best catalysts for the reaction has never stopped. Several catalysts were reported and new understanding of the reaction mechanism has emerged. Early studies on the catalytic properties of transition metal ions, specifically metal(II) ions, in aldol condensation reaction was sparked by the drive to understand the role of metal ion for the activity of Class II aldolases [158-160]. As the importance of aldol condensation reaction become very apparent, a lot more studies using different catalysts have taken place. In the literature, there exists study on aldol condensation reaction using metal(II) complexes [157, 161]. Apart from this, metal(II)-polymer complex catalyst [162] has also been used. In addition, there were also reports on using catalyst, such heterobimetallic asymmetric catalyst [163], molecular iodine [164], organo catalyst [165], and rare earth(III) pentafluorooctane [166].

Iwata and coworkers reported on the ability of copper(II) ion (from $CuCl_2.2H_2O$) to catalyze the mixed aldol condensation reaction between aldehydes and ketones to give benzylideneacetones. The scope and limitation of the aldol condensation was found through the use of various aldehydes and ketones. The authors noted that aromatic aldehydes, namely *p*-chlorobenzaldehyde and salicyldehyde, did not form condensation product when reacted with ketones. The explanations were: (a) occupation of the catalytic site of the metal ion by the electron-rich substituent, or (b) decreasing electrophilicity of the aldehyde group as a result of the inductive and resonance effects of the substituent. It was also found that aliphatic aldehydes, namely propanal and pentanal, gave no condensation products when reacting with acetone. The aldol reaction of aldehydes and 2-butanone showed that the aldehydes used attacked the methylene group at C3 of 2-butanone and not at C1, which is similar to the mineral-acid-catalyzed aldol condensation. In contrast to acetone, aliphatic aldehydes was found to give any condensation products when reacting with 2-butanone but with low yield. The author has also found that the following reactions did not give any condensation products: (a) acetophenone with *p*-anisaldehyde, (b) 2-pentanone with benzaldehyde, (c) 2-pentanone with *p*-anisaldehyde, (d) 2-pentanone with *o*-anisaldehyde, (e) 2-pentanone with 2,6-dimethoxybenzaldehyde, and (f) acetylacetone with *o*-anisaldehyde.

It was believed that the reaction of this mixed-aldol condensation reaction is similar with the enzymatic reaction of glyceraldehyde and dihydroxyacetone phosphate catalysed by Aldose (Class II). The reaction requires a divalent metal(II) ion to promote the same condensation reaction. Specifically, the Cu(II) ion in the reaction has played a dual role: (a) assisting the enolisation process of ketones, and (b) activation of aldehyde to be nucleophilically attacked by ketones. **Figure 2.25** shows the suggested mechanism of the reaction.

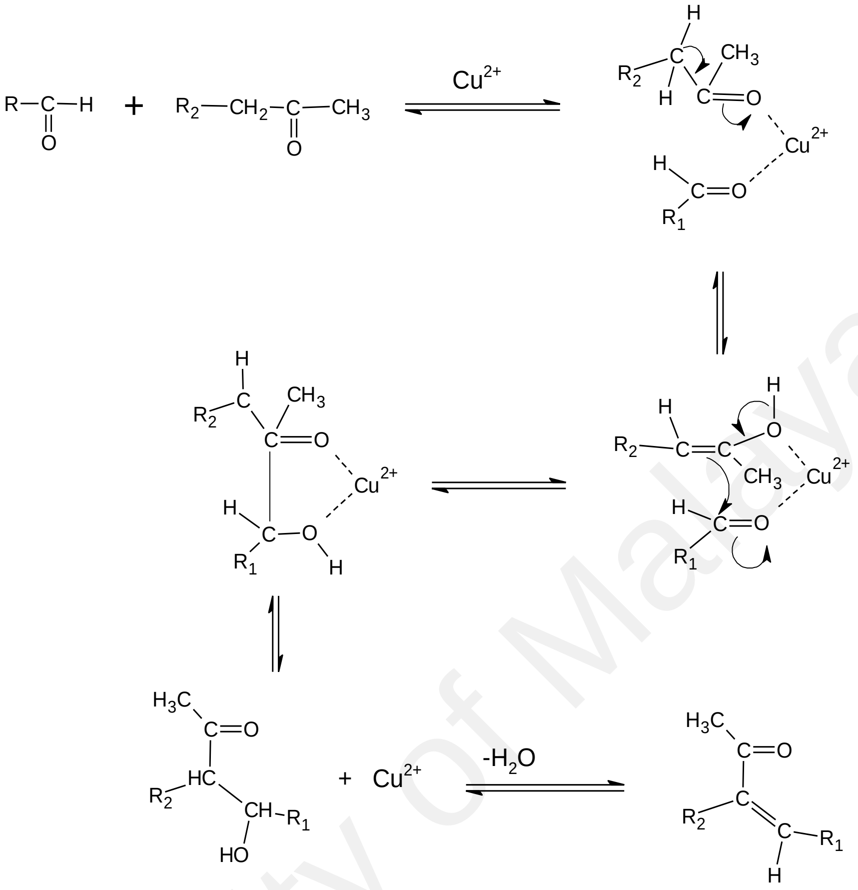
Figure 2.25: Aldol condensation reaction promoted by copper(II) ion

If this mechanism is truly a reality, it will resemble the one proposed for the Class II aldolases with respect to the role of metal(II) ions (**Figure 2.26**) [167-170].

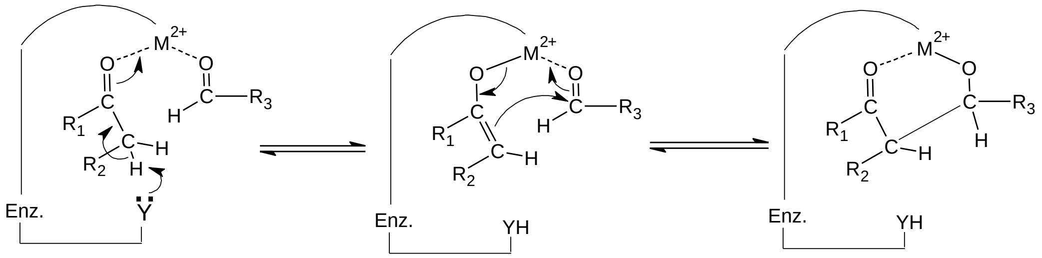
Figure 2.26: Mechanism of C-C bond-forming reaction for Class II aldolases

It was also found that the mixed condensation reaction predominates over the self-condensation of ketone, even with a large excess ketones present. Three major conclusions were proposed by the authors:

(a) Any ketone can be used as a solvent (reactant) for the reaction.

(b) A stable ketone-Cu(II) complex is unsuitable as a source of Cu(II) ion required for the reaction.

(c) Aryl alkyl ketones are unsuitable for the reaction. Only aliphatic ketones are suitable. As for the aldehydes, hydroxyl, halogeno and nitro substituents inhibit the reactions, while methoxy groups and hetero atoms in the aromatic will allow the reaction to take place.

The drawback of self-condensation and polycondensation, especially when a cross-coupling reaction is carried out using conventional base or acid catalysts, has also prompted considerable attention to be focused on directed coupling of two carbonyl compounds in a regioselective manner [171,172]. A very useful approach has been the reaction of a carbonyl compound with suitably reactive metal enolate or enol-ether derived regioselectively from the other carbonyl compound. Of the various metal derivatives, boron enolates were found to react most selectively with aldehydes [173-175]. In several cases, the desired aldol condensation products have also been obtained by using some transition-metal complexes as catalysts, namely Mn(II), Fe(II), Co(II), Ni(II), Cu(II) and Zn(II), with different ligands [176]. Among these complex, Co(II)-bipyridyl has been found to be more reactive, but it was mostly used for condensation reactions of aromatic aldehydes and only acetophenone in DMF.

The use of dinuclear copper(II) complex to mediate the regioselective aldol-type condensation has also been reported. The reaction involved the regioselective addition of α-methyl and/or α-methylene ketones, namely acetone, acetophenone, 2-butanone, 4-methyl-2-pentanone and *trans*-4-phenyl-3-butene-2-one, to one of the carbonyl groups of the symmetric 2-hydroxy-5-methyl-benzene-1,3-dicarbaldehyde through its dinuclear copper(II) complex. The formation of the complex is shown to activate the carbonyl group to become more susceptible to nucleophilic attack, thus leading to the C-C bond forming reaction to take place, giving a yield of the product of 50% to 70% [177]. Copper(II)-2,2'-bipyridine complex has also been shown to catalyze aldol condensation reaction of 2-butanone and benzaldehyde, primarily as a purpose of becoming a model for metal ion in the enzyme, under neutral condition to afford liberated α,β-unsaturated ketones without any by-product [160]. The yield of the product depends on the type of counter anion present in the complex, ranging from 0% to 60%, which is remarkably higher in comparison with that catalyzed by the copper(II) ion. The result of the study also shows that the aldol condensation took place at the C_1 position of 2-butanone. This was rather different compared to the aldol condensation catalyzed by $CuCl_2.2H_2O$, which took place at the C_3-position of 2-butanone [154]. It is important to note that the aldol condensation of 2-butanone and aldehyde with strong bases occurs preferentially at the C_1 position, while mineral acid-catalyzed condensation occurs preferentially at the C_3 position [178-180].

It is of great important to note that this C-C bond-forming reaction is largely affected by the kind of ligands bonded to the metal [157]. Under neutral condition, the following reaction:

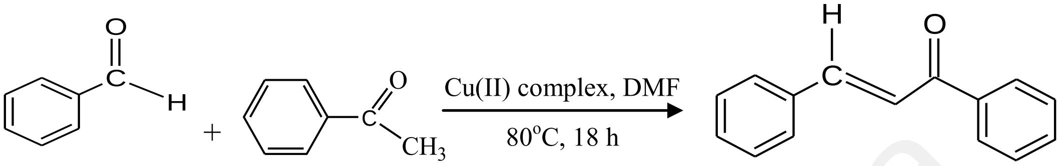

gave very low yield when carboxylic acids, namely $(COOH)_2$, $HSCCH_2COOH$ and NH_2CH_2COOH, were used as the ligands (0 to 17%) compared to when acetic acid was used as the coordinated ligand (53%). When aliphatic amines were employed, the yield of $C_6H_5CH{=}CHCOC_6H_5$ was comparable to that of acetic acid. The highest yield of the product were formed when tertiary aromatic amines, namely 2,2'-bipyridine and 1,10-phenanthroline, were used as the coordinated ligands (82%). However, ligands such as 6,6'-dimethyl-2,2'-bipyridine and 2,2':6',2"-terpyridine seemed to inhibit the reaction, with yields of 22-30% only. This could be ascribed as steric hindrance by the bulky ligand molecules. In all these reactions with several difference ligands, the driving force of the catalytic property of bipyridine ligand is the strongest, and can be explained by attributing it to the back π-bonding in the metal complex. That is, a higher positive charge is induced in the metal(II) ion by the coordination of the bipyridine ligand. The oxygen atoms in the carbonyl groups of the aldehyde and ketone may be more activated by the coordination to the Cu(II)-bipy complex than other coordinated ligands.

References

[1] J.D. Peterson, W.R. Murphy, R. Sahai, K.J. Brewer and R.R. Ruminski, *Coord. Chem. Rev.* 64 (1985) 261.

[2] P.J. Steel, *Coord. Chem. Rev.* 106 (1990) 227.

[3] C.T. Chen and K.S. Suslick, *Coord. Chem. Rev.* 128 (1993) 293.

[4] J.R.J. Sorenson, in: H. Sigel (Ed.), *Metal Ions in Biological Systems,* vol. 14, Marcel Decker, New York, 1982.

[5] E.G. Bakalbassis, M. Korabik, A. Michailidis, J. Mrozinski, C. Raptopoulo, S. Koulika, A. Terzis, and D. Tsaousis, *J. Chem. Soc., Daltons Trans.* (2001) 850.

[6] L. Sieron, M. Bukowska-Strzyzewska, M. Korabik and J. Mrozinski, *Polyhedron* 21 (2002) 2473.

[7] B. Kozlevcar, I. Leban. M. Petric, S. Petricek, O. Roubeu, J. Reedijk and P. Segedin, *Inorg. Chim. Acta* 357 (2004) 4220.

[8] B.P. Murphy and B.J. Hathaway, *Coord. Chem. Rev.* 124 (1993) 63.

[9] M. Melnik, M. Koman, D. Hudecova, J. Moncol, B. Dudova, T. Glowiak, J. Mrozinski and C. Holloway, *Inorg. Chim. Acta* 308 (2000) 1.

[10] J. Moncol, M. Palicova, P. Segl'a, M. Koman, M. Melnik, M. Valko and T. Glowiak, *Polyhedron* 21 (2002) 365.

[11] M. Melnik, *Coord. Chem. Rev.* 42 (1982) 259.

[12] M. Kato and Y. Muto, *Coord. Chem. Rev.* 92 (1988) 45.

[13] M.P. Suh, M.Y.Han, J.H. Lee, K.S. Min and C. Hyeon, *J. Am. Chem. Soc.* 120 (1998) 3819.

[14] Y.H. Chung, H.H. Wei, Y.H.Liu, G.H. Lee and Y. Wang, *Polyhedron* 17, (1988) 449..

[15] B. Zurowska and J. Mrozinski, *Inorg. Chim. Acta* 342 (2003) 23.

[16] B. Zurowska, J. Ochoki, Z. Ciunik, J. Mrozinski and J. Reedijk, *Inorg. Chim. Acta* 357 (2004) 755.

[17] C.J. O'connor, E.E. Eduok, F.R. Fronczek and O.Kahn, *Inorg. Chim. Acta* 105 (1985) 107.

[18] P.R. Levstein and R. Calvo, *Inorg. Chem.* 29 (1990) 1581.

[19] W.E. Hatfield and R. Whyman, *Transition Met. Chem.* 5 (1969) 47.

[20] R.J. Doedens, *Prog. Inorg. Chem.* 21 (1976) 209.

[21] J. Catterick and P. Thornton, *Adv. Inorg. Chem.* 20 (1977) 291.

[22] A.P. Ginsberg, *Inorg. Chim. Acta Rev.* 5 (1971) 313.

[23] S. Petricek and M. Petric, *Thermochim. Acta* 302 (1997) 35.

[24] A. Doyle, J. do Prado Felcman, M.T. Gambardella, C.N. Verani and M.L. Braganca Trisao, *Polyhedron* 19 (2000) 2621.

[25] N.E. Ghermani, C. Lecomte, C. Rapin, P. Steinmetz, J. Steinmetz and B. Malaman, *Acta. Cryst. Sec. B* 50 (1994) 157.

[26] T.R. Lomer and K. Perera, *Acta Cryst., Sect. B* 30 (1974) 2913.

[27] T.R. Lomer and K. Perera, *Acta Cryst., Sect. B* 30 (1974) 2912.

[28] R.L. Martin and H. Waterman, *J. Chem. Soc*. 1359 (1959).

[29] A.M. Greenaway, C.J. O'Connor, J.W. Overman and E. Sinn, *Inorg. Chem.* 20 (1981) 1508.

[30] P.J. Hay, J.C. Thibeult and R. Hoffman, *J. Am. Chem. Soc.* 97 (1975) 4884.

[31] S. Mukhopadhyay, D. Mandal, P.B. Chatterjee, C. Desplanches, J.P. Sutter, R.J. Butcher and M. Chaudhury, *Inorg. Chem.* 43 (2004) 8501.

[32] B. Zurowska and J. Mrozinski, *Inorg. Chim. Acta* 342 (2003) 23.

[33] S. Youngme, C. Pakawatchai, W. Somjitsripunya, K. Chinnakali and H.-K, Fun, *Inorg. Chim. Acta* 303 (2000) 181.

[34] M. Inoue and M. Kubo, *Inorg. Chem.* 9 (1970) 2310.

[35] E. Colacio, J.M. Dominguez-Vera, R. Kivekas, J.M. Moreno, A. Romerosa and J. Ruiz, *Inorg. Chim. Acta* 212 (1993) 115.

[36] R.L. Martin and H.J. Waterman, *J. Chem. Soc.* 1359 (1959).

[37] J.N. van Neikerk and F.R.L Schoening, *Acta Cryst.* 6 (1953) 227.

[38] F. Hanic, D. Stempelova and K. Hanovica, *Acta Cryst.* 17 (1964) 633.

[39] G.A. Barclay and C.H.L. Kennard, *J. Chem. Soc.* 17 (1961) 633.

[40] I.Y. Ahmed and A.L. Abu-Hijleh, *Inorg. Chim. Acta.* 61 (1982) 241.

[41] B.K.Koo, *Bull. Korean Chem. Soc*. 22(1) (2001) 113.

[42] J. Ploquin, *Bull. Soc. Chim. France*, 18 (1951) 757.

[43] M. Kato, H.B. Jonassen and J. C. Fanning, *Chem. Rev.* 64 (1964) 99.

[44] F. Hanic and J. Michalov, *Acta Cryst.* 13 (1960) 299.

[45] M. Inoue, M. Kishita and M. Kubo, *Inorg chem.*.3 (1965) 239.

[46] C.S. Fountain and W.E. Hatfield, *Inorg. Chem.* 4 (1965) 1368.

[47] W.E. Hatfield, C.S. Fountain and R. Whyman, *Inorg. Chem.* 5 (1966) 1855.

[48] F.G. Herring, B. Landa, R.C. Thompson and C.F. Schwerdtfeger, *J. Chem. Soc. (A)* (1971) 528.

[49] J. Lewis and R.C. Thompson, *Nature.* 200 (1963) 468

[50] J. Lewis, Y.C. Lin, L.K. Royston and R.C. Thompson, *J. Chem. Soc.,* (1965) 6464.

[51] J. Lewis, F.E. Mabbs, L.K. Royston, and W.R. Smail, *J. Chem. Soc. (A)* (1969) 291.

[52] M. Yamanaka, H. Uekusa, S. Ohba, Y. Saito, S. Iwata, M. Kato, T. Tokii, Y. Muto and O.M. Steward, *Acta Cryst.* B47 (1991) 344.

[53] O. Kahn, *Magneto-Structural Correlatios in Exchange Coupled System*, edited by R.D. Wilet, D. Gatteschi and O. Khan, 1985, pp. 37-56.

[54] T. Kawata, H. Uekusa, S. Ohba, T.Furukawa, T. Tokii, Y. Muto and M. Kato, *Acta Cryst.* B48 (1992) 253.

[55] L. Manojlovic-Muir, *Chem. Comm.* (1967) 1057.

[56] W. Harrison, S. Rettig and J. Trotter, *J. Chem. Soc, Dalton,* 2 (1972) 1852.

[57] M. Melnik, M. Dunaj-Jurco and M. Handlovc, *Inorg. Chim. Acta,* 86 (1984) 185.

[58] L. Strinna Erre, G. Micera, F. Cariai and G. Ciani, *Inorg. Chem.* 24 (1985) 2297.

[59] C.N. Banwell and E.M. McCash, *Fundamentals of Molecular Spectroscopy*, 4th Ed., Tata McGraw Hill, U.K, 2004

[60] D.A. Skoog and J.L. Leary, Principle of Instrumental Analysis. 4th ed. Philadelphia: Saunders College Publishing 1991 p.252.

[61] C.A. Agambar and K. G. Orrell, *J. Chem. Soc. A* (1969) 897.

[62] G.B. Deacon and R.J. Philips, *Coord. Chem. Rev.* 33 (1980) 227.

[63] I.A. Lee-Thorp, J.E. Ruede and D.A. Thornton, *J. Mol. Struc.* 50 (1978) 65.

[64] T.A. Stephenson, E. Bunnister and G.J. Wilkinson, *J. Chem. Soc.* (1964) 2538

[65] K. Nakamoto, Y. Morimota and A.E. Martell, *J. Am. Chem. Soc.* 83 (1961) 4528.

[66] G.B. Deacon and R.J. Philips, *Coord. Chem. Rev.* 33 (1980) 227.

[67] Y. Kuroda, J. Chem. Soc. Japan, *Pure Chem. Sect.* 82 (1961) 1624.

[68] Y. Kuroda, A. Sasano and M. Kubo, *Bull. Chem. Soc. Jpn.* 39 (1966) 1002.

[69] J. Kobylecke, B. Ptaszynski, R. Rogaczewski and A. Turek, *Thermochim. Acta* 407 (2003) 25.

[70] T. Inomata and T. Moriwaki, *Bull. Chem. Soc. Jpn*. 46 (1973) 1148.

[71] A. Turek, J. Kobylecka and B. Ptaszynski, *J. Therm. Anal. Cal.* 78 (2004) 513.

[72] W. Ference, A. Walkow-Dziewulska and P. Sadowski, *J. Therm. Anal. Cal.* 82 (2005) 513.

[73] P. Kogerler, P.A.M. Williams, B.S. Parajon-Costa, E.J. Baran, L. Lezama, T. Rojo and A. Muller, *Inorg. Chim. Acta.* 268 (1998) 239.

[74] G.B. Deacon and F. Huber, *Inorg. Chim. Acta.* 104 (1985) 41.

[75] F.A. Cotton and G. Wilkinson, *Advances in Inorganic Chemistry*,Wiley, New York, 2nd Ed. 1966.

[76] H.A. Jahn and E. Teller, Proc. Of the Royal Soc. (London) A161, 1937, 220.

[77] B. Bleany and K.D. Bowers, *Proc. R. Soc. London, Ser. A* 214 (1952) 451.

[78] M. Kondo and M. Kubo, *J. Phys. Chem.* 62 (1958) 1558.

[79] S. Yamada, H. Nakamura and R. Tushida, *Bull. Chem. Soc. Jpn.* 31 (1958) 303.

[80] J. Catterick and P. Thornton, *Adv. Inorg. Chem.* 21 (1976) 209.

[81] D.P. Graddon, *J. Inorg. Nucl. Chem.* 14 (1960) 1961.

[82] B.J. Hathaway and D. E. Billing, *Coord. Chem. Rev.* 5 (1970) 143.

[83] L. Dubicki and R.L. Martin, *Inorg. Chem.* 5 (1966) 2203.

[84] M.Getzlaff, *Fundamentals of Magnetism*, Springer, Berlin, 2008.

[85] G. I. Likhtenshtein, J. Yamauchi, S. Nakatsuji, A. I. Smirnov, and R. Tamura, *Nitroxides: Applications in Chemistry, Biomedicine, and Materials Science,* WILEY-VCH Verlag GmbH & Co. KGaA, Weinheim, chapter 1, 2008.

[86] G.A. Bain and J.F. Berry Journal of Chemical Education, 85(4) 2008 532-536.

[87] A.E. Martel and M. Clavin, *Chemistry of the Metal Chelate Compounds,* Prentice Hall, New York, N.Y., 1952: Chapter 6.

[88] P.W. Selwood, *Magnetochemistry,* Interscience Publishers, Inc., New York, N.Y., 1956, p.235.

[89] B.C. Guha, *Proc. R. Soc. London, Ser. A* 206 (1952) 353.

[90] J. Lifschitz, and E. Rosenbohm, *Electrochem.* 21 (1975) 499.

[91] T. Kawata, H. Uekusa and S. Ohba, *Acta Cryst.* B48 (1992) 253.

[92] B.N. Figgis and R.L. Martin, *J. Chem. Soc.* (1956) 3837.

[93] H. Koizumi, K. Osaki and T. Watanabe, *J. Phys. Soc. Jpn,* 18 (1963) 117.

[94] R. Kiriyama, H. Ibamoto and K. Matsuo, *Acta Cryst.* 7 (1954) 482.

[95] D.M.L Goodgame, N.J. Hill, D.F. Marsham, A.C. Skapski, and M.L. Smart *Chem. Commun*. (1969) 629.

[96] R.A. Zelonka and M.C. Baird, *Inorg. Chem.* 11 (1972) 134.

[97] R.L. Beddoes, J.A. Connor, D. Dubowski, A.C. Jones, O.S. Mills and R. Price, *J. Chem. Soc., Dalton Trans.* (1979) 781.

[98] R.W. Jotham, S.F.A. Kettle and J.A. Marks, *J. Chem. Soc. Dalton Trans.* (1972) 428.

[99] J. Mrozinski and K. Heyduck, *J. Coord. Chem.,* 13 (1984) 291.

[100] P.J. Hay, J.C. Thibeault, and R. Hoffman, *J. Am. Chem. Soc.* 97 (1975) 4884.

[101] S. Emori, H. Kurihara and Y. Muto, *Bull. Chem. Soc. Jpn*, 61 (1988) 3317.

[102] S. Emori, N. Morishita and Y. Muto, *Bull. Chem. Soc. Jpn,* 60 (1987) 1913.

[103] S. Emori, H. Nonaka and Y. Muto, *Bull. Chem. Soc. Jpn,* 61 (1988) 1812.

[104] S. Emori, Y. Tokoyama and Y. Muto, *Bull. Chem. Soc. Jpn,* 60 (1987) 4445.

[105] R.W. Jonathan, F.A. Kettle and J.A. Marks, *J. Chem. Soc., Dalton Trans.,* (1972) 428.

[106] D.F. Evans, *J. Chem. Soc.*, (1959) 2003.

[107] R.A. Zelonka and M.C.Baird, *Inorg. Chem,* 11, (1972) 134.

[108] A. M. Donia, *Thermochim. Acta,* 320 (1998) 187.

[109] S.P. Sovilj, K. Babic-Samardzija and D.M. Minic, *Thermochim. Acta* 370 (2001) 29.

[110] G. Liptay, E. Papp-Molnar and K. Burger, *J. Inorg. Nucl. Chem.* 31 (1969) 247.

[111] L.H.J. Lajunen, P. Kokkonen, A. Nissi and H. Ruotsalainen, *Thermochim. Acta,* 72 (1984) 219.

[112] D. Czakis-Sulikowska and A. Czylkowska, *J. Therm. Anal. Cal.* 71 (2003) 395.

[113] E. M. Abdullah and A.A. Said, *Thermochim. Acta* 405 (2003) 260.

[114] W. Brzyska and W. Wolodkiewicz, *Thermochim. Acta* 242 (1994) 131.

[115] Y. Akama, *J. Therm. Anal. Calor.* 45, (1995) 1501.

[116] K. Nejati, Z. Rezvani and B. Massoumi, *Dyes Pigm.*75 (2007) 653.

[117] W.W. Wendlandt and J.P. Smith, *J. Inorg. Nucl. Chem.* 25 (1963) 843.

[118] W.W. Wendlandt and L.A. Funes, *J. Inorg. Nucl. Chem.* 26 (1964) 1157.

[119] T. D. O'Brien and J.C. bailar, *J. Am. Chem. Soc.* 67 (1945) 856.

[120] J.L. Bear and W.Wendlandt, *J. Inorg. Nucl. Chem.* 17 (1961) 286.

[121] W.W. Wendlandt and L.A. Funes, *J. Inorg. Nucl. Chem.* 26 (1964) 1879.

[122] C. Valenzuela and A. Bernalte, *Thermochim. Acta* 156 (1989) 231.

[123] P.W. Bowman and L.B. Rogress, *J. Inorg. Nucl. Chem.* 28 (1966) 2215.

[124] A. Akhavein and J.E. House, *J. Inorg. Nucl. Chem.* 32 (1970) 1479.

[125] R. Farran and J. E. House, *J. Inorg. Nucl. Chem.* 34 (1972) 2219.

[126] P.Roman, A. Luque, J.I. Beitia and C. Guzman-Miralles, *Thermochim. Acta.* 231 (194) 113.

[127] P.Roman, J.I. Beitia and A. Luque, *Thermochim. Acta.* 233 (1994) 223.

[128] P.Roman, J.I. Beitia and A. Luque, *Thermochim. Acta.* 241 (1992) 113.

[129] D.T. Sawyer, W.R. Heinemen and J.M. Beebe (eds.) *Chemistry Experiments for Instrumental Methods,* John Wiley & Sons. Inc, 1984, pp.72-79.

[130] A.I. Vogel (ed.) *Quantitative Inorganic Analysis Including Elementary Instrumental Analysis*, John Wiley & Sons, Inc, (1978) pp 632-633.

[131] R. Greef, R. Peat, L.M. Peter, D. Pletcher and J. Robinson (eds.), *Instrumental Methods in Electrochemistry,* Ellis Horwood Ltd. Chichester, England (1985) pp 178-190.

[132] R.D Braun (ed.) *Introduction to Instrumental Analysis,* McGraw-Hill Book Company, New York (1987) pp. 785-793.

[133] J.P. Gisselbrecht, M. Gross, A.H. Alberts and J.M. Lehn, *Inorg. Chem.*, 19 (1980) 1386.

[134] E.F. Hasty, L.J. Wilson and D.N. Hendrickson, *Inorg. Chem.* 17 (1978) 1834.

[135] R.R. Gagne, R.P. Kreh, and J.A. Dodge, *J. Am. Chem. Soc.* 101 (1977) 6971.

[136] R.R. Gagne,C.A. Koval and T.J. Smith, *J.Am. Chem. Soc.* 99 (1977) 8367.

[137] D.E. Fenton, R.R. Schroder and R.L. Lintvedt, *J. Am. Chem. Soc*. 100 (1978) 1931.

[138] D.E. Fenton and R.L. Lintvedt, *J. Am. Chem. Soc.* 100 (1978) 6367.

[139] R.R Gagne, C.L. Spiro, T.J. Smith, C.A. Hamann, W.R. Thies and A.K. Shiemka, *J. Am. Chem. Soc.* 103 (1981) 4073.

[140] S.K. Mandal and K. Nag, *J. Chem. Soc. Dalton Trans.* (1983) 2429.

[141] H. Dhillon, K. Sharma, R. Gehlot and S. Kumbhat, *Electrochem. Commun.*11 (2009) 878.

[142] X. Zhou, X. Meng, W. Cheng, H. Hou, M. Tang and Y. Fan, *Inorg. Chim. Acta* 360 (2007) 3467.

[143] P. Amudha, M. Thirumavalavan and M. Kandaswamy, *Polyhedron* 18 (1999) 1363.

[144] A.M. Sosa, V.M. Ugalde-Saldiver, I. Gonzalez and L. Gasque, *J. Electroanal. Chem.* 579 (2005) 103.

[145] K. Shanmuga Bharati, S. Sreedaran, A. Kalilur Rahiman, K. Rajesh and V. Narayanan, *Polyhedron* 26 (2007) 3993.

[146] N. Sengottuvelan, J. Manomanni and M. Kandaswamy, *Polyhedron* 21 (2002) 2767.

[147] D. Saravanakumar, N. Sengottuvelan, G. Priyadarshni, M. Kandaswamy and H. Okawa, *Polyherdon* 23 (2004) 665.

[148] M.K. Taylor and J. Reglinsko, L.E.A. Berlouis and A.R. Kennedy, *Inorg. Chim. Acta* 359 (2006) 2455.

[149] B. Das, P. Thirpathi, I. Mahender and K. R. Reddy, *J. Mol. Catal. A: Chem.* 247 (2006) 182.

[150] A. Kawamata, K. Inoue, T. Inabe, M. Kiguchi, M. Kato and Y. Taniguchi, *Chem. Lett.* 249 (1996) 29.

[151] A.T. Nielsen and W.J. Houlihan, *Org. React.* 16 (1968) 1.

[152] R.L. Reeves, in: S. Patai (Ed.), C*hemistry of Carbonyl Group*, Wiley/Interscience, New York, 1966, pp. 580-593.

[153] C. Behrendt, S. Dabek, J. Heck, D. Courtney, A.R. Manning, M.J. McGlinchey, H.M. Bunx and Y. Ortin, *J. Organomet. Chem.* 691 (2006) 1183.

[154] J. March, *Advanced Organic Chemistry*, fourth ed., Wiley, New York, 1992, p. 937.

[155] C. Palomo, M. Oiarbide and J.M. Garcia, *Chem. Soc. Rev.* 33 (2004) 65.

[156] A. I. Vogel, *A Textbook of Practical Organic Chemistry*, John Wiley and Sons, N. Y., 1956, page 718.

[157] K. Irie and K. Watanabe, *Bull. Chem. Soc. Jpn.* 53 (1980)1366.

[158] M. Iwata and S. Emoto, *Chem. Lett*. (1974) 959.

[150] M. Iwata and S. Emoto, *Bull. Chem. Soc. Jpn.*, 49 (1976) 1369.

[160] K. Irie and K. Watanabe, *Chem. Lett.* (1978) 539.

[161] B. M. Trost, H. Ito and E. R. Silcoff, *J. Am. Chem. Soc*.123 (2001) 3367.

[162] K. Irie, A. Imazawa and K. Watanabe, *Chem. Lett.* (1979) 1401.

[163] M. Yoichi, A.Yamada, N. Yoshikawa, H. Sasai and M. Shibasaki, *Angew. Chem. Int. Ed. Engl.* 36(17) (1997)1871.

[164] B. Das, P. Thirupathi, I. Mahender and K. R. Reddy, *J. Mol. Catal. A: Chem* 247 (2006) 182.

[165] S. Samanta and C. G. Zhao, *Tetrahedron Lett.* 47 (2006) 3383.

[166] W.B. Yi and C. Cai, *J. Fluorine Chem.* 126 (2005) 1553.

[167] R.D. Kobes, R.T. Simpson, B.J. Valee and W.J. Rutter, *Biochem.* 8 (1969) 585.

[168] C.E. Harris, R.D. Kobes, D.C. Teller and W.J. Rutter, *Biochem.* 8, (1969) 2442.

[169] A.S. Mildvan, R.D. Kobes and W.J Rutter, *Biochem.* 10 (1971) 1191.

[170] E.J. Heron and R.M. Caprioli, *Biochem.* 13 (1974) 4371.

[171] T. Mukaiyama, *Org. React*. 28 (1982) 203.

[172] D.A. Evans, J.V. Nelson and T.R. Taber, *In Topic in stereochemistry* (edited by N.L. Allinger, E.L. Eliel and S.H. Wilen), Vol. 13, p.1. John Wiley, New York (1983).

[173] M. Hirama, D.S. Garvey, L.D.-L Lu and S. Masamune, *Tetrahedron Lett.* (1979) 3937.

[174] T. Inoue and T. Mukaiama, *Bull. Chem. Soc. Jpn.* 53 (1988) 174.

[175] D.A. Evans, J.V. Nelson, E. Vogel and T.R. Taber, *J. Am. Chem. Soc.*103 (1981) 3099.

[176] K. Irie and K. Watanabe, *Bull. Chem. Soc. Jpn.* 55 (1982) 3208.

[177] B. Adhikary, A.K. Biswas and K. Nag, *Polyhedron,* 6(6) (1987) 1473.

[178] M. Stiles, D. Wolf and G. V. Hudson, *J. Am. Chem. Soc.* 81 (1959) 628.

[179] T. Mukaiyama and T. Inoue, *Chem. Lett.* (1976) 559.

[180] T. Inoue, T. Uchimaru and T. Mukaiyama, *Chem. Lett.* (1977) 153.

CHAPTER 3

EXPERIMENTAL

The research focused on the synthesis, structural elucidation, physical (thermal, magnetic, redox) and chemical properties (the C-C bond-forming reaction) of copper(II) arylcarboxylates of general formula $[Cu_2(4\text{-}XC_6H_4COO)_4]$, where X = H, NO_2, OH, NH_2, F, Cl, Br, I) and $3,5\text{-}(NO_2)_2C_6H_3$ (a total of nine complexes).

These complexes were obtained by the metathesis reaction between copper(II) acetate and the corresponding arylcarboxylic acid [1], structurally analysed by CHN/O elemental analyses, AAS (for Cu), and FTIR and UV-vis spectroscopies. Their thermal properties were determined by TGA, TGA-MS and DSC, room-temperature effective magnetic moment by the Gouy method, and redox properties by cyclic voltammetry. Additional, X-ray crystallography was used for crystalline complexes.

In the C-C bond-forming reaction, $[Cu_2(4\text{-}XC_6H_4COO)_4]$, where X = H, NO_2, OH, Cl) were reacted with CH_3COCH_3. The scope of the reaction was then studied by reacting $[Cu_2(C_6H_5COO)_4]$ with a mixture of $C_6H_5COCH_3$ and C_6H_5CHO. The mechanism of the reaction was studied by UV-vis spectroscopy, and the products of the reaction was analysed by ^{1}H-NMR, ^{13}C-NMR, GCMS and TGA and DSC.

3.1 Chemicals

The chemicals used in the research were AnalaR reagents obtained from commercial sources, and used as received.

3.2 Synthesis of Copper(II) Arylcarboxylates: General Method

Arylcarboxylic acid (0.04 mol) was dissolved in hot ethanol (50 ml). Copper(II) acetate monohydrate (0.02 mol) was added portion wise to the magnetically-stirred hot solution. The mixture was further heated for an hour, and the solid obtained was filtered off from the hot solution, washed several times with hot ethanol, and dried in the oven at about 90°C for one hour.

3.3 Instrumental Analyses

3.3.1 Elemental Analyses

(a) Analysis for copper

The instrument used for the analysis for copper was a Perkin-Elmer AAnalyst 800 flame atomic absorption spectrometer with a slit width of 100 microns. The percentage transmissions were recorded at 324.7 nm using a band pass setting of 0.2 and converted to absorbance. Five standard solutions (2.0 ppm, 4.0 ppm, 6.0 ppm, 8.0 ppm and 10.0 ppm) were prepared from the commercially available copper stock solution of 1000 ppm by dilution. These standard solutions were used to construct the calibration curve.

A solution of each sample was prepared by nitric acid digestion of an accurately weight solid sample and then diluted to 100 ml. The concentration of copper in the real sample was then calculated from the calibration curve as percent copper.

(b) Analysis for other elements

The instrument used for the analysis for carbon, hydrogen, nitrogen and oxygen were Perkin Elmer, PE 2400 Series II CHNS/O analyzer and, Thermo Finnigan Flash EA 110. The pre-weighed samples (2.0 mg) were wrapped in tin capsules and were passed through a combustion/reduction tube at 975°C.

3.3.2 Fourier Transform Infrared Spectroscopy

The Fourier Transform Infrared spectra (FTIR) were recorded over the wavenumber ranges 4000 – 400 cm^{-1} using a FTIR SPECTRUM RX 1 Perkin-Elmer spectrometer. The samples were prepared as potassium bromide (KBr) discs. The spectra of the corresponding acids and their sodium salts were also obtained for comparison.

3.3.3 UV-vis Spectroscopy

The UV-vis spectra of solid samples were recorded using a Shimadzu UV-vis-NIR spectrophotometer, while the spectra of samples in solutions were recorded on a Perkin-Elmer Lambda 35 UV-vis spectrophotometer using 1-cm quartz cuvettes. The spectra were recorded from 1100 nm to 190 nm in tetrahydrofuran (THF), dimethylsulfoxide (DMSO), dimethylformamide (DMF), and in methanol-acetic acid (95:5 v/v). The molar absorptivity (ε) was calculated using the Beer-Lambert's law: $A = \varepsilon c l$.

3.3.4 Nuclear Magnetic Resonance Spectroscopy

The ^{1}H-NMR and ^{13}C-NMR were recorded on a Jeol 400 MHz NMR spectrometer using $CDCl_3$ as a solvent. The chemical shifts were referenced to that of the residual $CHCl_3$ in the deuterated solvent.

3.3.5 Gas Chromatography-Mass Spectrometry

The mass spectrum was recorded in acetone or methanol on a Perkin-Elmer Clarus 600 GCMS with Elite-5MS capillary column with dimension 30 m (L) x 0.25 mm (ID) x 0.25 μm (DF), or on a Shimadzu GCMS-QP2010 Plus with RTx®-5MS capillary column having dimension 30 m (L) x 0.25 mm (ID) x 0.25 μm (DF). (Abbreviation: L = length; ID = inner diameter; DF = film thickness).

3.3.6 Thermogravimetry

The thermogravimetric analyses (TGA) were determined on a Perkin-Elmer Thermogravimetric Analyser TGA 6. The heating rate of 20°C min^{-1} and the temperature range was from 30°C to 900°C. The sample (8 – 12 mg) was placed in a cylindrical ceramic crucible under N_2 gas purging at the flow rate of 20 cm^3 min^{-1}.

3.3.7 Thermogravimetry-Mass Spectroscopy

Thermogravimetry-mass spectroscopy (TGMS) was performed on a TA Instrument TGA Q500 connected to MS Termostar^{TM}. The measurement was made at a heating rate of 20°C min^{-1} from 30°C to 1000°C. The sample analysed was $[Cu_2(C_6H_5COO)_4(C_2H_5OH)_2]$. The sample (4.7 mg) was placed in a cylindrical ceramic crucible under N_2 gas purging at the flow rate of 20 cm^3 min^{-1}.

3.3.8 Differential Scanning Calorimetry

Differential Scanning Calorimetric Analysis (DSC) was performed on a Rheometric Scientific DSC instrument. The sample (about 10 mg) was placed in a cylindrical aluminium crucible and heated from 35°C to 300°C at the rate of 10°C min^{-1} under N_2 gas purging at the flow rate of 10 cm^3 min^{-1}.

3.3.9 Magnetic Susceptibility

The room-temperature magnetic susceptibility measurements were done on powdered samples using the Gouy method performed on a Sherwood Auto Magnetic Susceptibility Balance. From the observed susceptibility, the magnetic moment, μ_{eff}, was calculated using formula: $\mu_{eff} = 2.824\ [T(\chi_m^{corr} - N\alpha)]^{1/2}$ B.M. The diamagnetic correction was made using Pascal's constant, and the temperature-independent paramagnetism ($N\alpha$) was taken as 60 x 10^{-6} c.g.s e.m.u. for each copper(II) ion.

3.3.10 Cyclic Voltammetry

The cyclic voltammograms (CV) were recorded in the same solvent used in the UV-vis studies. The instrument used was a Gamry Instrument Reference 600 potentiostat/galvanostat/ZRA. A three-electrode cell, consisting of a glassy carbon electrode as the working electrode, saturated calomel electrode (SCE) as the reference electrode and platinum wire as the counter electrode, was used. The supporting electrolyte was tetrabutylammonium tetrafluoroborate (TBATFB). The molarity of the electrolyte and the sampel were 0.1 M and 0.0015 M respectively. The initial potential range was +2.0 V to -2.0 V, and the scan rates were 20 - 200 mV s^{-1}. The sample solution was bubbled with N_2 gas prior measurement and the working electrode was polished with alumina on chamois leather before and after used.

3.3.11 X-Ray Crystallography

The data was collected on a Bruker SMART APEX CCD diffractometer at about 100 K using graphite-monochromated Mo-Kα radiation (λ = 0.71073 Å).

3.4 The Carbon-Carbon Bond-Forming Reaction

3.4.1 Reaction of copper(II) benzoate with acetone

(a) The procedure

Copper(II) benzoate (2.0 g; 3.3 mmol), acetone (50 cm^3) and concentrated hydrochloric acid (5 cm^3) were mixed in a round-bottomed flask. The dark brown solution formed was refluxed in an oil bath for 8 hours, and the excess acetone gently evaporated off on a hotplate, leaving a black solid in a green filtrate. The black solid was filtered, washed with distilled water, left to dry overnight at room temperature, and dried in an oven at 90°C for one hour. The product was a black, shiny and brittle solid, and the yield was 1.45 g.

The black solid was analysed by elemental analyses, FTIR, UV-vis, TGA, DSC, ^{1}H-NMR, ^{13}C-NMR, and GCMS.

(b) Analysing the components of the black solid

The solid (about 1.4 g) was immersed in aqueous $NaHCO_3$ and heated to remove excess benzoic acid. The black solid residue was filtered and allowed to air dry. The yield was 1.3 g.

The solid (0.52 g) was dissolved with diethyl ether (30 ml) and the solution was transferred in a 250-ml separatory funnel, and washed with 30 ml distilled water twice. The organic layer was dried over anhydrous magnesium sulfate for 5 minutes, filtered and the solvent evaporated off to form a dark brown solid. The yield was 0.17 g. The brown solid was passed through silica gel column, using diethyl ether-hexane (1:4 v/v) as the eluant. The eluate was a pale yellow solid, and the yield was 0.0252 g. It was analysed by FTIR, NMR and GCMS.

(c) Deducing the mechanism of the reaction

The UV-vis spectrum of the solution (10 ml) was recorded at different time interval while the reaction mixture was heated under reflux. The spectrum was recorded at five time intervals: initial time (before heating), and after 2, 4, 6 and 8 hours of refluxing.

(d) The kinetics data

The kinetics of the reaction system was also measured by recording the UV-vis spectrum of the reaction mixture at different temperatures and different time intervals. This kinetic study was performed by preparing similar reaction mixture as above, prepared individually based upon the intended measuring temperatures. The absorbance (A) was measured at specific wavelength, λ_{max} at this particular temperature within several time intervals. Particularly for this study, four different temperatures were set (30, 40, 50, and 57^{o}C). Four absorbance readings were taken at each temperature at 30 minutes time interval. A plot of ln [A_t-A_o] against t was constructed and the value of the rate constant (k) at a particular temperature was calculated from the slope. Another plot of ln k against 1/T (T, temperature in Kelvin) was constructed to determine the activation energy.

3.4.2 Reaction of copper(II) benzoate with acetophenone and benzaldehyde

The carbon-carbon bond-forming reaction was further investigated, using a mixture of acetophenone and benzaldehyde.

(a) The procedure

In a 50-ml round bottom flask, copper(II) benzoate (0.5 g; 0.58 mmol) was suspended in acetophenone (10 ml). Then, concentrated HCl (2.5 ml) was added and the mixture was magnetically stirred at room temperature. Benzaldehyde (3.0 ml) was added to the solution. The reaction mixture was stirred until all solids dissolved. The solution was then refluxed for 8 hours in an oil bath. The solution was allowed to cool to room temperature overnight.

30 ml of diethyl ether was added to the cooled reaction mixture. The cloudy green-brown solution formed was filtered to give a brown solid (0.1367 g) and a greenish dark brown filtrate.

The filtrate was transferred into a 250-ml separatory funnel, washed with 30 ml of distilled water and the funnel shaken vigorously to give two layers, namely top brown ether solution and bottom light green aqueous solution.

The ether layer was dried over magnesium sulfate anhydrous for 5 minutes to give a clear orange brown solution. The ether was partially removed on a rotatory evaporator, and then put in a vacuum dessicator overnight to give a dark orange liquid. The yield was 6.9711 g. The dark orange liquid was analysed by FTIR, ^{1}H-NMR and GCMS.

The dark orange liquid was purified by using column chromatography. The liquid (3.7022 g) was passed through a silica column using diethyl ether-hexane (1:4 v/v) as the eluate to give a bright yellow solution. The solution was left to air dry to form yellowish crystalline solid (1.225 g; mpt 57-58^{o}C). It was analysed by GCMS.

3.4.3 *Reaction of copper(II) 4-nitrobenzate, copper(II) 4-hydroxybenzoate and copper(II) 4-chlorobenzoate with acetone*

The procedure was the same as for the reaction of copper(II) benzoate with acetone (**Section 3.4.1 (a)**). The products were analysed by elemental analyses, FTIR, UV-vis and GCMS.

Reference

[1] C.S. Fountain and W.E. Hatfield, *Inorg. Chem.*, 4 (1965) 1368.

CHAPTER 4

RESULTS AND DISCUSSION

4.1 INTRODUCTION

This research project is focused on the synthesis and study of selected physical and chemical properties of nine copper(II) arylcarboxylates. Eight of the complexes have the general formula [$Cu_2(4\text{-}XC_6H_4COO)_4$], where X = H, NO_2, OH, NH_2, F, Cl, Br, and I, and one other is [$Cu_2(3,5\text{-}(NO_2)_2C_6H_3COO)_4$]).

These complexes are grouped into four categories: (a) unsubstituted (X = H); (b) have strongly electron-withdrawing group (X = NO_2); (c) have strongly electron-donating group (X = OH, NH_2), and (d) halogenated (F, Cl, Br, I), which has opposing electron-donating (mesomeric) and electron-withdrawing (inductive) effects of decreasing strength.

It is noted that research on copper(II) benzoate (X = H) and its derivatives has attracted the interests of many scientists since 1960's. However, their main focus was on the interesting structures and magnetism of these complexes [1-4]. Additionally, it is noted that the structures of these complexes, either paddle-wheel or polymeric, depend on the synthetic method used. Since the objectives of this research were to enrich and/or further explore the chemistry of these complexes (magnetic, thermal and redox properties, and their role in the carbon-carbon bond-forming reaction), it is important to state the synthetic method used to prepare these complexes and to firmly establish their structures so that valid comparison with published results may be made.

The complexes in this work were obtained by the metathesis reaction between $[Cu_2(CH_3COO)_4]$ and the corresponding arylcarboxylic acid, RCOOH (R = $4\text{-}XC_6H_4$ or $3,5\text{-}(NO_2)_2C_6H_3$) in CH_3CH_2OH. The general equation for the reaction is shown below.

$$[Cu_2(CH_3COO)_4] + 4\ RCOOH \longrightarrow [Cu_2(RCOO)_4] + 4\ CH_3COOH$$

It is most likely that the driving force for this reaction is a combination of three main factors: (a) stronger RCOO-Cu bond due to back donation from the fully filled π orbitals (*xy, xz,* and *yz*) of Cu(II) to the vacant π* orbitals of the aromatic carbon atoms of the arylcarboxylate ligand; (b) the shift in equilibrium position to the product side of the equation as the less soluble $[Cu_2(RCOO)_4]$ deposited out of the reaction mixture, and (c) an increase in entropy due to the formation of CH_3COOH (a liquid) as the by-product.

The structural formulas of these complexes were deduced from the elemental analysis, FTIR and UV-vis spectroscopies. Their room-temperature magnetic susceptibilities were measured by the Gouy method, their thermal properties by thermogravimetry (TGA) and differential scanning calorimetry (DSC), and their redox properties by cyclic voltammetry. Finally, the carbon-carbon bond-forming reaction of specifically selected complexes with methylcarbonyls (CH_3COCH_3, and a mixture of $C_6H_5COCH_3$ and C_6H_5CHO) were studied.

4.2 COPPER(II) BENZOATE

Copper(II) benzoate (CuB) was obtained as a dark blue powder, and its yield was 41%. It was soluble in acetone, tetrahydrofuran, dimethylsulphoxide, acetonitrile, dimethylformamide and pyridine, partially soluble in diethyl ether and ethyl acetate, and insoluble in water and hexane.

4.2.1 Structural elucidation

(a) Elemental analysis

The results of the elemental analysis (53.9% C, 3.9% H and 17.6% Cu) are in good agreement with those calculated for the chemical formula $CuC_{16}H_{16}O_5$ or $[Cu(C_6H_5COO)_2(CH_3CH_2OH)]$ (formula mass, 351.5 g mol^{-1}; 54.6% C, 4.5% H, 18.1% Cu).

(b) FTIR spectroscopy

The FTIR spectrum is shown in **Figure 4.1**. Three inferences can immediately be made from the spectrum. Firstly, the absence of C=O peak at about 1680 cm^{-1} indicates the absence for C_6H_5COOH; secondly, the spectrum is simple, in agreement with the highly symmetrical structure; and thirdly, a broad and strong band at around 3450 cm^{-1}, characteristic of ν(OH) vibration [5-6], supports the presence of CH_3CH_2OH as indicated from the results of the elemental analysis.

However, the peaks in the fingerprint region (1600-1000 cm^{-1}) need careful assignments as they either overlap or are very close together. The strong peaks at 1562 cm^{-1} and 1408 cm^{-1} can confidently be assigned as asymmetric (ν_{as}) and symmetric (ν_s) COO vibrations, respectively. Thus, the value of $\Delta\nu$ ($\Delta\nu = \nu_{as} - \nu_s$) for CuB is 154 cm^{-1}, suggesting a bridging bidentate C_6H_5COO, and thus might indicate a dimeric paddle-wheel structure. These peaks have been reported at about the same wavenumbers by other researchers. For example, Kozlevcar et al. [7] reported values of 1572 and 1403 cm^{-1} ($\Delta\nu$ = 169 cm^{-1}) for $[Cu_2(C_6H_5COO)_4(2\text{-}H_2NC_5H_4N)_2]$, while Sequeira et. al [8] reported values of 1562 and 1408 cm^{-1} ($\Delta\nu$ = 154 cm^{-1}) for $[Cu_2(C_6H_5COO)_4(H_2O)_2]$.

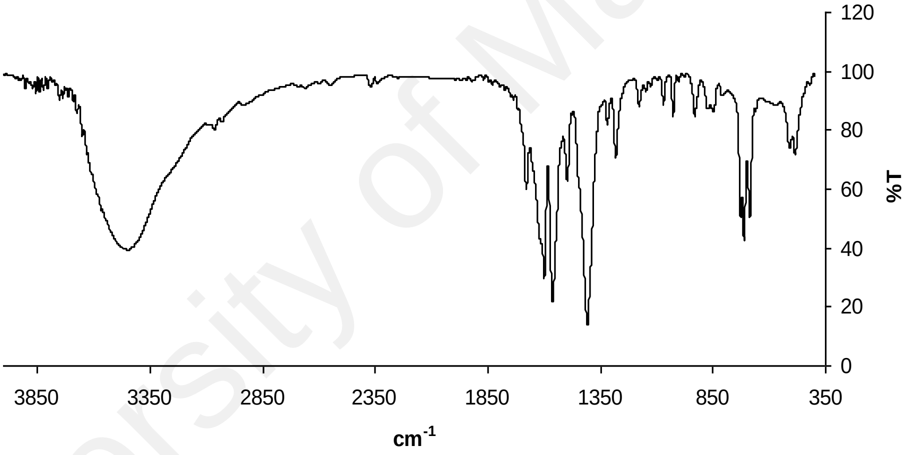

Figure 4.1: FTIR spectrum of CuB

(c) UV-vis spectroscopy

The UV-vis spectra were recorded as a solid sample and as solutions in different solvents so as to ascertain its geometry at Cu(II), nuclearity and structural stability.

The spectrum of the solid sample (**Figure 4.2**) shows *d-d* bands at 820 nm (a shoulder), 674 nm (broad), and 450 nm (a weaker shoulder), and a much stronger charge transfer band at 370 nm, and two overlapping strong intraligand bands at 265 nm and 227 nm. The *d-d* band at 674 nm, termed Band I, is typical for a complex with the square pyramidal geometry at Cu(II) [9-12].

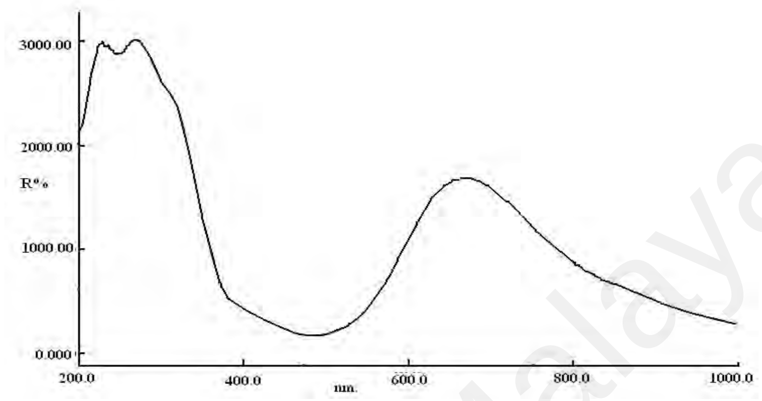

Figure 4.2: UV-vis spectrum of solid CuB

Thus, combining the results of the elemental analysis, and FTIR, UV-vis spectroscopies, it is proposed that CuB is a dimeric complex with the chemical formula $[Cu_2(C_6H_5COO)_4(CH_3CH_2OH)_2]$ and paddle-wheel structure as shown in **Figure 4.3**.

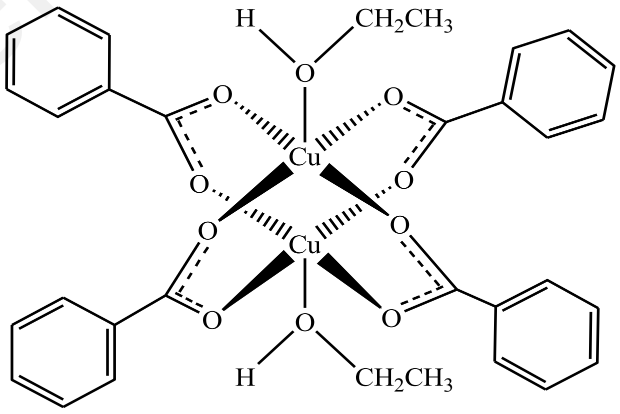

Figure 4.3: Proposed structural formula of CuB

The molecular orbital diagram for the dimer, drawn based on the C_{4v} local symmetry at [Cu(II)] centre and a triplet ground state (two unpaired electrons) is shown in **Figure 4.4**.

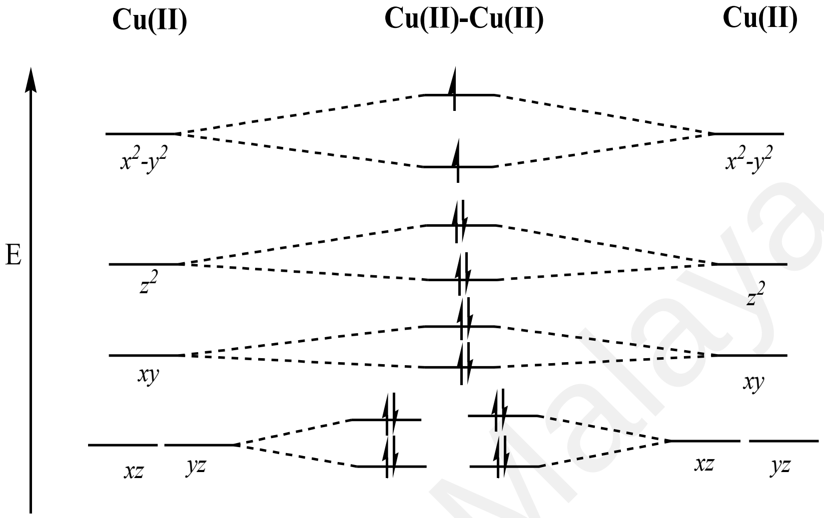

Figure 4.4: Molecular orbital diagram for CuB, showing only the interaction of the *d* orbitals and the triplet state (the diagram is not drawn to scale)

In is noted that there is no Cu-Cu δ bond, though the result of magnetic susceptibility study (*see later*) indicates the existence of magnetic coupling between the two Cu(II) centres. Based on the molecular orbital diagram above, the electronic transition associated with Band 1 ($xy \rightarrow x^2 - y^2$) is shown in **Figure 4.5**.

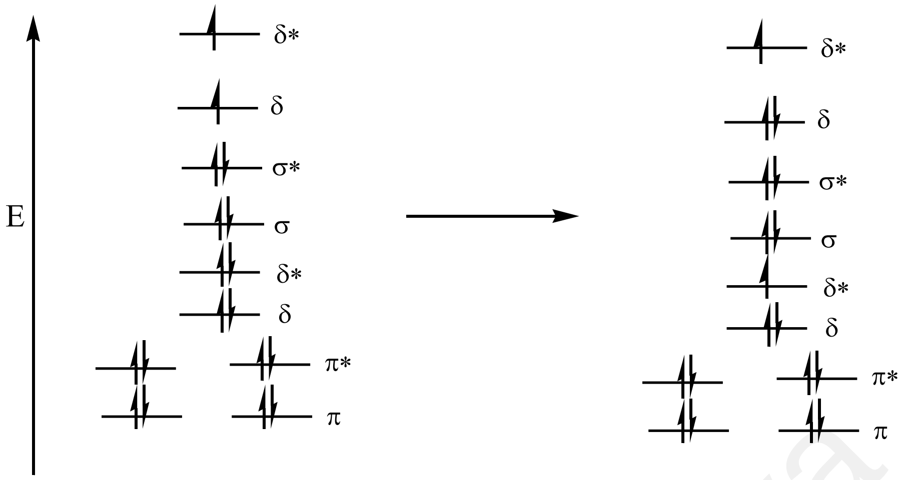

Figure 4.5: The electronic transition associated with Band 1 for CuB

It is noted that Band 1 for CuB (674 nm) is blue shifted compared to those reported in the literature. For example, Kozlevcar et. al reported a value of 726 nm for [$Cu_2(C_6H_5COO)_4(2\text{-}H_2NC_5H_4N)_2$] [7], while Melnik et. al reported a value of 714 nm for [$Cu_2(C_6H_5COO)_4(DMSO)_2$] [13]. However, the result is consistent with the weaker apical coordination of CH_3CH_2OH (a weaker Lewis base), resulting in stronger Cu-$O_{equatorial}$ bonds. The stronger ligand field effect of four C_6H_5COO ligands at Cu(II) leads to a larger increase in the energy of x^2-y^2 orbitals (or more antibonding orbital) [10].

The assignments of the electronic transitions for all peaks observed in the UV-vis spectrum are shown in **Table 4.1**. The weak shoulder at 820 nm is assigned to the $z^2 \rightarrow x^2–y^2$ electronic transition, the high energy shoulder at 400 nm is assigned to $yz,xz \rightarrow x^2$-y^2 electronic transitions, while a much stronger shoulder at 370 nm is assigned as the ligand-to-metal charge transfer band (LMCT) [14]. The latter band is also termed Band II, and its presence is indicative of a binuclear complex [15-17].

Table 4.1: The UV-vis band assignments for CuB

Band (nm)	**Assignment**
820 (shoulder)	$z^2 \rightarrow x^2 - y^2$
674	$xy \rightarrow x^2 - y^2$
450 (shoulder)	$yz, xz \rightarrow x^2 - y^2$
370	LMCT
275, 227	n → π*; π → π*

The spectrum also shows two strong bands at 275 nm and 227 nm for n → π* and π → π* electronic transition of the aromatic ligand, respectively [18]. It is noted that Kozlevcar et al. [7] reported such bands at lower energies (302 and 260 nm).

It is a fact that most Cu(II) complexes are labile in solution. Thus, to study the solution chemistry of CuB, such as its redox properties and C-C bond-forming reaction, it is important to ascertain its structural stability in different solvents. This is done by recording its UV-vis spectrum in DMSO, DMF, CH_3COCH_3 and CH_3OH-CH_3COOH (2:1). These solvents were specifically chosen for two reasons: (a) they readily dissolve the complex, and (b) they differ in their coordinating powers (strength as Lewis base). The spectrum for CuB in CH_3COCH_3 was also recorded as the information gained from it is important when discussing the C-C bond-forming reaction of this complex with this carbonyl compound.

It is noted that in the solid state, each axial position of CuB is occupied by a CH_3CH_2OH molecule, which has similar basic strength as CH_3OH, but a weaker donor compared to DMSO, DMF, CH_3COCH_3, and CH_3COOH. The order of coordinating strength is: DMSO > DMF > CH_3COCH_3 > CH_3COOH > CH_3CH_2OH, CH_3OH.

The UV-vis spectra of CuB in these solvents are shown in **Figure 4.6**, and the corresponding data in **Table 4.2**.

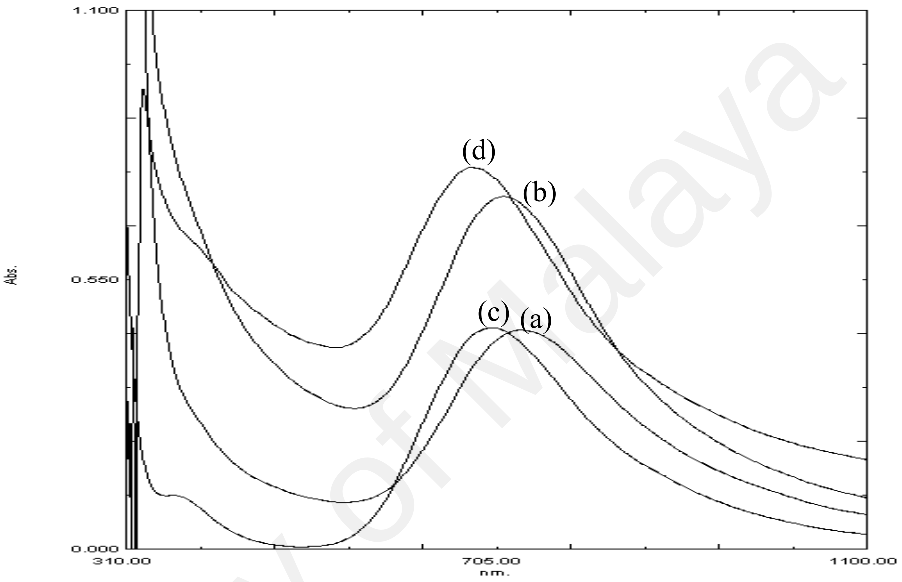

Figure 4.6: UV-vis spectra of CuB in: (a) DMSO; (b) DMF; (c) CH_3OH-CH_3COOH (2:1); and (d) CH_3COCH_3

Table 4.2: The UV-vis spectral data for CuB in different solvents

λ_{max}/nm (ε_{max}/$M^{-1}cm^{-1}$)]		**Solvent**
Band I	**Band II**	
674 (--)	370 (--)	None
729 (296)	-	DMSO
713 (480)	-	DMF
699 (295)	361 (71)	CH_3OH-CH_3COOH (20:1)
677 (530)	350 (sh)	CH_3COCH_3

--, not applicable; -, not observed

As expected, Band I in these solvents is red-shifted (bathochromic shift) compared to that of the solid sample, with the largest shift in DMSO.

The spectrum in DMSO shows a broad *d-d* band at 729 nm ($\boldsymbol{\varepsilon}_{max}$ = 296). The high value for λ_{max}, the relatively low value for ε_{max}, and the absence of Band II, suggest a mononuclear complex with either a distorted square pyramidal or octahedral geometry at Cu(II). The result seems to indicate that the strongly coordinating DMSO molecules at the axial positions of the dimeric CuB cause the C_6H_5COO-Cu equatorial bonds to weaken and finally break. The monomers formed then has a central Cu(II) bonded to two chelating bidentate $C_6H_5COO^-$ ions and DMSO molecule(s).

The spectrum in DMF also shows a broad *d-d* band at 713 nm ($\boldsymbol{\varepsilon}_{max}$ = 480). The lower value for λ_{max} and higher value for ε_{max} compared to those in DMSO, and the absence of Band II, similarly suggest a mononuclear complex but with less distorted square pyramidal geometry at Cu(II). The result is actually consistent with the weaker coordinating power of DMF. In this solvent, it is also proposed that the dimeric CuB dissociated to form monomers with Cu(II) bonded to two chelating bidentate $C_6H_5COO^-$ ions at the equatorial plane and a DMF molecule at the axial position.

The UV-vis spectrum in CH_3OH-CH_3COOH is consistent with the order of coordinating strength stated above. As expected, due to the weaker coordinating power of the mixed solvent molecules compared to DMSO and DMF, Band I is at a higher energy (λ_{max} = 699 nm; $\boldsymbol{\varepsilon}_{max}$ = 295) compared to DMSO (729 nm) and DMF (713 nm). The weaker axial effect also nicely explains the appearance of Band II in the latter solvent, indicating that the dimeric structure of the complex remained largely intact in this solvent.

The appearance of Band I at a lower energy (λ_{max} = 677 nm; **ε** = 530) in the spectrum of CuB in CH_3COCH_3 is consistent with its weaker coordinating power compared to DMSO, DMF and CH_3OH-CH_3COOH. The position of this band in this solvent is almost similar to that of solid CuB (λ_{max} = 674 nm), indicating similar binuclear structure. The significantly higher ε_{max} value compared to the mixed solvents strongly suggests a less symmetrical square pyramidal structure, which also agrees with the red-shifting of the band. The presence of Band II at 350 nm again indicates strongly that the complex remains dimeric in CH_3COCH_3.

4.2.2 Magnetic susceptibility

The value of the effective magnetic moment (μ_{eff}) at 298 K is 1.93 B.M. It is calculated from the values of χ_g (1.81 x 10^{-6} cm^3 g^{-1}), χ_d (-3.72 x 10^{-4} cm^3 mol^{-1}), and hence χ_m^{corr} (1.644 x 10^{-3} cm^3 mol^{-1}), and is shown in **Appendix 2**.

The calculated value is significantly lower than the expected spin-only value for a dinuclear Cu(II) complex (two unpaired electrons; μ_{eff} = 2.83 B.M.). However, it is in excellent agreement with the values of between 1.8-2.1 B.M. reported for $[Cu_2(CH_3COO)_4(H_2O)_2]$, which also have the dimeric, paddle-wheel structure [19,20].

The singlet and triplet energy level separation (or exchange integral), as a result of the electron spin interaction between the Cu(II) centres, or normally denoted as -2J, is calculated for CuB using the Bleaney-Bower equation [21,22]:

$$\chi_m = 2\frac{g^2N\beta^2}{3\kappa T}(1+\frac{1}{3}e^{\frac{-2J}{\kappa T}})^{-1} + 2N\alpha$$

In the calculation, the value of Lande' factor (g) is taken as 2.2 [23], the remaining constants have their usual meanings, and the value of Nα (temperature-independent paramagnetism) is taken as 60 x 10^{-6} cgs per Cu(II).

The calculated -2J value is 333 cm^{-1} (**Appendix 3**). This is in good agreement with those reported by Kawata et al. for $[Cu_2(C_6H_5COO)_4(L)_2]$, where L is benzoic acid, picoline, 4-methylquinoline, 7-methylquinoline, caffeine and 4,7-dichloroquinoline [23]. These complexes were shown to have the paddle-wheel structure, and the -2J values range from 316 cm^{-1} to 350 cm^{-1}. Similarly, the -2J value reported by Melnik et al. for $[Cu_2(C_6H_5COO)_4(DMSO)_2]$, which has similar structure, was 327 cm^{-1} [24].

Thus, it may be stated that there is a similarly strong antiferromagnetic interaction between the unpaired electrons of the two Cu(II) centres in CuB [21,22], which further strongly supports the proposed paddle-wheel structure (**Figure 4.3**). The magnetic interaction has been acknowledged to take place via the superexchange mechanism, where the unpaired electron in the x^2-y^2 orbital (singly occupied molecular orbital, SOMO) of each Cu(II) interacts through the molecular orbitals of the bridging ligand [25].

4.2.3 Thermal analysis

In addition to TGA and DSC, the thermal properties of CuB were also studied by thermogravimetric-mass spectroscopic analysis (TG-MS).

(a) TGA and TG-MS

The TGA thermogram (**Figure 4.7**) shows that the decomposition temperature for CuB is 254^{o}C. Thus, its thermal stability is comparable to that of [$Cu_2(C_6H_5COO)_4(H_2O)_2$] reported by Siqueira et al. (T_{dec} = 280^{o}C) [26].

The thermogram also shows an initial weight loss of about 9.6% at 90^{o}C assigned to the evaporation of CH_3CH_2OH molecules at the axial positions (expected, 13.1%). The lower than expected weight loss is explained by TG-MS (*see later discussion*). The next weight loss of 68.4% from 254^{o}C to about 500^{o}C with a total weight loss of 68.4% is assigned to the decomposition of C_6H_5COO ligand (expected, 68.8%). It is interesting to note that the decomposition temperature for CuB coincides closely with the boiling point of benzoic acid (249^{o}C), suggesting its formation when the complex was heated in an inert atmosphere. The possible correlation may be revealed from the TGA studies of CuB derivatives, discussed later.

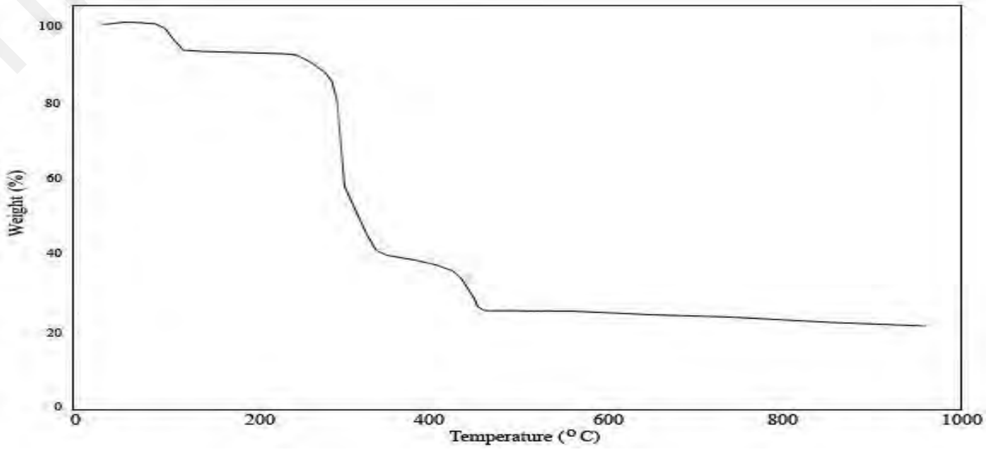

Figure 4.7: TGA of CuB

The amount of residue at temperatures above 500°C is 22.0%. Assuming that it is purely CuO [27-30], the expected value is 22.7%. The estimated formula mass of CuB, calculated using the concept of gravimetry, is 723 g/mol (**Appendix 4**). This is in good agreement with the value calculated from the proposed dimeric formula (703 g/mol).

Next, the thermal decomposition pathway of CuB was investigated by TG-MS as this technique enables the identification of volatile product(s) at each decomposition step. Plots of ion current versus temperature for each m/z detected by MS (**Figure 4.8**) show a few signals, with the highest intensity of the peaks in the temperature range of 80°C-150°C, and that most of the signals are observed in the temperature range of 200°C to 500°C.

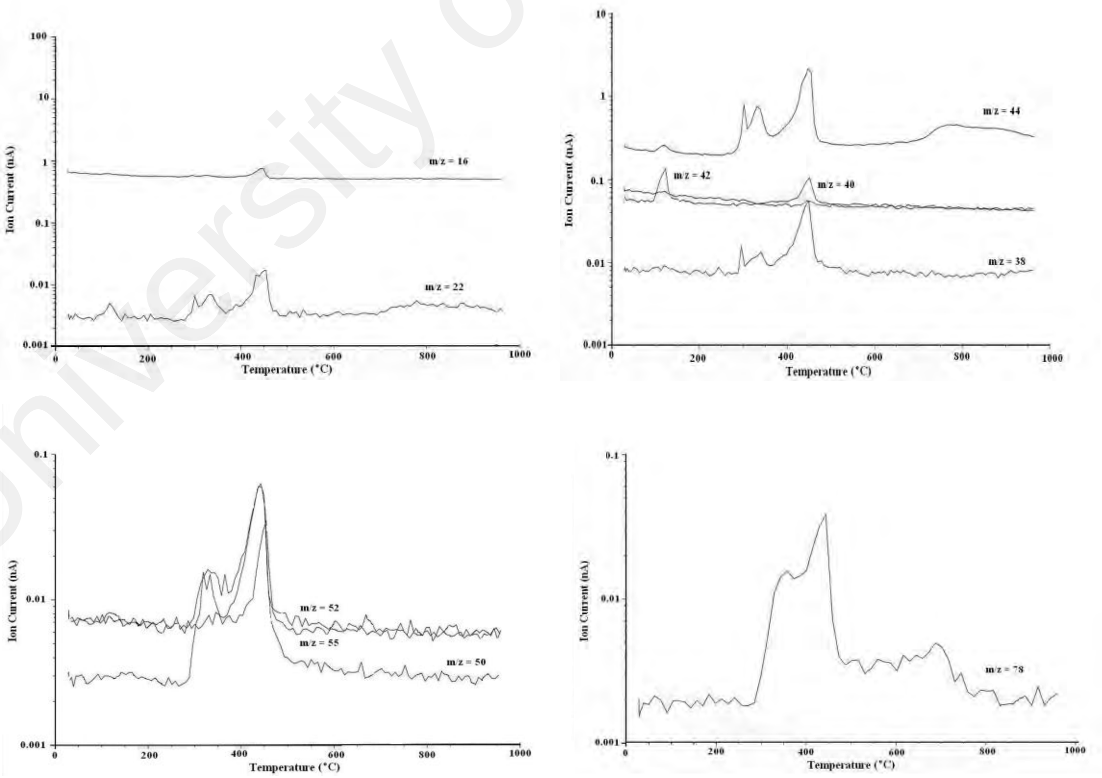

Figure 4.8: Plots of ion current versus temperature for each m/z detected by MS

By matching the current plot with the thermogram of CuB, the peaks observed depict the m/z values of gaseous products evolved at each decomposition step (**Figure 4.9).**

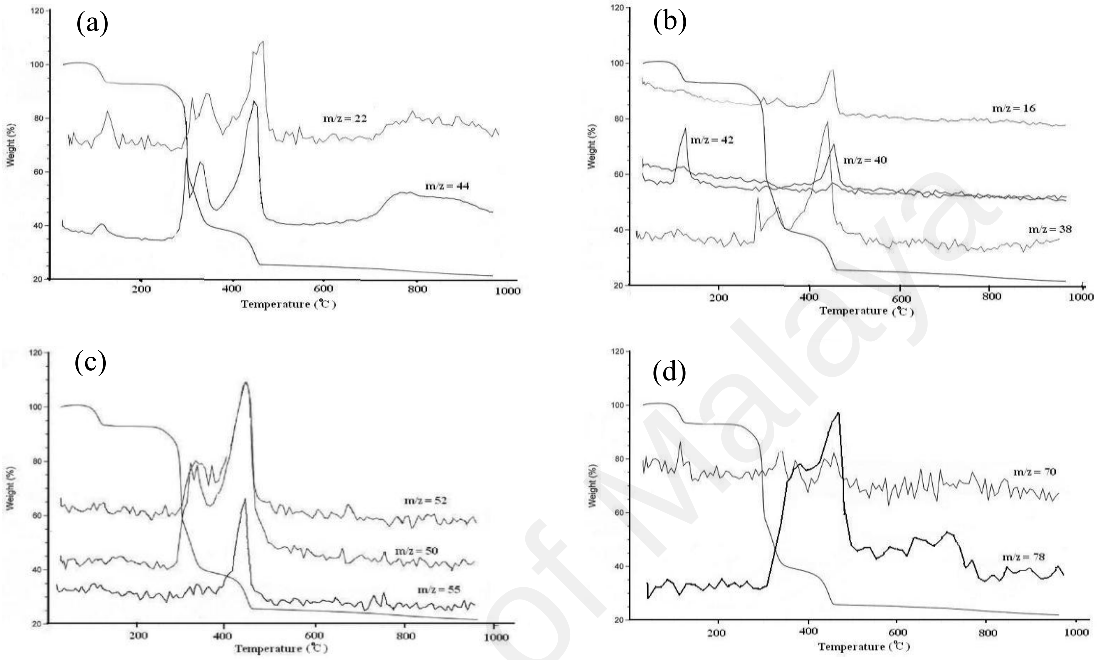

Figure 4.9: TG curve of CuB and mass spectra response curve for m/z: (a) 22, 44; (b) 16, 38, 40, 42; (c) 50, 52, 55; (d) 70, 78

The m/z values for the volatile product(s) evolved at each decomposition step are listed in **Table 4.3.**

Table 4.3: The m/z values of the gaseous products from the thermal decomposition of CuB

Stage	Temperature range (^{o}C)	m/z											
I	90-145	-	22	-	-	42	-	-	-	-	-	70	-
II	250-304	-	22	38	-	-	44	-	-	-	-	70	-
III	304-348	-	22	38	-	-	44	50	52	-	-	70	78
IV	348-477	16	22	-	40	-	44	50	52	55	57	70	78

The results shows that CO_2 (m/z = 22 (+2), 44 (+1)), is detected at each decomposition step. This suggests decarboxylation of C_6H_5COO• to C_6H_5• and CO_2. Also detected are the decomposition products of CH_3CH_2-O-CH_2CH_3 (m/z = 40, 42, 70), presumably formed from the condensation reaction of two CH_3CH_2OH molecules (**Scheme 4.1**). The formation of such products nicely explains the lower than expected weight loss of this molecule observed in TGA.

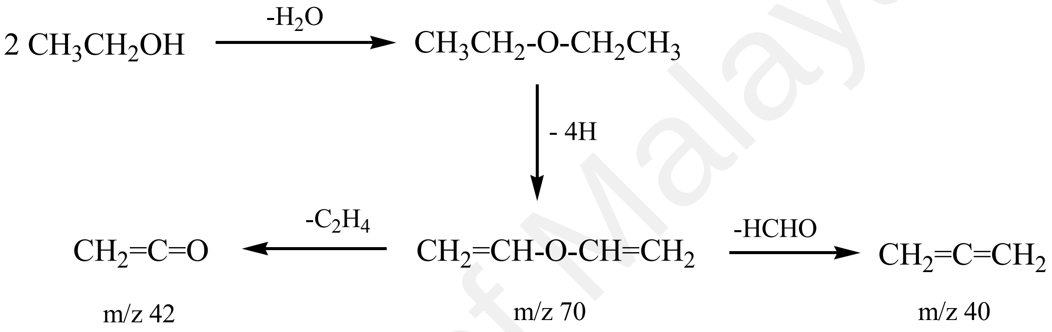

Scheme 4.1: Condensation of two CH_3CH_2OH molecules to CH_3CH_2-O-CH_2CH_3, and the thermal decomposition pathways of the latter

Also detected is C_6H_6 (m/z = 78) at stages III and IV, suggesting that C_6H_5• combined with H atom at higher temperatures. In addition, the m/z values of 50, 52, 55 and 57, detected at higher temperatures, suggest that the aromatic ring cracked to form simpler aliphatic conjugated organic volatiles [31].

Based on the TG-MS study, the decomposition pathway for CuB is proposed to occur after the loss of axial CH_3CH_2OH molecules. It involved the homolysis of the Cu-$OOCC_6H_5$ bond to form C_6H_5COO•, a process known as reductive elimination, followed by decarboxylation of C_6H_5COO• to C_6H_5•

and CO_2. Hence, it is postulated that the initial decomposition steps are as follows:

$$[Cu_2(C_6H_5COO)_4(CH_3CH_2OH)_2] \xrightarrow{\sim 90^{o}C} [Cu_2(C_6H_5COO)_4] + 2\ CH_3CH_2OH$$

$$[Cu_2(C_6H_5COO)_4] \xrightarrow{\text{homolysis}} [Cu_2(C_6H_5COO)_3]\bullet + C_6H_5COO\bullet$$

$$C_6H_5COO\bullet \xrightarrow{\sim 250^{o}C} CO_2 + C_6H_5\bullet$$

(b) DSC

The DSC trace (**Figure 4.10)** shows a weak endotherm at onset temperature 150°C ($\Delta H = +11.5$ kJ mol^{-1}), which is at a slightly higher temperature noted for the release of the apical ligand (from TGA). However, such discrepancy could be due to the multiple bond forming and breaking processes that take place at this stage, as shown in TGA-MS. Thus, the weak endothermic peak is postulated to represent the net energy involved for these processes.

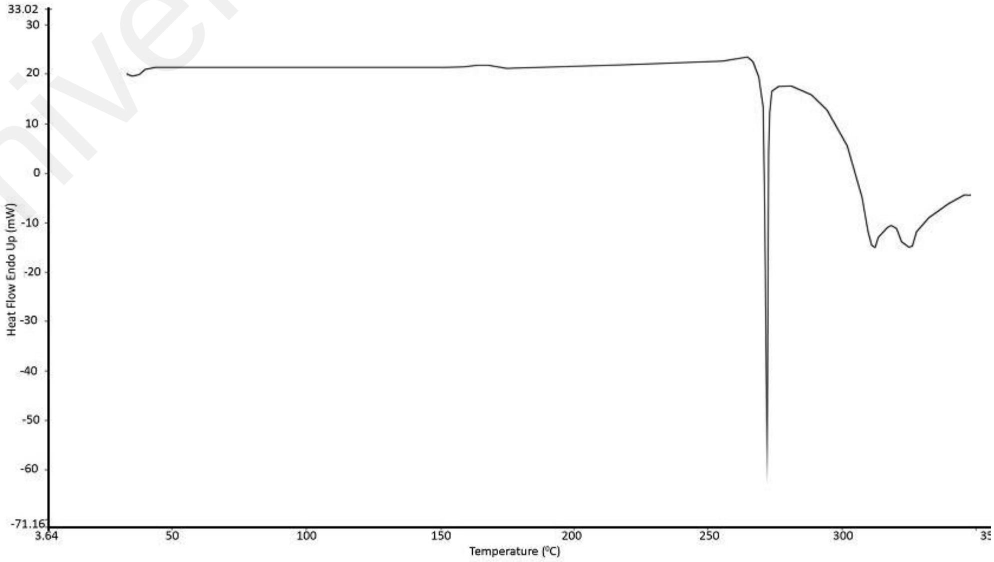

Figure 4.10: DSC of CuB

This is followed by a very strong and sharp exotherm at 269°C (ΔH = -295 kJ mol^{-1}) and overlapping exotherms at 300°C ($\Delta H_{combined}$ = -1480 kJ mol^{-1}). The temperatures of these exotherms are higher than the decomposition temperature of CuB (254°C from TGA). This clearly indicates the formation of volatiles, after C_6H_5COO ligand decarboxylates. The sharp exothermic peak indicates a very fast bond-forming process.

However, the absence of a strong endothermic peak associated with bond-breaking processes needs an explanation. It is likely that both endothermic and exothermic processes occurred almost simultaneously. The net heat was released as the decomposition products were stable volatiles.

The above thermal results were part of a published paper, entitled: "*Thermal stability and electrochemical behaviour of tetrakis-μ-benzoatodicopper(II),* Mohamad I. Mohamadin, Norbani Abdullah (2010) Central European Journal of Chemistry**,** Volume 8, Number 5, 1090-1096" (**Appendix 5**).

4.2.4 Cyclic voltammetry

The cyclic voltammograms (CV) of CuB in CH_3OH-CH_3COOH were scanned under several conditions in an attempt to probe the extent of redox reversibility, determined from the peak separations ($\Delta E = E_{anode} - E_{cathode}$), the anodic to cathodic peak currents ratio (I_{pa}/I_{pc}), and graph of peak current versus scan rate (ν).

It is to be noted from the UV-vis spectroscopic study (**Section 4.1(a)**) that the dimeric paddle-wheel structure of CuB is slightly distorted but remained intact in these solvents.

(a) Potential window = +1.5 V to -1.0 V; scan rate = 150 mV s^{-1}

The CV (**Figure 4.11**) shows three cathodic peaks at -0.13, -0.35 and -0.74 V, suggesting the presence of multiple species in solution [32], and two strong overlapping anodic peaks at +0.31 V (shoulder) and +0.46 V, indicating the occurrence of stepwise oxidation processes at almost similar potentials [33].

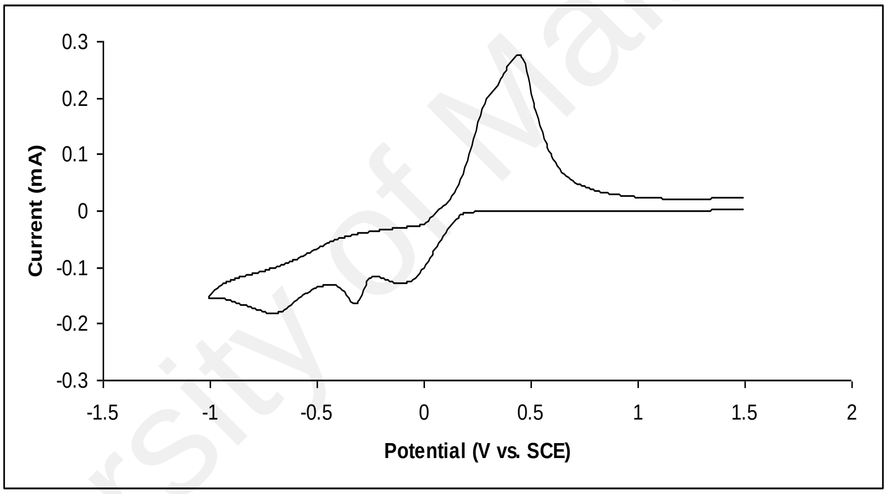

Figure 4.11: CV of CuB

The assignment of the cathodic peaks were made by referring to the CV of dinuclear [$Cu_2(CH_3COO)_4$] [34], mononuclear [$Cu(CH_3COO)_2(bpy)$] (bpy = 2,2'-bipyridine) [35], and mononuclear [$Cu(C_6H_4NH_2S)_2Cl$] [36].

The CV of dinuclear [$Cu_2(CH_3COO)_4$] shows two cathodic peaks at -0.2 V and -0.4 V, assigned to the reduction of [Cu(II)Cu(II)] to [Cu(II)Cu(I)] and [Cu(II)Cu(I)] to [Cu(I)Cu(I)], respectively. It is further noted that the CV also shows a sharp anodic stripping peak at 0 V, indicating the deposition of Cu metal on the electrode.

The CV of the mononuclear [Cu($CH_3COO)_2$(bpy)] and [Cu($C_6H_4NH_2S)_2$Cl] shows a cathodic peak at -0.38 V and -0.37 V, respectively, assigned to the reduction of [Cu(II)] to [Cu(I)].

Accordingly, the three cathodic peaks for CuB at -0.13, -0.35, and -0.74 V are assigned to the reduction of [Cu(II)Cu(II)] to the mixed-valence [Cu(II)Cu(I)], monomeric [Cu(II)] to [Cu(I)], and [Cu(II)Cu(I)] to [Cu(I)Cu(I)], respectively. It is postulated that the mononuclear [Cu(II)] was formed from the dissociation of the mixed-valence [Cu(II)Cu(I)], and not from the binuclear [Cu(II)Cu(II)]. This is based on the above UV-vis result that the latter complex was stable in these solvents.

To account for the strong overlapping anodic peaks, it is postulated that the binuclear [Cu(I)Cu(I)] formed was reoxidized to the mixed-valence [Cu(II)Cu(I)] at +0.31 V, which was then further reoxidized to binuclear [Cu(II)Cu(II)] at +0.46 V. At the same later potential, the mononuclear [Cu(I)] was reoxidised to the mononuclear [Cu(II)].

To summarise, CuB underwent an electrochemical-chemical (EC) mechanism for both redox reactions, as shown below.

$$[\mathrm{Cu(II)Cu(II)}] \xrightleftharpoons[+0.46\mathrm{V}]{-0.13\mathrm{V}} [\mathrm{Cu(II)Cu(I)}] \xrightleftharpoons[+0.31\mathrm{V}]{-0.74\mathrm{V}} [\mathrm{Cu(I)Cu(I)}]$$

$$[\mathrm{Cu(II)Cu(I)}] \xrightarrow{\textit{dissociation}} [\mathrm{Cu(II)}] + [\mathrm{Cu(I)}]$$

$$[\mathrm{Cu(II)}] \underset{+0.46\mathrm{V}}{\overset{-0.35\mathrm{V}}{\rightleftarrows}} [\mathrm{Cu(I)}]$$

It is further noted that the first cathodic potential for CuB (-0.13 V) is less negative compared to the same peak for [$Cu_2(CH_3COO)_4$] (-0.2 V). This means that CuB was more easily reduced compared to [$Cu_2(CH_3COO)_4$], and is probably due to the fact that the ligand C_6H_5COO, which is a weaker Lewis base compared to CH_3COO, forms a weaker σ coordinate bond with [Cu(II)], making it easier to distort the geometry, and producing a less energy antibonding x^2-y^2 orbital (**Figure 4.4**). Additionally, the positive charge density on Cu(II) is less neutralized by the electron pair from the ligand.

Also in contrast to [$Cu_2(CH_3COO)_4$] [34], there is no anodic stripping peak in the CV of CuB, suggesting that the dimeric [Cu(I)Cu(I)] formed was stabilized towards processes such as dissociation and/or disproportionation.

From the above cathodic and anodic potentials, the ΔE values for [Cu(II)Cu(II)]-[Cu(II)Cu(I)] and [Cu(II)Cu(I)]-[Cu(I)Cu(I)] couples are 590 mV and 1050 mV respectively. Since the value for a fully reversible redox reaction at 298 K is 59 mV, it may be concluded that CuB underwent stepwise quasireversible redox reactions as a result of extensive structural reorganization upon each reduction step. This result is actually consistent with redox processes involving electron(s) in an antibonding orbital.

(b) Potential window = +1.5 V to -1.0 V; scan rates = 40 - 100 mV s^{-1}

The CV of CuB was then recorded within the same potential window (+*1.5 V to -1.0 V)*, but at different scan rates, ranging from 40 mV s^{-1} to 100 mV s^{-1} (**Figure 4.12)**. This is to allow for the observation of potential and current dependency, which relate directly to the electrochemical reversibility of the overall redox reaction [37].

At first glance, the CV's obtained look similar. However, **Table 4.4** shows that the values of E_p and ΔE increase slightly with scan rate. Conceptually, a slow scan rate means a slow electron transfer. For example, at the very slow rate of 40 mV s^{-1}, the square pyramidal dimer had sufficient time to undergo a more extensive structural distortion to a less planar geometry. This allows for an easier reduction of [Cu(II)Cu(II)] to [Cu(II)Cu(I)] (E_{pc1}), and [Cu(II)Cu(I)] to [Cu(I)Cu(I)] (E_{pc3}). The converse applies during the fast scan rate.

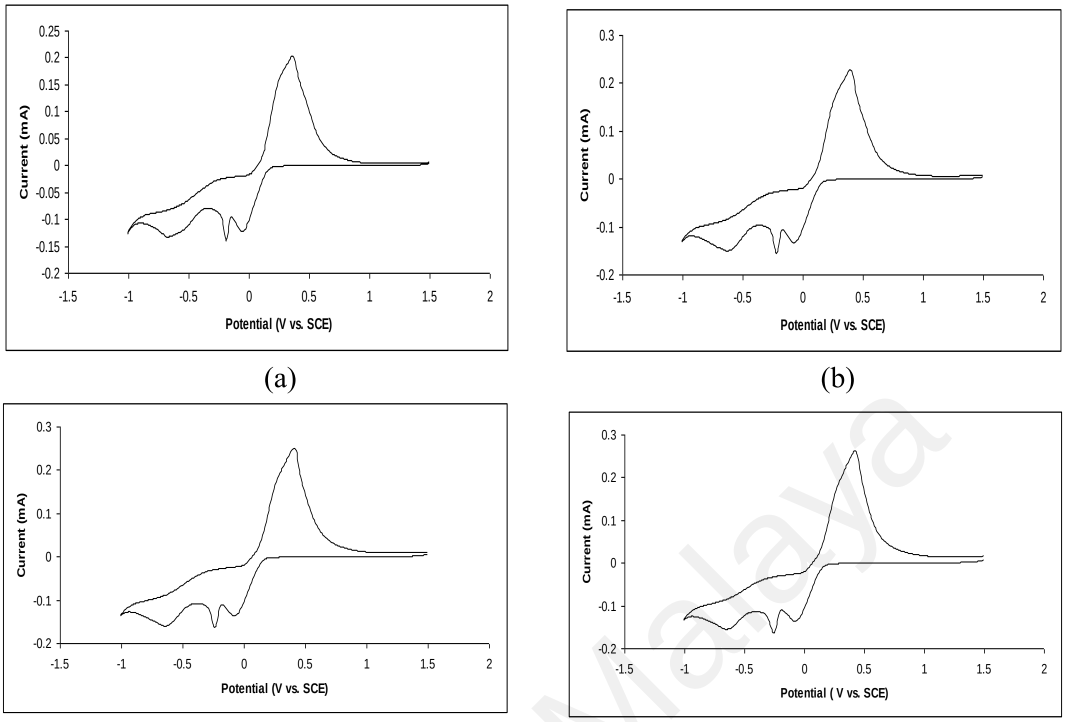

(a) (b)

(c) (d)

Figure 4.12: CV of CuB within a potential window +1.5 V to -1.0 V and scan rates (mV s^{-1}): (a) 40; (b) 60; (c) 80; and (d) 100

Table 4.4: The peak potential (E_p/V) and peak separation (ΔE/mV) for CuB in CH_3OH-CH_3COOH at each scan rate (mV s^{-1})

Scan rate	E_{pc1}	E_{pc2}	E_{pc3}	E_{pa1}	E_{pa2}	ΔE_1^*	$\Delta E_2^\#$
40	-0.07	-0.19	-0.60	+0.27	+0.37	440	870
60	-0.08	-0.22	-0.64	+0.28	+0.40	480	920
80	-0.09	-0.24	-0.66	+0.29	+0.41	500	950
100	-0.11	-0.27	-0.67	+0.30	+0.43	540	970
150	-0.13	-0.35	-0.74	+0.31	+0.46	590	1050

* $\Delta E_1 = E_{pa2} - E_{pc1}$; # $\Delta E_2 = E_{pa1} - E_{pc3}$

At each scan rate, the value of ΔE_2 is greater than that of ΔE_1. This suggests that structural reorganization was more extensive in [Cu(I)Cu(I)] compared to [Cu(II)Cu(I)]. The result is consistent with the fact that [Cu(I)] is less stable in a square planar geometry compared to [Cu(II)].

Additionally, a graph of the first cathodic peak current versus the square root of the scan rate is linear (**Figure 4.13**). This suggests that the reduction of [Cu(II)Cu(II)] to [Cu(II)Cu(I)] was diffusion-controlled [38].

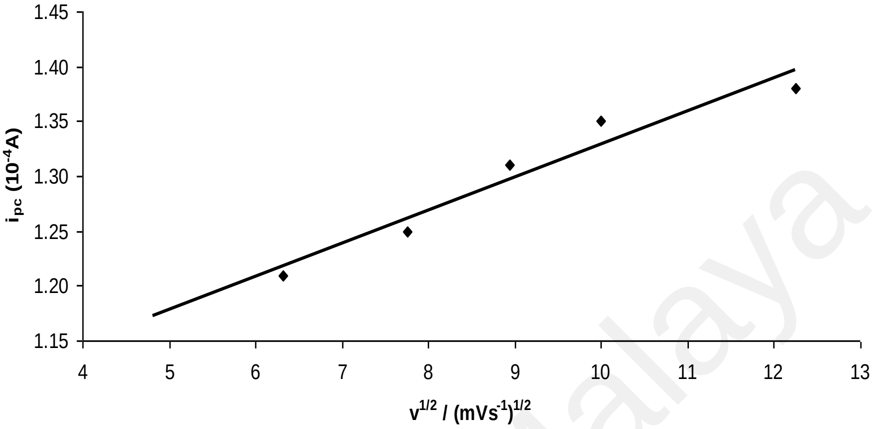

Figure 4.13: Graph of the first cathodic peak current versus square root of the scan rate for CuB

(c) Potential window = +0.5 V to -0.2 V; scan rate = 150 mV s^{-1}

The CV of CuB was next recorded within a shorter potential window (from +0.5 V to -0.2 V), but at a faster scan rate of 150 mV s^{-1}. The objective was to identify a redox couple. The voltammogram (**Figure 4.14**) shows a cathodic peak at -0.1 V, and two anodic peaks at +0.05 V and +0.18 V.

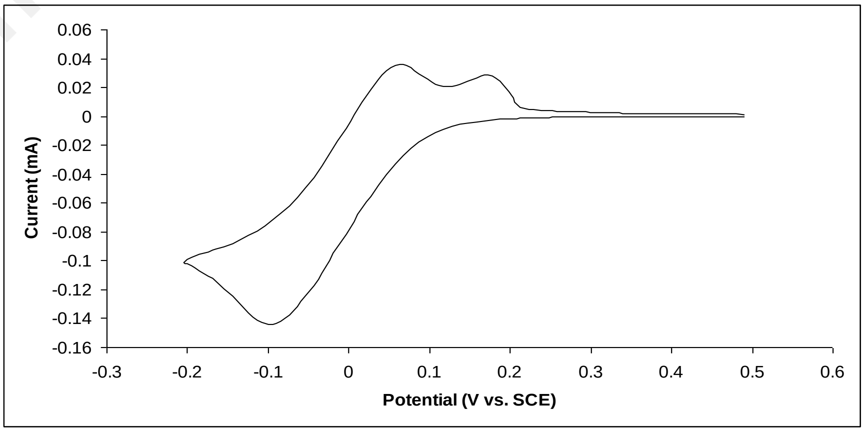

Figure 4.14: CV of CuB at potential window = +0.5 V to -0.2 V and scan rate = 150 mV s^{-1}

The result supports the suggestion made earlier that the first cathodic peak (at -0.1 V) was due to the reduction of the dinuclear [Cu(II)Cu(II)] to the mixed-valence [Cu(II)Cu(I)], which then dissociated to [Cu(II)] and [Cu(I)] (the EC mechanism). The first anodic peak at +0.05 V is assigned to the oxidation of the [Cu(I)] formed, while the second anodic peak at +0.18 V is assigned to the oxidation of [Cu(II)Cu(I)]. These assignments are based on the assumption that the mixed-valence complex was more difficult to be oxidized as it has a higher positive charge and expected to be stabilized by resonance compared to [Cu(I)]. Hence, the ΔE value for [Cu(II)Cu(II)]-[Cu(II)Cu(I)] couple is 280 mV, indicating a quasireversible process, as expected. The EC mechanism is shown below.

$$[\mathrm{Cu(II)Cu(II)}] \xrightleftharpoons[+\,0.18\ \mathrm{V}]{-0.1\ \mathrm{V}} [\mathrm{Cu(II)Cu(I)}]$$

$$[\mathrm{Cu(II)Cu(I)}] \xrightleftharpoons{\text{dissociation}} [\mathrm{Cu(II)}] + [\mathrm{Cu(I)}]$$

$$[\mathrm{Cu(I)}] \xrightarrow{+0.05\ \mathrm{V}} [\mathrm{Cu(II)}]$$

The peak current ratio (I_{pa}/I_{pc}) is 0.65, indicating the instability of the reduced complex.

(d) Potential window = +0.5 V to -0.2 V; scan rates = 40-100 mV s^{-1}

In order to probe deeper the electrochemical behaviour of CuB in this solvent, the CV analyses were repeated at a narrower potential window (+0.5 V to -0.2 V) and slower scan rates (40 mV s^{-1} to 100 mV s^{-1}). The results are shown in **Figure 4.15**, and the data is collected in **Table 4.5 (**which also shows the data at 150 mV s^{-1} scan rate for comparison).

As previously assigned, the first cathodic peak was due the reduction of [Cu(II)Cu(II)] to [Cu(II)Cu(I)]. At the slow scan rates, the mixed-valence [Cu(II)Cu(I)] formed has sufficient time to dissociate to [Cu(I)] and [Cu(II)]. Thus, the second cathodic peak may be due to the reduction of [Cu(II)] to [Cu(I)]* (the symbol * is used to signify a [Cu(I)] which has a different geometry than the first formed [Cu(I)] in order to justify the different potential for their oxidation).

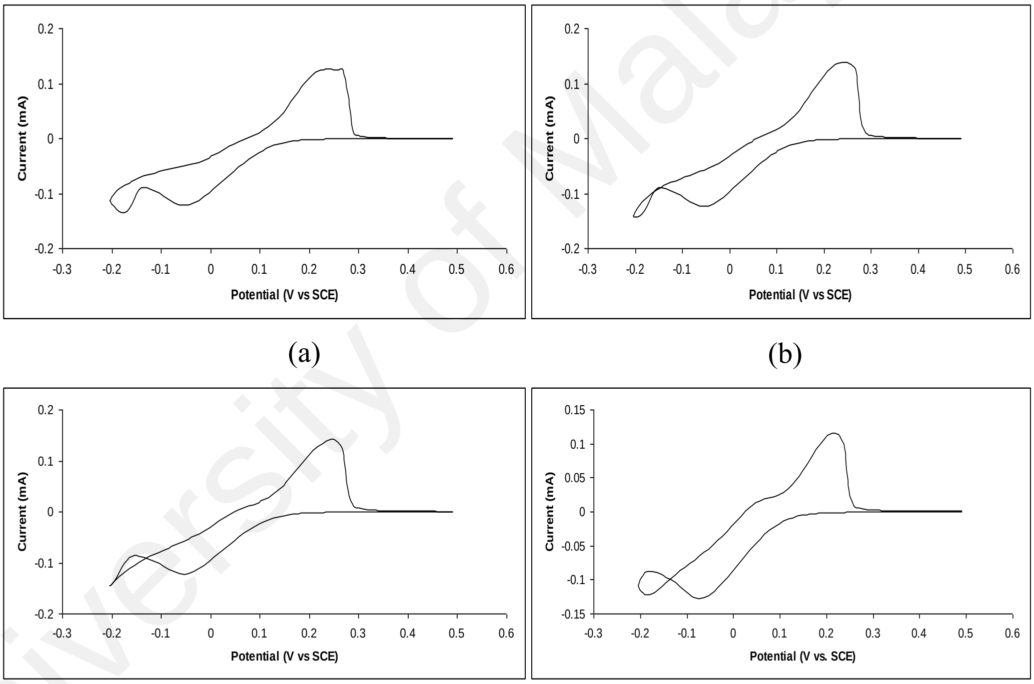

(a) (b)

(c) (d)

Figure 4.15: CV of CuB within a potential window of +0.5 V to -0.2 V and scan rates (mV s^{-1}): (a) 40; (b) 60; (c) 80; and (d) 100

Table 4.5: The electrode potential (E/V), peak separation (ΔE/mV) and ratio of peak currents (I_{pa}/I_{pc}) at different scan rate (mV s^{-1}) for CuB in CH_3OH-CH_3COOH

Scan rate	E_{pc1}	E_{pc2}	E_{pa1}	E_{pa2}	ΔE_1^*	$\Delta E_2^\#$	I_{pa}/I_{pc}
40	-0.05	-0.17	+0.23	+0.27	310	400	0.96
60	-0.05	-0.19	+0.23	+0.23	280	420	1.1
80	-0.05	-0.14$^@$	+0.25	+0.25	300	390	1.2
100	-0.07	-0.14$^@$	+0.22	+0.22	290	360	0.9
150	-0.1	-	+0.18	+0.18	280	-	0.65

-, not observed; $^@$, observed as an overpotential; $^*\Delta E_1 = E_{pa2} - E_{pc1}$; $^\#\Delta E_2 = E_{pa1} - E_{pc2}$

The overlapping anodic peaks are now assigned to the oxidation of [Cu(I)] and [Cu(I)]*, which occurred at almost the same potential as both complexes also have sufficient time to adopt similar environment and/or geometry. The redox processes at the scan rate of 40 mV s^{-1} are summarized below.

$$[\mathrm{Cu(II)Cu(II)}] \xrightarrow{-0.05\ \mathrm{V}} [\mathrm{Cu(II)Cu(I)}]$$

$$[\mathrm{Cu(II)Cu(I)}] \xrightarrow{\text{dissociation}} [\mathrm{Cu(II)}] + [\mathrm{Cu(I)}]$$

$$[\mathrm{Cu(II)}] \xrightarrow{-0.17\ \mathrm{V}} [\mathrm{Cu(I)}]^*$$

$$[\mathrm{Cu(I)}] \xrightarrow{+0.23\ \mathrm{V}} [\mathrm{Cu(II)}]$$

$$[\mathrm{Cu(I)}]^* \xrightarrow{+0.26\ \mathrm{V}} [\mathrm{Cu(II)}]^*$$

The next significant observation is that, at the scan rate of 80 and 100 mV s^{-1}, there is a crossing of the cathodic and anodic current curves at about -0.14 V, termed nucleation overpotential. This is not observed at the faster scan rate of 150 mV s^{-1}. The overpotential normally indicates the beginning of copper nucleation growth onto the electrode [39-40]. However, as pointed out above, no copper metal deposition was detected for CuB in this work. Thus, the observed overpotential is postulated to correspond to the change of the chemical species at the interface during the partial dissociation of the mixed-valence [Cu(II)Cu(I)], possibly with the formation of intermediates [41].

(e) The effect of solvents (potential window = +1.5 V to -2.0 V; scan rate = 100 mV s^{-1})

The redox properties of CuB were further pursued in different solvents in order to study the relationship between electrochemical reactions and stability of the paddle-wheel structure in solution. The solvents chosen were DMSO and DMF, as these solvents have stronger coordinating strength than CH_3OH-CH_3COOH (*refer to* ***Section 4.1(a)***)

The CV of CuB in DMSO and DMF are shown in **Figure 4.16**, and the corresponding data are depicted in **Table 4.6**. The values obtained in CH_3OH-CH_3COOH are included in the table for comparison.

It is noted that the CV in DMSO and DMF show the same number of cathodic and anodic peaks as in CH_3OH-CH_3COOH, and hence may be assigned as discussed above. It is also observed that the first and second reduction peaks in DMSO (for [Cu(II)Cu(II)] and [Cu(II)Cu(I)] respectively) occur at almost the same potentials (-0.15 and -0.79 V respectively) as those in CH_3OH-CH_3COOH (-0.13 V and -0.74 V). This suggests that the geometries of both [Cu(II)] centres in these complexes are about the same in these solvents.

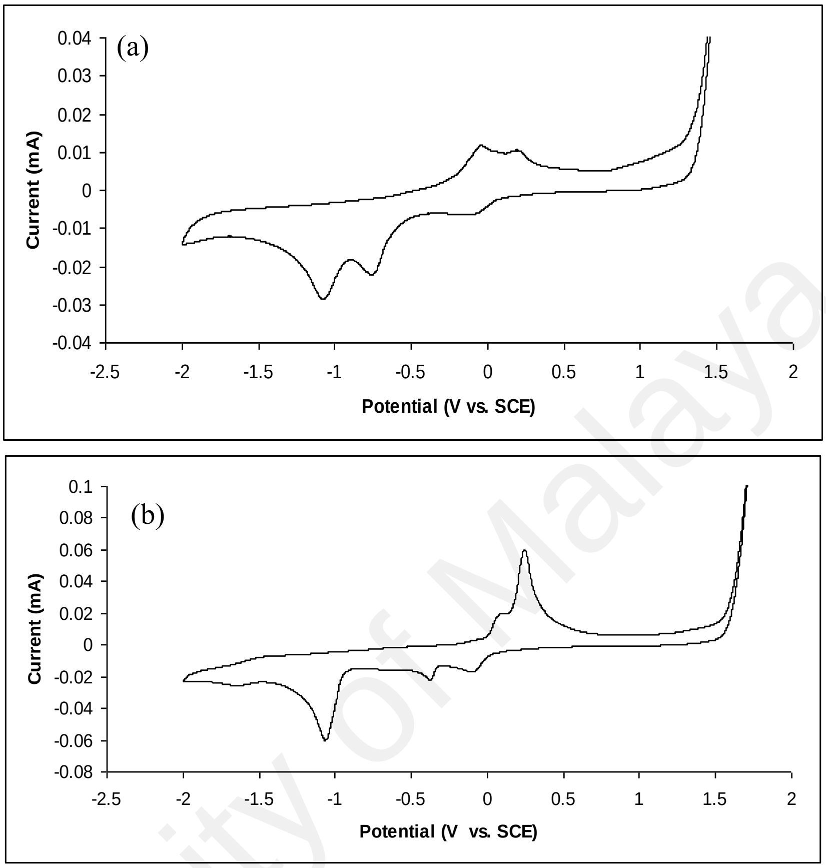

Figure 4.16: CV of CuB in (a) DMSO; and (b) DMF (molarity = 0.1 M; scan rate = 100 mV s^{-})

Table 4.6: The CV data of CuB in DMSO and DMF (molarity = 0.1 M; scan rate = 100 mV s^{-1}; potential window = +1.5 V to -2.0 V)

Solvent	Reduction			Oxidation	
	Peak 1	Peak 2	Peak 3	Peak 4	Peak 5
	E_{pc}	E_{pc}	E_{pc}	E_{pa}	E_{pa}
DMSO	-0.15	-0.79	-1.10	-0.01	+0.23
DMF	-0.13	-0.40	-1.10	+0.13	+0.26
CH_3OH-$CH_3COOH^{\#}$	-0.13	-0.74	*	-	+0.31

#, potential window -1.0 V to 1.5 V; *, not relevant; -, not observed

However, the fully reduced [Cu(I)Cu(I)] in DMSO was more easily oxidized (+0.23 V) compared to that in CH_3OH-CH_3COOH (+0.31 V). This suggest that the geometry of [Cu(I)] in DMSO is more planar or less tetrahedrally distorted than in CH_3OH-CH_3COOH. This may in turn explains the high reduction potential of [Cu(II)] (-1.10 V) and the corresponding very low oxidation potential of [Cu(I)] formed (-0.01 V) [42]. The behavior is also consistent with the stronger Lewis base strength of DMSO, as previously stated.

In DMF, the cathodic and anodic peaks, except for E_{pc2} (-0.40 V) and E_{pa1} (+0.13 V), are similar to those observed in DMSO, and thus may be similarly explained. The value for E_{pc2}, assigned to the reduction of [Cu(II)], is slightly more negative than that observed in CH_3OH-CH_3COOH (-0.35 V). Also, the value of E_{pa1}, assigned to the oxidation of the corresponding [Cu(I)], is less positive than that observed in CH_3OH-CH_3COOH (+0.46 V). These trends are consistent with the stronger Lewis base strength of DMF molecule.

Thus, the solvents CH_3OH-CH_3COOH, DMSO, and DMF exert similar effect on the reduction of [Cu(II)Cu(II)] to [Cu(II)Cu(I)]. The differences in the Lewis base strength of these solvents have a significant effect on increasing the reduction potential and decreasing the oxidation potential of the intermediate complexes.

4.2.5 Summary

The chemical formula of CuB is $[Cu_2(C_6H_5COO)_4(CH_3CH_2OH)_2]$, and it is proposed to have the paddle-wheel structure similar to copper(II) acetate and most other metal(II) carboxylates. The complex has a strong electronic communication between the two Cu(II) centres (μ_{eff} = 1.93 B.M.; - 2J = 333 cm^{-1}), and thermally stable (T_{dec} = 254^{o}C). The CV studies show that the complex undergoes two-steps and quasireversible redox processes involving an EC mechanism. The solvents CH_3OH-CH_3COOH, DMSO, and DMF exert almost similar effect on its redox properties.

4.3 COPPER(II) 4-NITROBENZOATE AND COPPER(II) 3,5-DINITROBENZOATE

It is of interest to know if the structure and properties of copper(II) arylcarboxylates can be tuned at will by simple substitution. With this in mind, the next two complexes studied have the aromatic ring substituted with strongly electron-withdrawing -NO_2 group at the 4- and 3,5- positions.

4.3.1 Copper(II) 4-Nitrobenzoate

Copper(II) 4-nitrobenzoate ($CuNO_2B$) was a pale blue powder, and the yield was 52%. Thus, its yield was higher than that of CuB (41%), suggesting lower solubility in ethanol. It was soluble in tetrahydrofuran, dimethylsulfoxide, dimethylformamide and pyridine, partially soluble in acetonitrile, and insoluble in other common organic solvents and in water.

4.3.1.1 Structural elucidation

The ligand, 4-$O_2NC_6H_4COO^-$ ion is a weaker Lewis base (weaker ligand) compared to $C_6H_5COO^-$ ion. This is because the corresponding acid, 4-$NO_2C_6H_4COOH$, is a stronger acid (pK_a = 3.43) than C_6H_5COOH (pK_a = 4.19). Accordingly, the ligand is expected to form a weaker 4-$O_2NC_6H_4COO$-Cu(II) σ coordinate bond.

Magnetic studies on these complexes [43,44] suggested that a weaker ligand has less tendency to form dinuclear complexes. This effect is attributed to the greater repulsion between the two Cu(II) centres. In contrast, a stronger ligand decreases the positive charge density on the metal ion, and consequently allows its valence orbitals to expand for better overlap [45]. Nevertheless, based on the analytical results presented below, it is proposed that $CuNO_2B$ adopted the dimeric paddle-wheel structure similar to that of CuB.

(a) Elemental analysis

The results of the elemental analysis (41.7% C, 2.9% H, 6.0% N and 15.2% Cu) are in good agreement with those calculated for the chemical formula $Cu_2C_{30}H_{24}O_{18}N_4$ or $[Cu_2(4\text{-}O_2NC_6H_4COO)_4(CH_3CH_2OH)(H_2O)]$ (855 g mol^{-1}; 42.1% C, 2.8% H, 6.5% N and 14.9% Cu).

(b) FTIR spectroscopy

The FTIR spectrum (**Figure 4.17**) is quite similar to that of CuB (**Figure 4.1**), suggesting similar structure. Specifically, there is a broad OH peak at 3410 cm^{-1} [8,9], and two strong peaks at 1567 cm^{-1} and 1414 cm^{-1} for $\nu_{as}COO$ and $\nu_{s}COO$ respectively. Hence, the value of $\Delta\nu$ is 153 cm^{-1}, suggesting a bridging bidentate $4\text{-}O_2NC_6H_4COO$ ligand. Also observed are a strong peak at 1628 cm^{-1} for the aromatic ring, two strong peaks at 1348 cm^{-1} and 1598 cm^{-1} for $R\text{-}NO_2$.

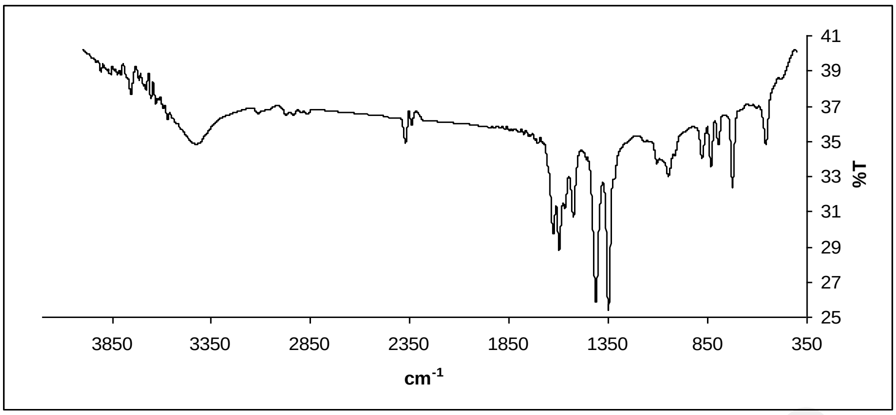

Figure 4.17: FTIR spectrum of $CuNO_2B$

(c) UV-vis spectroscopy

The UV-vis spectrum of solid $CuNO_2B$ (**Figure 4.18**) shows *d-d* bands at 700 nm, 850 nm, 440 nm, and 390 nm (shoulders), and two very strong bands at 309 nm and 239 nm. Thus, the spectrum is similar to that of CuB, and can be similarly assigned.

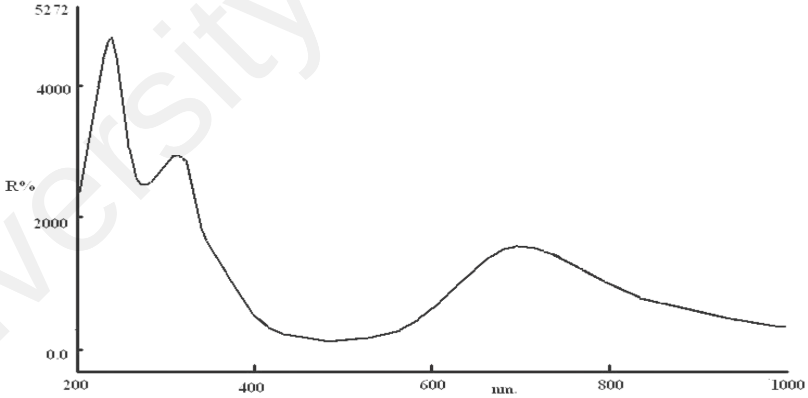

Figure 4.18: UV-vis spectrum of solid $CuNO_2B$

It is further noted that the peaks for $CuNO_2B$ are bathochromically shifted (lower energies) compared to those of CuB (**Table 4.7**). This is actually consistent with the proposed weaker 4-$O_2NC_6H_4COO$-Cu(II) σ coordinate bond. Such an effect is expected to result in a smaller splitting of the *d-d* energy level (or less energy antibonding x^2-y^2 orbital; refer to **Figure 4.4**) [10].

Table 4.7: The UV-vis band for $CuNO_2B$ and CuB

Electronic transition	$CuNO_2B$	CuB
$z^2 \rightarrow x^2 - y^2$	850	820
$xy \rightarrow x^2 - y^2$	700	674
$yz, xz \rightarrow x^2 - y^2$	440	400
LMCT	390	370
$n \rightarrow \pi^*; \pi \rightarrow \pi^*$	309, 239	275, 227

Accordingly, the proposed structure for $CuNO_2B$ is shown in **Figure 4.19**. The structure is similar to CuB (**Figure 4.3**), but more distorted (axial-equatorial bond angle greater than 90°) and have different apical ligands.

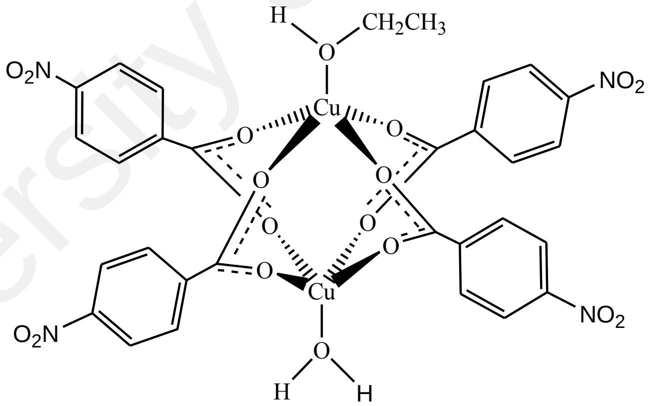

Figure 4.19: Proposed distorted paddle-wheel structure for $CuNO_2B$

As for CuB, the UV-vis spectra of $CuNO_2B$ were next recorded in different solvents, namely DMSO, DMF, and CH_3OH-CH_3COOH (20:1), in order to probe the stability of its structure in solution. The spectra are shown in **Figure 4.20,** and the corresponding data is in **Table 4.8**.

As observed for CuB, the position of Band I for $CuNO_2B$ is dependent on the coordinating power of the solvent molecules. It is further noted that in CH_3OH-CH_3COOH (20:1), the *d-d* band is at similar position as that of CuB (699 nm). This suggests similar geometrical environment around Cu(II) centres in both complexes. Accordingly, it is postulated that the structure of $CuNO_2B$ remained dimeric in these mixed solvents. Additionally, band II is not observed as may be hidden by the more intense intra-ligand band.

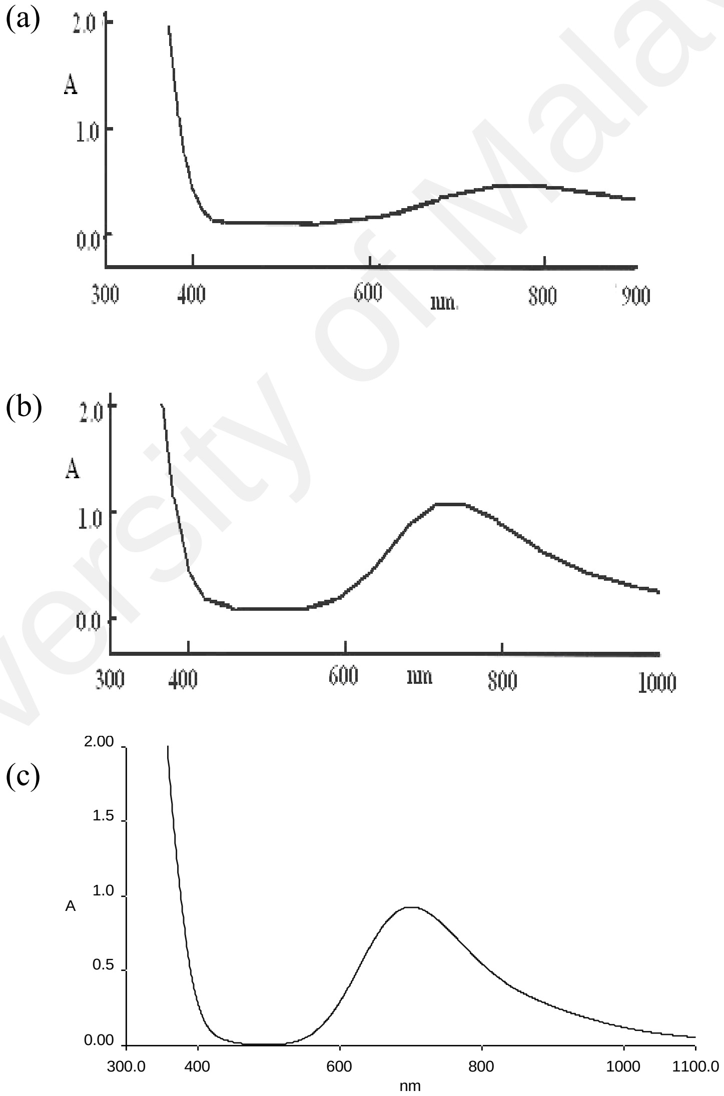

Figure 4.20: UV-vis spectrum of $CuDNO_2B$ in: (a) DMSO; (b) DMF and (c) CH_3OH-CH_3COOH (20:1)

Table 4.8: The UV-vis spectral data for $CuNO_2B$ in different solvents

λ_{max}/nm (ε/$M^{-1}cm^{-1}$)		Solvent
Band I	**Band II**	
700 (--)	390 (--)	None
769 (171)	-	DMSO
733 (397)	-	DMF
700 (315)	-	CH_3OH-CH_3COOH (20:1)

--, not applicable; -, not observed

The lower structural stability of $CuNO_2B$ in solution, compared to CuB, is further confirmed by the structures of crystals obtained when the complex was dissolved in DMSO-$CHCl_3$ (1:2). Initially, blue-green crystals were formed at the solvent surface after about four weeks of very slow evaporation at room temperature. These crystals were harvested from the solution, and after about a week later, another blue crystals formed at the bottom of the solution.

An X-ray crystallographic analysis of the blue-green crystal reveals the formation of three different structures (**Figure 4.21 (a), (b) and (c)**), showing a rare example of a 1:2:2 tri-component co-crystals, formula $[CuL_2(H_2O)(DMSO)]_2[CuL_2(H_2O)_2(DMSO)]$ $[CuL_2(H_2O)(DMSO)_2]$, where L = $4\text{-}NO_2C_6H_4COO$.

The crystal structure shown in **Figure 4.21(a)** is a centrosymmetric dimer. The coordination geometry at each Cu(II) centre is defined by carboxylate-O atoms, an aqua-O and an DMSO-O atom, resulting in the formation of five-coordinate O_5 square pyramidal geometry, as judged by the value of $\tau = 0.02$, which is determined by dividing the difference between two largest O-Cu-O angles by 60. ($\tau = 0$ for an ideal square pyramid and $\tau = 1.0$ for an ideal trigonal bipyramid [46]).

The axial position is occupied by the bridging $O1^i$ atom, which partially explains its elongated bond distance (tetragonal distortion). In contrast to the dinuclear structure observed in **Figure 4.21(a)**, both crystals shown in **Figure 4.21(b)** and **Figure 4.21(c)** are mononuclear.

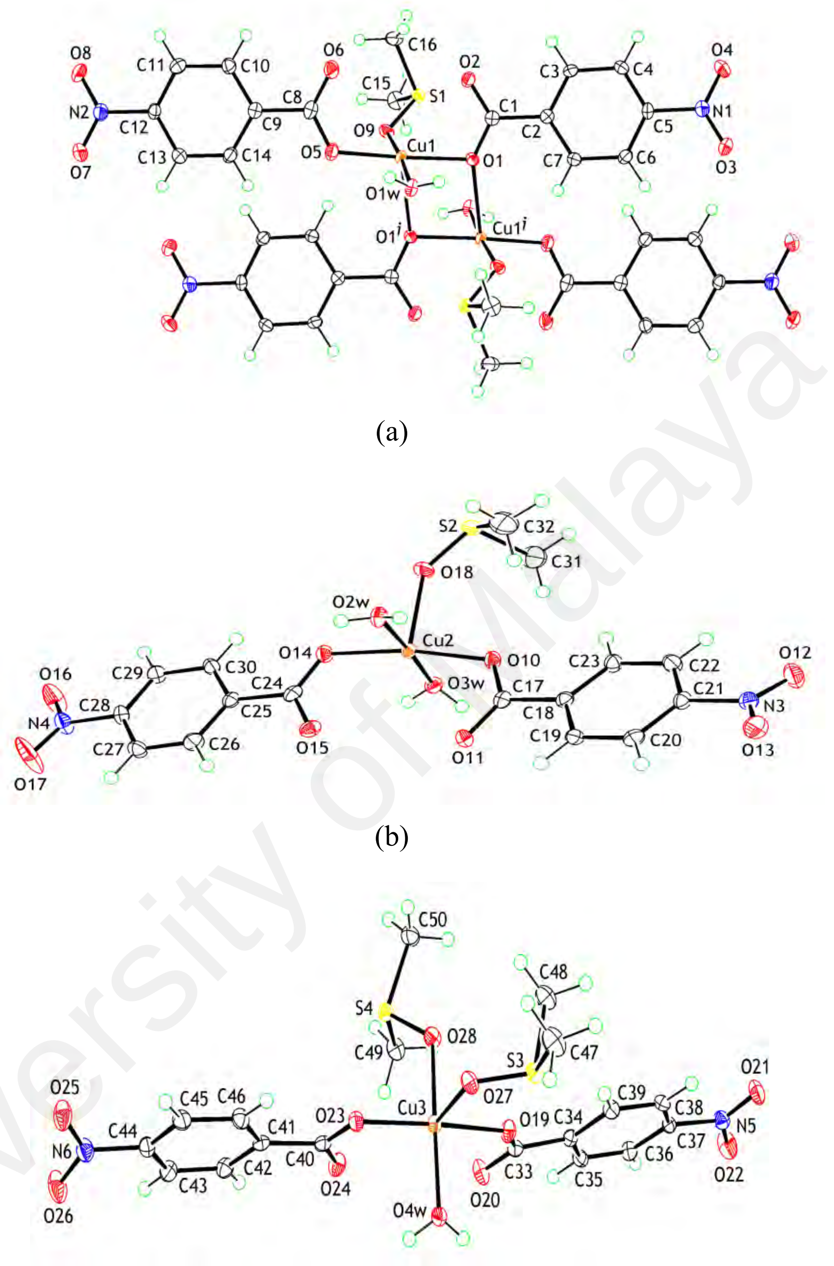

(a)

(b)

(c)

Figure 4.21: Molecular structures of the three independent molecules of the blue-green crystal: (a) $[CuL_2(H_2O)(DMSO)]_2$, a centrosymmetric dimer where symmetry operation *i* = -*x*, 1-*y*, 1-*z*, (b) $[CuL_2(H_2O)_2(DMSO)]$, with a *trans* disposition of aqua ligand, and (c) $[CuL_2(H_2O)(DMSO)_2]$, with a *cis* disposition of DMSO ligand. Diagrams are drawn at the 50% probability level (L = 4-$O_2NC_6H_4COO$).

In **Figure 4.21(b)**, the O_5 donor set is defined by the carboxylate-O atoms, two *trans*-disposed aqua-O atoms and a DMSO-O atom. In **Figure 4.21(c)**, the situation is reversed in that the O_5 donor set is completed by an aqua-O and *cis*-disposed DMSO-O atoms. A small deviation away from the ideal square pyramidal geometry is noted in **Figure 4.21(b)** with the DMSO-O18 atom in the axial position ($\tau = 0.11$); the value of τ is 0.02 for the crystals shown in **Figure 4.21(c)** with the DMSO-O27 in the axial position. It is noteworthy that the Cu-O27 distance in **Figure 4.21(c)** is considerably longer than the Cu-O28 distance formed by the other DMSO-O atom, again consistent with a tetragonal distortion.

The crystal packing of the blue-green crystal shows the formation of a penta-molecule aggregate containing a molecule of $[CuL_2(H_2O)(DMSO)]_2$, two molecules $[CuL_2(H_2O)_2(DMSO)]$ and two molecules, $[CuL_2(H_2O)(DMSO)_2]$, i.e. containing six copper atoms, as shown in **Figure 4.22(a)**. The aggregates are sustained by O–H...O hydrogen bonding where the donor atoms are the aqua-water molecules and the acceptor atoms are carbonyl-O atom. Hence, the O1w water molecule of **Figure 4.21(a)** is hydrogen bonded to the two carbonyl-O11,O15 atoms of **Figure 4.21(b)** giving rise to a ten-membered {...HOH...OCOCuOCO} synthon. The O2w and O3w water molecules form similar synthons, one (O2w) with two carbonyl atoms of **Figure 4.21(a)** and the other with the two carbonyl atoms of **Figure 4.21(c)**. Finally, the O4w aqua ligand of **1c** associates in the same way but with the two carbonyl atoms of **Figure 4.21(b)**.

Additional stability to the aggregates is provided by π...π interactions. The closest of these occur between the C9-C14 and C25-C30 rings, with the separation between the respective ring centroids being 3.6451(15) Å; the dihedral angle between planes is 5.68(12)º. The aggregates thus formed are assembled into layers in the *ac* plane, being stabilised by C–H...O contacts (C47...O14, C48...O18 and C16...O23). Interestingly, the same three DMSO-bound methyl groups provide the donor-H atoms for the inter-planar C–H...O interactions as well. A view of the crystal packing is shown in **Figure 4.22 (b)**.

On the other hand, the X-ray crystallographic analysis of the blue crystal shows an asymmetric unit comprises half a molecule of $[CuL_2(H_2O)(DMSO)_2]$ (L = $4\text{-}NO_2C_6H_4COO$), with the complete molecule being generated by the application of crystallographic 2-fold symmetry (**Figure 4.23**). The structure is interestingly the *trans*-DMSO isomer shown in **Figure 4.21(c)**. The axial position in the distorted O_5 square pyramidal geometry (τ = 0.20) is occupied by the aqua-O1w atom.

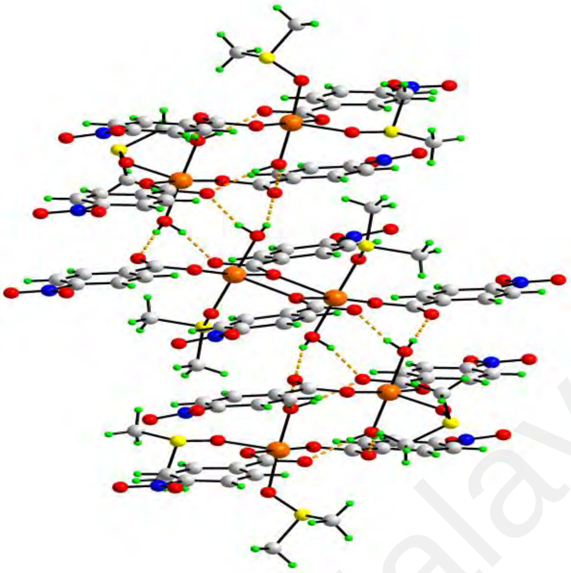

(a)

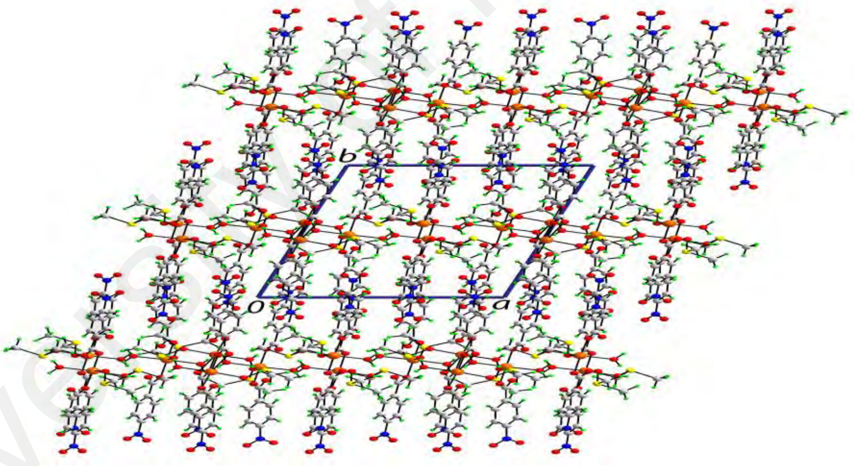

(b)

Figure 4.22: Crystal packing in blue-green crystal: (a) supramolecular aggregation via O–H…O hydrogen bonding (orange dashed lines) leading to five-molecule aggregates, and (b) view in projection down the *c* axis of the unit cell contents highlighting the layer-like nature of the crystal packing.

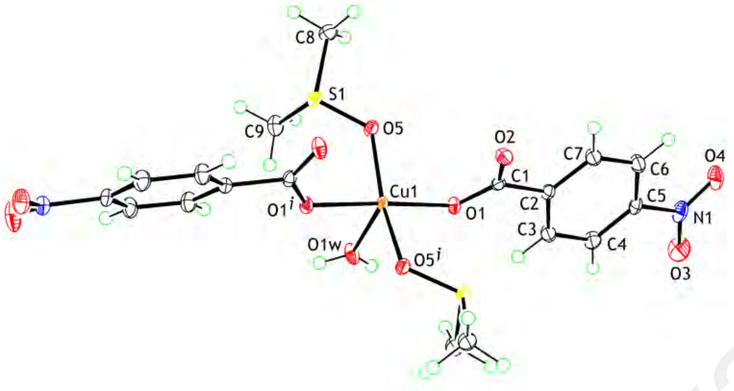

Figure 4.23: Molecular structure of [CuL$_2$(H$_2$O)(DMSO)$_2$], with a *trans* disposition of DMSO ligands, by contrast to the *cis* disposition illustrated for [CuL$_2$(H$_2$O)(DMSO)$_2$] in **Figure 4.21(c)**. The molecule has crystallographic 2-fold symmetry with the Cu and aqua-O atoms lying on the axis; symmetry operation i = 1-x, y, ½-z. Diagram is drawn at the 50% probability level.

The crystal packing in the blue crystal resembles that in the blue-green crystal in that the aqua molecule forms two hydrogen bonds with the carbonyl atoms of a translationally related molecule to form a linear supramolecular chain along the *b* axis (**Figure 4.24(a)**). Chains are linked by C–H...O interactions occurring between centrosymmetrically related DMSO molecules so that a layer is formed in the *bc* plane. These inter-digitate along the *a* direction (**Figure 4.24(b)**), in contrast to the blue-green crystal, there are no significant π-π interactions between the aryl rings.

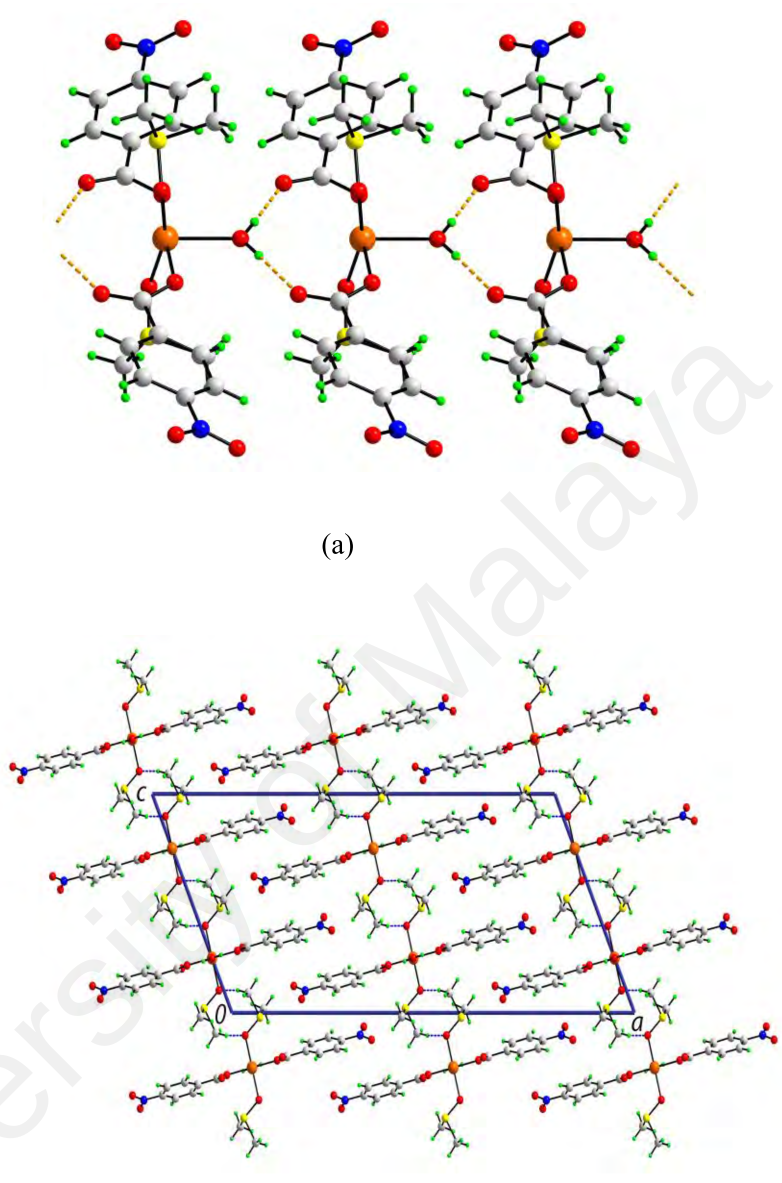

(a)

(b)

Figure 4.24: Crystal packing in the blue crystal: (a) supramolecular chain along the *b* axis sustained by O–H…O hydrogen bonding (orange dashed lines), and (b) view in projection down the *b* axis of the unit cell contents highlighting the stacking of layers.

Thus, the overall structure of the crystals is different from the proposed paddle-wheel structure for $CuNO_2B$. It is likely that a combination of weaker

$4\text{-}NO_2C_6H_4COO\text{-}Cu$ bond and stronger axial-coordination by DMSO molecules resulted in a slow rupture of the dimeric structure of the complex, which then self-assembled to form the observed crystals. The selected geometric parameters for both crystals are collected in **Table 4.9** and **Table 4.10**, and the crystallographic data for these crystals are shown in **Appendix 6**.

A paper on the crystal structure, spectroscopc and thermal studies of the above compound, entitled "*A three-component co-crystal and a mono crystal isolated from the same crystallisation of a copper(II) carboxylate*" has been accepted for publication in Zeitschrift fuer Kristallographie, 2011. (Manuscript Number zkri-D-11-1439R1; **Appendix 7**).

Table 4.9 Selected geometric parameters (Å, º) for the three independent molecules in the blue-green crystal, labelled as **a**, **b** and **c**,[a] and in the blue crystal

Parameter	**a**	Parameter	**b**	Parameter	**c**	Parameter	**Blue crystal**
Cu1–O1	1.9721(15)	Cu2–O10	1.9787(16)	Cu3–O19	1.9483(16)	Cu1–O1	1.9301(12)
Cu1...O2	2.8031(19)	Cu2...O11	3.0263(15)	Cu3...O20	3.125(2)	Cu1...O2	3.1562(12)
Cu1–O5	1.9356(16)	Cu2–O14	1.9786(16)	Cu3–O23	1.9624(16)	Cu1–O1$^{ii\ b}$	1.9301(12)
Cu1...O6	3.1369(16)	Cu2...O15	2.928(2)	Cu3...O24	2.8857(16)	Cu1...O2$^{ii\ b}$	3.1562(12)
Cu1–O9	1.9354(16)	Cu2–O18	2.2341(16)	Cu3–O27	2.2513(15)	Cu1–O5	1.9974(12)
Cu1–O1w	1.9609(17)	Cu2–O2w	1.9552(17)	Cu3–O28	1.9566(16)	Cu1–O5$^{ii\ b}$	1.9974(12)
Cu1–O1$^{i\ b}$	2.4407(16)	Cu2–O3w	1.9516(17)	Cu3–O4w	1.9680(17)	Cu1–O1w	2.2258(18)
O1–C1–C2–C3	163.8(2)	O10–C17–C18–C19	167.6(2)	O19–C33–C34–C35	176.3(2)	O1–C1–C2–C3	-20.5(2)
O5–C8–C9–C10	-169.8(2)	O14–C24–C25–C26	-176.3(2)	O23–C40–C41–C42	-178.1(2)	O1^{ii}–C1^{ii}–C2^{ii}–C3$^{ii\ b}$	-20.5(2)
O3–N1–C5–C4	172.8(2)	O12–N3–C21–C20	166.9(2)	O21–N5–C37–C36	174.2(2)	O3–N1–C5–C4	-5.7(3)
O7–N2–C12–C11	-176.7(2)	O16–N4–C28–C27	-170.6(3)	O25–N6–C44–C43	-164.1(2)	O3^{ii}–N1^{ii}–C5^{ii}–C4^{ii}	-5.7(3)
τ[c]	0.05	τ[c]	0.11	τ[c]	0.02	τ[c]	0.20

a, The labels **a**, **b** and **c** are based on **Figure 4.21(a)**, **Figure 4.21(b)** and **Figure 4.21(c)**; *b,* Symmetry operations *i*: -*x*, 1-*y*, 1-*z*; *ii*: 1-*x*, *y*, ½-*z*; *c,* τ is an indicator for the coordination geometry.

Table 4.10 Summary of intermolecular interactions (A–H…B; Å, º) operating in the crystal structures of the blue-green and blue crystal

A	H	B	A–H	H…B	A…B	A–H…B	Symmetry operation
$[CuL_2(OH_2)(DMSO)]_2[CuL_2(OH_2)_2(DMSO)][CuL_2(OH_2)(DMSO)_2]$							
O1w	H11	O11	0.832(15)	1.927(19)	2.729(2)	162(3)	*x*, *y*, *z*
O1w	H12	O15	0.84(2)	1.87(2)	2.685(2)	165(3)	*x*, *y*, *z*
O2w	H21	O2	0.84(3)	1.84(3)	2.663(2)	167(3)	*x*, *y*, *z*
O2w	H22	O6	0.836(17)	1.831(17)	2.664(2)	174(3)	*x*, *y*, *z*
O3w	H31	O20	0.83(2)	1.80(2)	2.621(3)	170(3)	*x*, *y*, *z*
O3w	H32	O24	0.83(3)	1.88(4)	2.684(3)	163(3)	*x*, *y*, *z*
O4w	H41	O11	0.84(3)	1.91(3)	2.697(3)	158(3)	*x*, *y*, *z*
O4w	H42	O15	0.84(2)	1.85(2)	2.671(2)	165(2)	*x*, *y*, *z*
C49	H49c	O14	0.98	2.35	3.318(3)	168	1-*x*, 1-*y*, -*z*
C50	H50b	O18	0.98	2.48	3.115(3)	162	1-*x*, 1-*y*, -*z*

Table 4.10 (cont.) Summary of intermolecular interactions (A–H…B; Å, º) operating in the crystal structures of the blue-green and blue crystal

A	H	B	A–H	H…B	A…B	A–H…B	Symmetry operation
$[CuL_2(OH_2)(DMSO)]_2[CuL_2(OH_2)_2(DMSO)][CuL_2(OH_2)(DMSO)_2]$							
C16	H16c	O23	0.98	2.49	3.426(3)	160	-1+*x*, *y*, *z*
C16	H16b	O22	0.98	2.55	3.500(3)	164	-1+*x*, 1+*y*, *z*
C50	H50c	O7	0.98	2.55	3.515(3)	169	1+*x*, -1+*y* ,*z*
C49	H49b	O8	0.98	2.56	3.521(3)	166	1+*x*, -1+*y* ,*z*
$[CuL_2(OH_2)(DMSO)_2]$							
O1w	H1	O2	0.84(2)	1.94(2)	2.7759(16)	177(2)	*x*, -1+*y*, *z*
C8	H8c	O5	0.98	2.53	3.461(2)	159	1-*x*, 1-*y*, 1-*z*

4.3.1.2 Magnetic susceptibility

The μ_{eff} value, similarly calculated as for CuB from the values of χ_g (0.221×10^5 cm^3 g^{-1}), χ_d (-4.21×10^{-4} cm^3 mol^{-1}), and hence χ_m^{corr} (2.313×10^{-3} cm^3 mol^{-1}), is 2.30 B.M. at 298 K, and the corresponding -2J value is 194 cm^{-1}. The results suggest antiferromagnetic interaction between the two Cu(II) centres.

However, the interaction is significantly weaker compared to that of CuB (μ_{eff} = 1.93 B.M, -2J = 333 cm^{-1}). This is actually consistent with the longer (weaker) 4-$NO_2C_6H_4COO$-Cu σ bonds (as suggested from UV-vis) and the more distorted geometry, which inhibit effective electronic communication via the superexchange pathway.

4.3.1.3 Thermal analysis

(a) TGA

The thermogram (**Figure 4.25)** indicates that $CuNO_2B$ is thermally stable up to 285°C. Thus, it is more thermally stable compared to CuB (T_{dec} = 254°C). It seems that the thermal stability is not governed by the arylcarboxylate-Cu bond strength, since the 4-$NO_2C_6H_4COO$-Cu bond is weaker than C_6H_5COO-Cu bond.

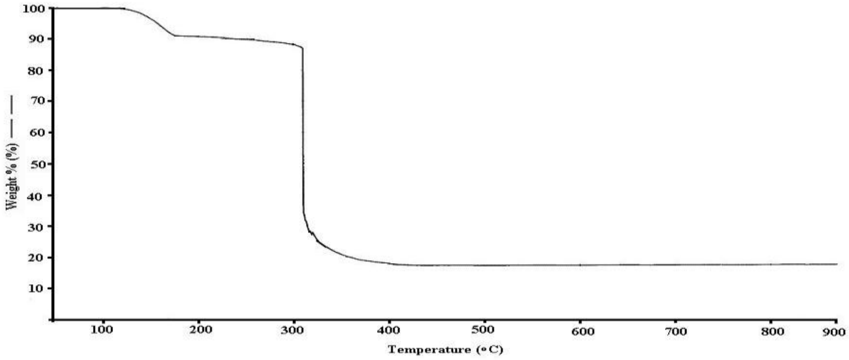

Figure 4.25: TGA of $CuNO_2B$

However, the decomposition process is postulated to involve the decarboxylation of the R-COO ligand to CO_2 and other volatiles. It is expected that the $4\text{-}NO_2C_6H_4\text{-}COO$ bond is stronger than the $C_6H_5\text{-}COO$ bond as a result of partial π bond (**Figure 4.26**), and therefore less easily decarboxylated.

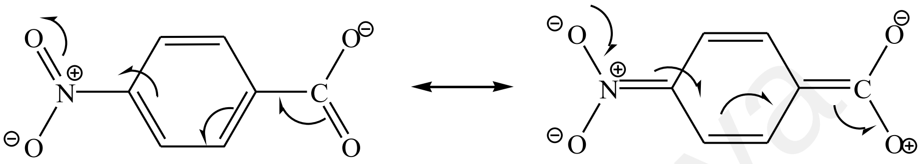

Figure 4.26: Electron delocalization in $4\text{-}NO_2C_6H_4COO^-$ ion

The thermogram also shows an initial weight loss of 8.0% at about 120°C, assigned to the evaporation of axially coordinated CH_3CH_2OH and H_2O molecules (expected, 7.5%). The next weight loss of 73.0% at 285°C is assigned to the decomposition of $4\text{-}NO_2C_6H_4COO$ ligand (expected, 77.7%). The amount of residue at temperatures above 400°C is 19.0%. Assuming that it was purely CuO as previously done in the case of CuB, the estimated formula mass for $CuNO_2B$ is 837 g/mol. This is in excellent agreement with the value calculated from the proposed chemical formula (855 g/mol).

(b) DSC

The DSC plot (**Figure 4.27**) shows a weak endothermic peak at about 120°C ($\Delta H = +122$ kJ/mol), assigned to the release of axially ligated CH_3CH_2OH and H_2O molecules, as suggested from TGA. This is followed by a very strong exotherm at 316°C ($\Delta H = -1581$ kJ/mol). The plot is actually quite similar to that of CuB, and thus may be similarly explained.

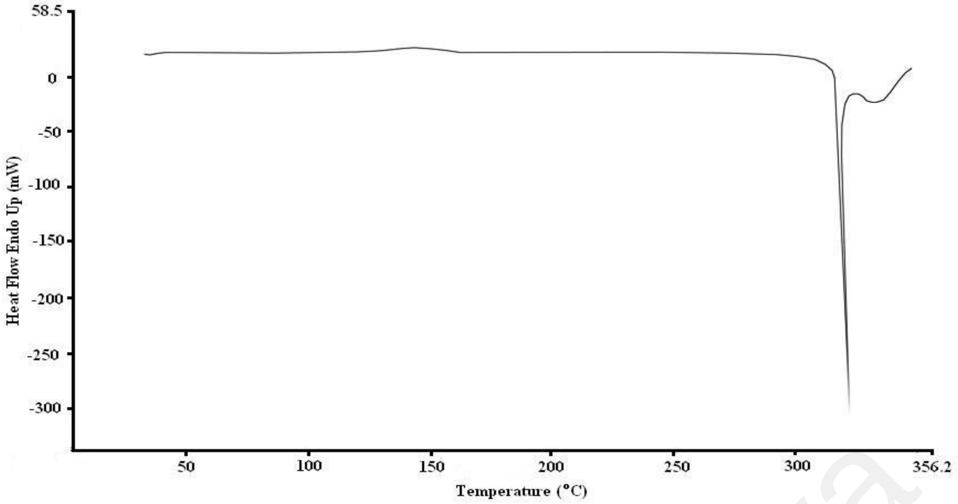

Figure 4.27: DSC of $CuNO_2B$

4.3.1.4 Cyclic voltammetry

As for CuB, the CV of $CuNO_2B$ in CH_3OH-CH_3COOH was scanned cathodically under several conditions in an attempt to investigate its electrochemical properties. It is important to recall that, based on the UV-vis spectroscopic study (**Section 4.3.1(c)**), the dimeric paddle-wheel structure of $CuNO_2B$ remained intact in these solvents.

(a) Potential window = +1.5 V to -1.5 V; scan rate = 100 mV s^{-1}

The CV (**Figure 4.28**) shows four cathodic peaks at -0.09 V, -0.32 V, -0.9 V and -1.1 V, and two anodic peaks at +0.21 V and +1.0 V respectively.

The first cathodic peak at -0.09 V is assigned to the reduction of [Cu(II)Cu(II)] to [Cu(II)Cu(I)]. It is noted that this process occurred at a less negative potential (easier reduction) compared to that of CuB (-0.13 V). This is in good agreement with the weaker 4-$NO_2C_6H_4COO^-Cu(II)$ σ coordinate bond, which "allows" for easier geometrical distortion towards tetrahedral.

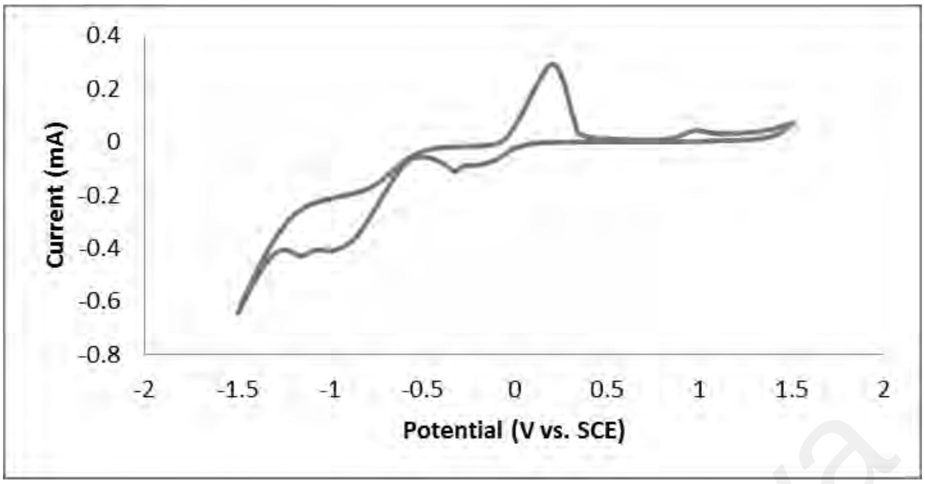

Figure 4.28: CV of $CuNO_2B$

As in the case of CuB, the mixed-valence [Cu(II)Cu(I)] formed from $CuNO_2B$ suffered partial dissociation to [Cu(II)] and [Cu(I)]. The mononuclear [Cu(II)] formed was then reduced to [Cu(I)] at a slightly lower potential compared to the mononuclear complex obtained from CuB (-0.35 V). This actually further supports the effect on the strong electron withdrawing NO_2 group, as explained above for the dimer.

It is interesting to note that the CV of $CuNO_2B$ shows another two cathodic peaks at more negative potentials (more difficult reduction) compared to CuB. The potential at -0.9 V is assigned to the reduction of the mixed-valence [Cu(II)Cu(I)] to [Cu(I)Cu(I)], which was observed at -0.74 V for CuB. This indicates that the mixed-valence complex formed from $CuNO_2B$ was more stable, which is consistent with the more extensive electronic delocalization involving the $–NO_2$ group, as suggested above. Another cathodic peak at -1.1 V is ascribed to the reduction of the $-NO_2$ group, which was reported in the literature to occur in the potential range of -1.2 V to -1.8 V [47].

The broad anodic peak at +0.21 V suggests an overlap of two or more overlapping peaks. Thus, it is assigned to an almost simultaneous oxidation of the [Cu(I)Cu(I)] to [Cu(I)Cu(II)], [Cu(I)] to [Cu(II)], [Cu(I)Cu(II)] to [Cu(II)Cu(II)] and the NO_2 group. The peak is at a much lower potential (easier oxidation) compared to CuB (+0.31 V). This is again consistent with a weaker $4\text{-}O_2NC_6H_4COO\text{-}Cu$ coordinate bond, which allows facile geometrical change to the preferred square planar geometry of Cu(II). The electrochemical-chemical (EC) mechanism is summarized below:

$$[\mathrm{Cu(II)Cu(II)}] \xrightleftharpoons[+0.21\ \mathrm{V}]{-0.09\ \mathrm{V}} [\mathrm{Cu(II)Cu(I)}]$$

$$[\mathrm{Cu(II)Cu(I)}] \xrightleftharpoons{\text{dissociation}} [\mathrm{Cu(II)}] + [\mathrm{Cu(I)}]$$

$$[\mathrm{Cu(II)}] \xrightleftharpoons[+0.21\ \mathrm{V}]{-0.32\ \mathrm{V}} [\mathrm{Cu(I)}]$$

$$[\mathrm{Cu(II)Cu(I)}] \xrightleftharpoons[+0.21\ \mathrm{V}]{-0.8\ \mathrm{V}} [\mathrm{Cu(I)Cu(I)}]$$

From the above cathodic and anodic potentials, the ΔE values for [Cu(II)Cu(II)]-[Cu(II)Cu(I)] and [Cu(II)Cu(I)]-[Cu(I)Cu(I)] couples are 300 mV and 1110 mV respectively. The high values strongly suggest quasireversible processes as a result of extensive structural changes. The greater value of ΔE for [Cu(II)Cu(I)-Cu(I)Cu(I)] process suggests a more extensive structural reorganization for this couple. However, it is noted that the ΔE value for [Cu(II)Cu(II)]-[Cu(II)Cu(I)] is much less than that of CuB

(590 nm), which is consistent with the a facile redox process of $CuNO_2B$ as a result of a weaker $4\text{-}NO_2C_6H_4COO^-Cu(II)$ σ coordinate bond.

(b) *Potential window = +1.5 V to -1.5 V; scan rates = 40 - 100 mV s^{-1}*

As for CuB, in order to further investigate the level of reversibility of the complex, the CV within the same potential window was recorded at different scan rate (40 – 100 mV/s). The voltammograms are shown in **Figure 4.29**.

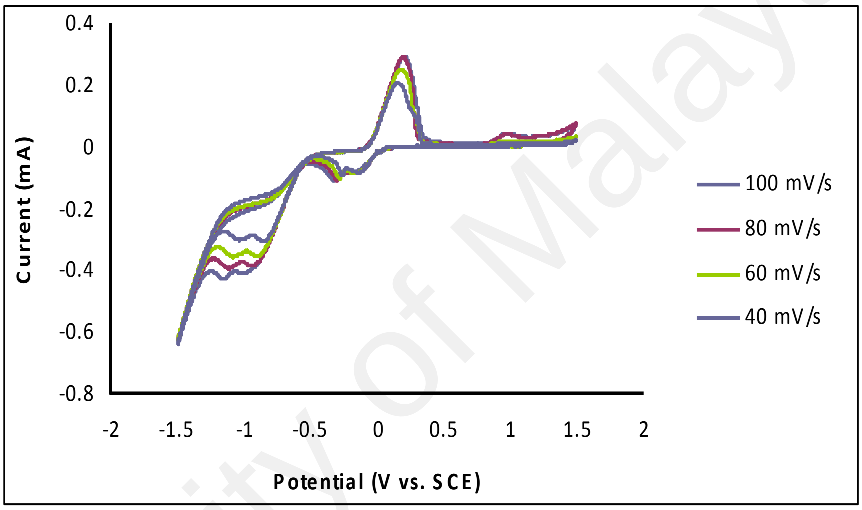

Figure 4.29: CV of $CuNO_2B$ at different scan rates

The potential and ΔE values at each scan rate are shown in **Table 4.11**. It could be observed that the potential for the first cathodic process increases as the scan rate increases. Similar trend was observed for CuB, and thus may be similarly explained.

The value of ΔE ranges from about 324 mV to 1110 mV at all scan rates. This suggests extensive structural reorganization upon reduction and confirming the quasireversibility of the process.

It is worth noting that at slower scan rate of 40 mV s^{-1}, the second anodic peak (observed at about +1 V for the faster scan rates) is observed as a new shoulder at much lower potential of +0.25 V. The plausible explanation is, at the slower scan rate, the reduced complex have sufficient time to undergo structural reorganization to a more planar geometry at Cu(I). Thus, the complex experiences easier oxidation to Cu(II), as proposed above.

Table 4.11: The peak potential (E_p/V) and peak separation (ΔE/mV) for $CuNO_2B$ in CH_3OH-CH_3COOH at each scan rate (mV s^{-1})

Scan rate	E_{pc1}	E_{pc2}	E_{pc3}	E_{pc4}	E_{pa1}	E_{pa2}	ΔE_1^*	$\Delta E_2^\#$
40	-0.074	-0.24	-0.80	-0.97	+0.12	+0.25(sh)	324	920
60	-0.078	-0.27	-0.81	-1.0	+0.15	-	228	960
80	-0.08	-0.28	-0.85	-1.0	+0.16	-	240	1010
100	-0.09	-0.32	-0.90	-1.1	+0.21	-	300	1110

* $\Delta E_1 = E_{pa2} - E_{pc1}$; # $\Delta E_2 = E_{pa1} - E_{pc3}$

Additionally, a graph of the first cathodic peak current versus the square roots of the scan rate is linear (**Figure 4.30**), indicating that the reduction of [Cu(II)Cu(II)] to [Cu(II)Cu(I)] was diffusion-controlled [37]. This is similar to CuB.

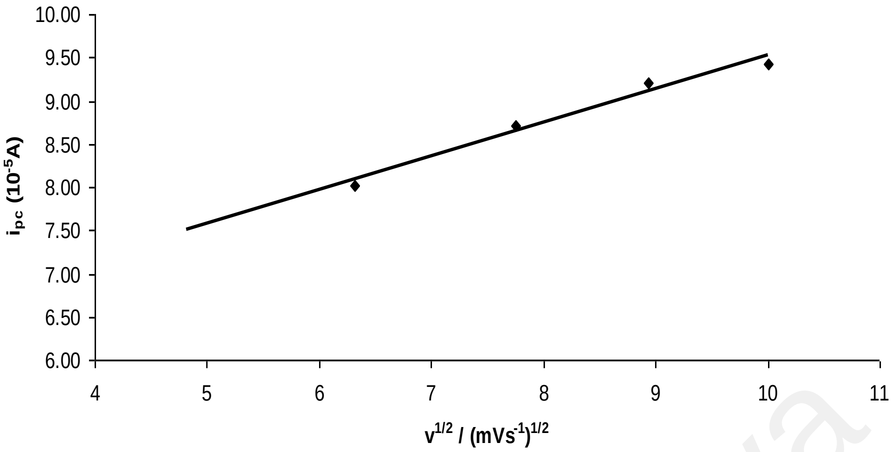

Figure 4.30: Graph of the first cathodic currents versus square root of the scan rates for $CuNO_2B$

4.3.1.5 Summary

The chemical formula for $CuNO_2B$ is $[Cu_2(4\text{-}O_2NC_6H_4COO)_4(CH_3CH_2OH)(H_2O)]$, and it is proposed to have the paddle-wheel structure similar to that of CuB. However compared to CuB, the RCOO-Cu coordinate bonds in $CuNO_2B$ are more easily disrupted in organic solvents, the antiferromagnetic interaction between the two Cu(II) centres is weaker, the thermal stability is higher and the reduction potential is lower. These suggest that the square pyramidal geometry at Cu(II) has a bond angle of greater than 90^o (highly distorted).

4.3.2 Cu(II) 3,5-Dinitrobenzoate

Copper(II) 3,5-dinitrobenzoate ($CuDNO_2B$) was obtained as a pale blue powder. Its yield (54.9%) is similar to that of $CuNO_2B$ (52.0%), suggesting similar solubility in ethanol. It was soluble in acetone, tetrahydrofuran, dimethylsulfoxide, dimethylformamide and pyridine, partially soluble in acetonitrile, and insoluble in other common organic solvents and in water.

4.3.2.1 Structural elucidation

Compared to the ligand of $CuNO_2B$ (the anion of $4\text{-}NO_2C_6H_4COOH$, $pK_a = 3.43$), the ligand of $CuDNO_2B$, $3,5\text{-}(NO_2)_2C_6H_3COO$, is a weaker Lewis base (pK_a value for $3,5\text{-}(NO_2)_2C_6H_3COOH$ is 2.82). Thus, it is postulated that the $3,5\text{-}(NO_2)_2C_6H_3COO\text{-}Cu$ σ coordinate bond will be weaker, and therefore more easily distorted. In addition, as a result of strong electron withdrawing effect of two $\text{-}NO_2$ groups, the positive charge on Cu(II) will be increased, which will incur greater repulsion between two Cu(II) centres. Therefore, the formation of dimeric, paddle wheel structure is less favourable. Also, the presence of two NO_2 groups can incur greater steric strain in the complex, which may become the dominant factor against the formation of the dinuclear complex [43, 46-48].

However based on the following analytical results, it is postulated that the chemical formula for $CuDNO_2B$ is $[Cu_2(3,5\text{-}(NO_2)_2C_6H_3COO)_4(H_2O)_2]$, and that it adopted similar dimeric paddle-wheel structure as proposed for $CuNO_2B$ (**Figure 4.19).**

(a) *Elemental analysis*

The results of the elemental analysis (33.2% C, 1.9% H, 10.7% N and 11.0% Cu) are in good agreement with those calculated for the chemical formula $CuC_{14}H_8O_{13}N_4$ or $[Cu(3,5\text{-}(NO_2)_2C_6H_3COO)_2(H_2O)]$ (formula mass, 503.5 g mol^{-1}; 33.4% C, 1.6% H, 11.1% N and 12.6% Cu).

(b) FTIR spectroscopy

The FTIR spectrum (**Figure 4.31**) is almost similar to that of $CuNO_2B$ (**Figure 4.17**). This, together with the Δv value of 140 cm^{-1}, suggests similarity in the structures of the two complexes.

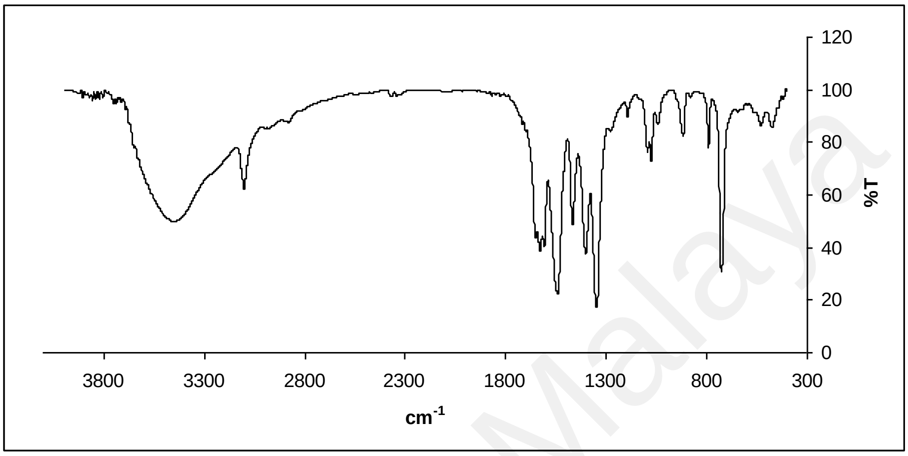

Figure 4.31: FTIR spectrum of $CuDNO_2B$

(iii) UV-vis spectroscopy

The UV-vis spectrum of solid $CuDNO_2$ (**Figure 4.32**) shows similar absorption peaks as that of $CuNO_2B$, and therefore may be similarly assigned and explained. However, the *d-d* absorption peaks for $CuDNO_2B$ are red-shifted by 20 nm compared to those of $CuNO_2B$ (**Table 4.12**) The shifts towards lower energies are actually expected and consistent with a much weaker 3,5-$(O_2N)_2C_6H_4COO$-Cu(II) σ coordinate.

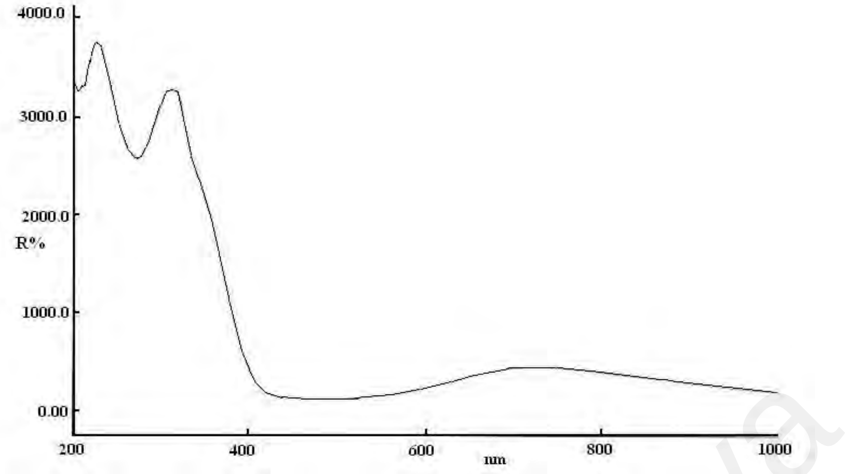

Figure 4.32: Solid state UV-vis spectrum of $CuDNO_2B$

Table 4.12: The UV-vis bands for $CuDNO_2B$ and $CuNO_2B$

Electronic transition	$CuDNO_2B$	$CuNO_2B$
$z^2 \rightarrow x^2 - y^2$	-	850
$xy \rightarrow x^2 - y^2$	720	700
$yz, xz \rightarrow x^2 - y^2$	-	440
LMCT	380	390
$n \rightarrow \pi^*; \pi \rightarrow \pi^*$	310, 225	309, 239

It is noted that the absorption bands for $z^2 \rightarrow x^2 - y^2$ and $yz, xz \rightarrow x^2 - y^2$ transitions are not observed as these might be red-shifted and overlapped with the broad $xy \rightarrow x^2-y^2$ band.

In order to further compare the structural stability of the compounds, the UV-vis spectra were studied in the same solvents as used for $CuNO_2B$, namely in DMSO, DMF and CH_3OH-CH_3COOH (20:1). These are shown in **Figure 4.33** and the corresponding spectral data in **Table 4.13**.

As in the case of $CuNO_2B$, the *d-d* absorption band for $CuDNO_2B$ seems to also depend on the strength of the coordinating solvent. In addition, its *d-d* band in CH_3OH-CH_3COOH (20:1) is at similar position as $CuNO_2B$ (700 nm), while Band II is also not observed.

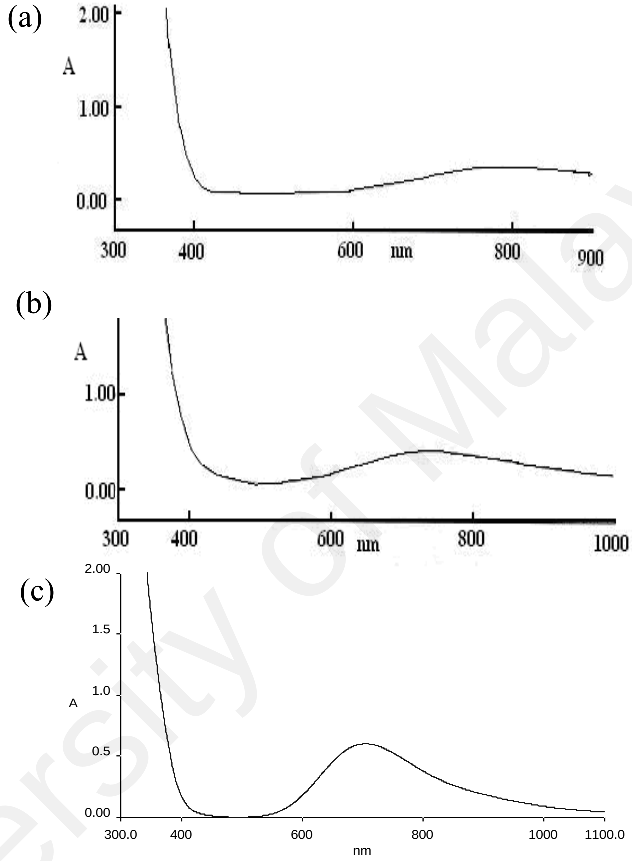

Figure 4.33: UV-vis spectra of $CuDNO_2B$ in: (a) DMSO; (b) DMF and (c) CH_3OH-CH_3COOH (20:1)

Table 4.13: The UV-vis spectral data for $CuDNO_2B$ in different solvents

λ_{max}/nm (ε_{max}/$M^{-1}cm^{-1}$)		**Solvent**
Band I	**Band II**	
700 (--)	390 (--)	None
794 (150)	-	DMSO
740 (173)	-	DMF
705 (233)	-	CH_3OH-CH_3COOH (20:1)

--, not applicable; -, not observed

The lower stability of the dimeric paddle-wheel structure proposed for $CuDNO_2B$ is further supported by the structures of crystals formed in solution. For example, blue-green prismatic crystals were obtained by dissolving the complex in THF, adding an equal mole of 2,2'-bypiridine, and slowly evaporating off the solvent at room temperature for two days. The crystallographic asymmetric unit of the crystal comprises a Cu(II) mononuclear complex and a THF molecule of crystallization (1:1 ratio). The molecular structure of the crystal is illustrated in **Figure 4.34** and selected geometric parameters and selected bond lengths are collected in **Table 4.14** and **Table 4.15**.

In the crystal structure, the Cu atom is penta-coordinate by two O atoms derived from two monodentate carboxylate ligand, two N atoms of the chelating 2,2'-bipyridine ligand, and an O atom derived from the coordinated water molecule. The resulting N_2O_3 donor set defines a square pyramidal geometry as indicated by the value of $\tau = 0.16$ (compare with $\tau = 0$ for an ideal square pyramid and $\tau = 1.0$ for an ideal trigonal bipyramid [49]). In this description, the coordinated water molecule occupies the apical position and each carboxylate-O atom is *trans* to a pyridine-N atom.

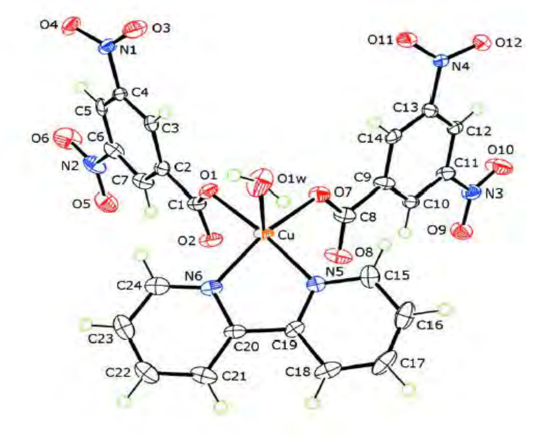

Figure 4.34: The molecular structure of the crystal, showing displacement ellipsoids at the 50% probability level. The disordered THF molecule is not shown.

Table 4.14: Selected geometric parameters for the blue-green prismatic crystals

$[Cu(C_7H_3N_2O_6)_2(C_{10}H_8N_2)(H_2O)]\cdot C_4H_8O$	$F(000) = 1500$
$Mr = 732.08$	$Dx = 1.614$ Mg m^{-3}
Orthorhombic, $Pca2_1$	Mo *Kα* radiation, λ = 0.71073 Å
Hall symbol: P 2c-2ac	
Cell parameters from 7872 reflections	
$a = 19.6424(7)$ Å	θ = 2.6–28.0°
$b = 23.2687(8)$ Å	μ = 0.81 mm−1
$c = 6.5897(2)$ Å	$T = 100$ K
$V = 3011.84(17)$ Å	Prism, green
$Z = 4$	0.26 × 0.07 × 0.07 mm

Table 4.15: Selected bond lengths (A°)

Cu—O7 1.951 (4)	Cu—N6 2.010 (4)
Cu—O1 1.972 (4)	Cu—O1W 2.198 (4)
Cu—N5 2.007 (4)	

The most prominent interactions operating in the crystal structure of the crystal are O–H···O contacts occurring between the hydrogen atoms of the coordinated water molecule and the carbonyl-O atoms of a translationally related molecule. As illustrated in **Figure 4.35**, the water-bound hydrogen atoms effectively form a bridge between the adjacent carbonyl atoms resulting in a ten-membered {···HOH···OCOCuOCO} synthon. The result of this hydrogen bonding is the formation of a supramolecular chain along the *c* axis. Each supramolecular chain is connected into a double chain along *c* with helical topology *via* C–H···O contacts whereby two bipyridine-H atoms form interactions with a carbonyl-O of the second chain, and a third bipyridine-H atom forms a C–H···O contact with a nitro-O within the chain (**Figure 4.36**). This arrangement brings into close proximity the 2,2'-bipyridine molecules which interdigitate, allowing for the formation of π–π interactions [ring centroid (N6,C20–C24)···ring centroid(N6,C20–C24)i = 3.527 (3) Å for i: -*x* + 1/2, *y*, *z* - 1/2]. The double chains pack in the *ac* plane to form layers that stack along the *b* axis (**Figure 4.37**).

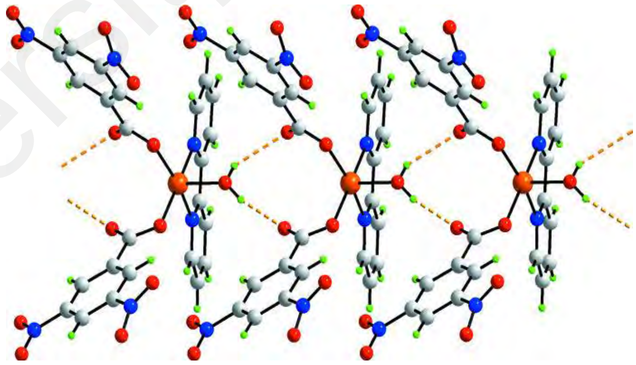

Figure 4.35: A portion of the supramolecular chain aligned along the *c* axis found in the crystal structure of (I) mediated by O–H···O hydrogen bonding (orange dashed lines). Colour code: Cu, orange; O, red; N, blue; C, grey; and H, green.

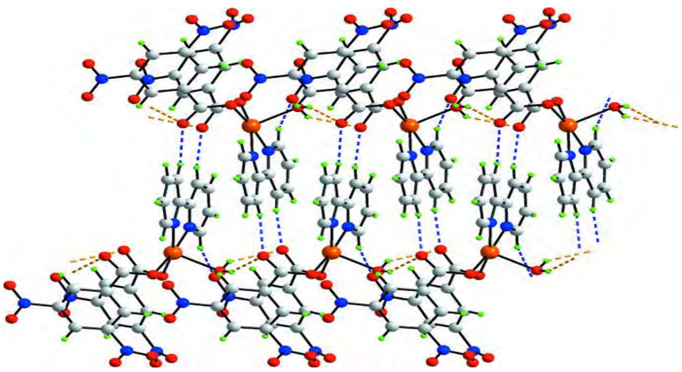

Figure 4.36: Double chain with helical topology mediated by O–H···O and C–H···O contacts shown as orange and blue dashed lines, respectively. Colour code: Cu, orange; O, red; N, blue; C, grey; and H, green.

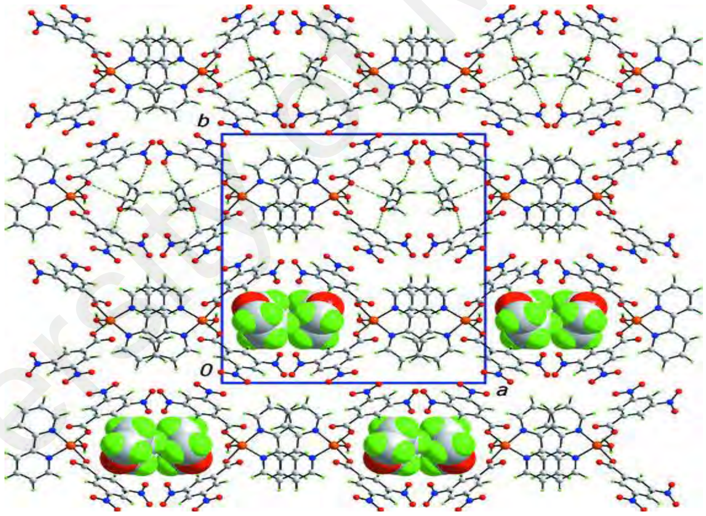

Figure 4.37: View of the unit-cell contents viewed in projection down the *c* axis. The double chains form layers in the *ac* plane which have large voids that are occupied by the solvent THF molecules; only the major component of the disordered molecules are shown. In the lower two layers, the solvent molecules are shown in space filling mode. In the upper two layers, the C–H···O interactions connecting the thf molecules to the layers are shown as green dashed lines. Colour code: Cu, orange; O, red; N, blue; C, grey; and H, green.

Within each layer, there are voids and these are occupied by the solvent THF molecules which are held in place by C–H···O interactions. Interactions between layers are primarily of the type C–H···O as detailed in **Table 4.16**.

Table 4.16: Hydrogen-bond geometry (A°)

D—H.....A	D—H	H.....A	D…..A	D—H…..A
O1w—H1w........O2i	0.84 (5)	2.01 (6)	2.766 (6)	150 (7)
O1w—H2w........O8i	0.84 (5)	2.35 (7)	3.048 (6)	141 (6)
C18—H18..........O8ii	0.95	2.17	3.060 (7)	155
C21—H21..........O2ii	0.95	2.41	3.087 (7)	128
C15—H15........O9i	0.95	2.43	3.285 (7)	150
C1s—H1s2........O7	0.99	2.53	3.451 (10)	155
C3—H3........O1s	0.95	2.58	3.520 (8)	169
C2s—H2s2........O11	0.99	2.49	3.385 (11)	150
C5—H5........O4iii	0.95	2.58	3.360 (7)	140
C12—H12........O12iii	0.95	2.43	3.263 (7)	146
C16—H16……O12iv	0.95	2.47	3.234 (8)	138

Symmetry codes: (i) x; y; z -1; (ii) -x +1/2; y; z -1/2; (iii) -x + 3/2; y; z + 1/2; (iv)-x + 1;-y + 2; z -1/2.

It is postulated that 2,2’-bipyridine molecules were able to rupture the “weaker” 3,5-$(NO_2)_2C_6H_3COO$-Cu coordinate bonds in the dimeric complex, and the “free” ions formed then self-assembled to form the mononuclear Cu(II) complex.

The above crystal structure was published as a paper in an ISI journal in 2010: N. Abdullah, M.I. Mohamadin, A.P. Safwan, E.R.T Tiekink, Acta Cryst. (2010). E66, m1055–m1056 (**Appendix 8)**.

4.3.2.2 Magnetic susceptibility

The μ_{eff} value, calculated as before from the values of χ_g (1.73 x 10^{-6} cm^3 g^{-1}), χ_d (-4.58 x 10^{-4} cm^3 mol^{-1}), and hence χ_m^{corr} (2.20 x 10^{-3} cm^3 mol^{-1}), is

2.25 B.M. at 298 K. The -2J value is 217 cm^{-1}. The results suggest antiferromagnetic interaction between the two copper(II) centres.

It is noted that the magnetic results are similar to those of CuNO$_2$B (μ_{eff} = 2.30 B.M.; -2J = 194 cm^{-1}). Hence, it may be suggested that the presence of an additional NO$_2$ group, and the different locations of this group at the aromatic ring, do not have a significant effect on the magnetic properties of these complexes.

4.3.2.3 Thermal analysis

(a) TGA

The thermogram (**Figure 4.38)** shows that CuDNO$_2$ is thermally stable up to 196^{o}C, which is much lower than CuNO$_2$B (285^{o}C). The decomposition temperature is expected to be higher due to the presence of two NO$_2$ groups per aromatic ring. However, the result is consistent with a proposed weaker 3,5-(NO$_2$)$_2$C$_6$H$_3$COO-Cu bond.

The first gradual weight loss of 3.5% from about 70^{o}C is assigned to the evaporation of two H$_2$O molecules (expected, 3.6%). The decomposition process is made up of two well-separated steps. The weight loss of 7.0% at about 196^{o}C is assigned to the loss of two CO$_2$ molecules from two of the four ligands (expected, 8.7%). The final rapid weight loss of 86.6% at 302^{o}C is assigned to further decomposition of all of the remaining ligands (expected 85.6%).

The amount of residue at temperatures above 400°C is 2.9%. The expected amount, assuming that it is purely CuO, is 7.5%. The result seems to indicate the formation of volatile Cu compound(s). This is interesting as it suggests that $CuDNO_2$ may be used as a precursor complex for deposition of a thin layer of CuO or Cu metal by chemical vapour deposition technique for nanotechnological applications.

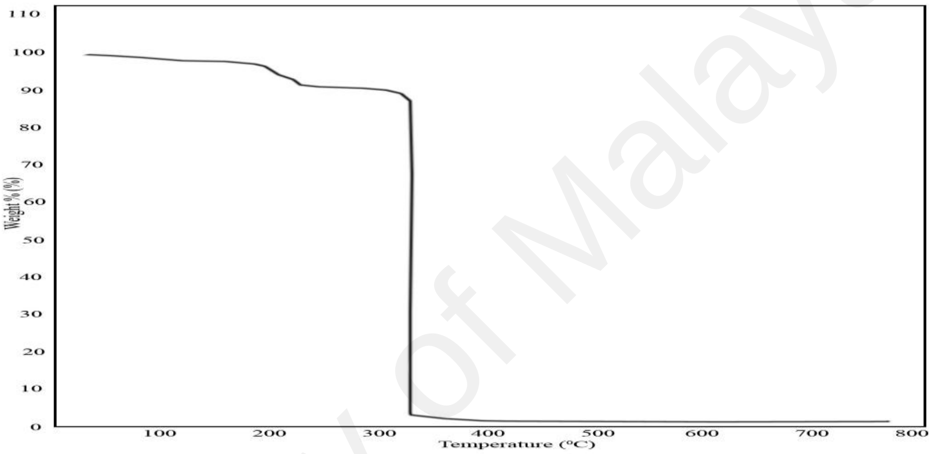

Figure 4.38: TGA of $CuDNO_2B$

(b) DSC

The DSC plot of $CuDNO_2B$ (**Figure 4.39**) shows the appearance of a small endothermic peak at 150°C ($\Delta H = +104$ kJ/mol). It is interesting to note that no exothermic peak is observed at this region to represent the formation of carbon dioxide (CO_2) gas. Thus it is postulated that the endothermic peak observed represents a net energy at this temperature which involved multiple bond breaking and formation processes. A very strong exothermic peak at 330°C ($\Delta H = -888$ kJ/mol) is also observed indicating the possible formation of highly stable volatiles. It is noted that the ΔH value for $CuDNO_2B$ is less negative than that for CuNO$_2$B (ΔH = -1581 kJ/mol at 316^{o}C), suggesting the formation of less stable volatiles for the former complex.

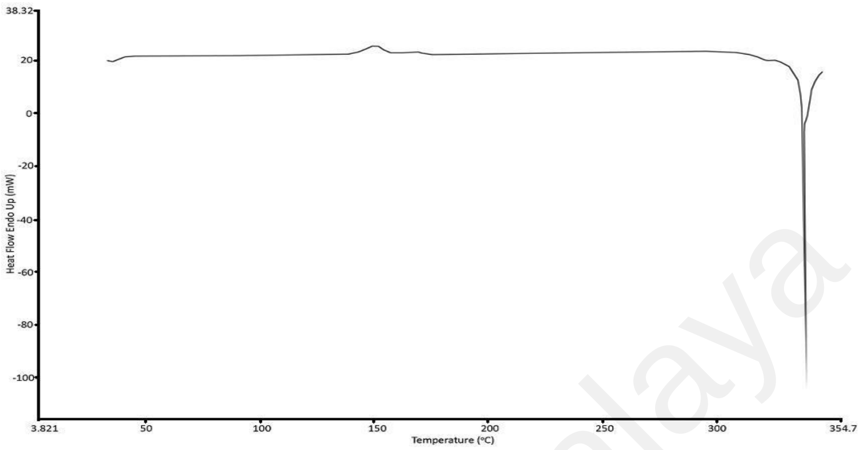

Figure 4.39: DSC of CuDNO$_2$B

4.3.2.4 Cyclic voltammetry

The CV of CuDNO$_2$B in CH$_3$OH-CH$_3$COOH was recorded under several conditions in order to investigate its electrochemical properties. Recall from the UV-vis spectroscopy that the dimeric paddle-wheel structure of CuDNO$_2$B remained intact in this solvents.

(a) Potential window = +1.5 V to -1.5 V; scan rate = 100 mV s^{-1}

It is immediately apparent that the CV for CuDNO$_2$B (**Figure 4.40**) shows some similarities to that of CuNO$_2$B. For example, it shows four cathodic peaks at -0.05, -0.29, -0.7 and -1.0 V, and broad and overlapping anodic peaks at +0.13 and +0.27 V (shoulder). As explained before, the unsymmetrical pattern of the peaks, which were also observed in the CV of CuNO$_2$B, depicts the quasireversibilty of the process as well as the occurrence of geometrical distortion during the redox process [37].

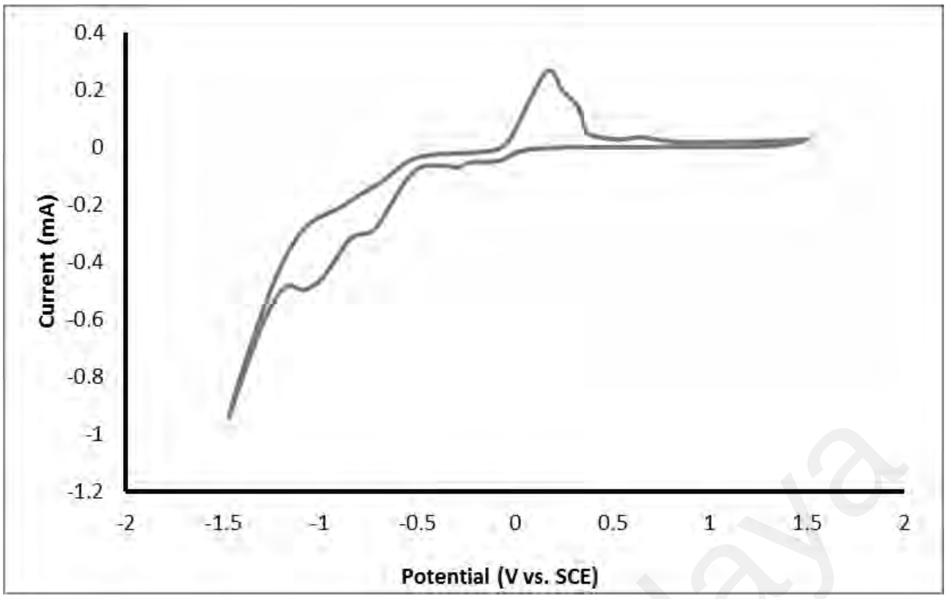

Figure 4.40: CV of $CuDNO_2B$

The cathodic peaks may be similarly explained and assigned as for $CuNO_2B$. However, the potentials for these peaks are lower than those recorded for $CuNO_2B$ (-0.09 V, -0.32 V, -0.9 V and -1.1 V). This is likely due to the higher residual positive change on Cu(II) centres due to the presence of two strongly electron-attracting NO_2 group in the former complex, and to a greater tetrahedrally distorted geometry at Cu(II) as a result of weaker 3,5-$(O_2N)_2C_6H_3COO$-Cu coordinate bond.

It is noted that the first potential for the oxidation process is also lower for $CuDNO_2B$ (+0.13 V) compared to $CuNO_2B$ (+0.21 V). Again, the easier oxidation of the [Cu(I)Cu(I)] complex is actually consistent with a weaker 3,5-$(O_2N)_2C_6H_3COO$-Cu coordinate bond, which allows for a less rigid geometry or easier distortion to the preferred square planar geometry for Cu(II).

The values of ΔE calculated for the redox couples, [Cu(II)Cu(II)]-[Cu(I)Cu(II)] and [Cu(II)Cu(I)]-[Cu(I)Cu(I)], are 320 mV and 830 mV respectively. The ΔE value for [Cu(II)Cu(II)]-[Cu(I)Cu(II)] couple is nearly similar to $CuNO_2B$ (300 mV), indicating insignificant effect of the number and positions of the NO_2 group on the first reduction process. However, the ΔE value for next redox couple, [Cu(II)Cu(I)]-[Cu(I)Cu(I)], is significantly lower (less extensive distortion) than $CuNO_2B$ (1100 mV). This is again consistent with a less rigid geometry of the mixed-valence from the former complex.

(b) Potential window = +1.5 V to -1.5 V; scan rates = 40 - 100 mV s^{-1}

In order to further probe the redox properties of $CuDNO_2B$, the CV was recorded at different scan rates, and the results are shown in **Figure 4.41**.

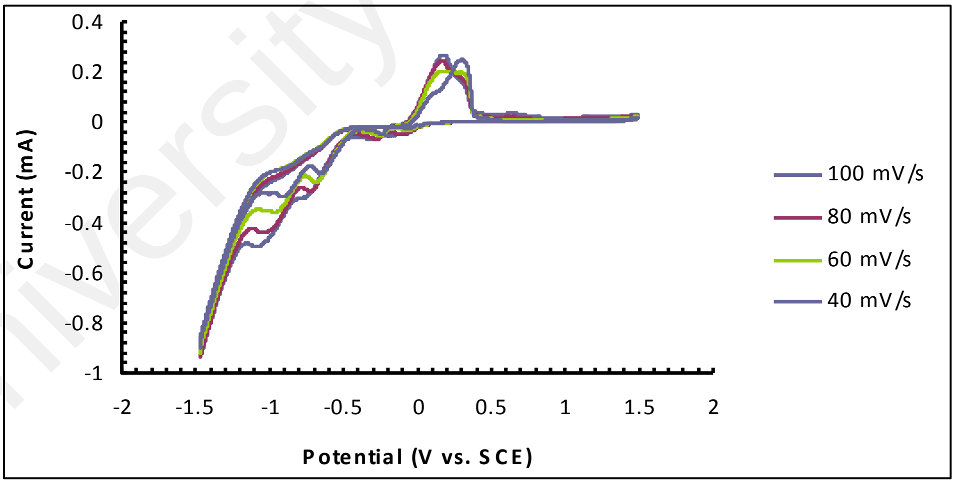

Figure 4.41: CVs of $CuDNO_2B$ at different scan rates

The potential and ΔE values for each scan rate (υ) are shown in **Table 4.17**. The trend is similar to that observed for $CuNO_2B$, and may be similarly explained.

The value of ΔE ranges from about 260 mV to 830 mV for all scan rates, suggesting an occurrence of extensive structural reorganization upon reduction and hence confirming the quasireversibility of the process. It is important to note that the ΔE values for CuDNO$_2$B are lower compared to those of CuNO$_2$B (324 mV to 1110 mV), suggesting a less extensive structural reorganization in the former complex. This is consistent with the weaker 3,5-(NO$_2$)$_2$C$_6$H$_3$COO-Cu coordinate bonds.

Table 4.17: The CV data (in V) for CuDNO$_2$B at different scan rate (υ/ mV s^{-1})

υ	E_{pc1}	E_{pc2}	E_{pc3}	E_{pc4}	E_{pa1}	E_{pa2}	ΔE_1^*	$\Delta E_2^\#$
40	-0.01	-0.20	-0.6	-0.87	+0.09(sh)	+0.25	260	690
60	-0.02	-0.21	-0.65	-0.9	+0.11	0.24 (sh)	260	760
80	-0.03	-0.23	-0.67	-0.9	+0.12	0.25(sh)	280	790
100	-0.05	-0.29	-0.7	-1.0	+0.13	+0.27(sh)	320	830

* $\Delta E_1 = E_{pa2} - E_{pc1}$; # $\Delta E_2 = E_{pa1} - E_{pc3}$

Additionally, a graph of the current of the first cathodic peak versus the square roots of the scan rate is linear (**Figure 4.42**). This indicates that the reduction of [Cu(II)Cu(II)] to [Cu(II)Cu(I) was diffusion-controlled.

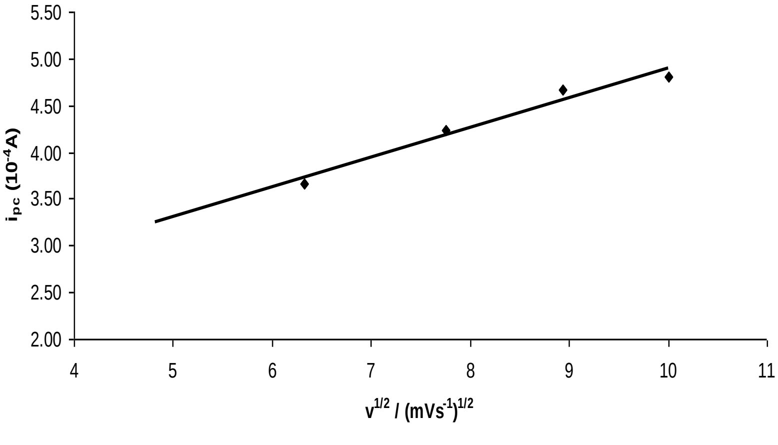

Figure 4.42: Graph of first cathodic current versus square root of scan rate for CuDNO$_2$B

4.2.3.5 Summary

The chemical formula for $CuDNO_2B$ is $[Cu_2(3,5\text{-}(O_2N)_2C_6H_3COO)_4(H_2O)_2]$, and it is proposed to have the distorted paddle-wheel structure similar to $CuNO_2B$. Thus, its magnetic and redox properties are similar to $CuNO_2B$, but it is much less thermally stable due to the higher polarizability of $3,5\text{-}(O_2N)_2C_6H_3COO$ ion.

4.4 COPPER(II) 4-HYDROXYBENZOATE AND COPPER(II) 4-AMINOBENZOATE

The next copper(II) benzoate derivatives studied have a strong electron-donating group, namely the hydroxyl (-OH) or amino ($–NH_2$) group, at the 4-position of the aromatic ring. The two ligands, $4\text{-}HOC_6H_4COO^-$ and $4\text{-}H_2NC_6H_4COO^-$, are the anions from weaker acids, $4\text{-}HOC_6H_4COOH$ (pK_a, 4.57) and $4\text{-}H_2NC_6H_4COOH$ (pK_a, 4.65) respectively, compared to that of CuB (C_6H_5COOH; pK_a, 4.19). Thus, these ligands are stronger conjugate bases than $C_6H_5COO^-$, and should form stronger coordinate bonds with Cu(II). Conceptually, this should reduce the residual positive charge on copper(II) ion. Thus the formation of dinuclear complex is more favourable [47,48,50]. In other word, these substituents should exert an opposite effect to that of the NO_2 group.

Earlier studies suggested that copper(II) 4-hydroxybenzoate has the dimeric paddle-wheel structure in dioxane [51]. However, it is important to note that the structure was proposed based solely on the electronic absorption spectra of samples as a solid and in solution.

In contrast, the structure of copper(II) 4-aminobenzoate was proposed to involve the coordination of 4-$H_2NC_6H_4COO^-$ through both the nitrogen atom of the -NH_2 group and the oxygen atom of the -COO group [52]. However, Alyariya et al. proposed that the same ligand coordinated to cadmium(II) only through the nitrogen atom [53]. Again, this deduction was solely made based on the IR analysis.

It is to the best of our knowledge that to date, no thorough work was undertaken to clarify the structure of these complexes.

4.4.1 Copper(II) 4-Hydroxybenzoate

Copper(II) 4-hydroxybenzoate (CuOHB) was a greenish blue powder, and the yield was 37.2%. Thus, its yield is slightly lower than CuB (41%), consistent with its higher solubility in CH_3CH_2OH. This is ascribed to the presence of – OH group, which can form H-bond with the solvent molecules.

The complex is also soluble in acetone, acetonitrile, tetrahydrofuran, dimethylsulfoxide, dimethylformamide and pyridine, but insoluble in water, hexane, ether and ethyl acetate.

4.4.1.1 Structural elucidation

(a) Elemental analysis

The results of the elemental analyses (42.8% C, 3.9% H and 16.8% Cu) are in good agreement with those calculated for the chemical formula $CuC_{14}H_{16}O_9$ or $[Cu(4\text{-}HOC_6H_4COO)_2(H_2O)].2H_2O$ (formula mass, 391.5 g mol^{-1}; 42.9% C, 4.1% H, 16.2% Cu). The presence of solvated H_2O molecules are to be expected from the ability of the –OH group of the ligand to participate in intermolecular H-bonding.

(b) FTIR spectroscopy

FTIR spectrum (**Figure 4.43**) is similar to CuB, indicating the presence of all of the expected functional groups. The value of $\Delta\nu$ ($\Delta\nu = \nu_{as} - \nu_s$) for CuOHB is 172 cm^{-1}, suggesting a bridging binding mode for the 4-HOC_6H_4COO ligand. It is interesting to note that the $\nu_{as}COO$ peak for CuOHB is shifted to higher frequency (1579 cm^{-1}) compared to CuB (1562 cm^{-1}). This is postulated to be due to the strong donating power of the – OH group, which increases the electron density at the -COO moiety, making the O-C-O bond stronger and possibly shorter.

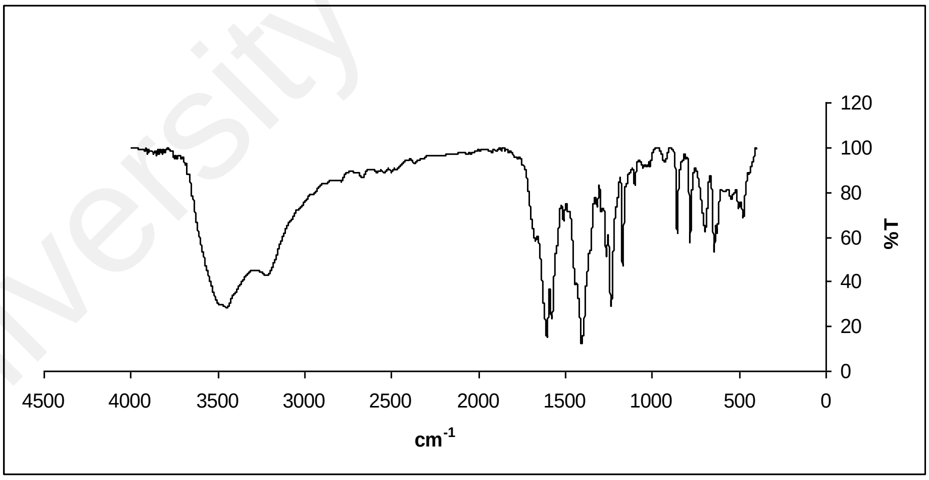

Figure 4.43: FTIR spectrum of CuOHB

(c) UV-vis spectroscopy

The UV-vis spectrum for solid CuOHB (**Figure 4.44**) is similar to that of CuB, and may be similarly assigned. It shows a broad, unsymmetrical *d-d* band at 686 nm (Band I) with a low energy shoulder at 800 nm, and another shoulder at about 380 nm (Band II). These support dimeric square pyramidal structure for the complex.

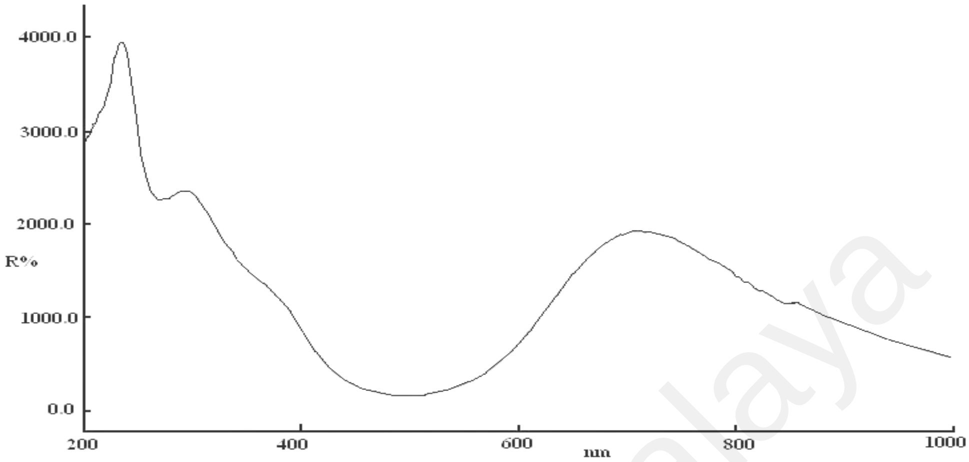

Figure 4.44: UV-vis spectrum of solid CuOHB

Compared to the spectrum of CuB, the *d-d* bands for CuOHB are clearly blue-shifted (higher energy). This is consistent with previous argument based on the RCOO-Cu bond strength. The stronger Lewis base 4-$HOC_6H_4COO^-$ forms a stronger σ coordinate bond with Cu(II), thus causing a bigger splitting of the *d-d* energy levels (or more energy antibonding x^2-y^2 orbital) [10].

To compare the structural stability of CuOHB with that of CuB and its nitro-substituted derivatives in solutions, its UV-vis spectra were recorded in the same solvents (**Table 4.18**).

Table 4.18: The UV-vis spectral data for CuOHB in different solvents

λ_{max}/nm (ε_{max}/M^{-1}cm^{-1})		Solvent
Band I	**Band II**	
696 (--)	380 (--)	None
716 (65)	-	DMSO
706 (114)	-	DMF
698 (509)	380 (--)	CH_3OH-CH_3COOH (20:1)

--, not applicable; -, not observed

The results are similar to those of CuB in these solvents, and may be similarly explained. For example, Band 1 of CuOHB is red-shifted, while Band II is not observed in DMSO and DMF, but observed in CH_3OH-CH_3COOH.

4.4.1.2 Magnetic susceptibility

The μ_{eff} value, calculated as before from the values of χ_g (0.156 x 10^{-5} cm^3 g^{-1}), χ_D (4.17 x 10^{-4} cm^3 mol^{-1}) and hence χ_M (1.638 x 10^{-3} cm^3 mol^{-1}), is 1.93 B.M. at 298 K. The -2J value, similarly calculated using the Bleaney-Bowers equation, is 333 cm^{-1}. It is noted that the values are similar to CuB (μ_{eff} = 1.93 B.M.; -2J = 333 cm^{-1}), suggesting similar antiferromagnetic interaction for both complexes. From these, it may be concluded that both complexes have similar structure, and that the -OH group does not exert a significant role in the superexchange pathway for the electronic communication, possibly because of its remote location from the –COO group.

4.4.1.3 Thermal analysis

(a) TGA

The thermogram (**Figure 4.45**) shows that CuOHB is thermally stable up to 250°C. Thus, the complex is as thermally stable as CuB (254°C). However, based on the stronger 4-HOC_6H_4COO-Cu coordinate bond compared to that of C_6H_5COO-Cu, CuOHB is expected to be more thermally stable. A possible explanation is that CuOHB decomposes by a different pathway, initiated by the breaking of the weakened H-OC_6H_4COOCu bond (**Figure 4.46**), while the decomposition of CuB was initiated by the breaking of the C_6H_5COO-Cu

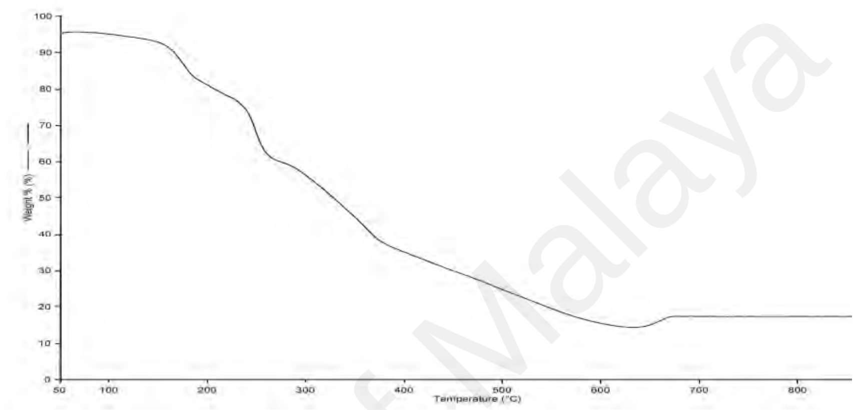

Figure 4.45: TGA of CuOHB

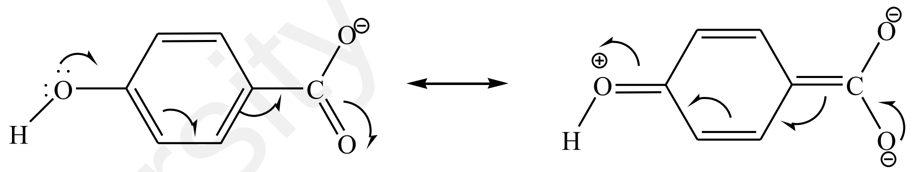

Figure 4.46: Weakening of H-OC_6H_4COO-Cu bond due to resonance and/or back bonding

The thermogram also shows a gradual weight loss process. The initial weight loss of 15.0% from about 50°C to about 170°C is assigned to the evaporation of axially ligated and solvated H_2O (expected, 13.8%). Above the decomposition temperature, the total weight loss of 70.0% is accounted for by the loss of 4-HOC_6H_4COO ligand (expected, 70.0%).

The amount of residue at about 630°C is 15.0%. It may be a mixture of CuO and Cu_2O (since there was a mass increase at temperatures above 630°C). Accordingly, the formula mass for CuOHB cannot be estimated as was previously done for the other complexes.

However, the result supports the above suggestion that the decomposition pathway for CuOHB differs from CuB. It is possible that the H atoms or H_2 molecules from the dissociation of H-O bond provide for a reducing atmosphere during the decomposition process.

(b) DSC

The DSC (**Figure 4.47**) shows a small and broad endotherm at 86°C (ΔH = +25 kJ mol^{-1}), which agrees fairly well with the release of coordinated and solvated H_2O molecules, in agreement with the suggestion from TGA. Then, a very strong exotherm is observed at 262°C (ΔH = -3188 kJ mol^{-1}), which occurs at a slightly higher temperature than its decomposition temperature (250°C from TGA). The results are similar as the previously discussed complexes, and may be similarly explained.

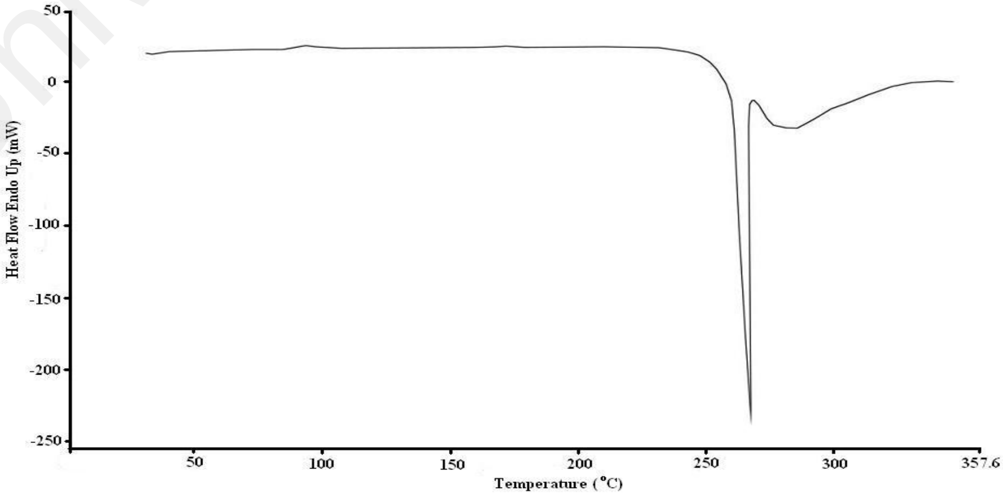

Figure 4.47: DSC of CuOHB

4.4.1.4 Cyclic voltammetry

The redox behaviour of CuOHB was investigated under similar conditions as for the previously discussed complexes. It is important to note from the UV-vis spectroscopy (**Section 4.4.1.1(c))** that the complex remained dimeric in these solvents.

The CV at the scan rate of 100 mV s^{-1} and potential range +1.5 V to -1.5 V (**Figure 4.48**) shows three cathodic peaks at -0.23, -0.40 and -0.77 V, and a broad anodic peak at +0.40 V. In fact, the CV is very similar to that of CuB (**Section 4.2.4**), which further support similar structure for the two complexes.

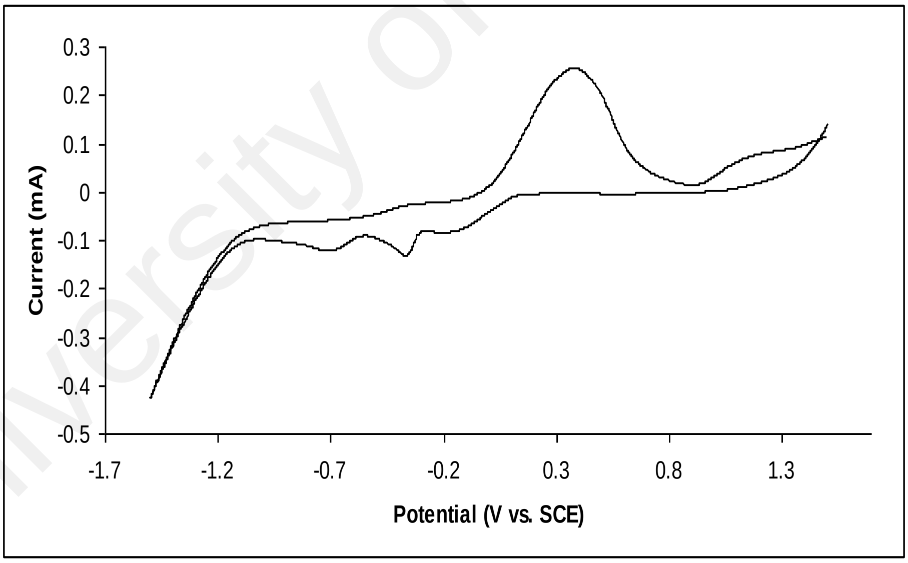

Figure 4.48: CV of CuOHB

However, it is noted that the first reduction potential for CuOHB is more negative (-0.23 V), or more difficult, compared to CuB (-0.13 V). This is likely due to the stronger Lewis basicity of 4-$HOC_6H_4COO^-$ ligand, resulting in increased electron density at copper(II) (or reduced positive charge).

From the cathodic and anodic potentials, the ΔE values for [Cu(II)Cu(II)]-[Cu(II)Cu(I)] and [Cu(II)Cu(I)]-[Cu(I)Cu(I)] couples are 640 mV and 1180 mV respectively. The values are slightly higher compared to the corresponding values for CuB (590 and 1050 mV), but are to be expected as the reduction potentials for CuOHB were more negative.

The CV at the different scan rates are shown in **Figure 4.49**, and the corresponding data is depicted in **Table 4.19.**

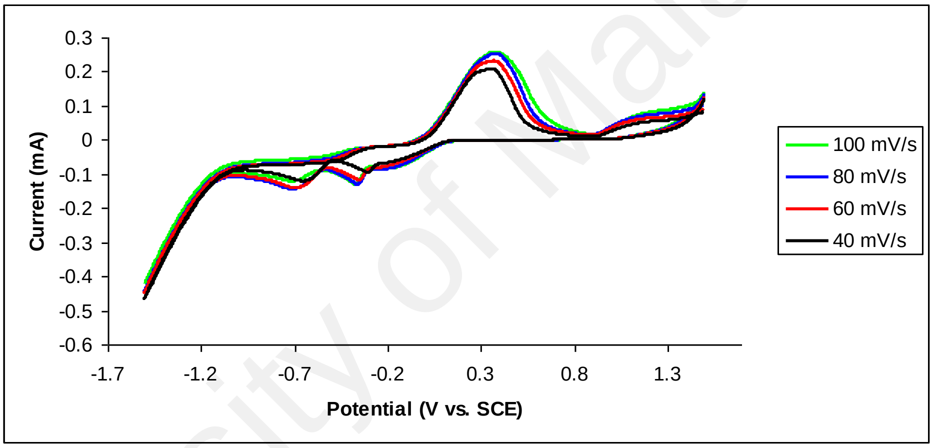

Figure 4.49: CV of CuOHB within the potential window +1.5 V to -1.5 V and scan rates 40, 60, 80 and 100 mV s^{-1}

Table 4.19: The peak potential (E_p/V) and peak separation (ΔE/mV) for CuOHB in CH_3OH-CH_3COOH at different scan rate (mV s^{-1})

Scan rate	E_{pc1}	E_{pc2}	E_{pc3}	E_{pa1}	ΔE_1^*	$\Delta E_2^\#$
40	-0.20	-0.33	-0.66	+0.39	590	1050
60	-0.21	-0.37	-0.70	+0.40	610	1100
80	-0.22	-0.38	-0.71	+0.41	630	1120
100	-0.23	-0.40	-0.77	+0.41	640	1180

* $\Delta E_1 = E_{pa1} - E_{pc1}$; # $\Delta E_2 = E_{pa1} - E_{pc3}$

As with the previously discussed complexes, the values of ΔE_1 and ΔE_2 increase with the scan rate, and the values of ΔE_2 are greater than that of ΔE_1. Thus similar conclusion could be made, specifically there occurs a more extensive structural reorganization for [Cu(I)Cu(I)] compared to [Cu(II)Cu(I)].

Similarly, a graph of first cathodic peak current versus the square roots of the scan rate is linear (**Figure 4.50**), indicating that the reduction of [Cu(II)Cu(II)] to [Cu(II)Cu(I)] was diffusion-controlled.

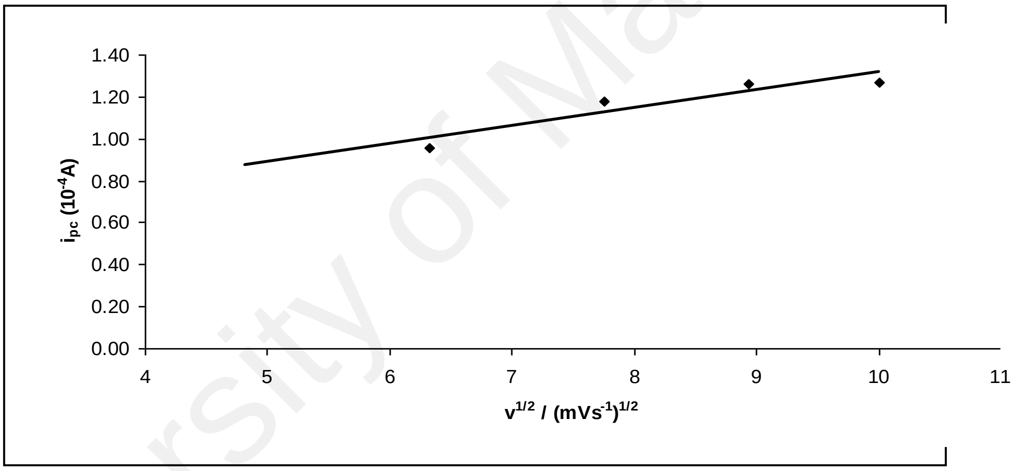

Figure 4.50: Graph of the first cathodic peak current versus the square root of the scan rate for CuOHB

4.4.1.5 Summary

The chemical formula for CuOHB is $[Cu_2(4\text{-}HOC_6H_4COO)_4(H_2O)_2].4H_2O$, and it is proposed to have similar paddle-wheel structure as CuB, but with stronger $4\text{-}HOC_6H_4COO\text{-}Cu$ bonds. Its magnetic, thermal and redox properties are also similar to CuB, but the complex was less easily reduced.

4.4.2 Copper(II) 4-Aminobenzoate

Copper(II) 4-aminobenzoate ($CuNH_2B$) was obtained as a dark green powder, and its yield (35.0%) was similar to CuOHB (37.2%), suggesting similar solubility in CH_3CH_2OH (the solvent used in the synthesis). The complex was also soluble in dimethylsulphoxide and pyridine, but insoluble in other common organic solvents or in water.

4.4.2.1 Structural elucidation

(a) Elemental analysis

The results of the elemental analyses (43.8% C, 4.0% H, 6.9% N, and 16.3% Cu) are in good agreement with those calculated for the chemical formula $CuC_{14}H_{18}O_7N_2$ or $[Cu(4\text{-}NH_2C_6H_4COO)_2(H_2O)].2H_2O$ (formula mass, 389.5 g mol^{-1}; 43.1% C, 4.6% H, 7.2% N, 16.3% Cu). It is interesting to note that its chemical formula is similar to that of CuOHB.

(b) FTIR spectroscopy

The FTIR spectrum (**Figure 4.51**) is similar to that of CuOHB, suggesting similar structure. Specifically, there are strong and very broad -OH bands at about 3450 cm^{-1} suggesting that the complex was highly hydrated, and the ν_{as}COO and ν_sCOO bands are at 1574 and 1397 cm^{-1} respectively. Accordingly, the $\Delta\nu$ value is 177 cm^{-1}, which is similar to that of CuOHB (172 cm^{-1}). Hence, $4\text{-}NH_2C_6H_4COO^-$ ion is coordinated to Cu(II) as a bridging bidentate ligand.

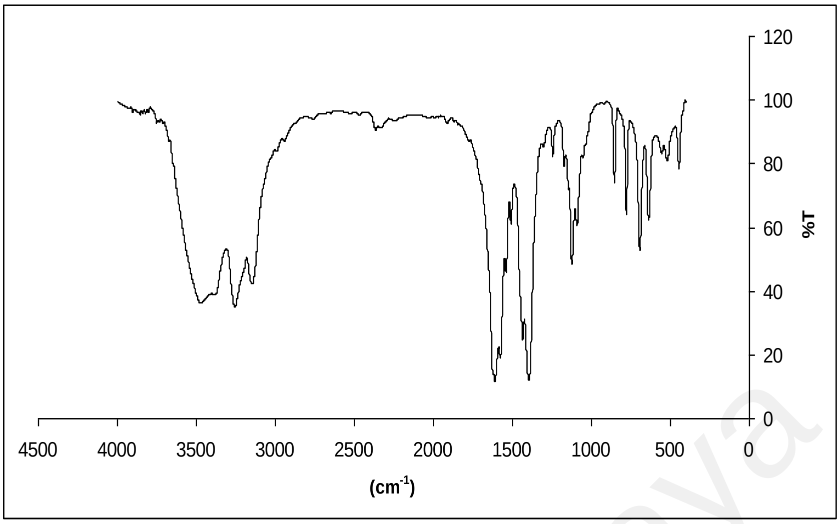

Figure 4.51: FTIR spectrum of $CuNH_2B$

(c) UV-vis spectroscopy

The UV-vis spectrum of solid $CuNH_2B$ (**Figure 4.52**) is also similar to that of CuOHB (**Figure 4.44**), and thus may be similarly assigned. The result further supports the similarity in their structures as proposed from FTIR. However, the broad *d-d* band is at a slightly higher energy (650 nm) compared to that of CuOHB (686 nm). This is indeed consistent with a stronger Lewis basicity of $4\text{-}H_2NC_6H_4COO^-$ ion, forming a stronger coordinate bond with Cu(II) ion. As a result, the SOMO is more antibonding. With similar reasoning, it is also further observed that a peak at 420 nm (for $yz, xz \rightarrow x^2 - y^2$ transition) and Band II absorption peak at 370 nm are blue shifted compared to CuOHB (450 nm and 380 nm respectively).

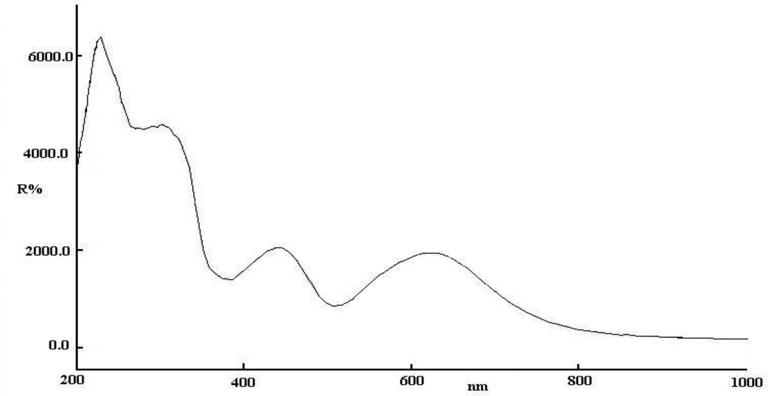

Figure 4.52: UV-vis spectrum of solid $CuNH_2B$

As previously done for the other complexes, the UV-vis spectra for $CuNH_2B$ were also recorded in various solvents in order to probe its structural stability in solutions. The results are shown in **Table 4.20**.

Table 4.20: The UV-vis spectral data for $CuNH_2B$ in different solvents

λ_{max}/nm (ε_{max}/$M^{-1}cm^{-1}$)		**Solvent**
Band I	**Band II**	
650 (--)	370 (--)	None
712 (291)	-	DMSO
702 (513)	-	DMF
696 (504)	380 (--)	CH_3OH-CH_3COOH (20:1)

--, not applicable; -, not observed

It is noted that the trend is similar to that shown by CuOHB in the same solvents, and thus can be similarly explained. It is further noted that the wavenumbers for Band I of $CuNH_2B$ in all solvents are at almost the same wavenumbers as those of CuOHB. These suggest that 4-$H_2NC_6H_4COO^-$ ligand exerts similar effect on the splitting of the 3*d* orbitals of Cu(II) as 4-$HOC_6H_4COO^-$ ligand.

However, on closer inspection, it is noted that the ε_{max} values for $CuNH_2B$ in DMSO and DMF are significantly higher compared to CuOHB in the same solvents (ε_{max} = 65 (DMSO), 114 (DMF); **Table 4.18**). The results suggest that the structure of $CuNH_2B$ is more distorted (lower symmetry) in these solvents compared to CuOHB.

4.4.2.2 Magnetic susceptibility

The μ_{eff} value, similarly calculated as for the other complexes from the values of χ_g (0.231 x 10^{-5} cm^3 g^{-1}), $\chi_{d,}$ (4.55 x 10^{-4} cm^3 mol^{-1}) and χ_m^{corr} (2.181 x 10^{-3} cm^3 mol^{-1}), is 2.32 B.M. at 298 K, and the -2J value is 221 cm^{-1}. These suggest antiferromagnetic interaction between the two Cu(II) centres.

It is noted that the μ_{eff} value for $CuNH_2B$ is higher than that of CuOHB (1.93 B.M.), indicating a weaker magnetic coupling between the two Cu(II) centers in the former complex. The result is actually consistent with the UV-vis spectroscopy, and in agreement with the postulation that a greater splitting between the singlet and triplet states leads to lower magnetic interaction [10].

4.4.2.3 Thermal analysis

(a) TGA

The thermogram (**Figure 4.53**) shows that $CuNH_2B$ is slightly less thermally stable (T_{dec} = 240°C) compared to CuOHB (T_{dec} = 250°C). As for CuOHB, the decomposition process is postulated to be initiated by the breaking of the much weaker H_2-NC_6H_4COOCu bond as a result of resonance or back-bonding.

The thermogram also shows an initial weight loss of 8.0% at 100°C, ascribed to the release of solvated H_2O molecules (expected, 9.2%). The next weight loss of 62.0% occurred gradually, starting at 240°C, which is assigned to the loss of coordinated H_2O and decarboxylation of 4-$NH_2C_6H_4COO$ ligands (expected, 74.5%). The amount of residue at temperatures above 800°C is 30.0% (expected, 20% assuming pure CuO). The results suggest incomplete decomposition of the ligand, and/or that the residue may be a mixture of CuO and Cu_3N_2.

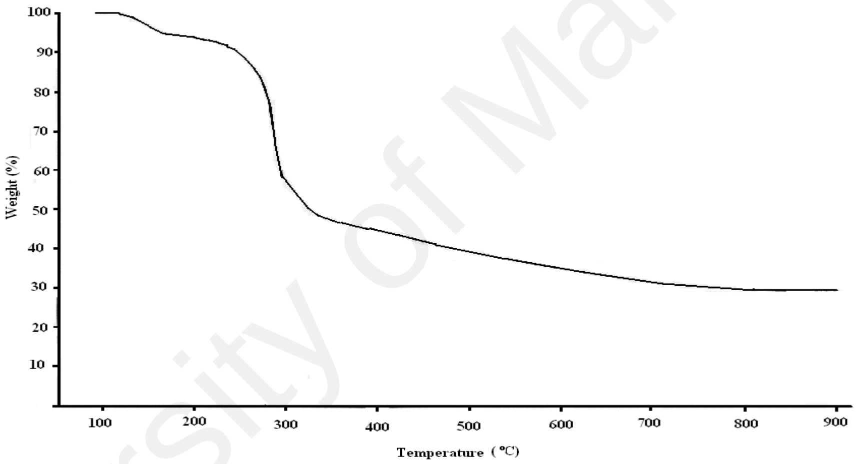

Figure 4.53: TGA of $CuNH_2B$

(b) DSC

The DSC curve for $CuNH_2B$ (**Figure 4.54**) showed a small and broad endotherm at about 125°C ($\Delta H = +82$ kJ mol^{-1}) and a strong exothermic peak at about 280°C ($\Delta H = -1309$ kJ mol^{-1}). The curve is similar to that obtained for CuOHB, and thus may be similarly explained.

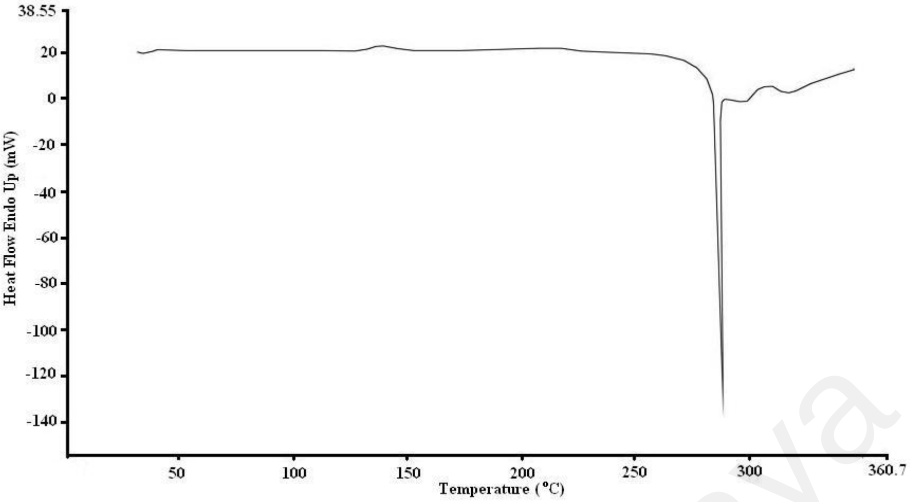

Figure 4.54: DSC of $CuNH_2B$

4.4.2.4 Cyclic voltammetry

The redox behaviour of $CuNH_2B$ was similarly investigated as for the previously discussed complexes. It is important to note that according to the UV-vis studies, the dimeric structure of the complex remained intact in the solvents used.

The CV with the scan rate of 100 mV s^{-1} and potential window +1.5 V to -1.5 V (**Figure 4.55**) is almost similar to that of CuOHB under the same conditions, and thus may be similarly assigned and explained.

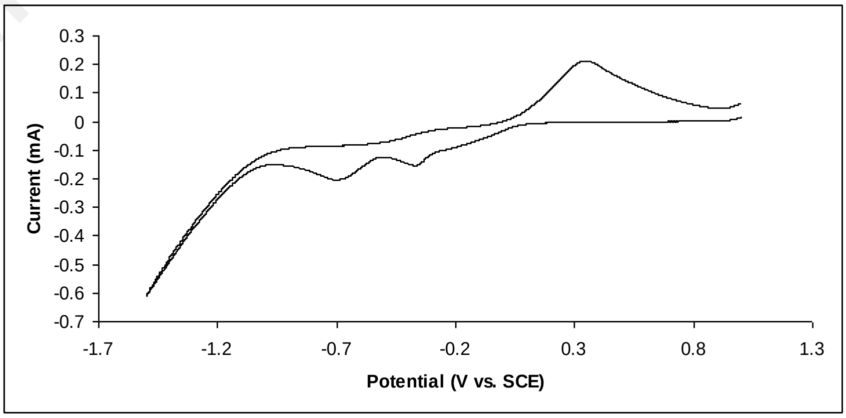

Figure 4.55: CV of $CuNH_2B$ (scan rate of 100 mV s^{-1}; potential window +1.5 V to -1.5 V)

It is further noted that the potentials for the three cathodic peaks ($E_{cathode}$ = -0.20 V, -0.37 V and -0.70 V) and the anodic peak (E_{anode} = +0.36 V) are similar to those of CuOHB ($E_{cathode}$ = -0.23, -0.40 and -0.77 V; E_{anode} = +0.40 V). Thus, it may be concluded that the NH_2 and OH group at the *para* positions of the arylcarboxylate ligands have similar effect on the redox properties of these complexes.

However, the ΔE values for the redox couples [Cu(II)Cu(II)]-[Cu(II)Cu(I)] and [Cu(II)Cu(I)]-[Cu(I)Cu(I)] (560 and 1060 mV respectively) are lower compared to CuOHB (640 mV and 1180 mV). These indicate that the reduced complexes from $CuNH_2B$ were less distorted compared to those from CuOHB, which is consistent with the stronger 4-$H_2NC_6H_4COO$-Cu bond in the former complex.

The CV at different scan rate (**Figure 4.56 and Table 4.21**) as well as the plot of current versus square roots of scan rates (**Figure 4.57**) are similar with CuOHB, and thus can be similarly explained.

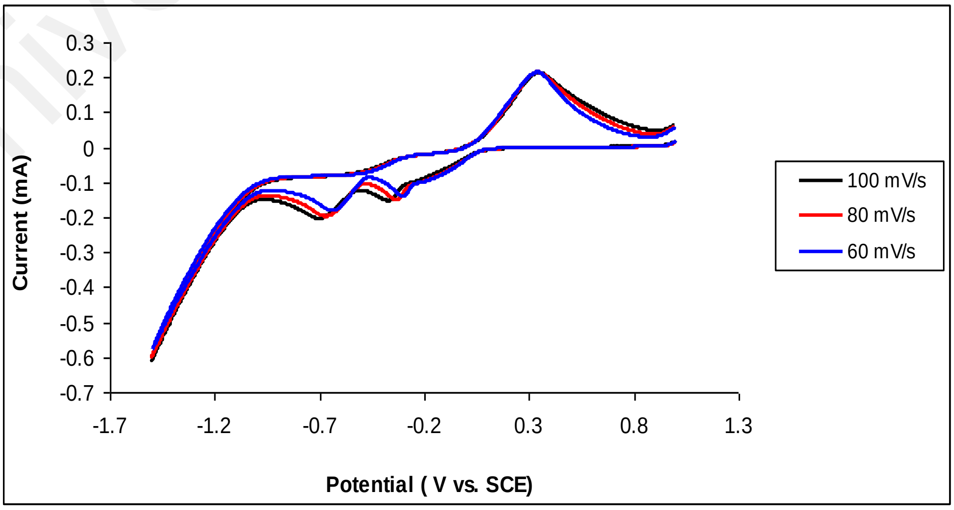

Figure 4.56: CV of $CuNH_2B$ at different scan rates

Table 4.21: The peak potential (E_p/V) and peak separation (ΔE/mV) for $CuNH_2B$ in CH_3OH-CH_3COOH at different scan rate (mV s^{-1})

Scan rate	E_{pc1}	E_{pc2}	E_{pc3}	E_{pa1}	ΔE_1^*	$\Delta E_2^\#$
60	-0.16	-0.28	-0.60	+0.30	460	900
80	-0.18	-0.30	-0.63	+0.31	490	940
100	-0.20	-0.37	-0.70	+0.36	560	1060

* $\Delta E_1 = E_{pa1} - E_{pc1}$; # $\Delta E_2 = E_{pa1} - E_{pc3}$

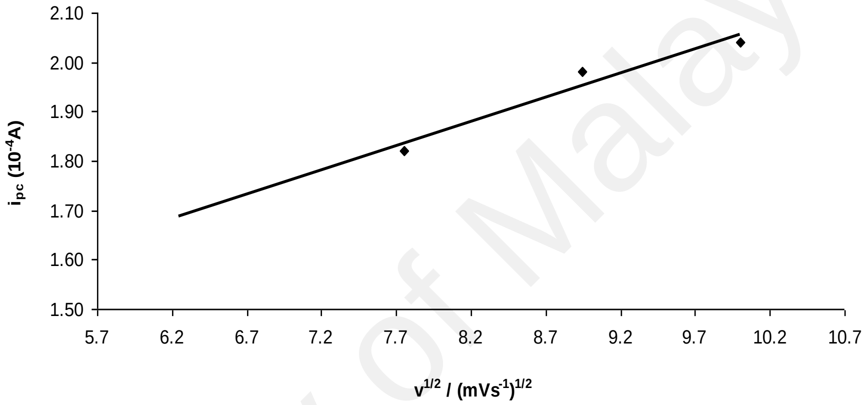

Figure 4.57: Graph of the first cathodic current versus square root of the scan rate for $CuNH_2B$

4.4.2.5 Summary

The chemical formula for $CuNH_2B$ is $[Cu_2(4\text{-}H_2NC_6H_4COO)_4(H_2O)_2].4H_2O$, and it is proposed to have similar paddle-wheel structure as CuOHB. Compared to CuOHB, its structure is more distorted in DMSO and DMF, and there exists a weaker antiferromagnetic interaction between the two Cu(II) centres. However, it has similar thermal stability and redox properties, and the geometries of the reduced complexes of $CuNH_2B$ are less distorted.

4.5 COPPER(II) 4-HALOBENZOATES

Copper(II) 4-halobenzoates ([Cu(4-$XC_6H_4COO)_2$]; X = F, Cl, Br, I) were studied with two main objectives: (a) to correlate the steric, inductive, and mesomeric effects with structure, physical and chemical properties; and (b) to compare these properties with previously discussed complexes (X = H, NO_2, OH and NH_2 groups).

It is noted that the pK_a values of 4-FC_6H_4COOH (4.14), 4-ClC_6H_4COOH (3.99), 4-BrC_6H_4COOH (4.00), and 4-IC_6H_4COOH (4.02) are almost the same. This means that the corresponding ligands have almost similar basicities, and may not account for any differences in the properties of these complexes. Therefore, the discussion will be focused on the differences in the steric ($F < Cl < Br < I$), inductive ($F > Cl > Br > I$), and mesomeric ($F > Cl < Br < I$) effects.

Additionally, the pK_a values of these 4-halobenzoic acids are compared with those of C_6H_5COOH (4.19), 4-$NO_2C_6H_4COOH$ (3.43), 4-HOC_6H_4COOH (4.57), and 4-$NH_2C_6H_4COOH$ (4.65). Thus conceptually, the Cu-O coordinate bonds in [Cu_2(4-$XC_6H_4COO)_4$] are expected to decrease in the following order: $H_2N > OH > H > F > I > Br > Cl > NO_2$.

These complexes were obtained by the same method as for previously discussed copper(II) arylcarboxylates in this report. The experimental data for these complexes are shown in **Table 4.22**.

Table 4.22: Experimental data for copper(II) 4-Xbenzoate

X	Label	Colour	Yield (%)
F	CuFB	🟦	41.0
Cl	CuClB	🟦	48.0
Br	CuBrB	🟦	49.6
I	CuIB	🟦	46.6

The percentage yields of these complexes are almost similar. This suggests that differences in size and electronic effect of the different halogens at the *para* position of the aromatic ring have insignificant effect on the solubility of these complexes in ethanol.

It is further noted that their yields are comparable to CuB (41%) and $CuNO_2B$ (52%), and slightly higher compared to CuOHB (37%) and $CuNH_2B$ (35%). The results are in agreement with the polarities of these complexes.

4.5.1 Copper(II) 4-Fuorobenzoate

4.5.1.1 Structural elucidation

The results of the **elemental analysis** (48.9% C, 2.9% H, 22.0% O and 14.1% Cu) are in a fairly good agreement with those calculated for the chemical formula $CuC_{16}H_{16}O_6F_2$ or $[Cu(4\text{-}FC_6H_4COO)_2(C_2H_5OH)].H_2O$ (formula mass, 405.5 g mol^{-1}; 47.4% C, 3.9% H, 23.6% O and 15.6% Cu).

The **FTIR** spectrum (**Figure 4.58**) is similar to that of CuB (**Figure 4.1**), $CuNO_2B$ (**Figure 4.17**), CuOHB (**Figure 4.43**), and $CuNH_2B$ (**Figure 4.51**).

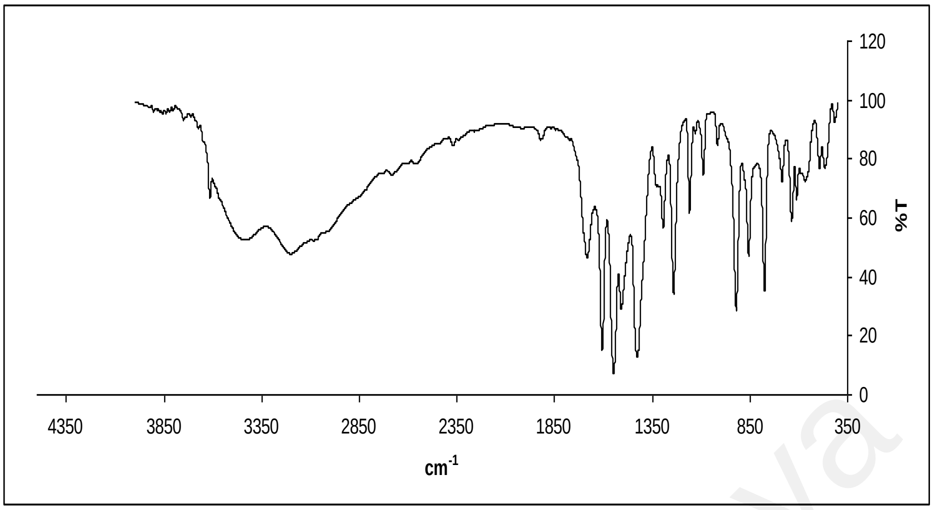

Figure 4.58: FTIR spectrum of CuFB

However, two differences are noted: (a) there are two broad peaks at 3420 cm^{-1} and 3180 cm^{-1}, suggesting the presence of H-bonded C_2H_5OH and H_2O, the presence of which are indicated from the elemental analyses; and (b) the values of ν_{as}COO and ν_{s}COO peaks are 1549 cm^{-1} and 1427 cm^{-1} respectively, and hence the value of $\Delta\nu$ (COO) is 122 cm^{-1}. This value is much lower compared to CuB (154 cm^{-1}), CuNO$_2$B (153 cm^{-1}), CuOHB (172 cm^{-1}) and CuNH$_2$B (177 cm^{-1}). Therefore, the structure of CuFB may differ from these complexes.

The **UV-vis spectrum** of solid CuFB (**Figure 4.59**) shows a very broad and weak *d-d* absorption band at 715 nm, suggesting square pyramidal geometry at Cu(II). However, the band is clearly red-shifted compared to CuB (674 nm), CuNO$_2$B (700 nm), CuOHB (686 nm) and CuNH$_2$B (650 nm). The result seems to suggest a more distorted geometry at Cu(II) centre.

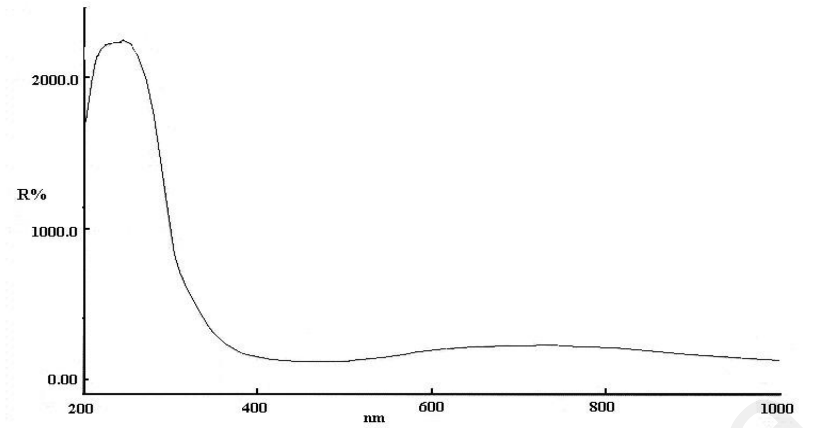

Figure 4.59: UV-vis spectrum of solid CuFB

The UV-vis spectrum of CuFB in solution was only recorded in CH_3OH-CH_3COOH (20:1) as it was not readily soluble in other solvents. The spectrum (**Figure 4.60**) shows two *d-d* peaks at 697 nm (ε_{max} = 430 M^{-1} cm^{-1}; Band 1) and 380 nm (ε = 66 M^{-1} cm^{-1}; Band 2) respectively. It is noted that Band 1 is at similar wavenumber as that of CuB (699 nm), $CuNO_2B$ (700 nm), CuOHB (698 nm) and $CuNH_2B$ (696 nm). Hence, CuFB is postulated to have similar structure in solution as the other previously discussed complexes. However, the higher ε_{max} value (430 M^{-1} cm^{-1}) for CuFB compared to CuB (295 M^{-1} cm^{-1}) suggests a less symmetrical structure in the former complex.

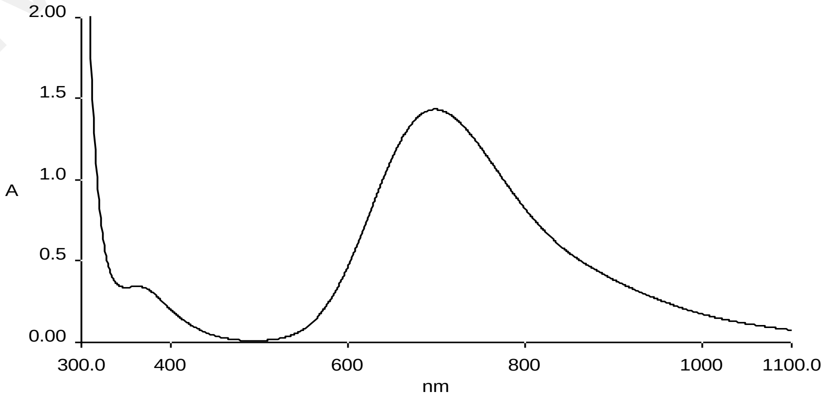

Figure 4.60: UV-vis spectrum of CuFB in CH_3OH-CH_3COOH

Based on the above results, it is proposed that CuFB has the distorted paddle-wheel structure similar to $CuNO_2B$ and $CuDNO_2B$ (axial-equatorial bond angle greater than 90°). From these, it may be suggested that arylcarboxylate ions substituted with strongly electron-attracting group (NO_2 and F in the present examples) tend to form binuclear copper(II) complexes with a distorted square pyramidal structure.

4.5.1.2 Magnetic susceptibility

The μ_{eff} value, calculated as before from the values of χ_g (2.97×10^{-6} cm^3 g^{-1}), χ_d (-3.77×10^{-4} cm^3 mol^{-1}), and hence χ_m^{corr} (2.786×10^{-3} cm^3 mol^{-1}), is 2.54 B.M. at 298 K, and the -2J value is 133 cm^{-1}. These suggest a weak antiferromagnetic interaction between the unpaired electrons of the two Cu(II) centres.

Additionally, the μ_{eff} value for CuFB is higher when compared to CuB (1.93 B.M), $CuNO_2B$ (2.30 B.M), CuOHB (1.93 B.M) and $CuNH_2B$ (2.32 B.M). The result is consistent with the weaker (longer) 4-FC_6H_4COO-Cu bond and with the proposed distorted structure.

4.5.1.3 Thermal analysis

The **TGA** of CuFB (**Figure 4.61**) shows that the complex is thermally stable up to 275°C. Thus, it is slightly more thermally stable compared to CuB (T_{dec} = 254°C), CuOHB (T_{dec} = 250°C) and $CuNH_2B$ (T_{dec} = 240°C), but slightly less stable compared to $CuNO_2B$ (T_{dec} = 285°C). It seems that there is no correlation between the thermal stabilities of these complexes with the Cu-O bond strengths. The important factor seems to be the resonance effect of F in 4-FC_6H_4COO, operating in a similar way (but weaker) as discussed for the NO_2 group in 4-$O_2NC_6H_4COO$ ligand (**Figure 4.25** in **Section 4.3.1.2**).

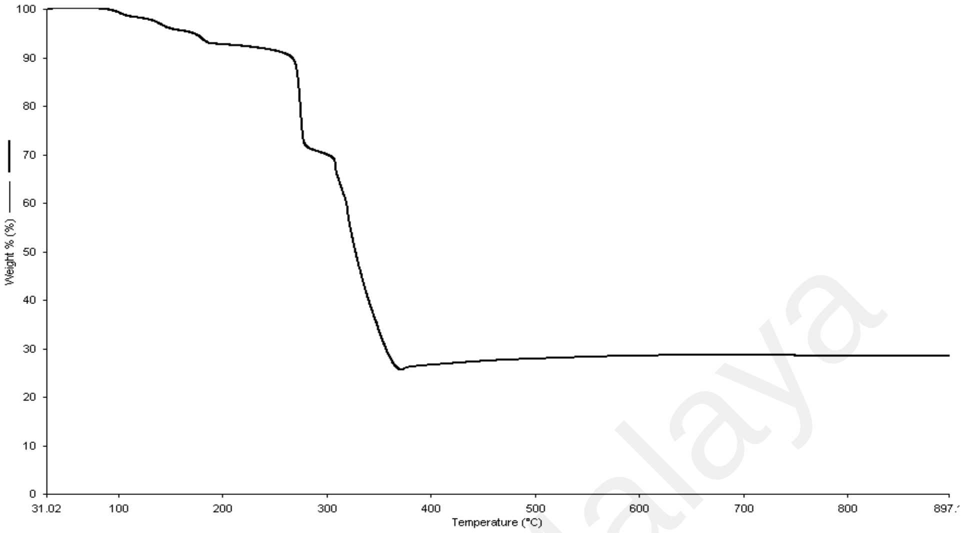

Figure 4.61: TGA of CuFB

The thermogram also shows a distinct three-step weight loss process. The first step is actually made up of multiple small steps at 100^{o}C, 150^{o}C and 180^{o}C, with a total weight loss of 9.5%. These are assigned to the evaporation of C_2H_5OH and H_2O molecules (expected, 15.8%). The lower than expected weight loss at this step is similarly observed for CuB, and may be similarly explained.

The next weight loss of 20.7% at 275^{o}C is followed by another of 43.9% at 298^{o}C (total, 64.6%) are assigned to the decarboxylation of 4-FC_6H_4COO ligand (expected, 68.6%). The amount of residue at temperatures above 500^{o}C is 25.9 %. This is in good agreement with the expected value of 28.3%, but only if it is assumed that the residue is a mixture of CuO and CuF_2.

The **DSC** plot (**Figure 4.62**) shows two weak overlapping endothermic peaks at 90^{o}C and 150^{o}C ($\Delta H_{combined}$ = +14.7 kJ/mol) and another weak endothermic peak at 180^{o}C (ΔH = +7.4 kJ/mol). The results are in agreement with the loss of weakly coordinated C_2H_5OH and H_2O molecules, as suggested from TGA.

Next, a weak endothermic peak at 280^{o}C, which is above its decomposition temperature (T_{dec} = 275^{o}C), followed immediately by strong exothermic peaks at 290^{o}C (ΔH = - 90.1 kJ/mol) and 312^{o}C (ΔH = - 90.1 kJ/mol), suggest concurrent breaking of Cu-O coordinated bond and formation of volatiles (mainly CO_2) from the ligand.

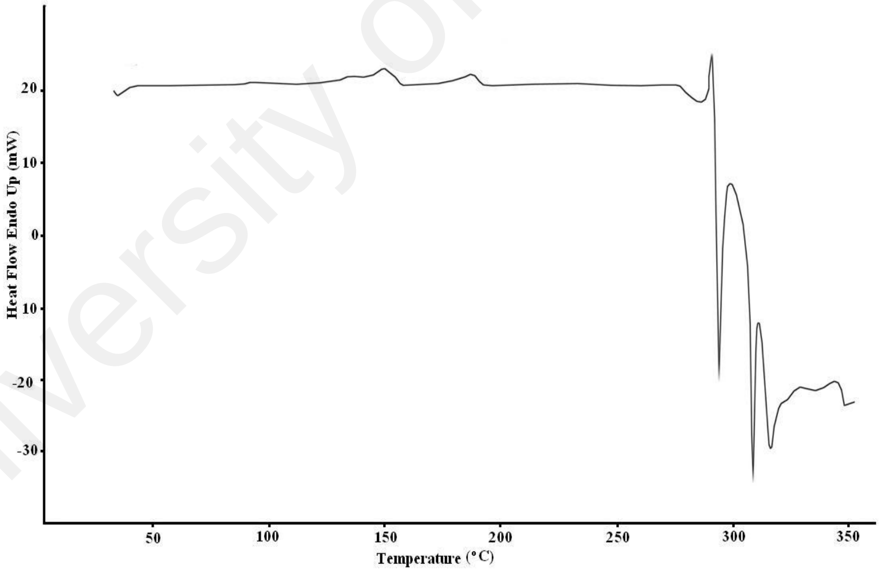

Figure 4.62: DSC of CuFB

4.5.1.4 Cyclic voltammetry

The CV of CuFB was similarly recorded in CH_3OH-CH_3COOH (20:1) under several conditions, as were done for the previously discussed complexes. It is again important to note that the complex remained dinuclear in these solvents.

(a) Potential window = +1.5 V to -1.5 V; scan rate = 100 mV s^{-1}

The CV (**Figure 4.63**) shows three cathodic peaks at -0.12, -0.28 and -0.80 V, and two overlapping anodic peaks at +0.20 V (shoulder) and +0.27 V. These peaks are similarly observed (but at different potentials) in the CVs of CuB, CuNO$_2$B, CuOHB and CuNH$_2$B, and may be similarly assigned.

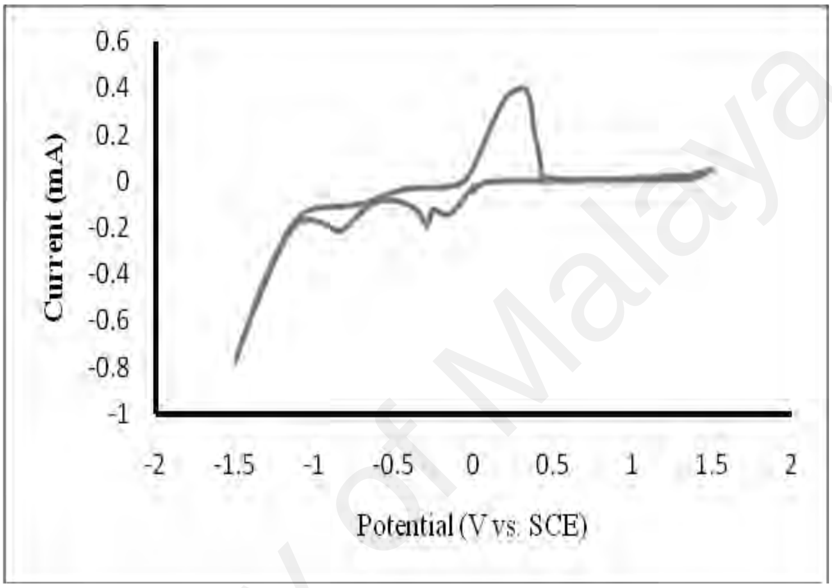

Figure 4.63: CV of CuFB

It is noted that [Cu(II)Cu(II)] in CuFB was reduced to [Cu(II)Cu(I)] at almost the same potential (-0.12 V) as CuB (-0.13 V), slightly higher potential than CuNO$_2$B (-0.09 V), and at a significantly lower potentials compared to CuOHB (-0.23 V) and CuNH$_2$B (-0.20 V). The geometries of Cu(II) for these complexes were almost similar in these solvents, as shown the UV-vis spectroscopic results. The CV results seem to suggest that the degree of structural distortion (towards less planar) is: CuNO$_2$B > CuB, CuFB > CuNH$_2$B, CuOHB.

From the potentials above, the ΔE values for [Cu(II)Cu(II)]-[Cu(II)Cu(I)] and [Cu(II)Cu(I)]-[Cu(I)Cu(I)] redox couples are 388 mV and 1000 mV respectively. These are similar with the other copper(II) arylcarboxylates, indicating the redox chemistry of CuF is also quasireversible with extensive structural reorganization upon reduction.

(b) Potential window = +1.5 V to -1.5 V; scan rates = 40 - 100 mV s^{-1}

The CV for the scan rates 40 – 100 mV s^{-1} are shown in **Figure 4.64**, and the values of peak potentials and ΔE are given in **Table 4.23.**

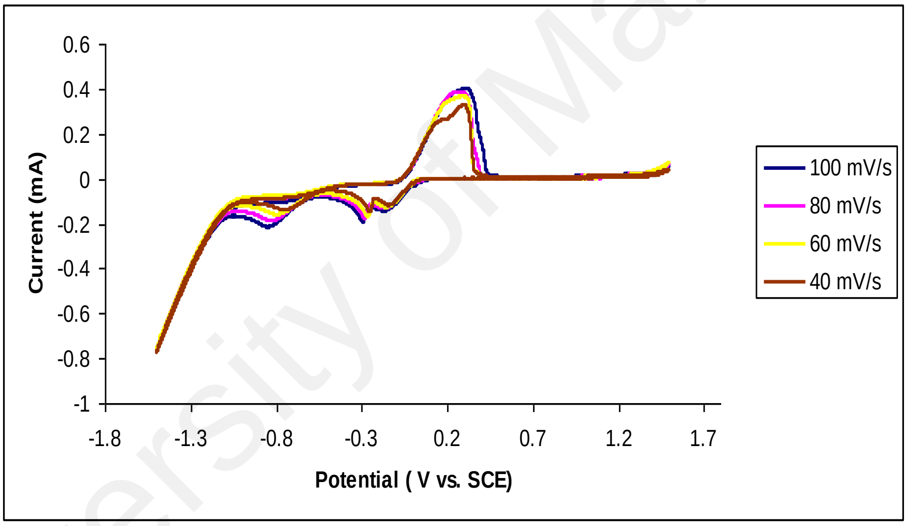

Figure 4.64: CV of CuFB at different scan rates

Table 4.23: The peak potential (E_p/V) and peak separation (ΔE/mV) for CuFB in CH_3OH-CH_3COOH at each scan rate (mV s^{-1})

Scan rate	E_{pc1}	E_{pc2}	E_{pc3}	E_{pa1}	E_{pa2}	ΔE_1^*	$\Delta E_2^\#$
40	-0.11	-0.24	-0.71	+0.20	+0.27	380	910
60	-0.11	-0.25	-0.75	+0.18	+0.27	380	930
80	-012	-0.27	-0.77	+0.20	+0.27	390	970
100	-0.12	-0.28	-0.80	+0.20	+0.27	390	1000

* $\Delta E_1 = E_{pa2} - E_{pc1}$; # $\Delta E_2 = E_{pa1} - E_{pc3}$

It is interesting to note that the values of ΔE_1 (the first reduction process) is almost independent on the scan rate. This is in contrast to the results obtained for CuB, $CuNO_2B$, CuOHB and $CuNH_2B$.

However at each scan rate, the much larger value for ΔE_2 compared to ΔE_1 is similar to that observed for the other complexes, and therefore may be similarly explained.

In addition, the graph of the first cathodic peak current versus the square root of the scan rate is linear **(Figure 4.65**), indicating that the reduction of [Cu(II)Cu(II)] to [Cu(II)Cu(I)] was also diffusion-controlled.

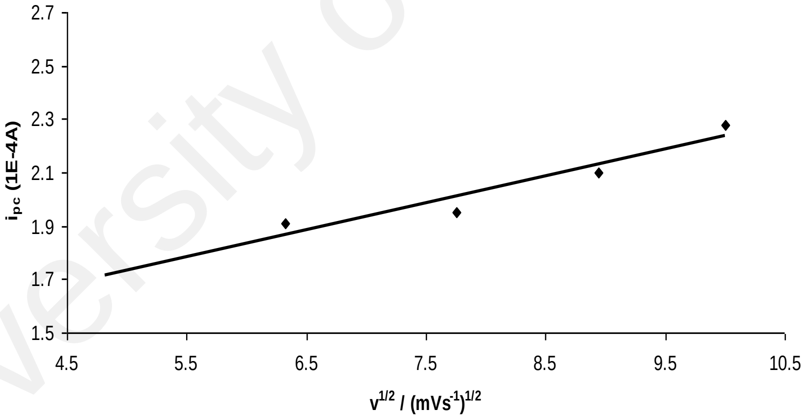

Figure 4.65: Graph of the first cathodic current versus square root of the scan rate for CuFB

The physico-structural studies of CuFB has been accepted for publication in the International Journal of Physical Sciences. ID number : IJPS-10-306 (**Appendix 9**).

4.5.1.5 Summary

The chemical formula of CuFB is $[Cu_2(4\text{-}FC_6H_4COO)_4(C_2H_5OH)_2].2H_2O$, and it is proposed to have a distorted paddle-wheel structure similar to $CuNO_2B$ and $CuDNO_2B$. However, its structure becomes more planar in $CH_3OH\text{-}CH_3COOH$ solvents. There exists a weak antiferromagnetic interaction between the two Cu(II) centres, its thermal stability is lower than $CuNO_2B$ but higher than CuB, $CuDNO_2B$, CuOHB and $CuNH_2B$, and its redox properties are similar to the previously discussed complexes in this study.

4.5.2 Copper(II) 4-Chlorobenzoate

4.5.2.1 Structural elucidation

The results of the **elemental analysis** (45.8% C, 3.3% H, 18.6% O and 15.6% Cu) are in excellent agreement with those calculated for the chemical formula $CuC_{16}H_{14}O_5Cl_2$ or $[Cu(4\text{-}ClC_6H_4COO)_2(C_2H_5OH)]$ (formula mass, 420.5 g mol^{-1}; 45.7% C, 3.3% H, 19.0% O, 15.1% Cu).

Its **FTIR** spectrum (**Figure 4.66**) is similar to those of the previously discussed complexes. For example, it shows a broad ν(OH) vibration at about 3400 cm^{-1}, and the values for ν_{as}COO and ν_sCOO bands are 1562 cm^{-1} and 1408 cm^{-1} respectively. Hence, the $\Delta\nu$(COO) value is 153 cm^{-1}, indicating a bridging bidentate coordination mode of the ligand. The value is similar to that of CuB (154 cm^{-1}). Thus, it may be suggested that the structure of CuClB is also paddle-wheel.

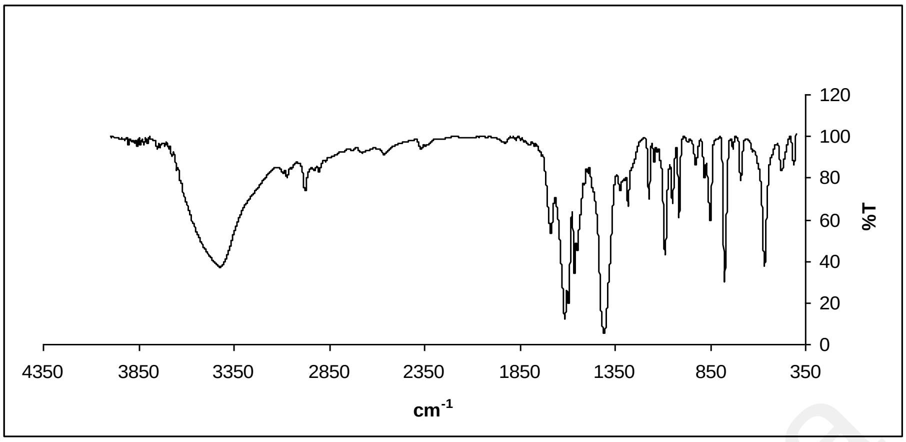

Figure 4.66: FTIR spectrum of CuClB

The **UV-vis** spectrum of solid CuClB (**Figure 4.67**) shows a broad *d-d* band at 703 nm, indicating a square pyramidal geometry at Cu(II) centres. The band is stronger and slightly blue-shifted compared to CuFB (715 nm). This further supports a less distorted structure for CuClB.

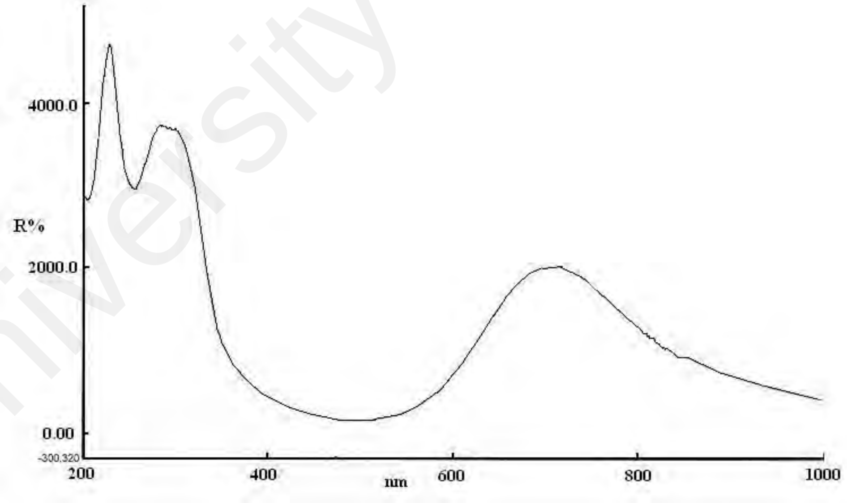

Figure 4.67: UV-vis spectrum of solid CuClB

The UV-vis spectrum of CuClB dissolved in CH_3OH-CH_3COOH (20:1) (**Figure 4.68**) is similar to those of the previously discussed complexes. The two *d-d* peaks at 700 nm (ε_{max} = 283 M^{-1} cm^{-1}) and 380 nm

(ε_{max} = 66 M^{-1} cm^{-1}) suggest that its binuclear square pyramidal geometry remained intact in these solvents.

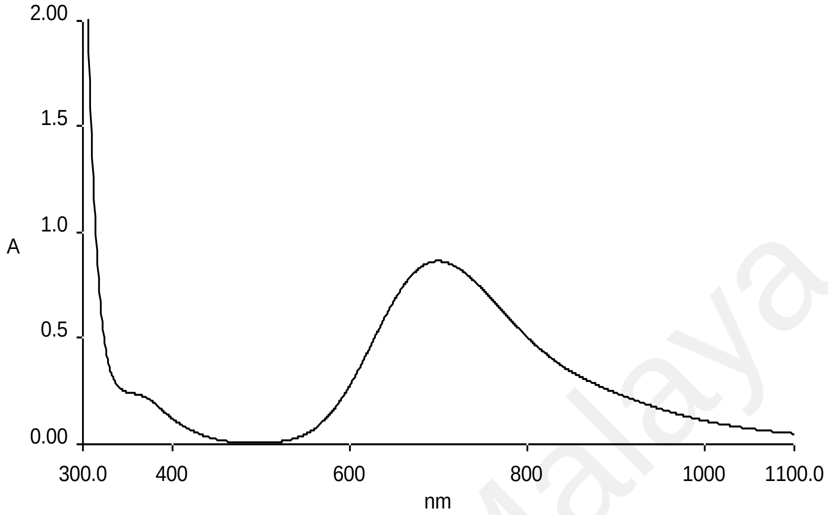

Figure 4.68: UV-visible spectrum of CuClB in CH_3OH-CH_3COOH

The lower ε_{max} value for Band 1 of CuClB (283 M^{-1} cm^{-1}) compared to CuFB (430 M^{-1} cm^{-1}) further supports the more symmetrical paddle-wheel structure for the former complex.

4.5.2.2 Magnetic susceptibility

The μ_{eff} value, similarly calculated from the values of χ_g (1.15 x 10^{-6} cm^3 g^{-1}), χ_d (-4.63 x 10^{-4} cm^3 mol^{-1}), and hence χ_m^{corr} (1.43 x 10^{-3} cm^3 mol^{-1}), is 1.80 B.M. at 298 K, and the -2J value is 381 cm^{-1}. The lower μ_{eff} value (stronger antiferromagnetic interaction) compared to CuFB (2.54 B.M.) and similarity with that of CuB (1.93 B.M.) further supports the above suggestion about its structure.

4.5.2.3 Thermal analysis

The **TGA** trace (**Figure 4.69**) shows that CuClB is just slightly more thermally stable (T_{dec} = 288°C) compared to CuFB (T_{dec} = 275°C). Based on the respective pK_a value of the corresponding arylcarboxylic acid, the 4-ClC_6H_4COO-Cu bond is expected to be slightly weaker than that of 4-FC_6H_4COO-Cu. The results seem to suggest that thermal stability of these complexes depends more on their structure and polarity of the arylcarboxylate ligands than on the metal-ligand bond strength.

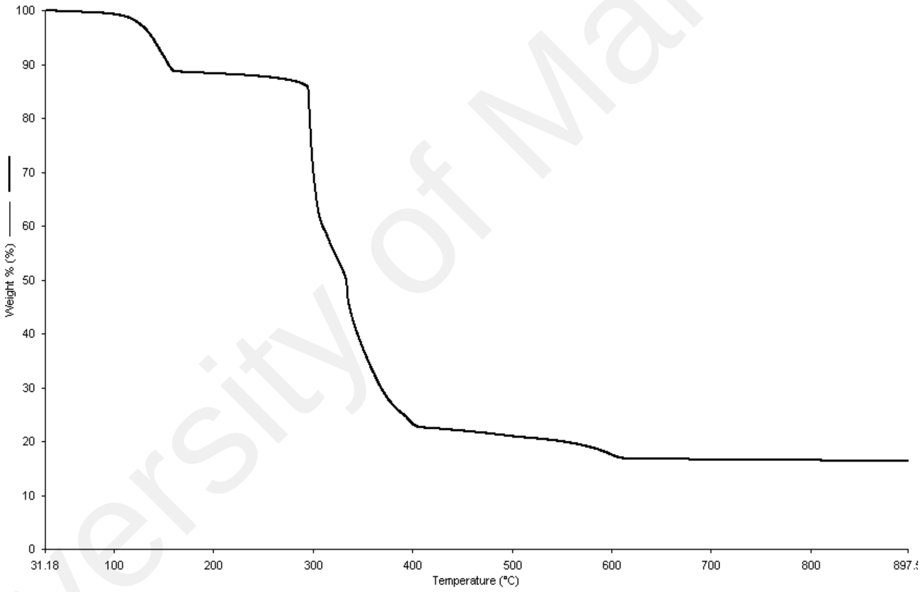

Figure 4.69: TGA of CuClB

The thermogram also shows an initial weight loss of 11% at 100°C, assigned to the evaporation of the axially-coordinated CH_3CH_2OH molecules (expected, 11%). The major weight loss of 72% at 288°C is assigned to the decarboxylation of 4-ClC_6H_4COO ligand (expected, 70%). The amount of residue at temperatures above 700°C is 17%, which is in excellent agreement with the expected value of 18.9%, calculated assuming that it is mainly CuO.

Additionally, using the gravimetric concept, the estimated formula mass for CuClB is 845 g mol^{-1}, which is in good agreement with the value calculated based on its proposed structural formula (841 g mol^{-1}).

The **DSC** plot (**Figure 4.70)** shows a weak endothermic peak at 100°C (ΔH = +154 kJ/mol) and a very strong exothermic peak at 295°C (ΔH = - 502 kJ/mol). The results are similar to previously discussed complexes (except CuFB), and hence may be similarly explained.

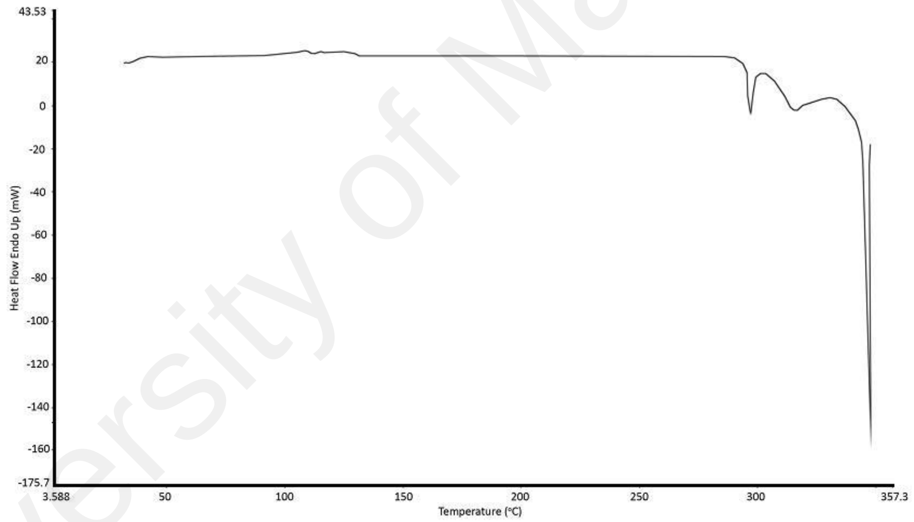

Figure 4.70: DSC of CuClB

4.5.2.4 Cyclic voltammetry

The CV of CuClB was similarly recorded in CH_3OH-CH_3COOH. Again, it is important to note that its dimeric structure remained intact in these solvents.

(a) *Potential window = +1.5 V to -1.5 V; scan rate = 100 mV s^{-1}*

The CV (**Figure 4.71**) shows three cathodic peaks at -0.13, -0.27 and -0.82 V and two overlapping anodic peaks at +0.21 V and +0.30 V (shoulder). The result is similar to CuFB, and may be similarly assigned.

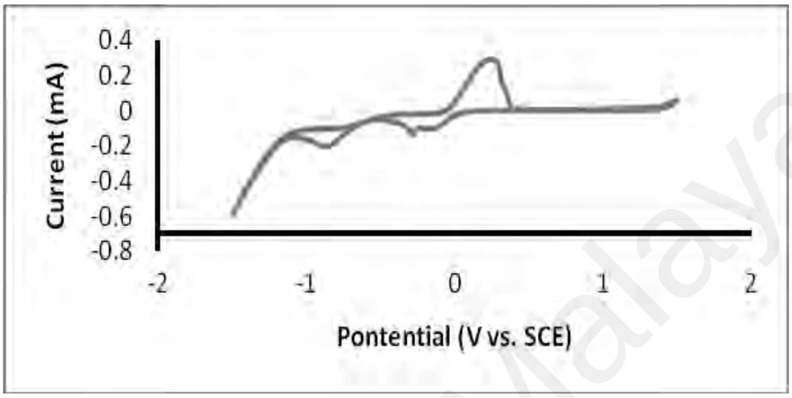

Figure 4.71: CV of CuClB

The results suggest that Cl exerts a similar effect as F on the redox properties of these copper(II) 4-haloarylcarboxylates. This may be due to the almost similar basicities of the two ligands, and to similar structure in these solvents.

(b) Potential window = +1.5 V to -1.5 V; scan rates = 40 - 100 mV s^{-1}

The CVs of CuClB at different scan rates are shown in **Figure 4.72**, the corresponding data in **Table 4.24**, and a graph of the current of the first cathodic peak versus the square roots of the scan rate in **Figure 4.73.** The results are similar to those of CuFB, which further support the above suggestions.

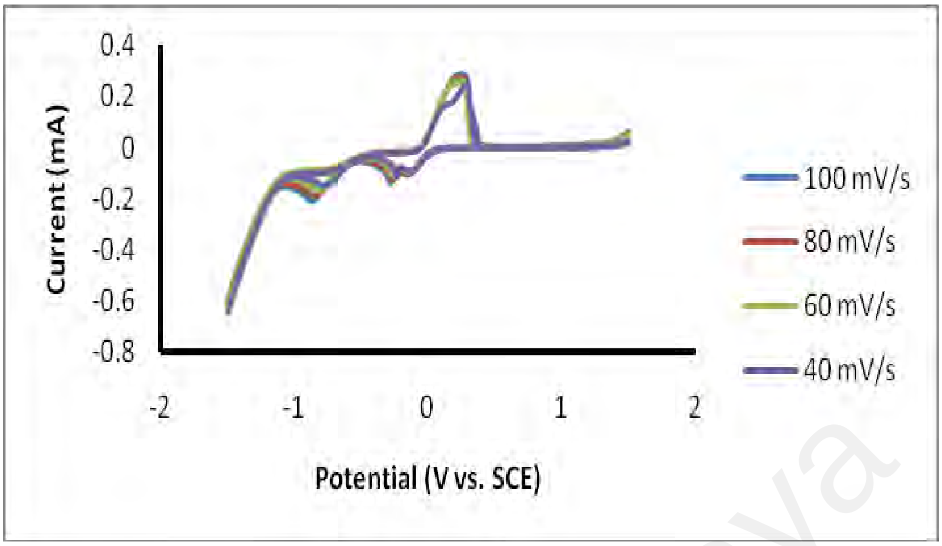

Figure 4.72: CV of CuClB at different scan rates

Table 4.24: The peak potential (E_p/V) and peak separation (ΔE/mV) for CuClB in CH_3OH-CH_3COOH at each scan rate (mV s^{-1})

Scan rate	E_{pc1}	E_{pc2}	E_{pc3}	E_{pa1}	E_{pa2}	ΔE_1^*	$\Delta E_2^\#$
40	-0.10	-0.24	-0.73	+0.11	+0.23	330	840
60	-0.11	-0.25	-0.78	+0.15	+0.25	360	930
80	-012	-0.27	-0.81	+0.19	+0.27	390	1000
100	-0.13	-0.27	-0.82	+0.21	+0.30	430	1030

* $\Delta E_1 = E_{pa2} - E_{pc1}$; # $\Delta E_2 = E_{pa1} - E_{pc3}$

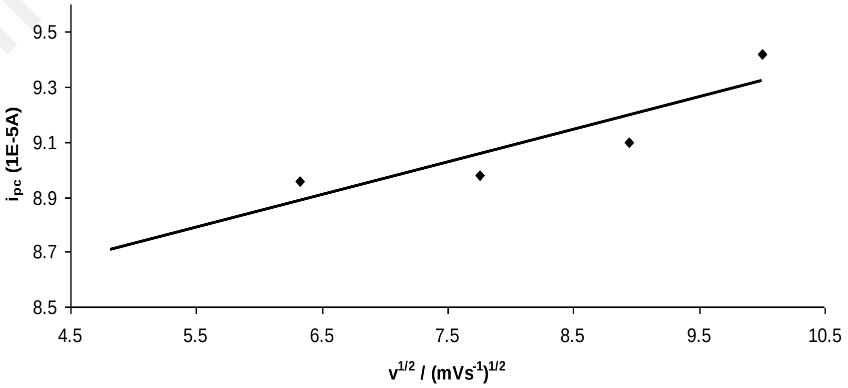

Figure 4.73: Graph of the first cathodic current versus square root of the scan rate for CuClB

4.5.2.5 Summary

The chemical formula for CuClB is $[Cu_2(4\text{-}ClC_6H_4COO)_4(C_2H_5OH)_2]$, and it is proposed to have similar paddle-wheel structure as for the previously discussed complexes, in the solid state and especially in solution. It shows a strong antiferromagnetic interaction between the two Cu(II) centres, its thermal stability is similar to $CuNO_2B$ and higher than CuFB, while its redox properties are similar to CuFB.

4.5.3 Copper(II) 4-Bromobenzoate

4.5.3.1 Structural elucidation

The results of the **elemental analysis** (38.0% C, 2.7% H, 16.1% O and 12.3% Cu) are in good agreement with those calculated for the chemical formula $CuC_{16}H_{14}O_5\ Br_2$ or $[Cu(4\text{-}BrC_6H_4COO)_2(CH_3CH_2OH)]$ (FW, 509.3 g mol^{-1}; 37.7% C, 2.7% H, 15.7% O and 12.3% Cu).

The **FTIR** spectrum (**Figure 4.74**) is very similar with that of CuClB. Specifically, there is a broad OH peak at 3400 cm^{-1}, and the values for the $\nu_{as}COO$ and $\nu_{s}COO$ stretching bands are 1560 cm^{-1} and 1407 cm^{-1} respectively. Thus, $\Delta\nu(COO)$ value (153 cm^{-1}) is the same as CuClB (153 cm^{-1}). Hence, it may be stated that the coordination mode of $4\text{-}BrC_6H_4COO^-$ ligand in CuBrB is also bidentate bridging.

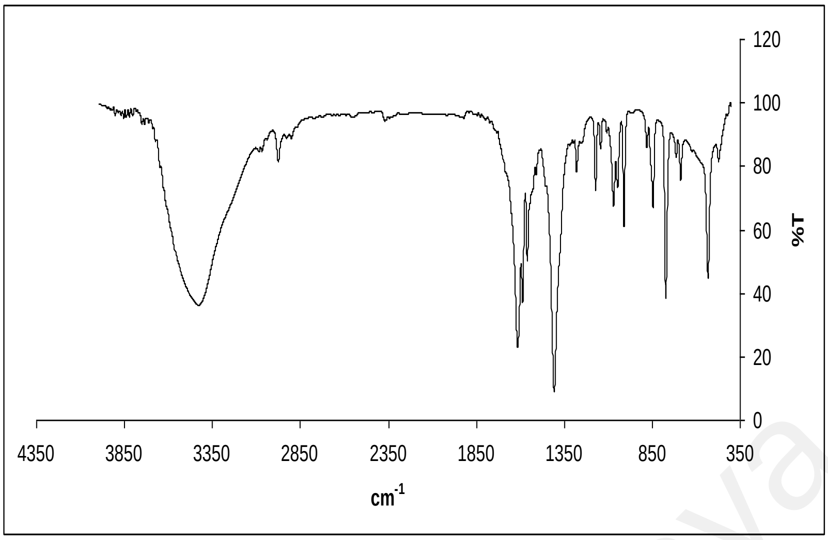

Figure 4.74: FTIR spectrum of CuBrB

The **UV-vis** spectrum of solid CuBrB (**Figure 4.75**) shows a broad *d-d* peak (Band 1) at 701 nm as well as peaks at 400, 380, 276 and 233 nm. The spectrum is very similar to that of solid CuClB (Band 1 at 703 nm), suggesting similar structure of the two complexes, as was suggested from FTIR.

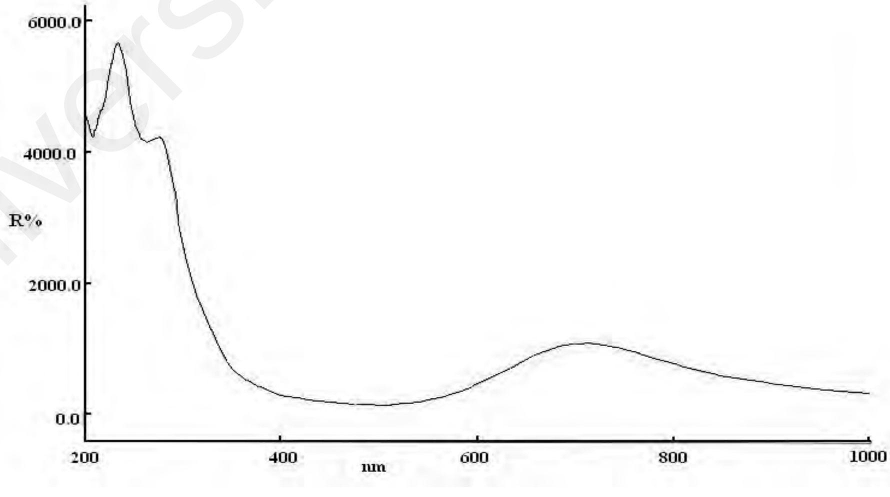

Figure 4.75: UV-vis spectrum of solid CuBrB

As expected, the UV-vis spectrum of CuBrB (**Figure 4.76**) in CH_3OH-CH_3COOH is also similar to that of CuClB. It shows *d-d* bands at 700 nm

(ε = 299 $M^{-1}cm^{-1}$) and at 384 nm (ε = 66 $M^{-1}cm^{-1}$). From these, it is highly probable that the structures of the two complexes are similar in these solvents (binuclear pyramidal).

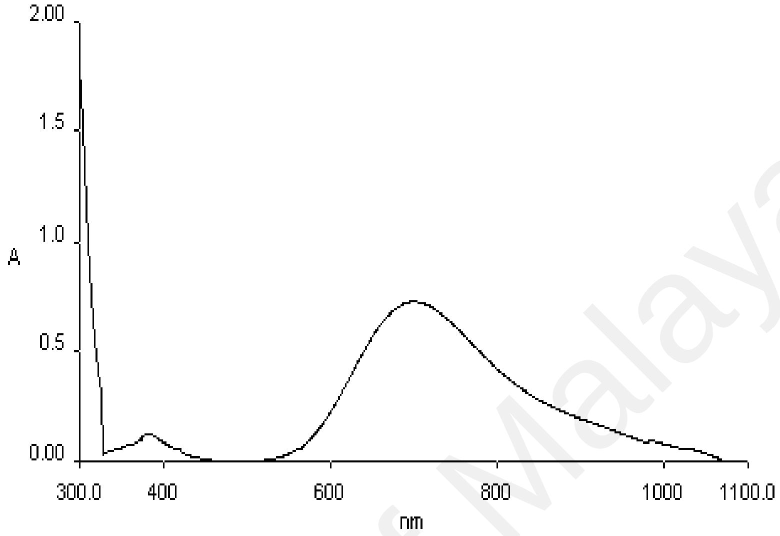

Figure 4.76: UV-vis of CuBrB in CH_3OH-CH_3COOH

4.5.3.2 Magnetic susceptibility

The μ_{eff} value, calculated as before from the values of χ_g (0.90 x 10^{-6} cm^3g^{-1}), χ_d (-5.09 x 10^{-4} cm^3mol^{-1}), and hence χ_m^{corr} (1.426 x 10^{-3} cm^3mol^{-1}), is 1.80 B.M. at 298 K, while the -2J value is 381 cm^{-1}. The values are the same as for CuClB (μ_{eff} = 1.80 B.M., -2J = 381 cm^{-1}), confirming the similarity in their structures.

4.5.3.3 Thermal analysis

The **TGA** trace (**Figure 4.77**) shows that the complex is thermally stable up to 293°C, which is slightly higher than CuClB (288°C). As it is proposed that both complexes have similar structures with similar metal-ligand coordinate bond strength, the higher thermal stability of CuBrB may be due to the lower inductive and mesomeric effects of Br atom. As a result, the 4-$BrC_6H_4COO^-$ ion is less easily decarboxylated compared to 4-$ClC_6H_4COO^-$ ion. This is in line with the above suggestion that thermal stability of these complexes depends on their structure and polarity of the arylcarboxylate ligands, namely a less polar ligand is more thermally stable.

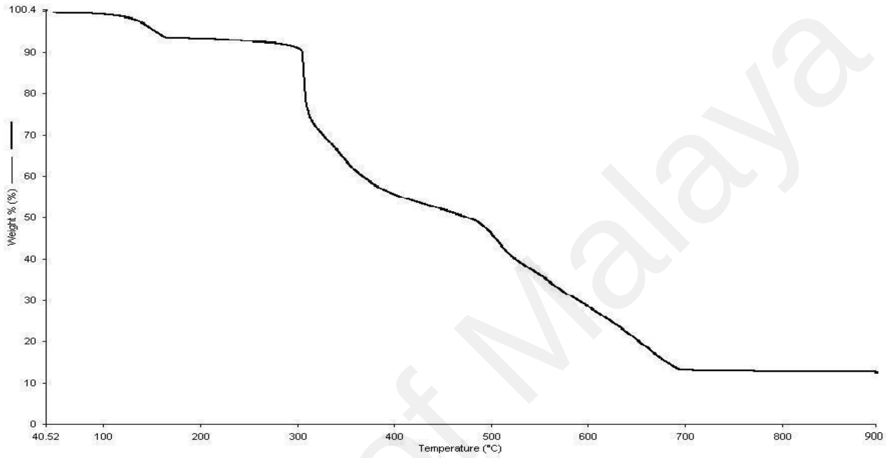

Figure 4.77: TGA of CuBrB

The TGA also shows an initial weight loss of 8.5% at 120°C assigned to the loss of axially-coordinated CH_3CH_2OH (expected, 9.0%). This is followed by a major weight loss of 76.0% at 293°C, assigned to the decomposition of 4-BrC_6H_4COO ligand (expected, 78.1%).

The amount of residue at temperatures above 700°C is 15.5%. From this, the estimated formula mass for CuBrB is 1026 g mol^{-1}. The result is good agreement with the formula mass calculated from the proposed chemical formula (1018 g mol^{-1}).

The **DSC** plot (**Figure 4.78**) shows a weak endothermic peak at 124°C (ΔH = +73.6 kJ/mol) and a strong exothermic peak at 310°C (ΔH = -2315 kJ/mol). The plot is actually very similar to that of CuClB, and may be similarly assigned and explained.

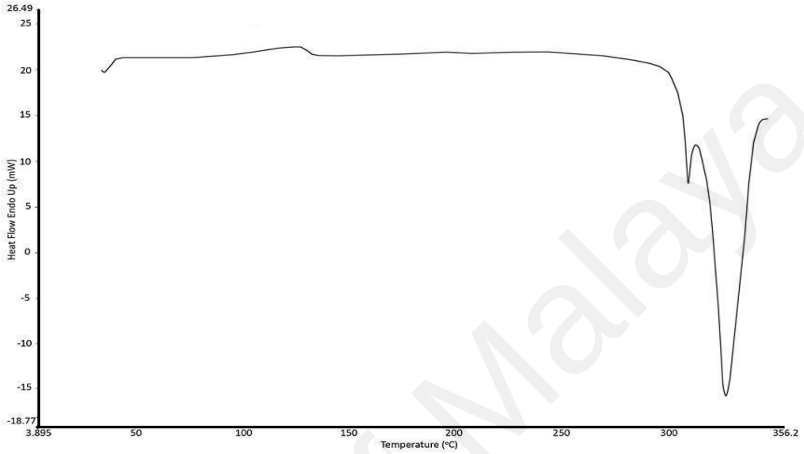

Figure 4.78: DSC of CuBrB

4.5.3.4 Cyclic voltammetry

As for the other complexes, the CV of CuBrB was also recorded in CH_3OH-CH_3COOH. Also, it is to be noted that the dimeric structure of the complex remained intact in this solvent.

(a) Potential window = +1.5 V to -1.5 V; scan rate = 100 mV s^{-1}

The CV (**Figure 4.79**) shows three cathodic peaks at -0.15, -0.29 and -0.85 V, and a broad anodic peak at +0.26 V. As expected, these are at almost the same potentials as for CuClB (-0.13, -0.27, -0.82, +0.21, +0.30 V) and CuFB (-0.12, -0.28, -0.80, +0.20, +0.27 V), and may be similarly assigned and explained.

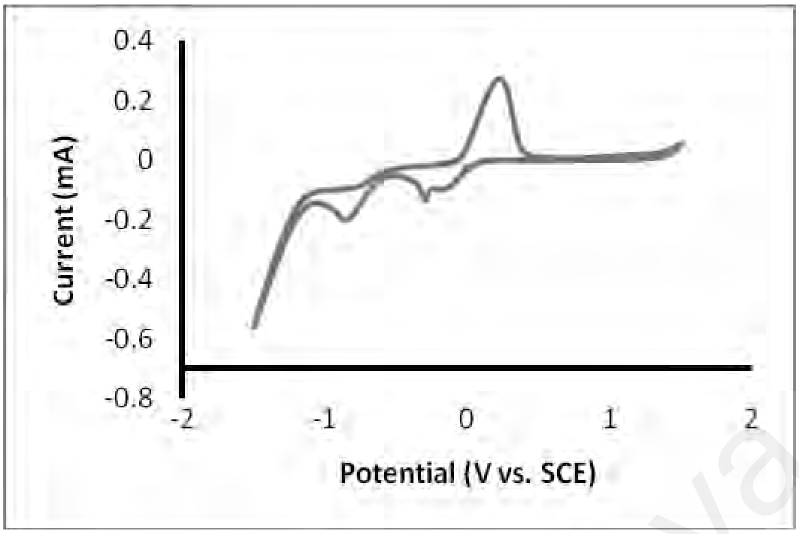

Figure 4.79: CV of CuBrB

The results suggest that Br exerts a similar effect as Cl and F on the redox properties of these copper(II) 4-haloarylcarboxylates. This further supports the correlation between redox properties and basicities of ligands and structure of complexes.

(b) Potential window = +1.5 V to -1.5 V; scan rates = 40 - 100 mV s^{-1}

The CVs recorded at different scan rates are shown in **Figure 4.80,** the corresponding data in **Table 4.25**, and a graph of the first cathodic peak current versus the square root of the scan rate in **Figure 4.81**. As expected, the results are similar to CuClB and CuFB, which further support the correlation proposed above.

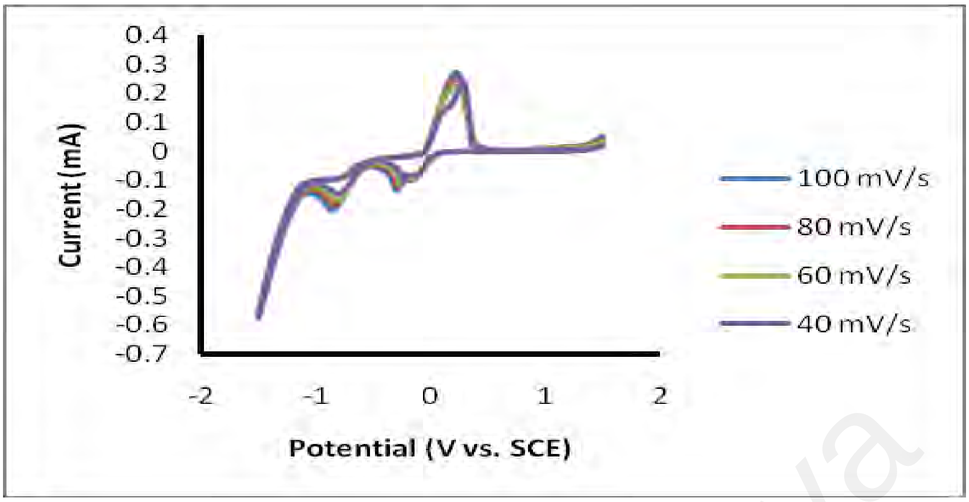

Figure 4.80: CV of CuBrB at different scan rates

Table 4.25: The peak potential (E_p/V) and peak separation (ΔE/mV) for CuBrB in CH_3OH-CH_3COOH at different scan rate (mV s^{-1})

Scan rate	E_{pc1}	E_{pc2}	E_{pc3}	E_{pa1}	E_{pa2}	ΔE_1^*	$\Delta E_2^\#$
40	-0.11	-0.25	-0.76	+0.13	+0.29	404	891
60	-0.12	-0.26	-0.80	+0.19	+0.28	400	890
80	-013	-0.28	-0.81	+0.22	-	350	1030
100	-0.15	-0.29	-0.85	+0.26	-	410	1090

* $\Delta E_1 = E_{pa2} - E_{pc1}$; # $\Delta E_2 = E_{pa1} - E_{pc3}$

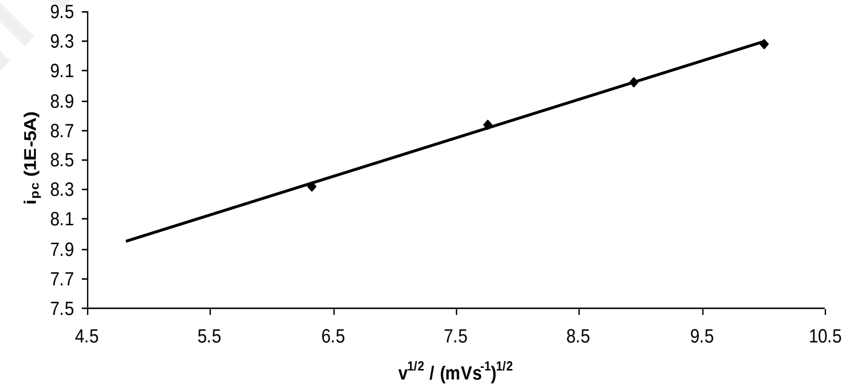

Figure 4.81: Graph of the first cathodic currents versus square root of the scan rates for CuBrB

4.5.3.5 Summary

The chemical formula for CuBrB is $[Cu_2(4\text{-}BrC_6H_4COO)_4(C_2H_5OH)_2]$, and it is proposed to have similar paddle-wheel structure as the previously discussed complexes, in the solid state and especially in solution. Its thermal stability is slightly higher than, while its magnetic and redox properties are similar to, CuClB. Thus, substituting Br for Cl or F in the aromatic ring of the arylcarboxylate ligands does not seem to have a significant effect on the structure, thermal, magnetic and redox properties of these complexes.

4.5.4 Copper(II) 4-Iodobenzoate

4.5.4.1 Structural elucidation

The results of the **elemental analysis** (31.2% C, 2.3% H, 14.3% O and 11.0% Cu) are in good agreement with those calculated from the chemical formula $CuC_{16}H_{14}O_5I_2$ or $[Cu(4\text{-}IC_6H_4COO)_2(CH_3CH_2OH)]$ (formula mass, 603.3 g mol^{-1}; 31.8% C, 2.3% H, 13.3% O and 10.5% Cu).

The **FTIR** spectrum (**Figure 4.82**) is similar to the previously discussed complexes. It shows a broad peak at about 3400 cm^{-1} for OH group, and the values for ν_{as}(COO) and ν_s(COO) at 1580 and 1420 cm^{-1} respectively. Thus, the $\Delta\nu$(COO) value is 160 cm^{-1} indicating a bridging bidentate coordination mode of the ligand.

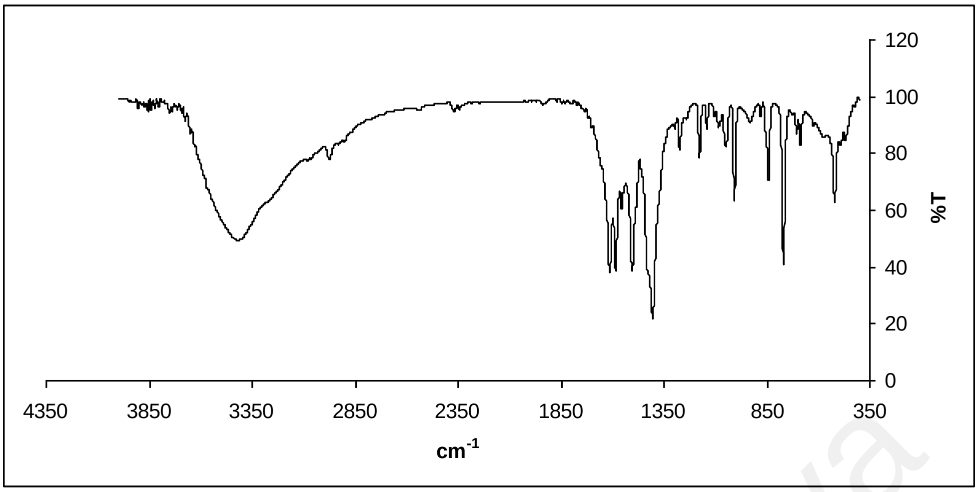

Figure 4.82: FTIR spectrum of CuIB

The **UV-vis** spectrum of solid CuIB (**Figure 4.83**) shows a broad *d-d* peak at 707 nm, which is at similar wavenumber as that of CuBrB (701 nm) and CuClB (703 nm). This suggests similar square pyramidal geometry at Cu(II) with these complexes.

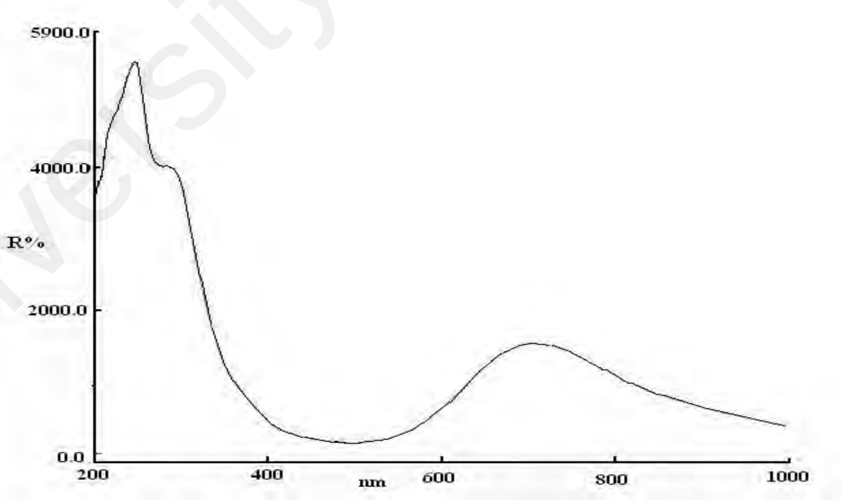

Figure 4.83: UV-vis spectrum of solid CuIB

The spectrum of CuIB in CH_3OH-CH_3COOH (**Figure 4.84**) is also similar to all of the previously haloarylcarboxylate copper(II) complexes, suggesting similar structures in solution. For example, its *d-d* peaks are at

700 nm (ε = 280 $M^{-1}cm^{-1}$) while the value for CuFB is 697 nm (430 $M^{-1}cm^{-1}$), CuClB is 700 nm (283 $M^{-1}cm^{-1}$), and CuBrB is 700 nm (299 $M^{-1}cm^{-1}$).

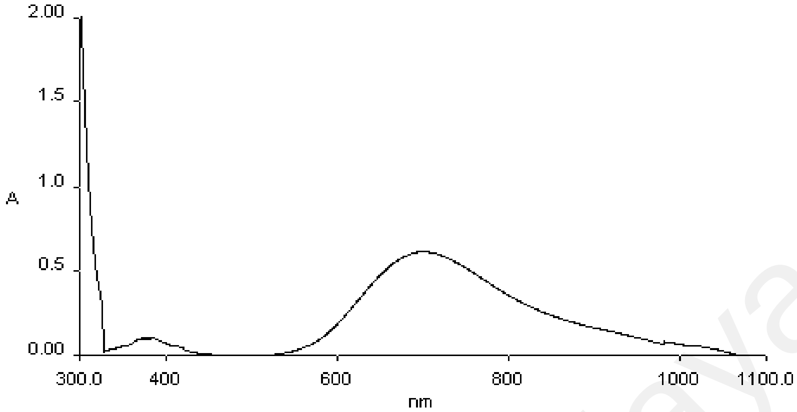

Figure 4.84: UV-vis spectrum of CuIB in CH_3OH-CH_3COOH

In order to ascertain the stability of CuIB in solution, it was dissolved in THF and an equimolar amount of 2,2'-bypiridine was added at room temperature. The mixture formed crystals suitable for X-ray analysis after two days of slow evaporation. The structure is shown in **Figure 4.85**, and the corresponding crystal data and selected bond lengths and angles are shown in **Table 4.26** and **Table 4.27**.

The structure shows that the Cu(II) atom is N,N'-chelated by a 2,2'-bipyridine and coordinated by two monodentate carboxylate ions and a water molecule in a distorted square-pyramidal geometry (τ = 0.13). The apical site is occupied by one of the carboxylate O atoms. The water molecule forms intramolecular hydrogen bonds to the uncoordinated carboxyl O atoms.

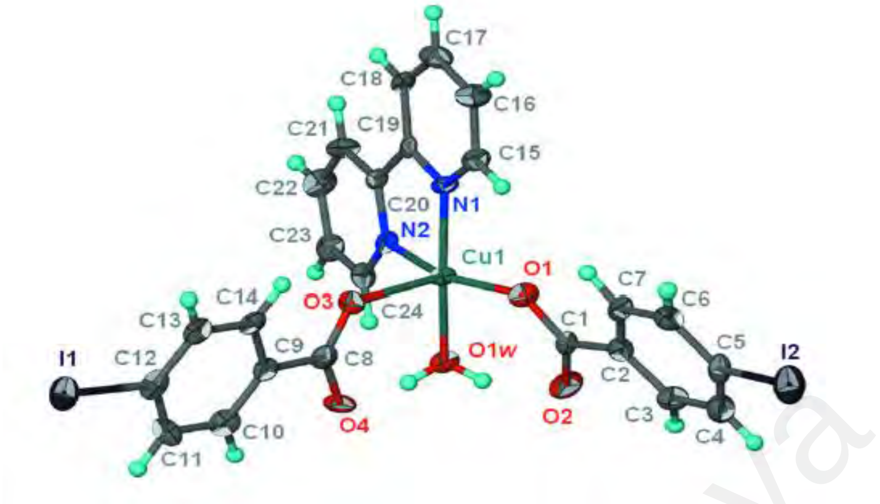

Figure 4.85: Thermal ellipsoid plot of $Cu(H_2O)(C_{10}H_8N_2)(C_7H_4IO_2)_2$ at the 70% probability level; hydrogen atoms are drawn as spheres of arbitrary radius

Table 4.26: Crystal data

$[Cu(C_7H_4IO_2)_2(C_{10}H_8N_2)(H_2O)]$
$M_r = 731.74$
Monoclinic, $P21/c$
Hall symbol: -P 2ybc
$a = 13.0571$ (2) Å
$b = 16.0724$ (2) Å
$c = 11.9605$ (2) Å
$\beta = 103.298$ (1)°
$V = 2442.72$ (6) Å^3
$Z = 4$

$F(000) = 1404$
$D_x = 1.990$ Mg m^{-3}
Mo $K\alpha$ radiation, $\lambda = 0.71073$ Å
Cell parameters from 1215 reflections
$\theta = 2.5$–24.2°
$\mu = 3.46$ mm^{-1}
$T = 100$ K
Cube, blue
0.30 × 0.30 × 0.30 mm

Table 4.27: Selected bond lengths (Å)

Cu1—N1 1.982 (7)
Cu1—N2 2.009 (6)
Cu1—O1 1.977 (5)

Cu1—O3 2.216 (6)
Cu1—O1W 1.959 (5)

Probably due to a large size of the iodine atom, there is no significant intermolecular interaction observed in the crystal packing of the molecule (no supramolecular network). However, there exists intramolecular interaction in the crystals involving hydrogen from H_2O molecule and the uncoordinated carboxyl O atoms (**Table 4.28**). The crystallographic asymmetric unit of the crystal only comprises a copper(II) complex without the presence of THF molecules. This is in contrast to the crystals obtained from a similar reaction between $CuDNO_2$ and 2,2'-bipyridine (**Figure 4.33**), where an intermolecular interaction is dominant by hydrogen bonding.

Table 4.28: Hydrogen-bond geometry (Å)

D—H.....A	D—H	H.....A	D…..A	D—H…..A
O1w—H11.....O2	0.84	1.79	2.560 (9)	152
O1w—H12.....O4	0.84	1.79	2.575 (8)	154

Thus, the paddle-wheel structure of CuIB dissociated in solution, the "species" formed then self-assembled to a form a more stable structure. This is as expected from the weaker 4-IC_6H4COO-Cu bond.

The above crystal structure was published in an ISI journal: Mohammad Isa Mohamadin, Norbani Abdullah, Kong Mun Lo and Seik Weng Ng, *Aqua(2,2'-bipyridine-κ^{2}N,N')bis(4-iodobenzoato-κO)copper(II)*, Acta Cryst. (2010). E66, page 1530 (**Appendix 10**).

4.5.4.2 Magnetic susceptibility

The μ_{eff} value for CuIB, calculated from the values of χ_g (0.82 x 10^{-6} cm^3 g^{-1}), χ_d (-5.65 x 10^{-4} cm^3 mol^{-1}), and hence χ_m^{corr} (1.555 x 10^{-3} cm^3 mol^{-1}), is 1.88 B.M. at 298 K, and the corresponding -2J value is 352 cm^{-1}. These values are similar to CuB, CuClB and CuBrB, indicating similar magnetic properties, and hence similar structure in the solid state.

4.5.4.3 Thermal analysis

The **TGA** trace (**Figure 4.86)** shows that CuIB was thermally stable up to 310^{o}C. Thus, it is the most thermally stable complexes of all of the copper(II) arylcarboxylates studied in this study. The result further enhances the above postulation on the correlation between thermal stability and polarisability of the arylcarboxylate ligands.

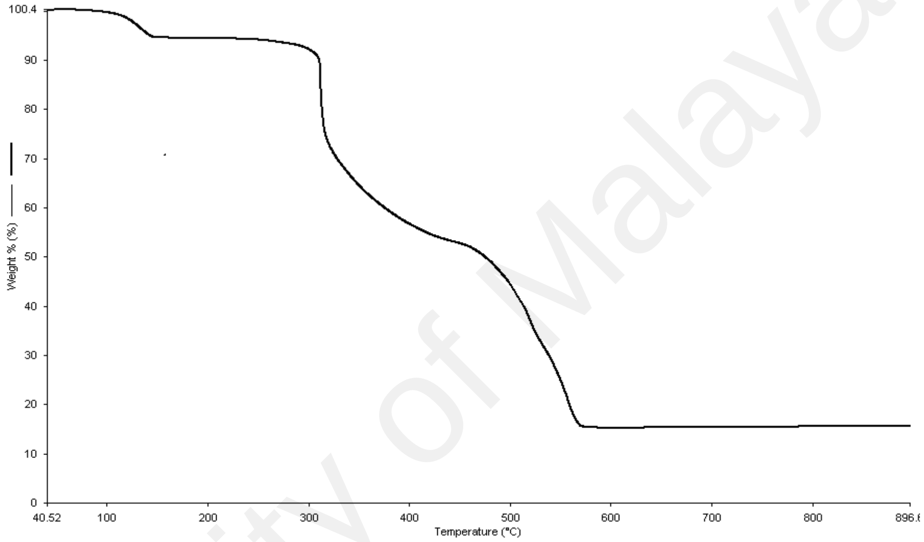

Figure 4.86: TGA of CuIB

The TGA also shows an initial weight loss at of 5.4% at 120^{o}C, assigned to the evaporation of coordinated CH_3CH_2OH (expected, 7.6%). The major weight loss of 81.1% at temperatures above 310^{o}C, assigned to decomposition of 4-IC_6H_4COO ligand (expected, 79.2%). The amount of residue at temperatures above 600^{o}C is 13.5 %, which is in excellent agreement with the expected value of 13.2%, assuming that it is purely CuO.

The **DSC** plot of CuIB (**Figure 4.87**) is similar to the other complexes. It shows a small endotherm at 160^{o}C ($\Delta H = +177$ kJ/mol), ascribed to the release of the apical CH_3CH_2OH ligand, in agreement with TGA. This is then followed by a strong exothermic peak at 312°C (ΔH = -261 kJ/mol) as a result of the formation of volatiles from the decomposition of the ligands.

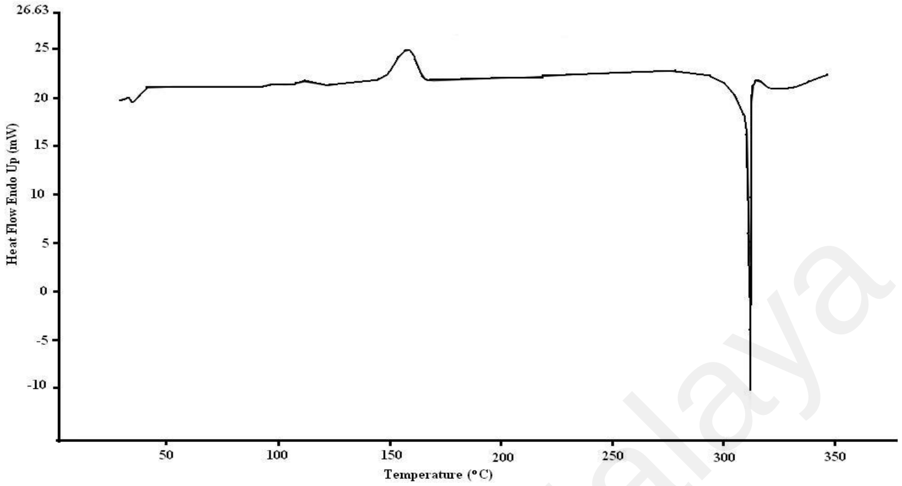

Figure 4.87: DSC of CuIB

4.5.4.4 Cyclic voltammetry

The CV of CuIB is similarly recorded in CH_3OH-CH_3COOH. It is again important to note that its structure remained dimeric in these solvents.

(a) Potential window = +1.5 V to -1.5 V; scan rate = 100 mV s^{-1}

The CV (**Figure 4.88**) shows three cathodic peaks -0.18, -0.33 and -0.92 V. These peaks are also found at about the same potentials in the CVs of the previously discussed copper(II) haloarylcarboxylates, and may be similarly assigned.

However compared to the other halo complexes, there are three oxidation peaks at +0.15, +0.27 (shoulder) and +0.54 V ("new"), suggesting step-wise oxidation process. The difference may not be due to a more extensive geometrical distortion and complex dissociation as these complexes were shown to have similar structures in these solvents, and similar 4-

XC_6H_4COO-Cu bond strengths. It is proposed that the "new" peak arises from the oxidation of iodine atom at the aromatic ring, which should be easier compared to the other halogens due to its larger size and higher negative charge density.

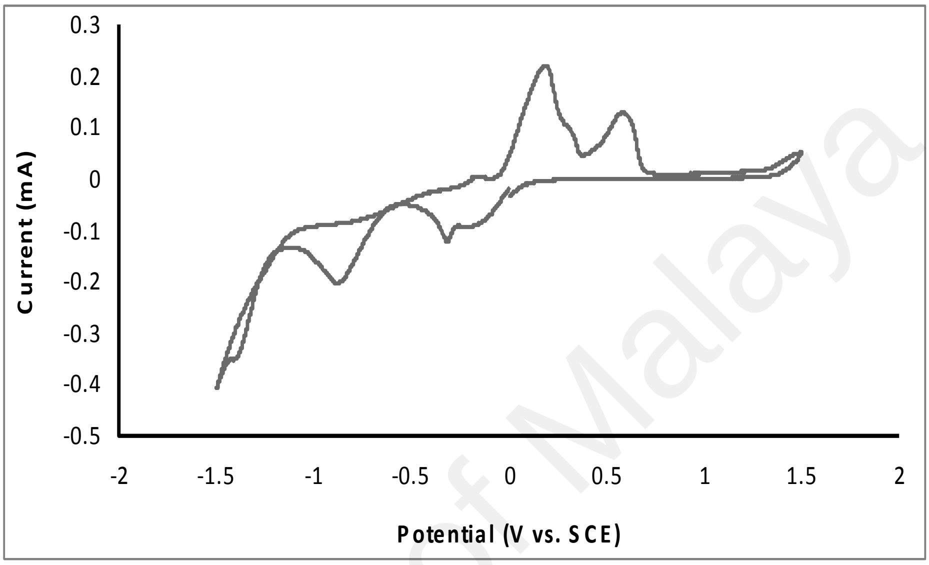

Figure 4.88: CV of CuIB

Similar to the previously discussed copper(II) complexes, the ΔE values for Cu(II)Cu(II)-Cu(II)Cu(I) and Cu(II)Cu(I)-Cu(I)Cu(I) redox couples are 720 mV and 1070 mV respectively, indicating quasireversible redox reactions.

(b) Potential window = +1.5 V to -1.5 V; scan rate = 40 - 100 mV s^{-1}

The CV of CuIB was also recorded at different scan rates. The voltammogram (**Figure 4.89**), the corresponding data (**Table 4.29**), and a graph of the first cathodic peak current versus the square root of the scan rate (**Figure 4.90**) are similar to the other copper(II) arylcarboxylates studied, and may be similarly explained. The obvious difference is a more extensive structural distortion of the reduced complexes formed from CuIB.

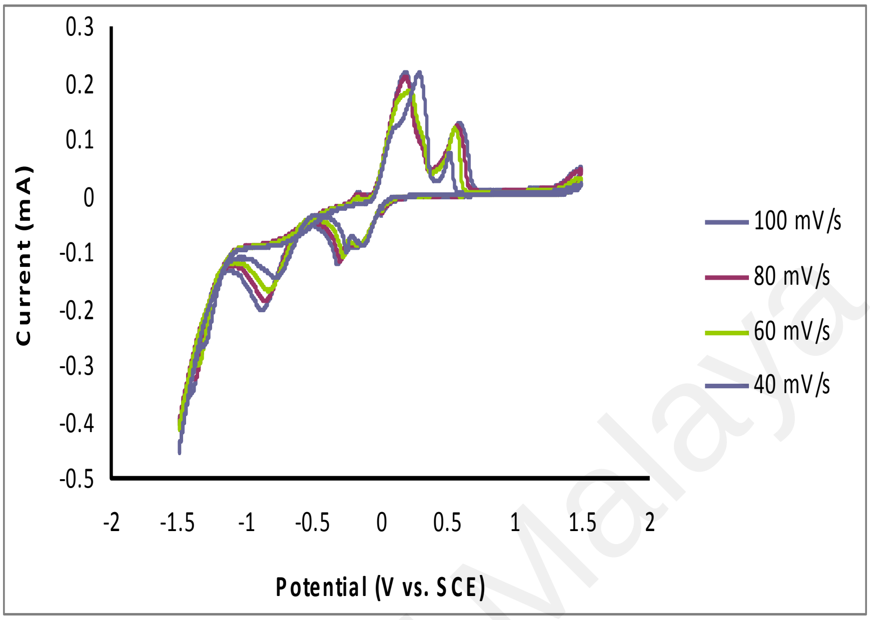

Figure 4.89: CV of CuIB at different scan rates

Table 4.29: The peak potential (E_p/V) and peak separation (ΔE/mV) for CuIB in CH_3OH-CH_3COOH at different scan rate (mV s^{-1})

Scan rate	E_{pc1}	E_{pc2}	E_{pc3}	E_{pa1}	E_{pa2}	E_{pa3}	ΔE_1^*	$\Delta E_2^\#$
40	-0.14	-0.26	-0.82	+0.11	+0.29	0.49	634	927
60	-0.15	-0.28	-0.87	+0.13	+0.26	0.53	681	995
80	-0.16	-0.30	-0.90	+0.15	+0.26	0.54	700	1049
100	-0.18	-0.33	-0.92	+0.15	+0.27	0.54	720	1070

* $\Delta E_1 = E_{pa3} - E_{pc1}$; # $\Delta E_2 = E_{pa1} - E_{pc3}$

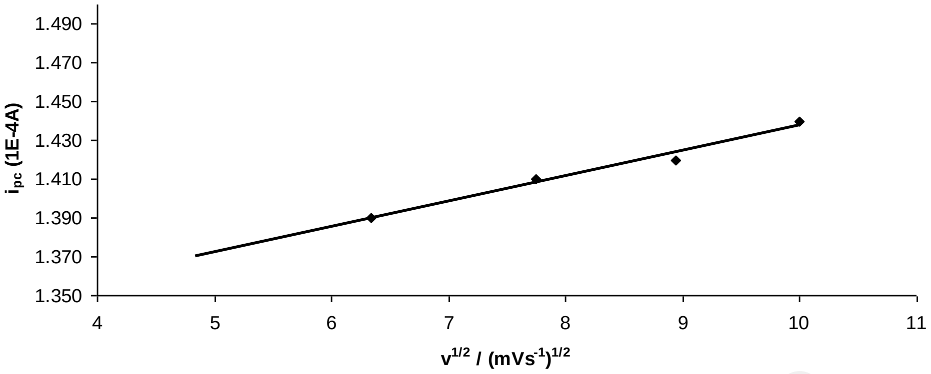

Figure 4.90: Graph of the first cathodic current versus square root of the scan rate for CuIB

4.5.4.5 Summary

The chemical formula for CuIB is [$Cu_2(4\text{-}IC_6H_4COO)_4(CH_3CH_2OH)_2$], and it is proposed to have similar paddle-wheel structure as previously discussed complexes in this study, both in the solid state and in CH_3OH-CH_3COOH, similar magnetic and redox properties (except for an easier oxidation of substituted iodine atom), and has the highest thermal stability.

Thus, substituting iodine for H, NO_2, OH, NH_2, F, Cl, or Br has increased the thermal stability, but had not affected significantly the structure, magnetic, and redox properties of copper(II) arylcarboxylates.

4.6 REACTION WITH CARBONYLS

Most literature reports on dinuclear copper(II) carboxylates mainly focused on their structures in correlation with the magnetic properties [46-53,54-59], but hardly any on their chemical properties.

Conceptually, the paddle-wheel structure adopted by most dinuclear copper(II) carboxylates [60,61] would enable them to act as templates-cum-catalysts for many chemical reactions, based on the following arguments: (a) there are two accessible axial positions at Cu(II) centres to act as templates for reactants with electron-pair donor atom (Lewis bases); (b) two Cu(II) centres in close proximity increase the electron-attracting ability of the complex as well as stabilizing it as a mixed-valence [Cu(II)-Cu(I)] complex. This would prevent the active catalyst from being deposited out of the reaction medium as insoluble Cu metal; (c) these complexes have tunable physical properties, such as solubility, and air and thermal stabilities; and (d) they are nonpoisonous and not easily poisoned, and may be easily synthesized from cheap and readily available starting materials.

The next focus of this research project is to identify the product(s) formed from the reaction of copper(II) arylcarboxylates with carbonyls under acidic conditions, and to understand the reaction mechanism. The impetus of the study originates from the accidental finding that a mixture of $[Cu_2(C_6H_5COO)_4]$, CH_3COCH_3 and HCl reacted to form a shiny and brittle black plates [62], which have yet to be fully characterized. Such compounds are attractive as potential processable and tunable solar cell materials due to its black colour, shiny appearance, and ease of preparation from cheap and readily available starting materials.

Current knowledge on the above reaction after refluxing for two or four hours, and on the product(s), indicates an incomplete redox and C-C bond formation reactions. Thus, this work is an attempt to fully comprehend the reaction, maximize the yield by a longer refluxing time of 8 hours, study the selectivity and tunability of the product (the electronic effect of substituent on the arylcarboxylate ligands), and to extend the scope of the reaction to other carbonyls (acetophenone and benzaldehyde).

4.6.1 Reaction of CuB with Acetone

The product obtained from the reaction of CuB with acetone (CH_3COCH_3) in the presence of concentrated HCl after refluxing for 8 hours was black, shiny and brittle plates in good yield (63% w/w based on CuB). It was observed that the colour of the reaction mixture changed from dark brown at initial time to orange brown after refluxing for 4 hours, and then to dark brown again after 6 hours.

The black solid was not obtained in a controlled experiment when either CuB or HCl was omitted from the reaction mixture.

It is envisaged that in the presence of a strong acid, such as HCl, CuB will react to form $CuCl_2$ and C_6H_5COOH. However, the results of the C,H elemental analyses of the black solid is 65.99% C and 8.47% H, while the values calculated for C_6H_5COOH is 68.85% C and 4.92% H. These suggest the presence of organic compound(s) other than C_6H_5COOH in the black solid.

The black solid was readily soluble in most polar organic solvents, namely acetone, chloroform, ethyl acetate, diethyl ether, THF, pyridine and ethanol, forming a dark brown solution, but insoluble in water and hexane.

4.6.1.1 Spectroscopic analysis

The **FTIR** spectrum of the black solid (**Figure 4.91)** shows a strong and broad peak at about 3500 cm^{-1} for the H-bonded –OH group, and a medium broad peak at 1680 cm^{-1} for C=O group. The absence of two asymmetric and symmetric vibrations of –COO, normally observed at 1609 – 1542 cm^{-1} and 1434 – 1348 cm^{-1} respectively for CuB, is noted. In fact, the spectrum is almost similar to that of C_6H_5COOH, suggesting its presence.

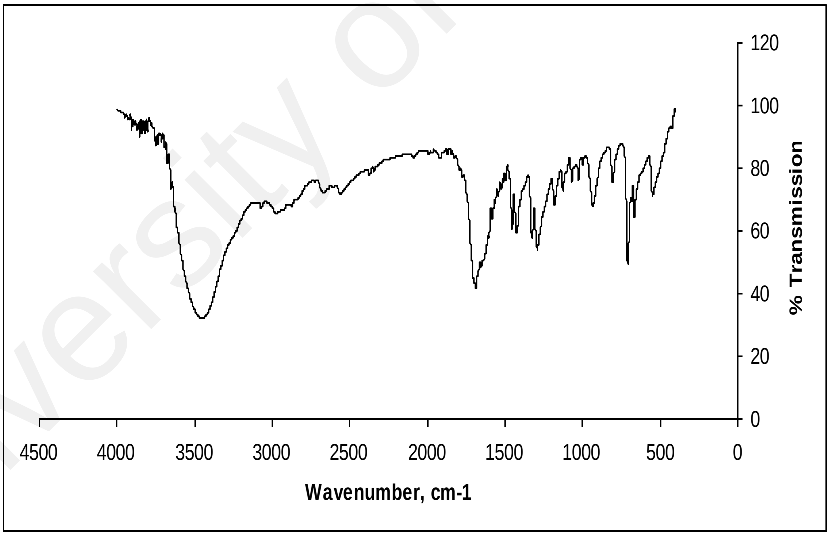

Figure 4.91: FTIR spectrum of the black solid

The **UV-visible spectrum** of the black solution (**Figure 4.92(a)**), formed when the black solid was dissolved in CH_3COCH_3, shows a gradually increasing absorbance from 1100 nm to about 600 nm with a plateau at 800 nm, and a much higher absorbance below 500 nm. Thus, the *d-d* peak expected for Cu(II) from 600 nm to 800 nm, is not distinctly obvious from the spectrum. The much higher absorbance peak at about 500 nm may arise from the MLCT transition involving Cu(I) [63-65].

It was observed that the colour of the solution gradually changed from black to yellow after about a month at room temperature. The UV-vis spectrum of the yellow solution (**Figure 4.92(b))** shows a very weak and broad *d-d* peak at about 700 nm, indicating the presence of square pyramidal Cu(II), and a highly intense MLCT band below 500 nm, reinforcing the above suggestion for Cu(I).

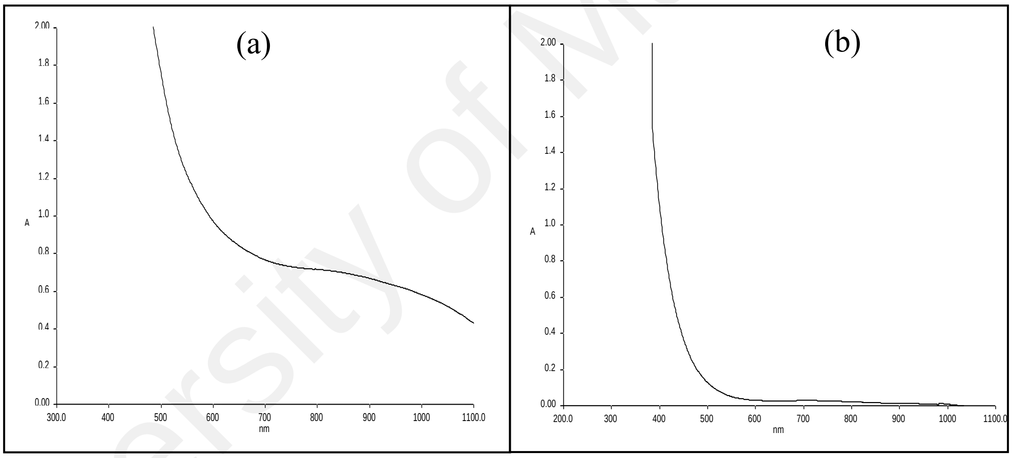

Figure 4.92: UV-visible spectrum of the black solid in acetone: (a) at initial time; (b) after one month at room temperature

The UV-vis spectroscopy was then used to "follow" the progress of the reaction. First, the spectrum of a blue solution of CuB in CH_3COCH_3 (**Figure 4.93; red)** was recorded. It shows a *d-d* band at 685 nm (ε_{max} = 54.8 M^{-1} cm^{-1}) and a shoulder at 380 nm (ε_{max} = 10.5 M^{-1} cm^{-1}), indicating a binuclear, square-pyramidal geometry at Cu(II). Immediately upon adding concentrated HCl, the spectrum of the brown reaction mixture formed (**Figure 4.93; blue**) shows the *d-d* band at a significantly red-shifted position of 875 nm (ε_{max} = 44 M^{-1} cm^{-1}), suggesting an octahedral geometry around Cu(II). The spectrum also shows a new band at 518 nm assigned to Cu(I), while the "noise" below 400 nm may be due to vibronic coupling.

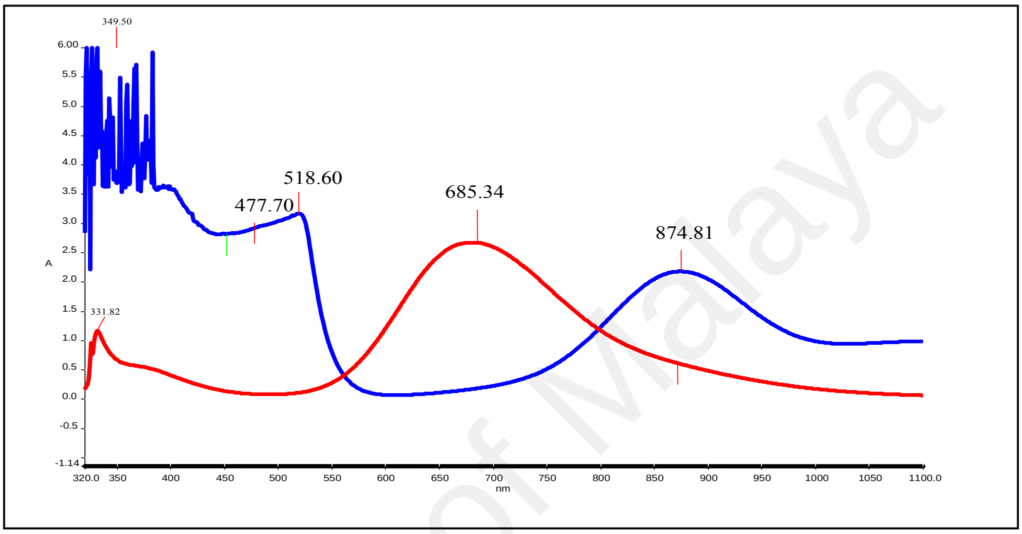

Figure 4.93: UV-vis spectra of CuB in CH_3COCH_3: before (red); and after (blue) adding HCl

It was stated above that in the presence of a strong acid, such as HCl, CuB was expected to dissociate to form $CuCl_2$ and C_6H_5COOH. However, the UV-vis spectrum of a sample of $CuCl_2$ in CH_3COCH_3 in the presence of HCl shows a broad *d-d* band at a shorter wavelength, 860 nm (ε_{max} = 46 M^{-1} cm^{-1}), and a sharp peak at 475 nm (ε_{max} = 125 M^{-1} cm^{-1}). This is a good indication that the Cu(II) complex presence in the reaction mixture involving CuB may be quite different from that involving $CuCl_2$ under similar conditions.

Then, the CuB reaction mixture was refluxed and its UV-visible spectra were recorded every two hours for six hours (**Figure 4.94)**. It is clearly seen that the intensity of the *d-d* band at 875 nm for Cu(II) gradually diminishes as the reflux time increases. At the same time, the intensity of the band at 518 nm for Cu(I) increases. This suggests reduction of Cu(II) to Cu(I) as the reaction progressed, and that after six hours, both ions were present in the reaction mixture.

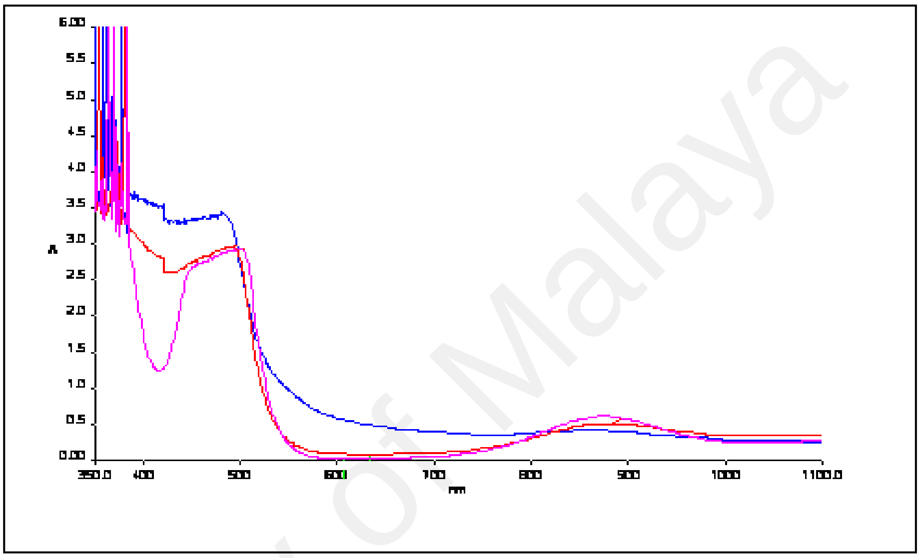

Figure 4.94 UV-vis spectra of the reaction mixture at different refluxing time: 2 hr (pink); 4 hr (red); 6 hr (blue)

From the above results, it may be inferred that the black solid is a mixed-valence [Cu(II)Cu(I)] complex, and that it loses its colour on standing in solution due to the dissociation of its ligand(s) (most likely a neutral one). It is to be noted that Type-III mixed-valence complexes, according to the Robin-Day classification, have dark colours due to an extensive electronic delocalization [66]. Thus, similar delocalisation may also be inferred for the black solid.

The ^{1}**H-NMR** spectrum of the black solid dissolved in $CDCl_3$ **(Figure 4.95)** shows four sharp peaks at 7.2, 7.4, 7.6 and 8.1 ppm for the aromatic protons of C_6H_5COO [67], and two broaden peaks centered at 1.2 and 2.2 ppm for the aliphatic protons. The integration ratio for the aromatic:aliphatic protons is 1:2.

It is known that paramagnetic complexes will be either NMR-inactive or give broad peaks. Thus, the observed sharp peaks for the aromatic protons suggest that C_6H_5COO may be closer to the diamagnetic Cu(I), while the broaden peaks suggest that the aliphatic protons are either closer to the paramagnetic Cu(II), or rotating at the same frequency as that of the NMR instrument used [68].

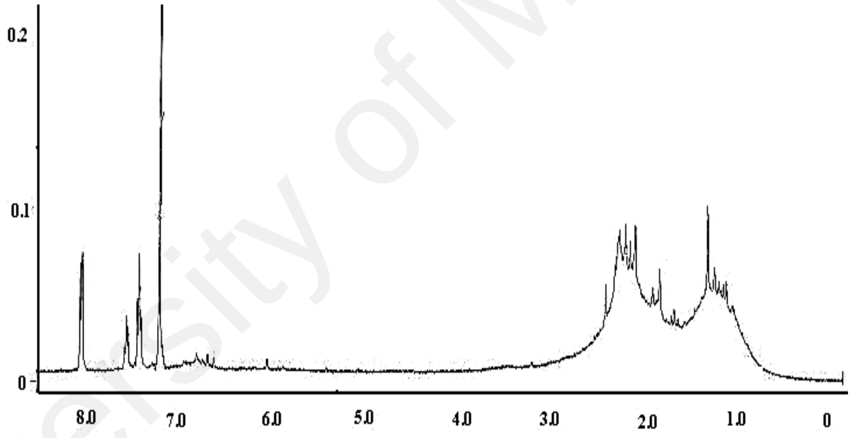

Figure 4.95: ^{1}H-NMR spectrum of the black solid

The **^{13}C-NMR** spectrum of the black solid dissolved in $CDCl_3$ (**Figure 4.96)** shows distinct peaks for the aromatic and aliphatic carbons. The peaks at 128.5 (2 CH; s), 129.2 (C; w), 130.2 (2 C; s) and 133.7 ppm (CH; w) are assigned to the aromatic carbons of C_6H_5COO [67], while a weak peak at 170.9 ppm is assigned to the carbonyl carbon (C=O). Another set of weak peaks are observed at 20.5, 21.3, 24.0, 36.0 and 48.0 ppm, as well as at 109.3 ppm. These peaks are indicative of aliphatic, sp^3- and sp^2-hybridized carbons. Therefore, the ^{13}C-NMR of the black solid supports the deductions made from FTIR and ^{1}H-NMR spectra.

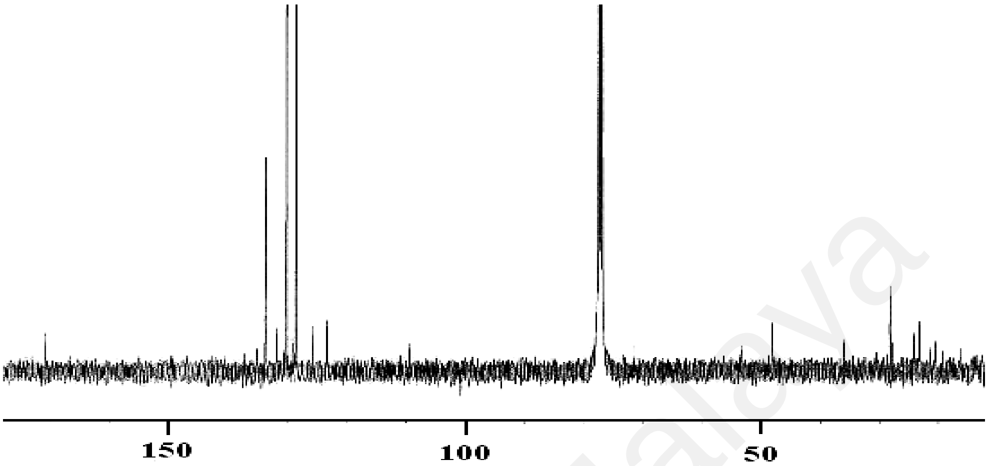

Figure 4.96: ^{13}C-NMR spectrum of the black solid dissolved in $CDCl_3$ (the sharp and strong peak at 77.0 ppm is due to the solvent)

4.6.1.2 GCMS

The GCMS spectrum of the black solid dissolved in CH_3COCH_3 (**Figure 4.97)** shows a strong peak at R_t = 8.65 min (m/z = 122) assigned to C_6H_5COOH (94.3%), followed by several weak peaks and finally a very broad peak (0.7%) at R_t above 22.4 min

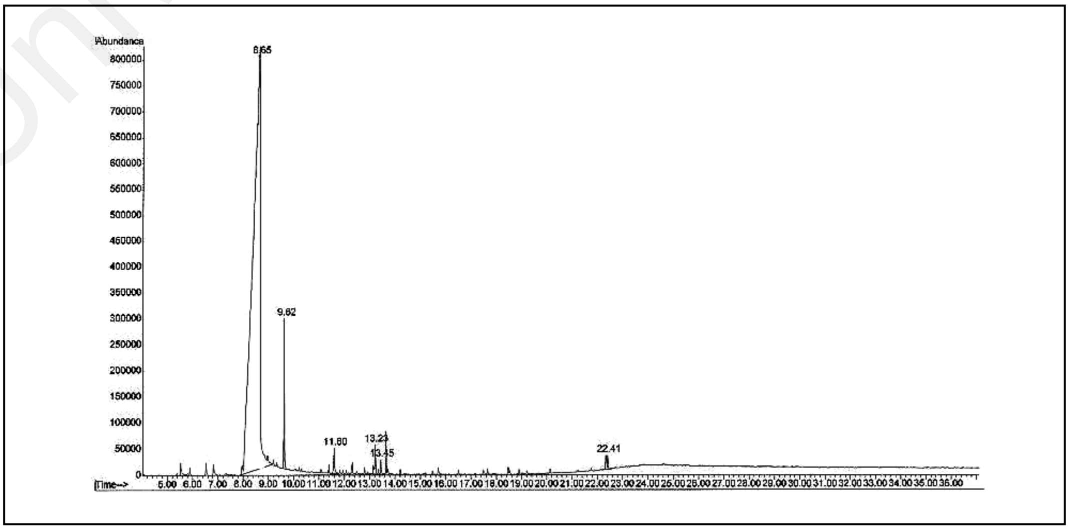

Figure 4.97: GCMS spectrum of the black solid

In order to identify the neutral components of the black solid, it was passed through a silica gel column using hexane:diethyl ether (4:1) as the eluent. A total of ten eluates were collected but only four were analysed by GCMS (**Appendix 11**). It was observed that the colour of the eluates changed from brown to pale yellow. Besides the expected peak for C_6H_5COOH (85%), the spectrum also show a new peak at $R_t = 3.7$ min (**Figure 4.98)** assigned to 4-hydroxy-4-methyl-2-pentanone, $CH_3COCH_2C(OH)(CH_3)_2$ (6.5%), and peaks with R_t greater than 10 minutes which could not be assigned with high confidence as the library database shows a very low probability.

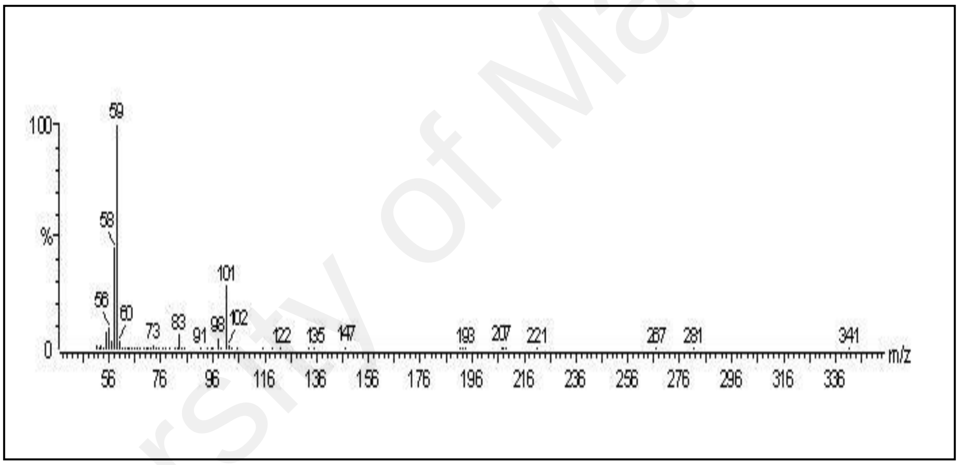

Figure 4.98: Mass spectrum of $CH_3COCH_2C(OH)(CH_3)_2$

In order to detect other minor components in the black solid, C_6H_5COOH was removed by heating it in an aqueous solution of $NaHCO_3$, followed by diethyl ether extraction. The dark brown solid obtained was then passed through a silica gel column as before. A total of six eluates (pale yellow solids) were analysed by GCMS (**Appendix 12**). The results show two significant peaks at $R_t = 3.3$ min and 3.7 min, and based on their mass spectra (**Figure 4.99**), are assigned to 4-methyl-3-penten-2-one, $CH_3COCH=C(CH_3)_2$ and 4-hydroxy-4-methyl-2-pentanone, $CH_3COCH_2C(OH)(CH_3)_2$, respectively.

It is to be noted that $CH_3COCH_2C(OH)(CH_3)_2$ is a product of the C-C bond-forming reaction of two CH_3COCH_3 molecules, while $CH_3COCH{=}C(CH_3)_2$ is a conjugated enone formed from the dehydration of $CH_3COCH_2C(OH)(CH_3)_2$ [69]. It is a fact that the dehydrated aldol product is usually formed, especially at high temperatures [70].

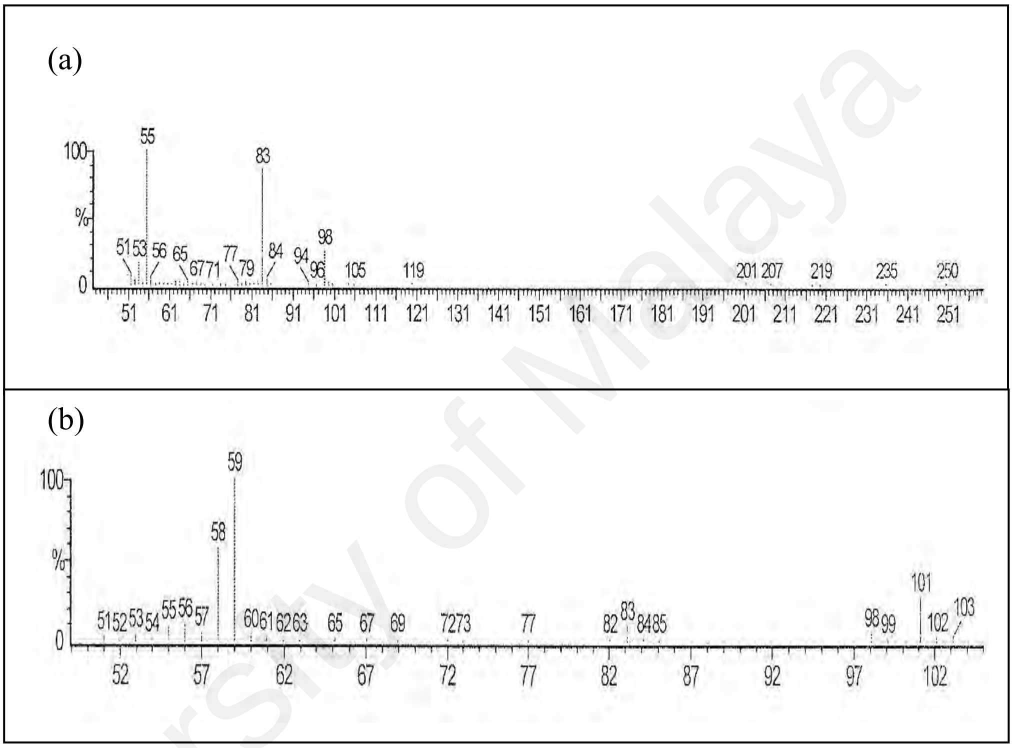

Figure 4.99: Mass spectra for peaks at R_t (min): (a) 3.3; and (b) 3.7

4.6.1.3 TGA and DSC

The **TGA** thermogram (**Figure 4.100**) shows that the black solid is thermally stable up to 126°C. Thus, it is significantly less thermally stable than CuB (T_{dec} = 254°C). However, this is to be expected for a complex involving neutral organic ligand(s).

The thermogram also shows an initial slow weight loss of 4.4% at 50°C, assigned to the evaporation of non-coordinated CH_3COCH_3 (expected, 4.6%).

This was followed by a more rapid weight loss of 83.8% from 126°C to 250°C, assigned to the loss of $CH_3COCH_2C(OH)(CH_3)_2$, C_6H_5COOH (boiling point 249°C) and C_6H_5COO ligand as CO_2 and other organic volatiles [71] (expected, 82.7%).

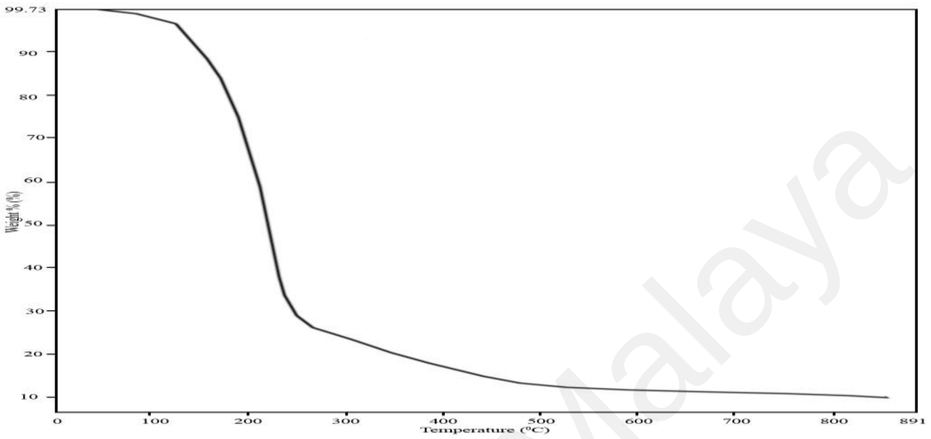

Figure 4.100: TGA of the black solid

The amount of residue formed at temperatures above 500°C is 11.8%. Thus, this is a conclusive evidence for the presence of Cu(I) and/or Cu(II) in the black solid. If the black solid is a [Cu(II)Cu(I)] mixed-valence complex, the residue may be a mixture of CuO and Cu_2O. Using the gravimetric concept, the formula mass of the black solid is estimated to be 1279 g mol^{-1} (**Appendix 13**).

At this stage, the chemical formula that may be suggested for the black solid is $[Cu(II)Cu(I)(R)_3(RH)_2(CH_3COCH_2C(OH)(CH_3)_2)_4].CH_3COCH_3$, where R is C_6H_5COO (formula mass, 1256 g mol^{-1}). The suggested chemical formula agrees quite well with ^1H-NMR (aliphatic:aromatic ratio = 2:1), and with TGA (4.6% CH_3COCH_3, 82.1% $CH_3COCH_2C(OH)(CH_3)_2$, $C_6H_5COO^-$

and C_6H_5COOH). The proposed reaction for the formation of $CH_3COCH_2C(OH)(CH_3)_2$ (circled) is shown in **Scheme 4.2** (for clarity, the paddle-wheel structure of CuB shows only one C_6H_5COO ligand).

Step 1: *Axial ligation by acetone, one-electron reduction of Cu(II), breaking of Cu-$OOCC_6H_5$ equatorial bond, and formation of an enone*

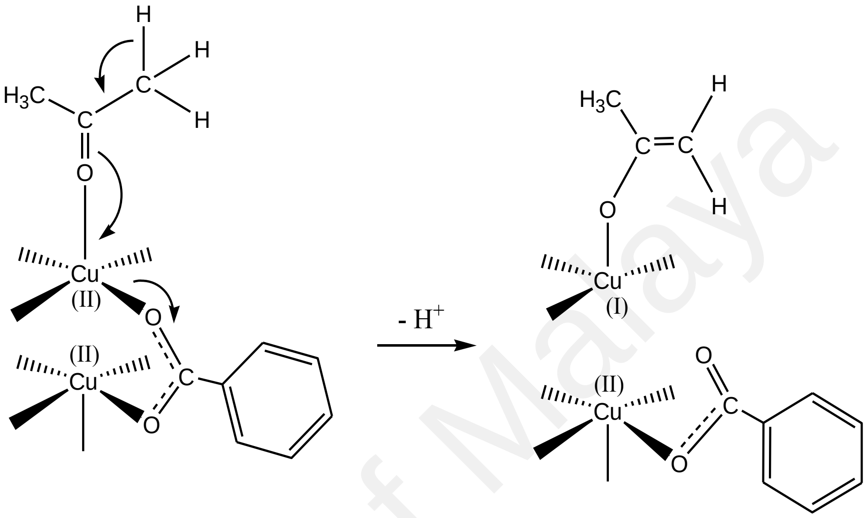

Step 2: *Protonation of acetone to form a carbocation (an enophile)*

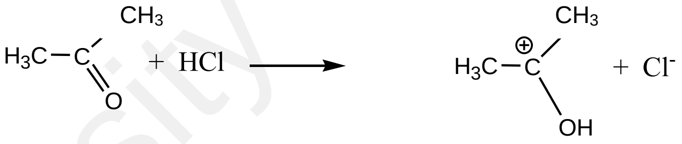

Step 3 *The C-C bond-forming reaction between the enone and the enophile*

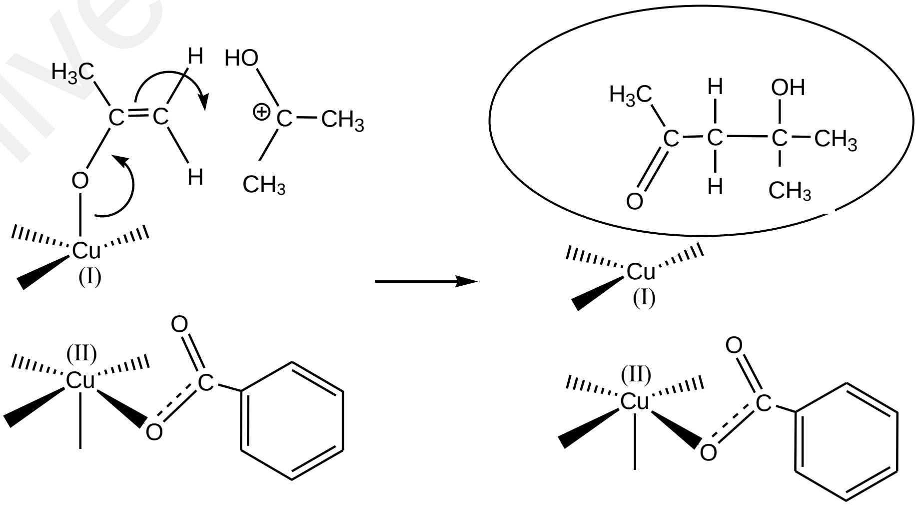

Scheme 4.2: The formation of $CH_3COCH_2C(OH)(CH_3)_2$ from the reaction of CuB with CH_3COCH_3 in the presence of HCl

The **DSC** scan of the black solid (**Figure 4.101)** shows a broad endotherm at onset temperature 50°C, and two overlapping endotherms at 112°C and 115°C ($\Delta H_{combined}$ = 297.4 kJ mol^{-1}). These endotherms occur at lower temperatures than its decomposition temperature (126°C).

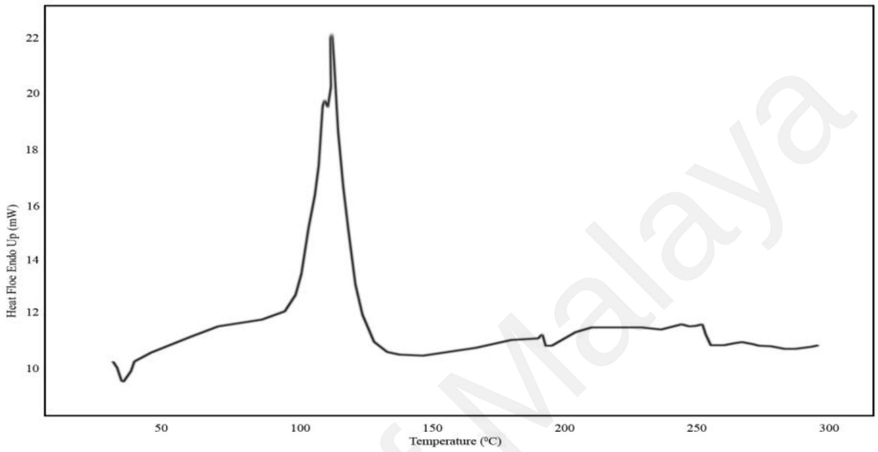

Figure 4.101: DSC of the black solid

By referring to its proposed chemical formula, the first endotherm is assigned to the evaporation of non-coordinated CH_3COCH_3 ($T_{boiling}$ = 56°C), while the overlapping endotherms are assigned to the concurrent melting of the black solid and the "freed" C_6H_5COOH ($T_{melting}$ = 122°C). The high enthalpy changes for these processes indicate the presence of strong bond(s), which are consistent with the coordinated $CH_3COCH_2C(OH)(CH_3)_2$, possibly also intra- and inter- molecularly H-bonded to the other ligands (C_6H_5COOH and C_6H_5COO), and strong H-bonds between C_6H_5COOH molecules.

The unexpectedly low melting point for a copper complex is rather interesting as generally copper(II) complexes have high melting points (above 200°C; decomposed) [72]. Such a low melting point could be due to the low molecular symmetry of the overall structure of the black solid as well as the presence of highly-branched alkyl chains [73-75]. This is again in tandem with the proposed chemical formula.

4.6.1.4 Magnetic susceptibility

The μ_{eff} value of the black solid at room temperature (298 K) is 1.33 B.M. The value is calculated from χ_g (0.08 x 10^{-6} cm^3 g^{-1}), χ_d (7.09 x 10^{-4} cm^3 mol^{-1}) and χ_m^{corr} (8.10 x 10^{-4} cm^3 mol^{-1}), and the estimated value for -2J is 556 cm^{-1}. These magnetic data indicate a very strong antiferromagnetic interaction between the two copper centres, which further supports the proposed extensive electron delocalization in a mixed-valence [Cu(II)Cu(I)] complex.

4.6.1.5 Cyclic voltammetry

The proposed mixed-valence [Cu(II)Cu(I)] complex for the black solid is strongly supported by cyclic voltammetry, recorded anodically in THF from 0 V, within the potential window of +1.0 V to -1.5 V, and at the scan rate of 100 mV s^{-1}. The CV (**Figure 4.102)** shows one anodic peak at +0.70 V, and on reversing the scan at +1.0 V, two cathodic peaks at +0.53 V and -0.90 V.

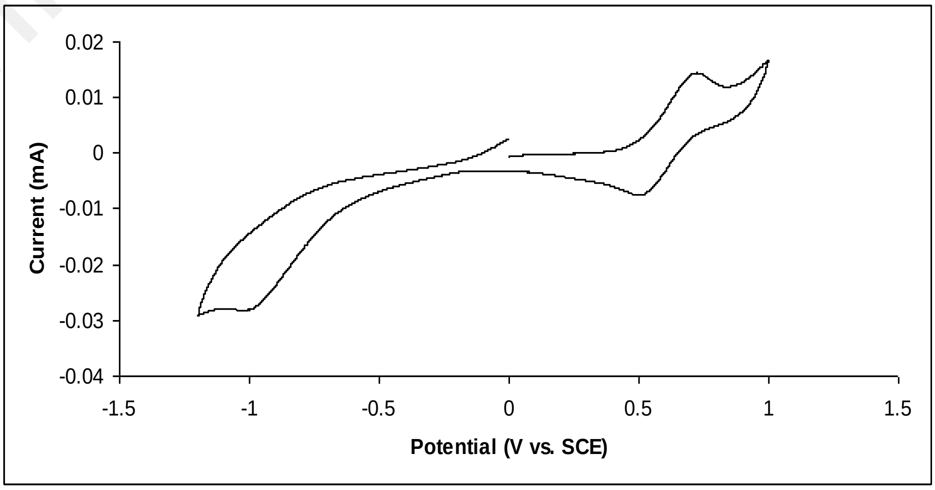

Figure 4.102: CV of the black solid

The anodic peak at +0.70 V is assigned to the oxidation of [Cu(II)Cu(I)] to [Cu(II)Cu(II)], which was then reduced to [Cu(II)Cu(I)] at +0.53 V. The value of ΔE is 170 mV, indicating a quasireversible redox reaction due to slight structural reorganisation. The I_{pc}/I_{pa} value for this process is 0.78, indicating that the "newly" formed [Cu(II)Cu(I)] mixed-valence complex was chemically unstable. The mixed-valence complex was then irreversibly reduced at -0.9 V to [Cu(I)Cu(I)]. The redox processes are summarized below.

$$\text{[Cu(I)Cu(I)]} \xrightleftharpoons{-0.9\text{V}} \text{Cu(II)Cu(I)]} \xrightleftharpoons[+0.53\text{V}]{+0.70\text{V}} \text{[Cu(II)Cu(II)]}$$

The CV results were then used to calculate the energy band gap, which would further facilitate the conclusion on the presence of highly delocalized electron in the mixed-valence complex. The oxidation process corresponds to removal of electron from the HOMO energy levels, whereas the reduction cycle corresponds to addition of electron to the LUMO level [76,77]. Importantly, if the oxidation/reduction processes can be measured using the same electrolyte/solvent system, then the difference between the two onset potentials should match the optical bandgap. This value can be directly compared with the existing bandgap value of other materials and will give valuable information on future application of the solid.

From the voltammogram (**Figure 4.102**), the onset potential of reduction and oxidation processes are -0.682 V and 0.493 V respectively. Adding 4.4 V to each of the potentials, the LUMO and HOMO energy levels, E_{LUMO} and E_{HOMO}, is 3.718 eV and 4.893 eV [78]. The difference between these two energy levels is the band gap energy, which is 1.2 eV. The value is very small, indicating that the LUMO and HOMO of the complex is close to each other, and thus allowing for an extensive electronic delocalization. The value is also comparable to the reported semiconductors (the bandgap energy around 1.0 eV) [79-81]. Hence, such a low band gap could suggest that the solid is a potential photovoltaic cell material.

To summarise, CuB reacted with CH_3COCH_3 in the presence of HCl to form a black solid, proposed to be a mixed-valence complex with the chemical formula $[Cu(II)Cu(I)(R)_3(RH)_2(CH_3COCH_2C(OH)(CH_3)_2)_4].CH_3COCH_3$ ($R = C_6H_5COO$). The complex has a low melting point (112^{o}C), is magnetic with a strong antiferromagnetic interaction between the two Cu centres, and has low bandgap energy of 1.2 eV.

A paper on the spectroscopic, magnetic, thermal and cyclic voltammetric studies of the black solid, entitled "*Mixed-Valence Low Bandgap Photovoltaic Material:* $[Cu(II)Cu(I)(R)_3(RH)_2L_4].CH_3COCH_3$ *(*$R = C_6H_5COO$*;* $L = CH_3COCH_2C(OH)(CH_3)_2$*)*" has been accepted for publication in the Journal of Advanced Materials Research (Manuscript Number E2763). **Appendix 14**).

4.6.1.6 Kinetics study

Kinetics study on the reaction between CuB and CH_3COCH_3 in the presence of HCl was undertaken in order to deduce its mechanism and the feasibility of the reaction. The UV-vis spectroscopy offers a fast and facile technique in this case. It involves measuring the absorbance at a selected wavelength of the reaction mixture at different time and temperature, and then determining the rate constant and activation energy of the reaction. In this study, the *d-d* band at 877 nm for Cu(II) ion was chosen as its integrity is unquestionable.

In the study, the spectrum of the brown reaction mixture at 30, 40, 50, and 57°C (the boiling point of acetone) were recorded at time interval of 30 minutes for two hours. **Figure 4.103(a)** shows the spectrum at 50°C, while **Figure 4.103(b)** shows the close-up view at the chosen wavelength at that temperature. It clearly shows the decrease of the absorbance at 877 nm as the reaction time increases, signifying involvement of Cu(II) in the reaction. Similar spectra were obtained for the reactions at other temperatures.

From the spectra, graphs of absorbance versus time at different temperature were plotted (**Figure 4.104),** and the value of A_o, which was the absorbance at $t = 0$ s, was determined.

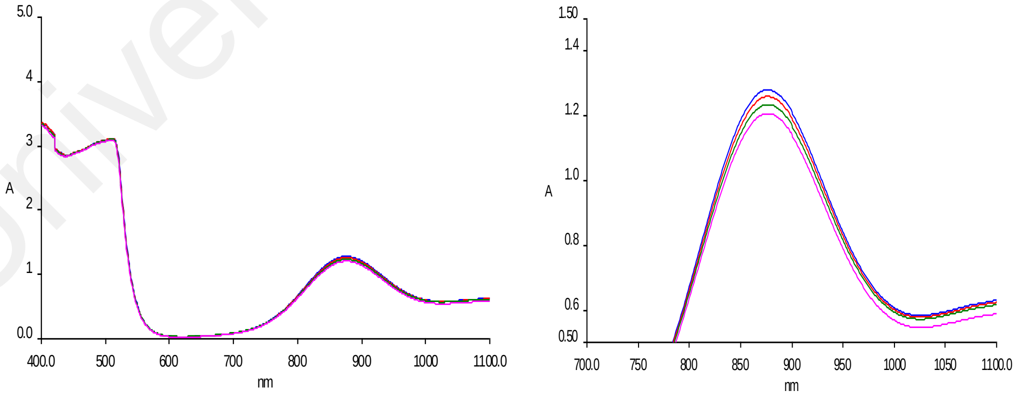

(a) (b)

Figure 4.103: UV-vis spectra of the reaction mixture at 50°C recorded every 30 minutes for 2 hours

The rate constant (k) at each temperature was determined from the slope of the graph of ln[A_t/A_o] versus *t* (**Figure 4.105**). The results are shown in **Table 4.30.**

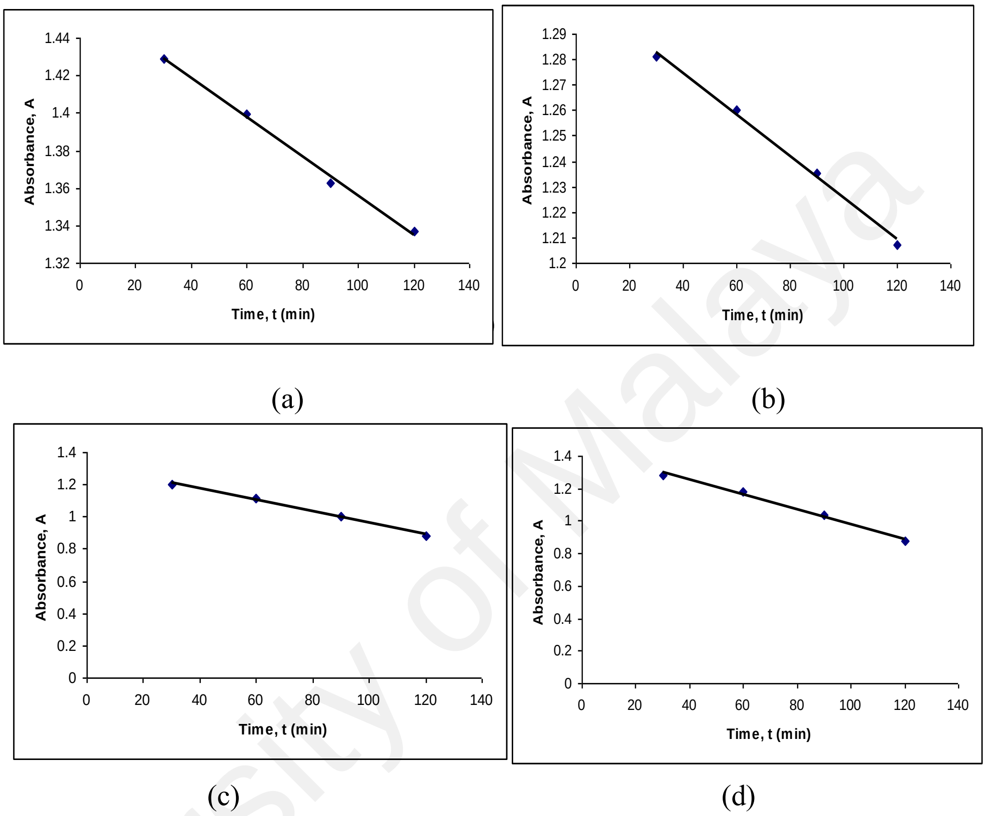

Figure 4.104: Graphs of absorbance versus time at different temperature (λ_{max} = 877 nm): (a) 30 ^oC; (b) 40 ^oC ; (c) 50 ^oC and (d) 57 ^oC

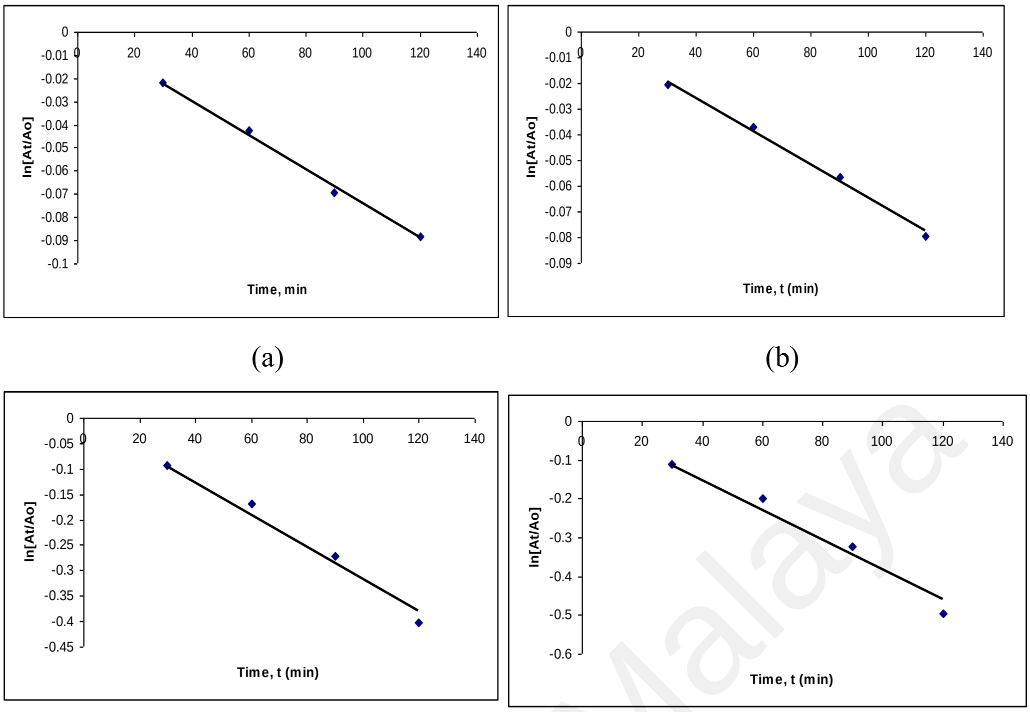

(a) (b)

(c) (d)

Figure 4.105: Graphs of ln[A_t/A_o] versus *t* at different temperature (λ_{max} = at 877 nm): (a) 30°C; (b) 40°C; (c) 50°C; and (d) 57 °C

Table 4.30: The rate constant at different temperature

Temperature (°C)	Rate constant, k (10^{-4} min^{-1})
30	7
40	8
50	32
57	38

The activation energy (E_a) for the reaction, calculated from the Arrhenius plot of ln k versus T^{-1} (**Figure 4.106**), is 63 kJ/mol.

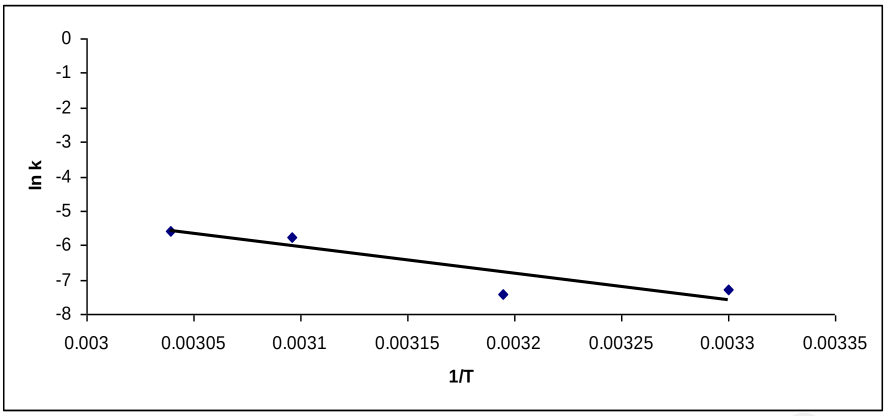

Figure 4.106: The Arrhenius plot

Kustrowski et al. [82] obtained the activation energies of 36 kJ/mol and 57 kJ/mol for the aldol reaction of acetone in the presence of a base catalyst, $Ba(OH)_2$ or $Sr(OH)_2$, respectively. Thus, these values are indeed comparable with the value obtained in this study. From this, it may be suggested that there is a direct relationship between the rate of disappearance of Cu(II) and the rate of formation of the aldol product.

4.6.2 Reaction of CuB with acetophenone and benzaldehyde

The C-C bond-forming reaction between CuB and CH_3COCH_3 was then extended to other carbonyls in order to study the scope of the reaction. As a preliminary work, the carbonyls chosen were acetophenone ($C_6H_5COCH_3$) and benzaldehyde (C_6H_5CHO). These carbonyls were chosen as it is known that they reacted to form $C_6H_5COCH{=}CHC_6H_5$ (the crossed-aldol condensation product) and $C_6H_5COCH{=}C(CH_3)C_6H_5$ (the self-condensation product of $C_6H_5COCH_3$). For example, in the presence of NaOH at 15-30^oC, the yield of $C_6H_5COCH{=}CHC_6H_5$ was 85% [83].

The reaction between CuB and a mixture of $C_6H_5COCH_3$ and C_6H_5CHO in the presence of concentrated HCl was carried out in the same manner as for CH_3COCH_3 (**Section 4.7.1)**. The expected products from the reaction were C_6H_5COOH, $C_6H_5COCH{=}CHC_6H_5$ and $C_6H_5COCH{=}C(CH_3)C_6H_5$. The initial product obtained was a blackish orange liquid (4.0 g) with distinctive smell of $C_6H_5COCH_3$. The liquid gave a pale yellow crystal after being subjected to column chromatography.

The **FTIR** spectrum of the blackish orange liquid (**Figure 4.107**) shows a broad peak at 3500 cm^{-1} for -OH, two sharp and medium peaks at 3060 and 3028 cm^{-1} tentatively assigned to vinylic and aromatic hydrogens, a very strong absorption peak at 1684 cm^{-1} for C=O, and two very strong peaks at 1598 and 1494 cm^{-1} for aromatic C=C. It is noted that the spectrum has common peaks with that of the black solid obtained from the reaction involving CH_3COCH_3 (**Figure 4.91**).

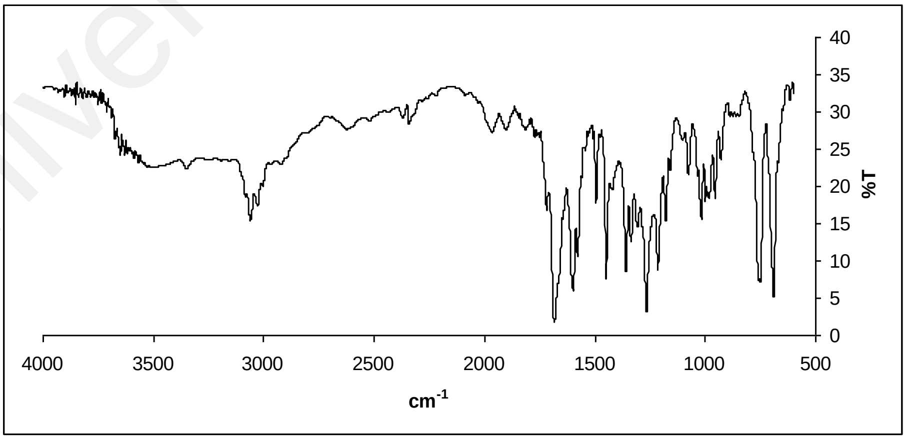

Figure 4.107: FTIR spectrum of the blackish orange liquid

The **^{1}H-NMR** spectrum of the blackish orange liquid dissolved in $CDCl_3$ (**Figure 4.108)** shows unresolved multiplets in the region of 7 - 8 ppm for the aromatic and –CH=C protons, and distinct peaks in the region of 1 - 4 ppm for the aliphatic protons. It is interesting to note that the –COOH peak for C_6H_5COOH, expected at about 12 ppm, is not observed, and that the aliphatic hydrogen peaks are not broad as was shown for the product obtained from the reaction involving CH_3COCH_3 (**Figure 4.95**).

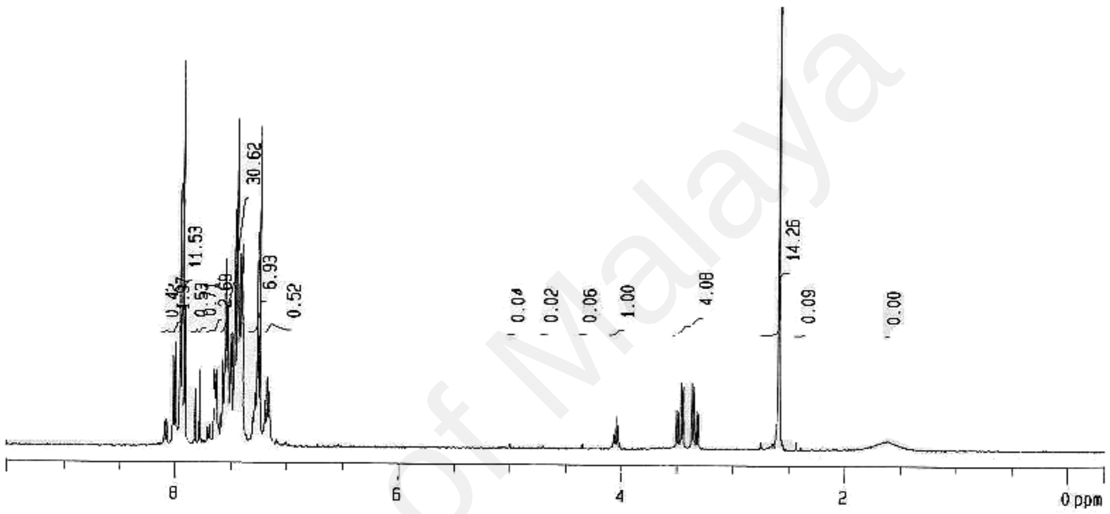

Figure 4.108: ^{1}H-NMR spectrum of the blackish orange liquid

In the above ^{1}H-NMR spectrum, the strong singlet at 2.5 ppm (integral, 14.26) is assigned for CH_3, most likely from the unreacted $C_6H_5COCH_3$ and one of the expected products, $C_6H_5COCH=C(CH_3)C_6H_5$. The two doublets at 3.5 ppm are assigned to -CH=CH- of $C_6H_5COCH=CHC_6H_5$. From the integral of this doublets (4.08), it is estimated that there was about 33% of $C_6H_5COCH=CHC_6H_5$ in the blackish orange liquid (**Appendix 15)**, which translates into the yield of the product as 1.35 g (23.4 %).

The **GCMS** of the blackish orange liquid (**Figure 4.109)** shows well separated strong peaks at R_t = 6.34 min (37.2%), 14.25 min (31.2%) and

18.96min (23.3%), a weak peak at 14.28 min (5.3%) and a broader peak at 25.49 min (2.8%).

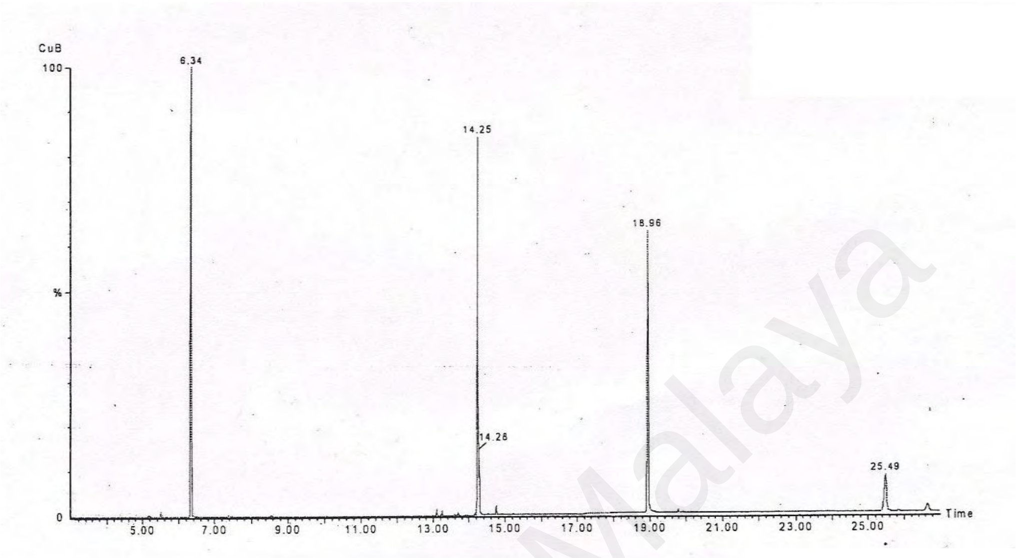

Figure 4.109: GC of the blackish orange liquid

These peaks were assigned (**Table 4.31)** based on their mass spectra (**Appendix 16**).

It is noted that, apart from the unreacted $C_6H_5COCH_3$ (37.2%), the two expected C-C bond-forming products, $C_6H_5COCH{=}CHC_6H_5$ and $C_6H_5COCH{=}C(CH_3)C_6H_5$, were obtained in good yields (combined 36.5%). The much higher yield for the cross-aldol condensation product is conceptually correct as C_6H_5CHO (an aldehyde) is more reactive than $C_6H_5COCH_3$ (a ketone). It is also noted that the peak expected for C_6H_5COOH at 8.66 minute is not observed in the spectrum. However, the unexpected product was 1,3,5-triphenyl-1,5-pentanedione (23.3%), postulated to form from the condensation of two $C_6H_5COCH_3$ with one C_6H_5CHO molecules. At the moment, there is not enough evidence to postulate how this product may be formed. The peak at 25.49 minute cannot be assigned confidently as the library search gave a very low percentage probability (< 50%).

Table 4.31: GCMS data and assignments for the blackish orange liquid

R_t (min)	Structural formula	%
6.34	$C_6H_5COCH_3$	37.2
14.25	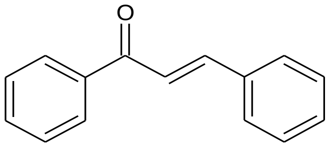 1,3-diphenyl-2-propen-1-one	36.5
14.28	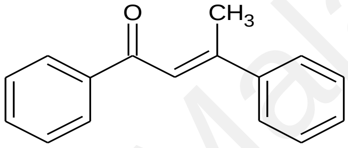 1,3-diphenyl-2-buten-1-one	
18.96	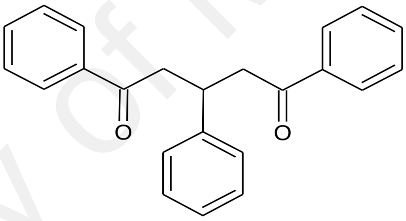 1,3,5-triphenyl-1,5-pentanedione	23.3

4.6.2.1 Analysis of the pale yellow crystal

The products present in the blackish orange liquid were isolated by column chromatography (silica gel column; eluate, diethyl ether-hexane 1:4). The pale yellow solution eluated from the column formed a pale yellow crystal (yield, 15%) upon slow evaporation of the solvents at room temperature. Its melting point was 57-58°C. The GC of the crystal (**Figure 4.110)** shows only one peak at R_t of 14.10 min, indicating a highly pure crystal.

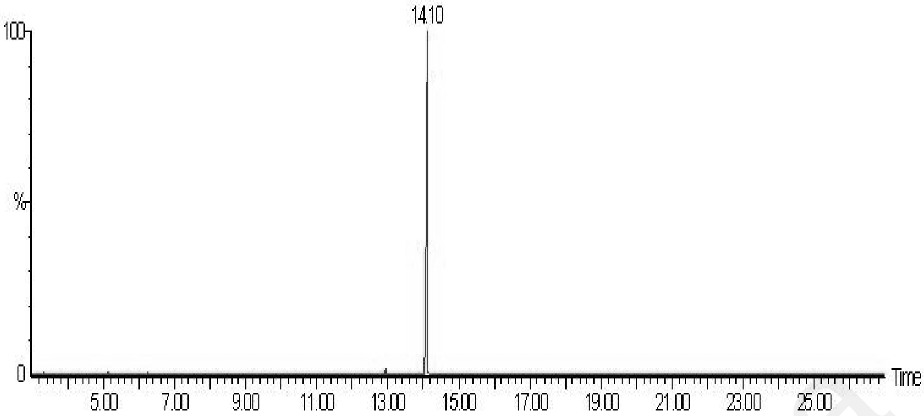

Figure 4.110: GC of the pale yellow crystal

From the melting point and mass spectrum (**Figure 4.111),** the crystal is identified as $C_6H_5COCH{=}CHC_6H_5$. Hence, this confirms the C-C bond-forming reaction between $C_6H_5COCH_3$ and C_6H_5CHO.

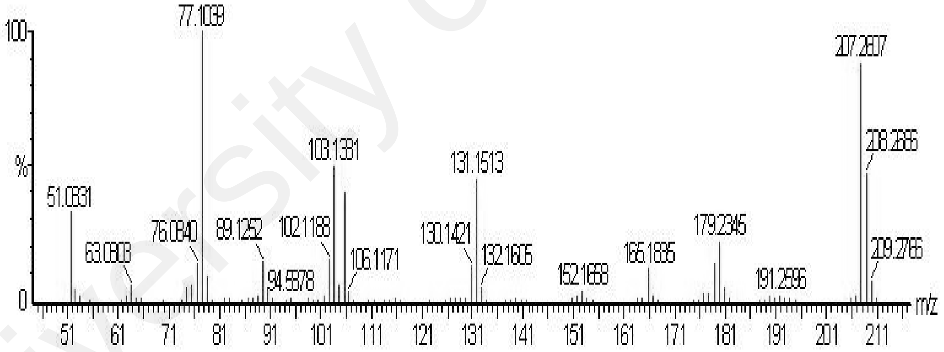

Figure 4.111: Mass spectrum of the pale yellow crystal

It is important to note that only the dehydrated form of the product was isolated. The findings is again consistent with the work of Kutsrowski et al., which found that the dehydrated form was the dominant species when the reaction takes place at higher temperatures [84].

4.6.2.2 Controlled experiments

In order to probe the role of HCl and CuB in the reaction, two controlled experiments were done, firstly by omitting HCl, and then by omitting CuB, from the reaction mixture.

In the absence of HCl, CuB was refluxed with a mixture of $C_6H_5COCH_3$ and C_6H_5CHO for eight hours and then left to cool to room temperature for 7 days. It is reminded that the chemical formula of CuB in this work was $[Cu_2(C_6H_5COO)_4(CH_3CH_2OH)_2]$ (**Section 4.2**). However, small blue block crystals with the chemical formula $[Cu_2(C_6H_5COO)_4(C_6H_5COOH)_2]$ (**Figure 4.112**) was obtained from the reaction mixture. The X-ray crystallographic data as well as selected bond lengths and angles are given in **Appendix 17** and **18**.

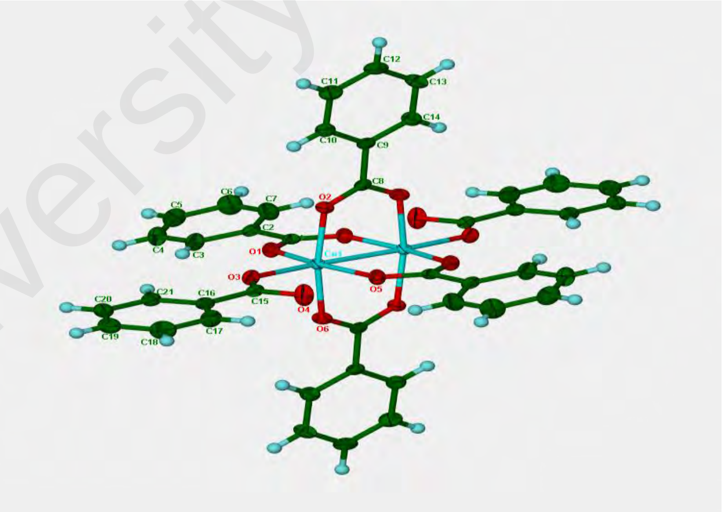

Figure 4.112: An ORTEP drawing of $[Cu_2(C_6H_5COO)_4(C_6H_5COOH)_2]$, showing the paddle-wheel structure with C_6H_5COOH molecules at the axial positions

The crystal structure of $[Cu_2(C_6H_5COO)_4(C_6H_5COOH)_2]$ obtained is similar with the published results [23]. The structure shows a centrosymmetric dinuclear units, with four bidentate C_6H_5COO ligands forming *syn-syn* bridges between the two Cu(II) centres separated by about 2.6067 Å. At each Cu(II) are four bridging C_6H_5COO ligands at the basal plane, and an C_6H_5COOH at the axial position. The axial ligand bond is almost perpendicular to the basal plane. Thus, the coordination geometry about the Cu atom is square pyramidal (neglecting the Cu-Cu interaction and considering only the five bonded oxygen atoms as the Cu-Cu distant is longer than the 2.56 Å, the interatomic distance in metallic copper [57]).

As the crystal structure shows the presence of C_6H_5COOH, it is suggested that this acid was formed from the oxidation of C_6H_5CHO either by air and/or $[Cu_2(C_6H_5COO)_4(CH_3CH_2OH)_2]$. This is expected to happen as aldehydes are easily oxidized by weak oxidizing agents.

In the second controlled experiment, a mixture of $C_6H_5COCH_3$, C_6H_5CHO and HCl was refluxed for eight hours in the absence of CuB, and then left to cool to room temperature. The product was an orange brown liquid as the top layer and a colourless liquid as the bottom layer. The mixture was then separated by ether extraction to afford a yellow brown solution, which was further separated by column chromatography as before. The product was a yellow powder in low yield (7.1%), and its melting point was 56 – 58°C. The GC of the yellow powder (**Figure 4.113)** shows a broaden peak at R_t = 19.5 min, and another peak at R_t = 26.6 min (not shown in the chromatogram; refer to **Appendix 19**).

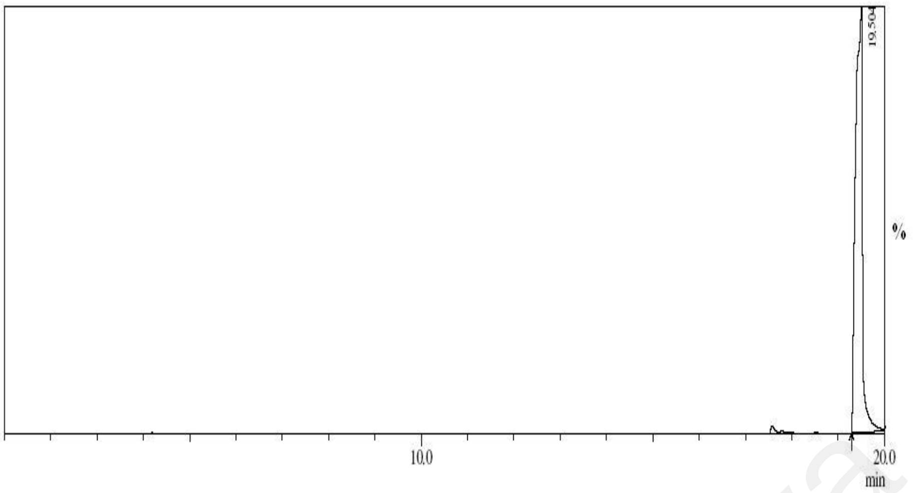

Figure 4.113: GC of the yellow powder

From the mass spectrum (**Figure 4.114**), the peak at R_t = 19.6 min is identified as $C_6H_5COCH{=}CHC_6H_5$, the expected crossed aldol condensation product of $C_6H_5COCH_3$ with C_6H_5CHO. However, another peak at R_t = 26.6 min (**Figure 4.115**) is identified as 1,3,5-triphenyl-1,5-pentanedione (4%). Hence, in the absence of CuB, the C-C bond-forming products were formed, but in much lower yields.

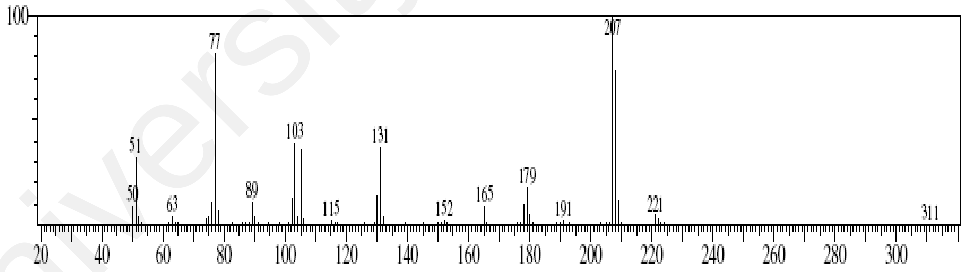

Figure 4.114: Mass spectrum of the yellow powder at R_t = 19.6 min

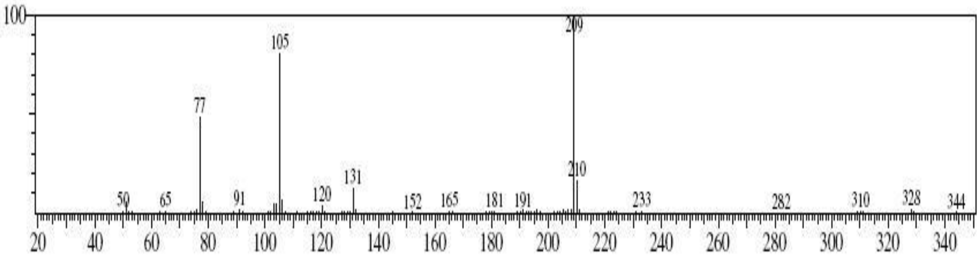

Figure 4.115: Mass spectrum of the yellow powder at R_t = 26.6 min

It is important to note that the retention times for the products are different in the controlled experiment compared to those obtained in the presence of CuB. This is because different GCMS instruments were used in both analyses (**Chapter 3**).

To summarise, CuB acted as a template for the C-C bond-formation reaction of $C_6H_5COCH_3$ with C_6H_5CHO. It is postulated that initially, $C_6H_5COCH_3$ molecules, through its -C=O group, were axially coordinated to CuB. As a result, the Cu-$OOCC_6H_5$ equatorial bonds were weaken and/or broken, allowing for ligation of Cl^- (from HCl) and a geometrical change at Cu(II) to less planar or more tetrahedral. Such geometrical change facilitated reduction of Cu(II) to Cu (I), and oxidation of $C_6H_5COCH_3$ to an enone. Additionally, the H^+ ion in the solution protonated the carbonyls ($C_6H_5COCH_3$ and C_6H_5CHO) to enophilic intermediates, which then reacted with the enone, forming the aldol products.

The proposed reaction for the formation of 1,3-diphenyl-2-propen-1-one (the crossed-aldol product shown inside a circle) is shown in **Scheme 4.3** (for clarity, the paddle-wheel structure of CuB shows only one C_6H_5COO ligand).

Step 1: *Axial ligation by acetophenone, one-electron reduction of Cu(II), breaking of Cu-OOCC$_6$H$_5$ equatorial bond, and formation of an enone*

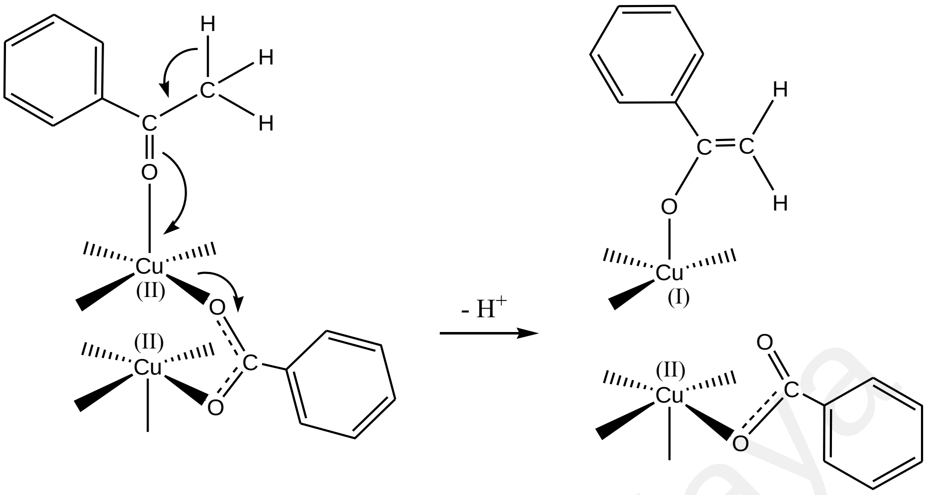

Step 2: *Protonation of benzaldehyde to form a carbocation (an enophile)*

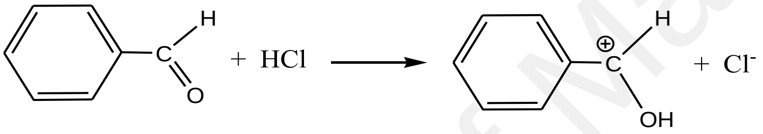

Step 3 *The C-C bond-forming reaction between the enone and the enophile*

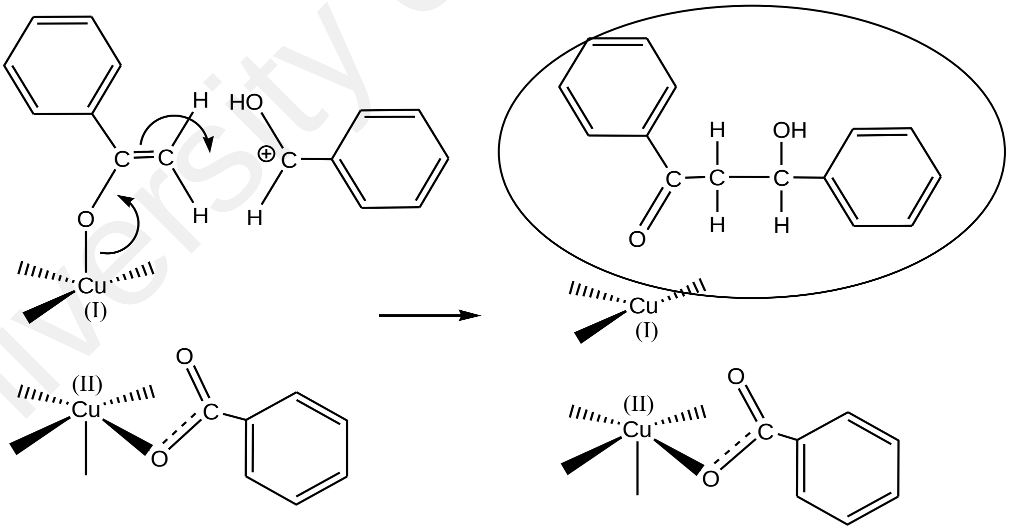

Step 4 *Dehydration of the crossed-aldol product*

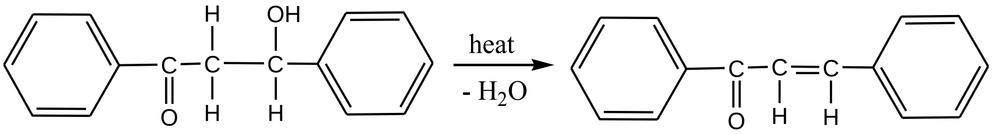

Scheme 4.3: The formation of $C_6H_5COCH_2CH(OH)C_6H_5$ from the reaction of CuB with a mixture of $C_6H_5COCH_3$ and C_6H_5CHO in the presence of HCl

4.6.3 Reaction of [$Cu_2(4\text{-}XC_6H_4COO)_4$] (X = NO_2, OH, Cl) with acetone

It is important to know if the reaction of [$Cu_2(4\text{-}XC_6H_4COO)_4$] with carbonyls may be tuned by the different electronic effect of X. Keeping this in mind, the reaction was extended to copper(II) arylcarboxylates substituted with 4-NO_2, 4-OH, and 4-Cl. Recall that for this reaction, the proposed mechanism involved coordination of CH_3COCH_3 at the "free" axial position of the complex, and reduction of [Cu(II)Cu(II)] to [Cu(II)Cu(I)].

4.6.3.1 Reaction of [$Cu_2(4\text{-}NO_2C_6H_4COO)_4$] with acetone

The rate of reaction for a complex with a strongly electron-withdrawing substituent, such as the NO_2 group, is expected to be faster (and therefore higher yield) for two main reasons: (a) the increased charge on Cu(II) centers should allow for the formation of a stronger coordinate bond (more stable intermediate complex); and (b) the [Cu(II)Cu(II)] will be easier to be reduced. This is actually supported by the CV result, which showed that [Cu(II)Cu(II)] from $CuNO_2B$ was reduced at a less negative potential (-0.09 V) compared to that of CuB (-0.13 V).

Accordingly, it was discovered that under similar experimental conditions as for CuB, $CuNO_2B$ reacted with CH_3COCH_3 to give a dark brown solid, and the yield was 77% (w/w based on $CuNO_2B$), which is expectedly higher compared to CuB (63% w/w based on CuB).

The results of the **C,H elemental analysis** of the dark brown solid were 55.7% C, 6.2% H and 2.8% N. These indicate the presence of organic compound(s) in the solid other than 4-$NO_2C_6H_4COOH$ (expected, 50.3% C, 3.0% H and 8.3% N).

The **FTIR** spectrum of the dark brown solid (**Figure 4.116**) is different compared to the black solid obtained from CuB (**Figure 4.91**). The spectrum is much simpler and the peaks were broad, indicating more symmetrical structure with more extensive electron delocalization. The broad and strong peak at about 3400 cm^{-1} indicates H-bonded –OH group, the split peaks at about 2900 cm^{-1} suggest the presence of C-H stretching bands of an alkyl group from the C-C bond-forming reaction, and two very strong absorption peaks at 1647 cm^{-1} and 1376 cm^{-1}, are assigned to C=O and -NO_2 respectively.

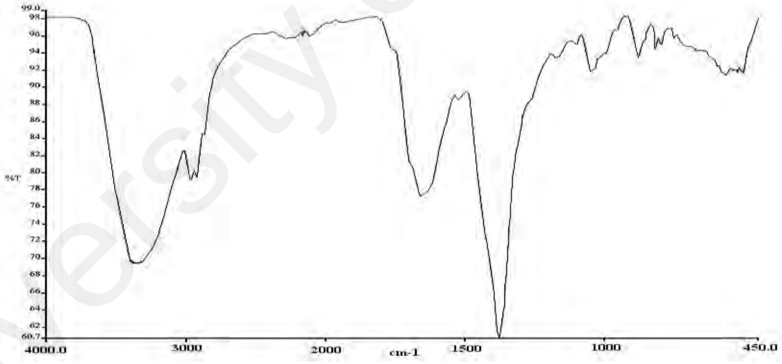

Figure 4.116: FTIR spectrum of the dark brown solid obtained from the reaction of $CuNO_2B$ with acetone

The **UV-vis** spectra of the dark brown solid, dissolved in acetone, were recorded after several time intervals (**Figure 4.117**). The spectra are similar with those of the black solid from CuB. At initial time, the spectrum shows a band at around 470 nm assigned as the MLCT transition involving Cu(I). This band slowly disappeared, and then a new band was observed at around 700 nm after 14 days, indicating the presence of square pyramidal Cu(II).

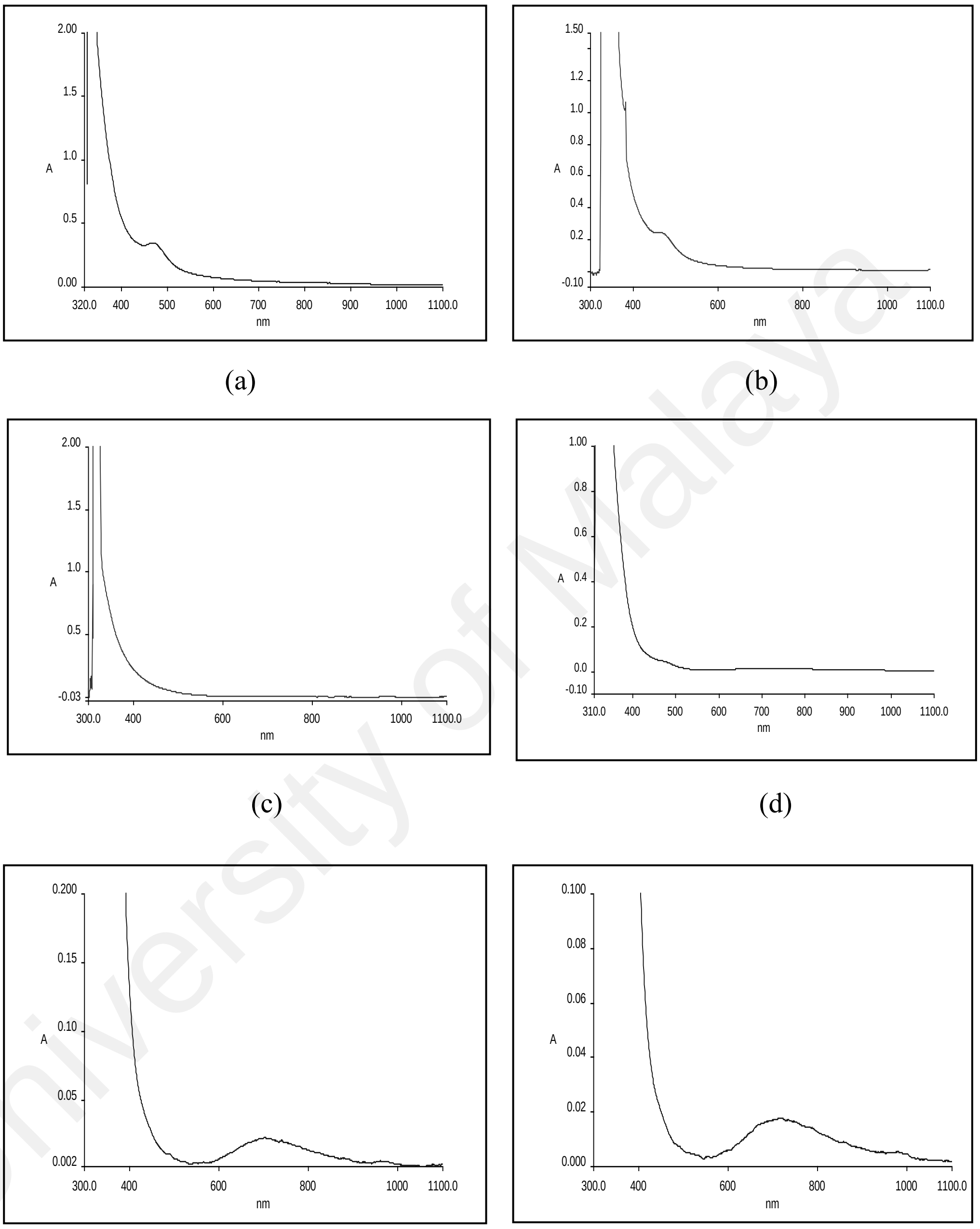

(a) (b)

(c) (d)

(e) (f)

Figure 4.117: UV-vis spectra of the dark brown solution at (a) initial time; and after (b) 3 days; (c) 7 days; (d) 10 days; (e) 14 days; and (f) 24 days

As previously done, the components of the dark brown solid were separated by column chromatography, and a total of 10 eluates were collected (but only three were analysed) by GCMS (**Appendix 20**). The first eluate was an orange-yellow sticky solid (10.9%). In contrast to the GC of the black solid obtained from CuB, the GC of the first eluate showed many peaks (**Figure 4.118**). Moreover, few significant peaks observed could not be confidently assigned due to the low probability during library search process. An exception is for the peak at R_t = 4.18 min (46%), which is assigned to ($CH_3COCH_2C(OH)(CH_3)_2$) from its mass spectra. In contrast to the product from the reaction with CuB, its dehydrated product ($CH_3COCH=C(CH_3)_2$) was not detected.

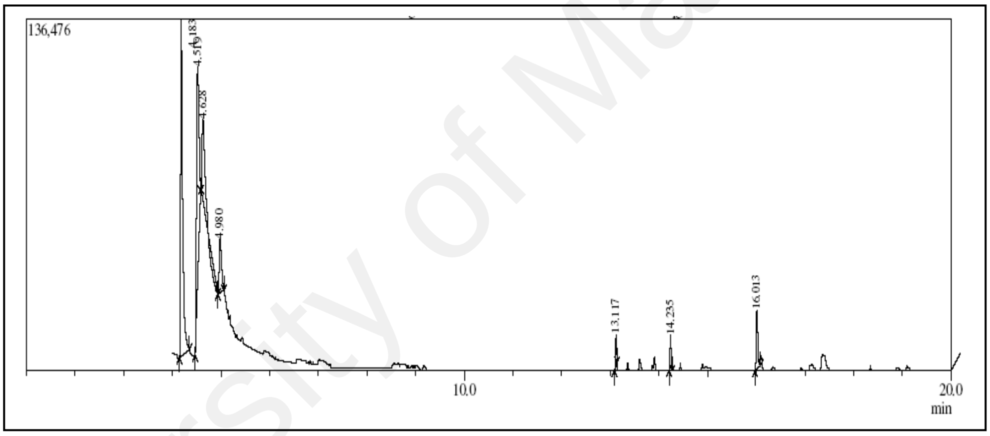

Figure 4.118: GC of eluate 1

Combining the above results, the proposed chemical formula for the dark brown solid is $[Cu(II)Cu(I)(R)_3(RH)_2(L)_{10}].3CH_3COCH_3$, where R = $4\text{-}O_2NC_6H_4COO$, L = $CH_3COCH_2C(OH)(CH_3)_2$ (formula mass = 2293; C,H,N: calculated = 54.8% C; 6.9% H; 3.0% N; found = 55.7% C; 6.2% H; 2.8% N).

4.6.3.2 Reaction of [$Cu_2(4\text{-}HOC_6H_4COO)_4$] with acetone

The presence of a strong electron-donating group, such as -OH, in copper(II) arylcarboxylate is expected to have the opposite effect to that of NO_2. Specifically, the rate of the reaction and the yield of the product are expected to be lower.

It was found that under the same experimental conditions as for CuB, CuOHB reacted with CH_3COCH_3 to give a black solid. As expected, the yield (60% w/w based on CuOHB) is much lower compared to that of $CuNO_2B$ (77%). These results strongly support the proposed mechanism for the C-C bond-forming reaction involving copper(II) arylcarboxylates.

The **C,H elemental analysis** of the solid gave 59.8% C and 5.76% H, indicating the presence of organic compounds other than $4\text{-}OHC_6H_4COOH$ in the solid (expected, 60.9% C, 4.3% H).

The **FTIR** spectrum of the black solid (**Figure 4.119**) shows a strong broad peak at about 3400 cm^{-1} for H-bonded -OH group, a broad peak at about 2600 – 2900 cm^{-1} for the C-H stretching mode of alkyl group, and a strong peak at about 1670 cm^{-1} for C=O. It is noted that the asymmetric and symmetric stretching COO bands, found at 1579 cm^{-1} and 1407 cm^{-1} respectively for CuOHB, are no longer obvious in this spectrum. Also, in contrast to the dark brown solid obtained from $CuNO_2B$, the spectrum of the black solid from CuOHB is quite similar to the black solid from CuB (**Figure 4.91).**

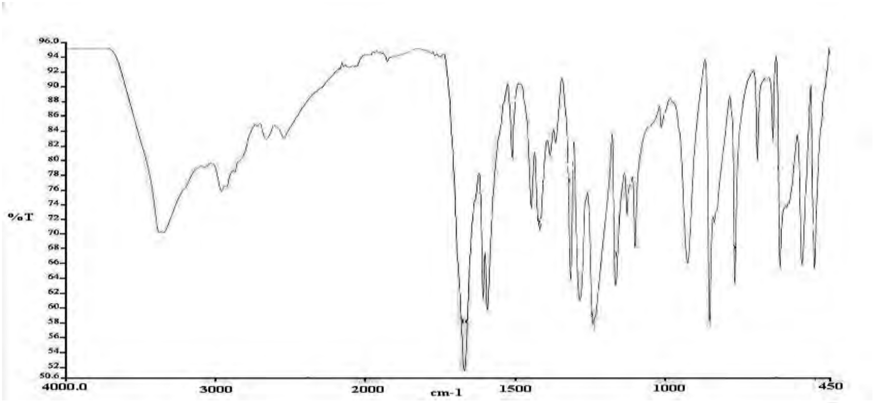

Figure 4.119: FTIR spectrum of the black solid obtained from the reaction of CuOHB with acetone

The **UV-vis** spectra of the black solid in CH_3COCH_3 at room temperature were recorded after several days interval (**Figure 4.120**).

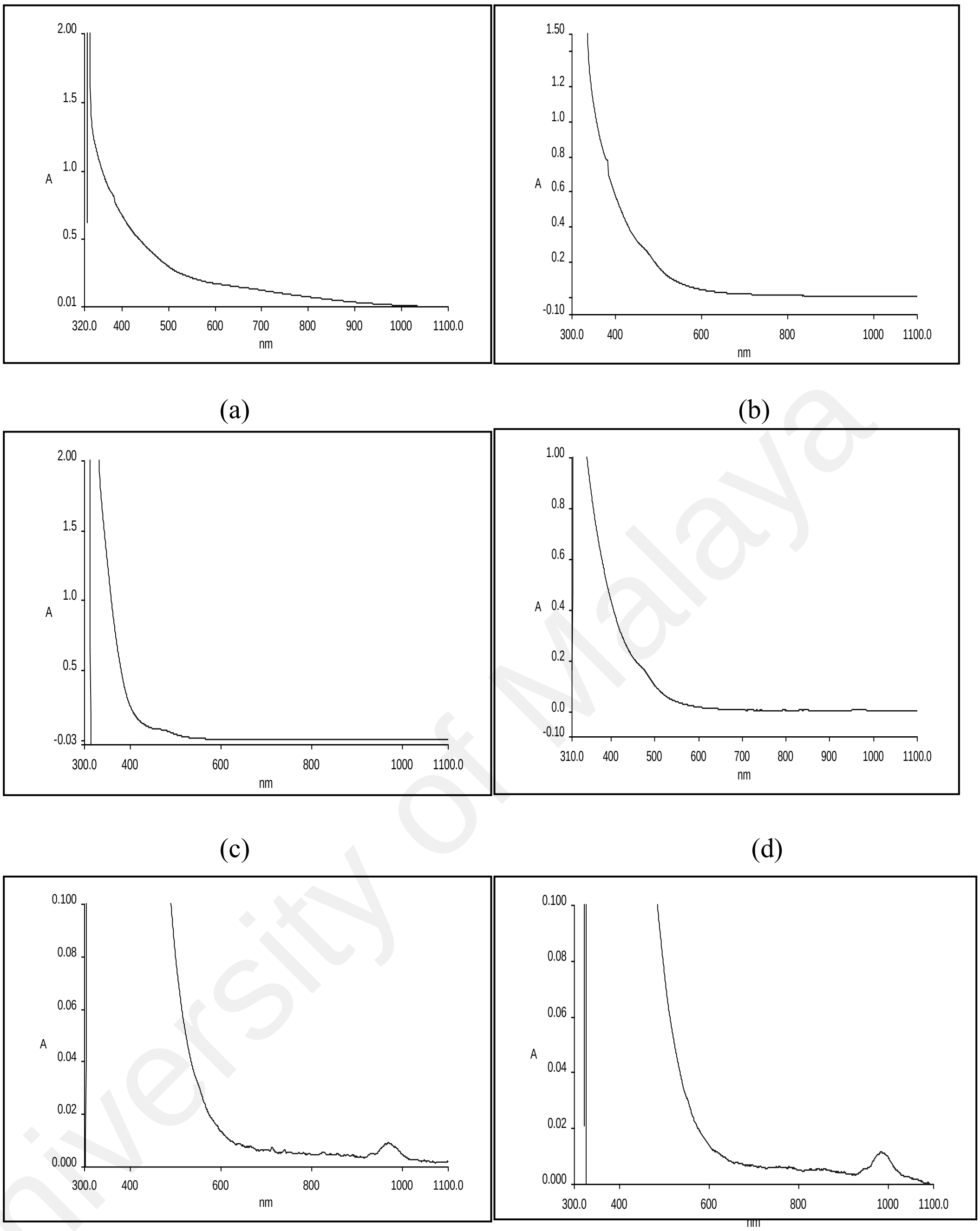

(a) (b)

(c) (d)

(e) (f)

Figure 4.120: UV-vis spectra of the black solid in CH_3COCH_3 at (a) initial time; and after (b) 3 days; (c) 7 days; (d) 10 days; (e) 14 days; and (f) 24 days

As in the case of CuB, the spectrum did not show distinct *d-d* peak for copper(II) at initial time. However, after 14 days, a shoulder at about 600 nm (for square planar Cu(II)) and a very weak and broad peak at about 1000 nm were observed. These peaks were still shown in the spectrum, recorded after 24 days. The very low energy for the latter peak suggests Cu(II) in a tetrahedral geometry.

From the above observations, it may be suggested that the black solid is also a mixed-valence complex similar to those obtained from CuB and $CuNO_2B$. On standing in acetone, its Cu(I) was slowly oxidized to copper(II).

As previously done, the component(s) of the black solid was/were similarly analysed by GCMS. A total of 11 eluates were collected but only 5 were analysed (**Appendix 21**).

As in the case of $CuNO_2B$, the GC spectrum of the black solid from CuOHB shows many peaks (**Figure 4.121**). However, the peak at R_t = 4.18 min indicates the presence of $CH_3COCH_2C(OH)(CH_3)_2$. As expected, the yield of this product is lower (26%) compared to that found in the dark brown solid obtained from $CuNO_2B$ (46%). It is also worth noting that its dehydrated product $CH_3COCH{=}C(CH_3)_2$ was not observed.

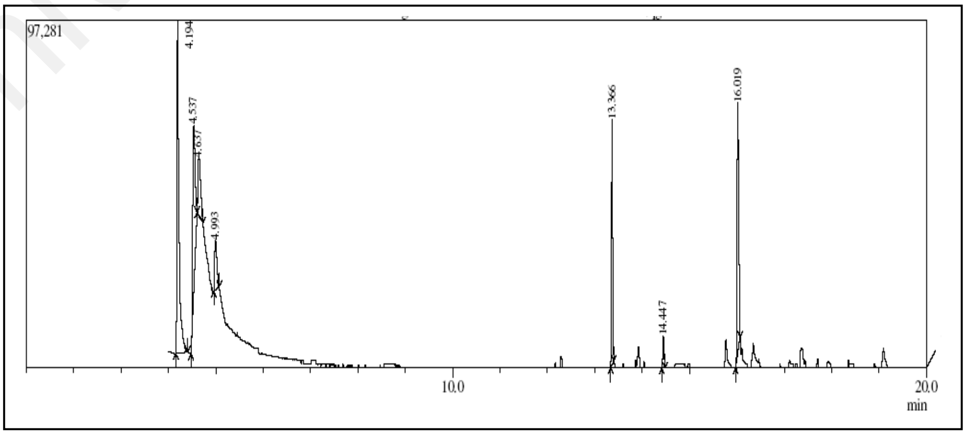

Figure 4.121: GC spectrum for eluate 1

Based on the results discussed above, the proposed chemical formula for the black solid is $[Cu(II)Cu(I)(R)_3(RH)_5(L)_5].CH_3COCH_3$, where R = 4-$HOC_6H_4COO$; L = $CH_3COCH_2C(OH)(CH_3)_2$ (formula mass, 1766 g mol^{-1}; C,H: calculated = 59.1% C; 5.9% H; found = 59.8% C; 5.8% H).

4.6.3.3 Reaction of $[Cu_2(4\text{-}ClC_6H_4COO)_4]$ with acetone

The strong inductive effect of the halogen group has been shown to have a direct effect on the physico-structural feature of the compounds. In the reaction of carbonyl, where the complex is suggested to act as a template in the redox reaction, the low electron density on copper(II) will cause the reaction to be more favourable. Hence, a higher yield of the product is expected from the reaction using copper(II) halobenzoates. In order to test this hypothesis, CuClB was reacted with acetone. This complex was deliberately chosen due to its similar structure and redox properties with CuB.

Under the same experimental conditions as CuB, CuClB reacted with acetone to give a black solid, and the yield was 67.5% (w/w based on CuClB). As expected, the yield is similar to that from CuB (63%).

The **C,H elemental analysis** of the solid gave 57.3% C and 7.6% H, indicating the presence of organic compounds other than 4-ClC_6H_4COOH (expected, 53. % C, 3.2% H).

The **FTIR** spectrum of the black solid (**Figure 4.122)** is different compared to the spectrum of CuClB and 4-ClC_6H_4COOH. It shows a strong and broad peak at about 3400 cm^{-1} assigned to H-bonded –OH group, and two asymmetric and symmetric COO vibrations at 1545 and 1382 cm^{-1} respectively. Hence, the value of $\Delta\nu$ (COO$^-$) is 163 cm^{-1}, which is similar to that of CuClB (153 cm^{-1}). Thus it could be inferred that, the overall structure and geometry of copper(II) remained intact in the black solid. It is also important to note that the peak at about 1680 cm^{-1} is rather broad, indicating an overlapping peaks for C=O, aromatic ring and C=C groups. Another significant observation in the spectrum is the presence of a strong and sharp band at 2900 cm^{-1}, assigned for presence of C-H stretching bands of an alkyl group.

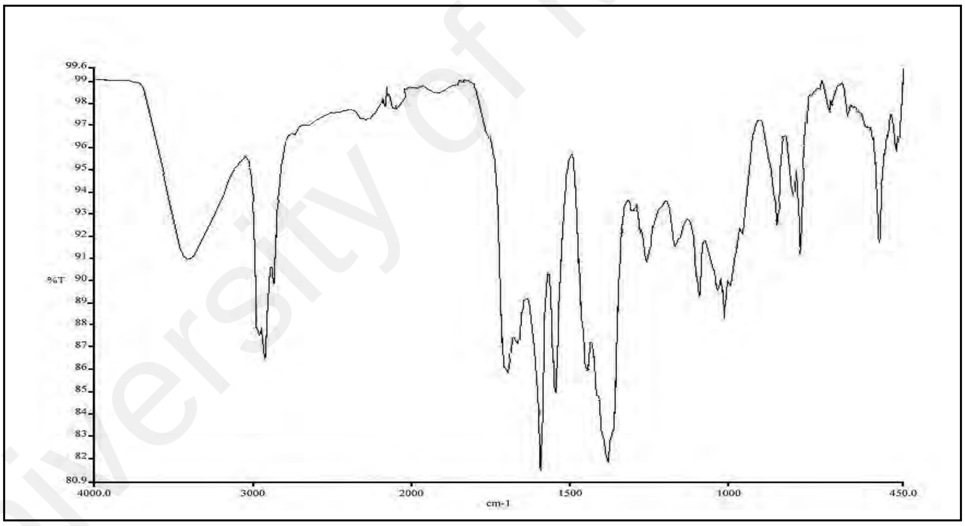

Figure 4.122: FTIR spectrum of the black solid obtained from the reaction of CuClB with acetone

The **UV-vis** spectrum of the black solid dissolved in acetone was taken a few times at several days apart (**Figure 4.123**). The spectrum shows a very intense MLCT at about 500 nm, indicating the presence of Cu(I). After about two weeks, a very broad and weak *d-d* peak is observed at about 700 nm and another one at about 1000 nm. These suggest the presence of two Cu(II) in a different geometry (square pyramidal and tetrahedral).

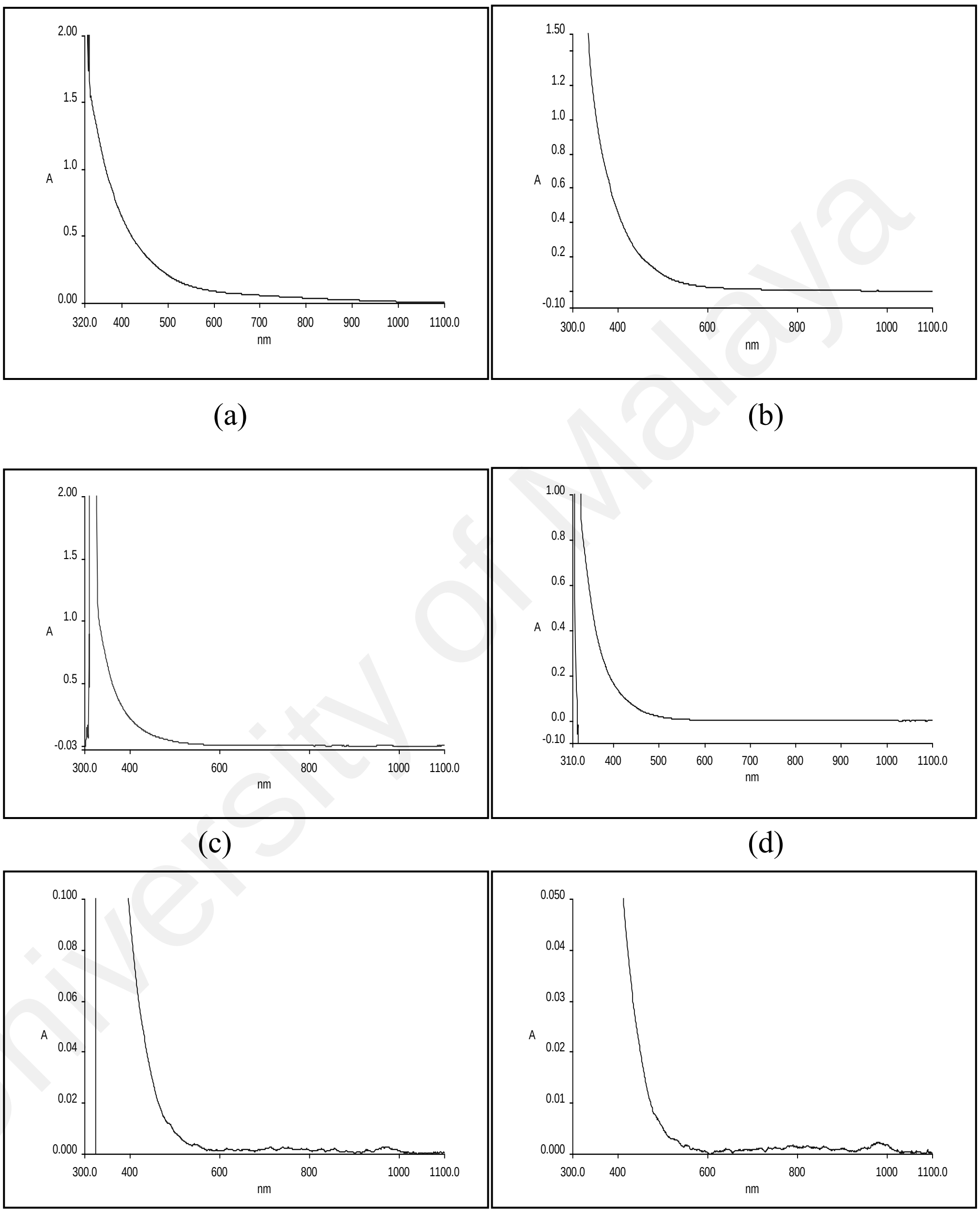

(a) (b)

(c) (d)

(e) (f)

Figure 4.123: UV-vis spectra of the black solution at: (a) initial time; and after (b) 3 days; (c) 7 days; (d) 10 days; (e) 14 days; and (f) 24 days

In order to detect the minor components, the solid was dissolved in ethyl ether and passed through a silica gel column using hexane-diethyl ether (4:1) as the eluent. A total of 13 eluates were collected, but only 5 were analysed by GCMS (**Appendix 22**).

Eluate 1 was a yellow gummy solid (17%) and its GC spectrum (**Figure 4.124**) shows peaks that could be completely assigned due to low probability during library search process. The exception is the peak at R_t = 4.18 minu (16.6%), assigned to 4-hydroxy-4-methyl-2-pentanone, $CH_3COCH_2C(CH_3)(OH)CH_3$.

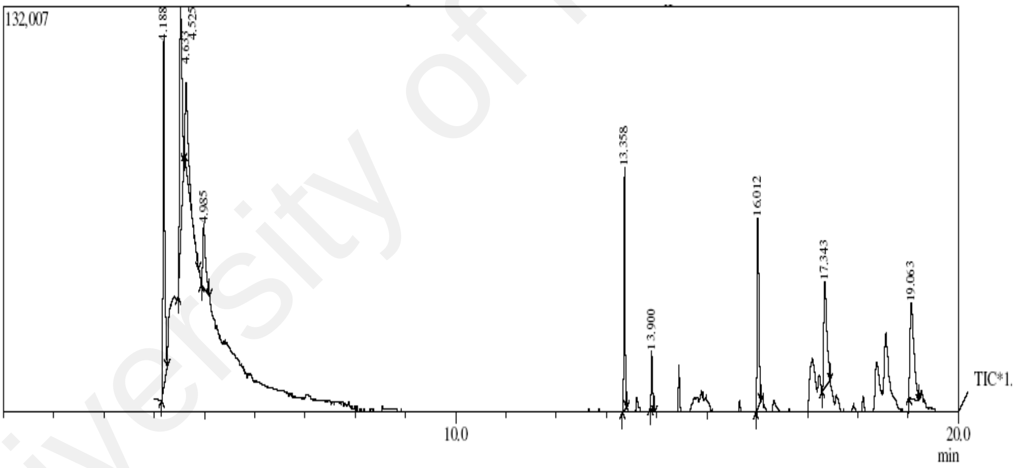

Figure 4.124: GC spectrum for eluate 1

Accordingly, the proposed chemical formula for the black solid is $[Cu(II)Cu(I)(R)_3(RH)_2(L)_{15}].CH_3COCH_3$, where R = $4\text{-}ClC_6H_4COO$, L = $CH_3COCH_2C(OH)(CH_3)_2$ (formula mass, 2704 g mol^{-1}; C,H: calc. = 56.8% C; 8.0% H; found = 57.3% C; 7.6% H).

To summarise, the reaction between $[Cu_2(4\text{-}XC_6H_4COO)_4]$ (X = H, NO_2, OH, Cl) with CH_3COCH_3 under acidic condition leads to the formation of an organic neutral ligand, $CH_3COCH_2C(OH)(CH_3)_2$, which is a product from the carbon-carbon bond-forming reaction of CH_3COCH_3, and a mixed-valence [Cu(II)Cu(I)] complex. The reaction is faster and the yield is higher when the arylcarboxylate ligand is substituted with a strong electron-withdrawing group (NO_2).

References

[1] C.S. Fountain and W.E. Hatfield, *Inorg. Chem,* 4(9) (1965) 1368.

[2] J. Lewis, Y.C. Lin, L.K. Rayston and R.C. Thompson, *J. Chem. Soc.* (1965) 6464.

[3] J. Lewis and F. Mabbs, 1964, *J. Chem. Soc.* (1964) 3894.

[4] S. Emori, H. Suenaga and N. Goto, *Bull. Chem. Soc. Jpn,* 64 (1991) 3460.

[5] G.B. Deacon and R.J. Phillips, R.J., *Coord. Chem. Rev*., 33 (1980) 227.

[6] B.S. Manhas and A.K. Trikha, *J. Indian Chem. Soc*., 59 (1982) 315.

[7] B. Kozlevcar, N. Lah, D. Zlindra, I. Leban and P. Segedin, *Acta Chim Slov*., 48 (2001) 363.

[8] A. B. Siqueira, A.B., Y. Elias, E.Y. Ionashiro, T.C. Cláudio, B. Gilbert, C.R. Emanuel and I. Massao, *Quim. Nova,* 30(2) (2007) 318.

[9] J.E. Weder, T.W. Hambley, B.J. Kennedy, P.A. Lay, D. MacLachlan, R. Bramley, C.D. Delfs, K.S. Murray, B. Moubaraki, B. Warwick, J.R. Biffin, J.R. and H.L. Regtop, *Inorg. Chem. 38 (1999)* 1736.

[10] M. Kato, and Y. Muto, *Coord. Chem. Rev*. 92 (1988) 45.

[11] C. Dendrinou-Samara, P.D. Jannakoudakis, D.P. Kessissoglou, G.E. Manoussakis, D. Mentzafos, and A. Terzis, *J. Chem. Soc., Dalton Trans.* (1992) 3259.

[12] G.W. Reimann, G.F. Kokoszka, and G. Gordon, *Inorg. Chem.* 4 (1965) 1082.

[13] M. Melnik and M. Dunaj-Jurco, *Inorg. Chim. Acta,* 86 (1984) 185.

[14] J. Catterick, and R. Thornton, *P. Adv. Inorg. Chem. Radiochem.* (1977) 291.

[15] L. Dubicki and R.L. Martin, *Inorg. Chem, 5* (1996) 2203.

[16] A.L. Abuhijleh, *J. Inorg. Biochem, 55* (1994) 255.

[17] M. Melnik, I. Potocnak, L. Macaskova, D. Miklos and C.E. Holloway, *Polyhedron,*15, (1996) 215.

[18] D.P. Graddon, *J. Inorg. Nucl. Chem.17* (1961) 222.

[19] M. Kato, H.B. Jonassen, and J.C. Fannng, *Chem. Rev.* 64 (1964) 99.

[20] S.P. Ja and C.H. Dae, *Bull. Kor. Chem. Soc*. 43(3) (1999) 351.

[21] B.N. Figgis and R.L Martin, *J. Chem. Soc*. (1956) 3837.

[22] B. Bleaney and K. Bowers, *Proc. R. Soc. London, Ser. A (1952)* 451.

[23] T. Kawata, H. Uekusa, S. Ohba, T. Furukawa, T. Tokii, Y. Muto and M. Kato, *Acta Cryst.* B48 (1992) 253.

[24] M. Melnik, M. Dunaj-Jurco and M. Handlovc, *Inorg. Chim. Acta* 86 (1984) 185.

[25] R.A. Zelonka and M.C. Baird, *Inorg. Chem.* 11(1) (1972) 134.

[26] A.B. Siqueira, E.Y. Ionashiro, C.T de Carvalho, G. Bannach, E.C. Rodrigues and M. Ionashiro, *Quim. Nova* 30(2) (2007) 318.

[27] W. Ference, A. Walkow-Dziewulska, and P. Sadowski, *J. Therm. Anal. Cal.* 82 (2005) 365.

[28] A. Turek, J. Kobylecka and B. Ptaszynski, *J. Therm. Anal. Cal*. 78 (2005) 513.

[29] F.Q. Wang, D.F. Weng, X.J. Zheng, J.J. Zhang, H. Mad and L.P. Jin, *Inorg. Chim. Acta* 360 (2007) 2029.

[30] M. Arshada, S. Rehmanb, S.A. Khanb, K. Masudc, N. Arshad and A. Ghani, *Thermochim. Acta*, 364 (2000)143.

[31] D. Czakis-Sulikowska and A. Czylkowska, *J. Therm. Anal. Cal.* 71 (2003) 395.

[32] S.P. Perlepes, E. Libby, W.E. Streib, K. Folting and G. Chrsitou, *Polyhedron*, 11(8) (1992) 923.

[33] P. Kogerler, P.A.M. Williams, B.S. Parajon-Costa, E.J. Baran, L. Lezama, T. Rojo and A. Muller, *Inorg. Chim. Acta,* 268 (1998) 239.

[34] I. Toledo, M. Arancibia, C. Andrade and I. Crivelli, *Polyhedron*, 17(1) (1998) 173.

[35] B. K. Moo, *Bull. Korean. Chem. Soc.* 22(1) (2001) 113.

[36] H. Dhillon, K. Sharma, R. Gehlot and S. Kumbhat, *Electrochem. Commun.* 11 (2009) 878.

[37] P. Zanello, *Inorganic Electrochemistry. Theory, Practice and Application*, The Royal Society of Chemistry, 2003.

[38] X. Zhou, X. Meng, W. Cheng, H. Hou, M. Tang and Y. Fan, *Inorg. Chim. Acta* 360 (2007) 3467.

[39] A.M. Sosa, V.M. Ugalde-Saldivar, I. Gonzalez and L. Gasque, *J. Electroanal. Chem.,* 579 (2005) 103.

[40] D. Grujicic and B. Pesic, *Electrochim. Acta.* 47 (2002) 2901.

[41] C. Nila and I. Gonzalez, *J. Electroanal. Chem.* 401 (1996) 171.

[42] R. Kannapan, R. Mahalakshmy, T.M. Rajendran, R. Venkatesan and P. S. Rao, *Proc. Indian Acad. Sci. (Chem. Sci.*), 115(1) (2003) 1.

[43] J. Lewis, F.E. Mabbs, L.K. Royston and W.R. Smail, *J. Chem. Soc.* (1969) 291.

[44] J. Lewis and R.C. Thompson, *Nature* (1963) 468.

[45] J. Lewis, Y.C. Lin, L.K. Royston and R.C. Thompson, *J. Chem. Soc.* (1965) 6464.

[46] A. W. Addison, T. N. Rao, J. Reedijk, J. van Rijn and G. C. Verschoor, *J. Chem. Soc. Dalton Trans*., (1984) 1349.

[47] S. Zolezzi, E. Spodine and A. Decinti, *Polyhedron*, 21 (2002) 55.

[48] G.F.kokosza and G. Gordon, *Transition Met. Chem*., 5 (1969)181.

[49] A. W. Addison, T.N. Rao, J. Reedijk, J. van Rijn, and G.C. Verschoor, *J. Chem. Soc. Dalton Trans.* (1984) 1349.

[50] F.G. Herring, B. Landa, R.C. Thompson and C.F. Schwerdtfeger, *J. Chem. Soc. (A)*, (1971) 528.

[51] S. Yamada, H. Nishikawa and S. Miki, *Jpn. Chem. Soc. Bull*., 37(4) (1964) 576.

[52] T. Inimata and T. Moriwaki, *Bull. Chem. Soc. Jpn*., 46 (1973) 1148.

[53] M.K. Alyariya, T. Saideliev and Y.T. Tashpulatov, *Zh. Neorgan Khim.,* 10 (1965) 1493.

[54] G. Micera, P. Pilu and l. Strinna Erre, *Thermochim. acta* 84 (1985) 175.

[55] W.E. Hatfiled, C.S. Fountain and R. Whyman, *Inorg. Chem.* 5 (1966) 11.

[56] F. Hanic and J. Michalov, *Acta. Cryst*. 13 (1960) 299.

[57] M.Inoue, M. Kishita and M. Kubo. *Inorg. Chem.* 3 (1964) 239.

[58] C.S. Fountain and W.E. Hatfield. *Inorg. Chem.* 4 (1965) 1368.

[59] W.E. Hatfield, C.S. Fountain and R. Whyman. *Inorg. Chem.* 5 (1966) 1855.

[60] M. Melnik, *Coord. Chem. Rev.*, 36 (1981) 1.

[61] R.W. Jonathan, F.A. Kettle and J.A. Marks, *J. Chem. Soc., Dalton Trans.*(1972) 428.

[62] N. Abdullah and M. H. Chisholm, *Role of $Cu_2(XC_6H_4COO)_4$ in facile C-C bond-forming reaction of carbonyls,* International Conference on Molecular Chemistry, (2008) 54.

[63] A.B.P. Lever, D.R. McMillin, and K.M. McNett, Chem. Rev. 98 (1998) 1201.

[64] V. Kalsani, M. Schmittel, A. Listorti, G. Accorsi, and N. Armaroli, *Inorg. Chem.* 45 (2006) 2061.

[65] W. F. Fu, X. Gan, J. Jiao, Y. Chen, M. Yuan , S. M. Chi, M. M. Yu, and S. X. Xiong. *Inorg. Chim. Acta,* 360 (2007) 2758.

[66] M.B. Robin and P.Day, *Adv. Inorg. Chem. Radiochem.* 10 (1967) 247.

[67] http://www.aist.go.jp/RIODB/SDBS (National Institute of Advanced Industrial Science and Technology, 21 Februrary 2011).

[68] G. C. Campbell and J. F. Haw, *Inorg. Chem.,* 27 (1988) 3706.

[69] J. McMurry, *Organic Chemitry* 3rd Edn. Brooks/Cole Publishing Company, USA, Chapter 23 (1992).

[70] P. Kutrowski, D. Sulkowska, R. Pytlowany and R. Dziembaj *React. Kinet. Catal. Lett.*, 81(1) (2004) 3-11.

[71] M. I. Mohamadin and N. Abdullah. *Cent. Eur. J. Chem*. 8 (2010) 1090.

[72] Y. Akama, *J. Therm. Anal. Cal.*, 45 (1995) 1501.

[73] A.M. Giroud-Godquin. *Coord. Chem. Rev*., 178 (1998) 1485.

[74] R. Paschke, D. Balkow and E. Sinn. *Inorg. Chem*. 41(7) (2002) 1949.

[75] G. S. Attard and P. R. Cullum. *Liq. Cryst*. 8(3) (1990) 299.

[76] R. Cervini, X.C. Li, G.W.C. Spencer, A.B. Holmes, S.C. Moratti and R.H. Friend, *Synth. Met.* 84 (1997) 359.

[77] Y.F. Li, Y. Cao , J. Gao, D. Wang, G. Yu and A. J. Heeger, *Synth. Met*. 99 (1999) 243.

[78] D.M. de Leeuw, M.M.J Simenon, A.R. Brown and R.E.F Einerhand, *Synth. Met*. 87 (1997) 53.

[79] R.L. Sproull, and W.A. Phillips, *Modern Physics: The Quantum Physics of Atoms, Solids and Nuclei*, Wiley, (1980).

[80] R.J. William, *Modern Physics from A to Z*, Wiley 1994.

[81] S. Banerjee, *Solid State electronic Devices* (5th ed.). New Jersey. Prentice Hall. (2000) p. 524.

[82] P. Kustrowski, D. Sulkowska, R. Pytlowany and R. Dziembaj, *React. Kinet. Catal. Lett.* 81(1) (2004) 3.

[83] R. Mahrwald, *Modern Aldol reaction : Enolates, organocatalysi, biocatalysis and natural product synthesis*, Wiley-VCH, 1-53 (2004).

CHAPTER 5

CONCLUSIONS AND SUGGESTIONS FOR FUTURE WORKS

5.1 Conclusions

The metathesis reaction [1] between [$Cu_2(CH_3COO)_4$] and the corresponding arylcarboxylic acid was a suitable method for the preparation of dimeric copper(II) arylcarboxylates of general formula [$Cu_2(4\text{-}XC_6H_4COO)_4$], where X = H, NO_2, OH, NH_2, F, Cl, Br, and I, and [$Cu_2(3,5\text{-}(NO_2)_2C_6H_3COO)_4$]. The yields were in the range of 35-54.9%. The yield was highest for 3,5-$(NO_2)_2$- and lowest for NH_2- substituted complexes.

All complexes adopted the paddle-wheel structure similar to other metal(II) carboxylates reported in the literature [2,3], with CH_3CH_2OH and/or H_2O at the axial positions. However, complexes having strong electron withdrawing group namely X = NO_2, 3,5-$(NO_2)_2$ and F, have a more distorted geometry around copper(II). Their dimeric structures were also maintained in CH_3OH-CH_3COOH. Labile complexes are formed from a weaker Lewis base (X = NO_2), or when coordinated with a strong coordinating molecules at the axial positions.

The room-temperature magnetic susceptibilities for these complexes were comparable to other dimeric copper(II) carboxylates [4-6]. The values of the effective magnetic moments (μ_{eff}) and -2J were in the range of 1.8 – 2.5 B.M. and 133-381 cm^{-1} respectively. The strength of the antiferromagnetic interaction depends on the distortion of the square pyramidal geometry at Cu(II); a less distorted complex has a stronger interaction. The order of increasing antiferromagnetic interaction is:

$F < NH_2 < NO_2 < 3,5\text{-}(NO_2)_2 < OH, H < I < Br, Cl.$

In general, these complexes were thermally stable up to 240°C. The main residue from the decomposition was CuO. The decomposition process involved decarboxylation of the arylcarboxylate ligands to mainly CO_2. The thermal stability depends on the polarisability of the arylcarboxylate ligands. Ligands substituted with a stronger electron-attracting or electron-donating group are more polarisable and therefore less thermally stable. The order of increasing thermal stability is: $3,5\text{-}(NO_2)_2 < NH_2 < OH < H < NO_2 < F < Cl < Br < I$.

The redox properties of these complexes showed stepwise one-electron reduction: [Cu(II)Cu(II)] → [Cu(II)Cu(I)] → [Cu(I)Cu(I)]. The mixed-valence [Cu(II)Cu(I)] complexes formed partially dissociated, while the fully reduced [Cu(I)Cu(I)] complexes were not further reduced to metallic Cu. The overall redox processes were accompanied by extensive structural reorganizations, indicated by the high value of ΔE ranging from 590 to 1050 mV. The first reduction potential of these complexes increases in the following order:

$3,5\text{-}(NO_2)_2 < NO_2 < H < F < Cl < Br < I < NH_2 < OH$

$[Cu_2(4\text{-}XC_6H_4COO)_4]$, where X = H, NO_2, OH, Cl, acted as a redox template for the C-C bond-forming reaction of carbonyls. In the reaction with CH_3COCH_3, the percentage yield of the product follows the reducibility of the complex: NO_2 > Cl, OH, H. The products were mixed-valence [Cu(II)Cu(I)] complexes. The chemical formulas of the mixed-valence complexes obtained from CuB, $CuNO_2B$, CuOHB and CuClB are shown in **Table 5.1**.

Table 5.1: The mixed-valence complex formed from the C-C bond-forming reaction of $[Cu_2(4\text{-}XC_6H_4COO)_4]$ with CH_3COCH_3

X	Chemical formula*	Colour
H	$[Cu(II)Cu(I)(RCOO)_3(RCOOH)_2(L)_4].CH_3COCH_3$	Black
NO_2	$[Cu(II)Cu(I)(R)_3(RH)_2(L)_{10}].3CH_3COCH_3$	Dark brown
OH	$[Cu(II)Cu(I)(R)_3(RH)_5(L)_5].CH_3COCH_3$	Black
Cl	$[Cu(II)Cu(I)(R)_3(RH)_2(L)_{15}].CH_3COCH_3$	Black

* R, $4\text{-}XC_6H_4COO$; L, $CH_3COCH_2C(OH)(CH_3)_2$

CuB (X = H) also reacted with a mixture of $C_6H_5COCH_3$ (benzophenone) and C_6H_5CHO (benzaldehyde), under the same conditions, to form the C-C bond-forming products, $C_6H_5COCH{=}CHC_6H_5$, $C_6H_5COCH{=}C(CH_3)C_6H_5$ and $C_6H_5COCH_2CC_6H_5CH_2COC_6H_5$.

5.2 Suggestions for Future Works

The pursuit to obtain crystals of these dimeric complexes should be continued in order to make the correct correlation between the structure, physical and chemical properties with the electronic effect of the substituent.

The C-C bond-forming reaction should be further studied in order to find the optimum conditions, in terms of refluxing time and molarity of HCl, as well as the effect of other mineral acids (examples, HF, HBr, HI, H_2SO_4, HNO_3), organic acids (example, CH_3COOH) and Lewis acids (example, $AlCl_3$). It would also be worthwhile to test the scope of the reactions to other carbonyls, such as diketones (acetylacetone) and carbohydrates (glucose), which may produce mixed-valence copper complexes with interesting physical properties (extended conjugation, water-solubility). Also, it would be interesting to find out if the reaction can be extended to other transition metal ions, such as Ni(II), Co(II), Fe(II), and Mn(II).

Similar studies (especially redox and C-C bond-forming reaction) should be extended to other copper(II) arylcarboxylates and to copper(II) complexes with substituents at other position of the aromatic ring, especially the *ortho*- position, to see the steric effect, as well as for fully-substituted fluorinated complex ($[Cu_2(C_6F_5COO)_4]$) to see the cumulative effect of a strong electron-attracting group, and for copper(II) alkylcarboxylates of either linear of branched chains which may exhibit metallomesogenic properties.

Further studies on the black solids obtained from the C-C bond-forming reaction may lead to cheaper and easily prepared low band-gap photovoltaic materials.

References

[1] D.D. Ebbing. *General Chemistry*. Hughton Mifflin Company, Boston, USA, 1996.

[2] B. Kozlevcar, N. Lah, D. Zlindra, I. Leban and P. Segedin, *Acta Chim. Slov*. 48 (2001) 363.

[3] A. B. Siqueira, Y. Elias, E.Y. Ionashiro, T.C. Cláudio, B. Gilbert, C.R. Emanuel and I. Massao, *Quim. Nova* 30(2) (2007) 318.

[4] M. Kato, H.B. Jonassen and J.C. Fang, *Chem. Rev.* 64 (1964) 99.

[5] S.P. Ja and C.H. Dae, *Bull. Kor. Chem. Soc*. 43(3) (1999) 351.

[6] T. Kawata, H. Uekusa, S. Ohba, T. Furukawa, T. Tokii, Y. Muto and M. Kato, *Acta Cryst.* B48 (1992) 253.